‘Evaluation of Electrostatic Precipitation to Capture and Inactivate Viral Particles from Bioaerosols.’

Candidate Number: C1716818

Candidate Name: Hannah Elizabeth Preston

School: Cardiff School of Medicine

Division: Division of Cancer and Genetics (DCG)

Supervisors: Professor Alan Parker, Dr Rebecca Bayliss, Dr Jason Brewer and Dr Dominic Griffiths

Degree Award: Full Time Master of Philosophy (MPhil)

Year of Presentation: 2022/2023

Word Count: 33,444

Date: 31/10/2022

Abstract

Background: Ultravision™ technology has been developed to clear surgical smoke during laparoscopic surgery. Ultravision™ operates by 'electrostatic precipitation' (EP), whereby solid particles are removed from a gas via electrical energy. Previous studies have shown that EP can capture airborne pathogens. However, little is known regarding the effects of EP on viral activity. The ability to successfully capture and inactivate aerosolised viral particles may limit the spread of respiratory diseases, potentially enabling elective laparoscopic surgical procedures to continue during periods of viral pandemics.

Methods: To mimic the release of bioaerosols that occurs during surgery, model systems designed to resemble open and closed surgery were constructed. Two viruses were used to evaluate the effects of Ultravision™ on both enveloped and non-enveloped virus particles: a Lenti-SARS Pseudovirus and Adenovirus serotype 5. A known concentration of each virus sample was aerosolised into the model systems, exposed to Ultravision™, and collected from a BioSampler for experimental analysis. Additionally, parameters affecting the efficiency of EP were altered to identify optimal conditions for Ultravision™ usage. All collected samples were analysed for viral presence by qPCR and for viral activity by transduction and plaque assays.

Results: Virus particles were successfully captured and inactivated by Ultravision™, in both model systems. Ultravision™ functioned most efficiently at 10kV. Likewise, using two discharge electrodes at 8kV, as opposed to one, enhanced the efficiency of electrostatic precipitation.

Conclusion: Although this study highlights Ultravision™ as an efficient device for the capture and inactivation of viral particles, the exact mechanisms underpinning viral inactivation remain unknown. It was hypothesised that the discharge electrode generated virucidal reactive species that degraded the aerosolised virus particles. Future work using more representative models is required to confirm findings from this study and to elucidate mechanisms of viral inactivation caused by Ultravision™.

Acknowledgements

First and foremost, I would like to thank my excellent academic supervisors, Professor Alan Parker, and Dr Rebecca Bayliss. They have provided me with plentiful support, advice, and guidance, of which I am hugely grateful for. In addition, I would like to extend my thanks to the entire Parker-Lab team, for their support and encouragement throughout my degree. I would also like to thank my supervisors from Alesi Surgical Ltd, Dr Dominic Griffiths and Dr Jason Brewer. Their sharing of knowledge and experience has greatly improved my understanding and broadened my skill set in a field that was unfamiliar to me at the start of my MPhil. I would also like to thank Dr Neil Warren, Dr Michael Shinkwin and Dr James Davies, for providing invaluable preliminary data and offering helpful suggestions and assistance as I continued the research they had pioneered. Finally, I am deeply grateful to Professor Nigel Temperton and Dr Martin Mayora Neto from the Medway School of Pharmacy, for their generous collaborations and contributions towards my project.

Table of Contents

Figures

Tables

Chapter 1. Introduction

1.1 Airborne Transmission of Respiratory Viruses

Over 4 million deaths are caused annually by acute respiratory viruses, making them the leading cause of mortality from infectious diseases worldwide (Fink, et al. 2020). Key transmission of respiratory pathogens occurs via the dispersion of bioaerosols from infectious patients. Contaminated aerosol droplets can be released by coughing, sneezing, breathing, and talking, spreading the virus to those within 2 metres of the infectious individual. Additionally, aerosol droplets that land on and contaminate surfaces (fomites) can also cause viral transmission following direct contact (Wang, et al. 2021).

Numerous factors affect the spread of airborne viruses, and conditions that promote dissemination are accountable for superspreading events. Environmental factors such as temperature, humidity, UV radiation and airflow all contribute to the transportation and stability of viral aerosols. For example, a study by Chan (2011), found that in typical air-conditioned environments (22°C), at a relative humidity of 40-50%, SARS CoV2 that was deposited onto smooth surfaces remained stable for over 5 days. However, following an increase in room temperature and relative humidity, virus viability was rapidly reduced by >3$\log_{10}$ (Chan, et al. 2011). Additionally, physical properties such as aerosol droplet size, air-space volume and fomite material can influence viral spread and stability (Scheuch. 2020). Van Doremalen (2020) identified that SARS CoV-2 was more stable and remained viable for longer, when deposited onto plastic or stainless steel, as opposed to copper (Van Doremalen, et al. 2020). This thereby implies that certain materials possess intrinsic virucidal properties, whilst others allow the spread of respiratory viruses. Another factor influencing viral transmission is the minimum infectious dose required to initiate disease. The minimum infectious dose is highly dependent on host susceptibility, the site of droplet deposition within the respiratory tract and the type of virus itself (Wang, et al. 2021). For example, Smither (2020) discovered that at medium relative humidity (40-60%), SARS CoV-2 had a half-life of 1.25 hours, compared to the Influenza Virus, which had a half-life of 32 minutes in the same experimental conditions (Smither, et al. 2020). This study therefore suggested that different virus species can survive aerosolisation for different

periods of time, irrespective of the external conditions. As well as this, Tate (2021) showed that Adenoviruses are also capable of surviving aerosolisation, with respects to Pressurised Intraperitoneal Aerosolised Virotherapy (PIPAV) procedures. Additionally, the physical structure of a virus plays an integral role in its stability and transmission. When exposed to extreme environments, non-enveloped viruses have shown more resistance, compared to enveloped viruses (Doms. 2016). In a study by Firquet (2015), various virus preparations were applied to Petri dishes, left to dry in biosafety cabinets and were then recovered at multiple time points and analysed via qPCR for infectious viral titers. Enveloped viruses remained viable for less than 5 days, compared to non-enveloped viruses, which remained infectious for 6 weeks or longer (Firquet, et al. 2015). Therefore, we must not only strive to better understand the vast number of components that affect aerosol transmission, but also establish and enforce effective precautionary measures based on our understanding of such factors.

The 2020 SARS CoV-2 pandemic highlights the extreme importance of understanding airborne viral transmission, to reduce mortality, morbidity and the devastating socio-economic impacts we are currently facing. Mitigation strategies such as mask wearing, personal protective equipment (PPE), quarantining of infected individuals, social distancing, regular hand-washing and vaccination, have been enforced and encouraged by the government and health authorities. Data obtained from Ferguson (2020), who mathematically modelled the predicted spread of SARS CoV-2 with and without the addition of precautionary measures, aided the formulation of our current mitigation methods (Ferguson, et al. 2020). However, the cases of SARS CoV-2 continue to fluctuate at high levels, due to the appearance of new viral strains, and the easing of government-enforced restrictions (UK Government, 2022). Additionally, in May 2022, only 70% of the populations in 57 high-income countries were vaccinated (at least one dose), with approximately one billion people in low-income countries remaining unvaccinated (World Health Organisation, 2022). This may be due to political, personal, or health-related reasons, as well as a potential lack in vaccine confidence (Hou, et al. 2021). Therefore, a large proportion of the global population are still at high risk, emphasising the need for novel safety and precautionary interventions. The aim to reduce the spread of disease is not limited to SARS CoV-2, but accounts for all viral and bacterial pathogenic outbreaks that may lead to future epidemics and pandemics.

Developing a device that is capable of eliminating airborne pathogen transmission would be a breakthrough discovery and has the potential to save an immeasurable number of lives globally.

1.2 Socio-economic Impacts of the 2020 SARS-CoV-2 Pandemic

Presently (October 2022), the 2020 SARS-CoV-2 pandemic has directly caused >6.58 million deaths worldwide, >205,000 of which occurred in the UK alone. Additionally, there have been >629 million global cases, >22,200,000 of which were reported in the UK (UK Government, 2022). Of course, it is likely that these statistics were at least a third higher, as values stated by the Government only accounted for reported cases. It is therefore abundantly clear that the pandemic has had devastating and long-lasting socio-economic impacts. The speed of viral spread across the nation has placed unprecedented demands on the NHS, health care staff, hospital facilities and intensive care units (ICUs). These unprecedented demands and pressures on the health service have required retired health care workers to be redeployed, and newly graduated students to be prematurely recruited, in an attempt to battle staff shortages (Propper, 2020).

It is estimated that hundreds of thousands of medical procedures were delayed or cancelled as a result of the pandemic, in turn creating enormous backlogs of untreated and undiagnosed patients, increasing the demand for private health care (Propper, 2020). In order to treat severely ill COVID-19 patients, 30,000 hospital beds in NHS England were provided by postponing non-urgent surgeries. Bioaerosol generating procedures, such as tracheostomy, laparoscopy, open suctioning, administration of nebulised treatment and manual ventilation, were at the highest risk of cancellation, due to the likelihood of airborne transmission to staff and other patients (Fink, 2020). Individuals that were already experiencing medical issues, other than COVID-19, were left helpless and unaided, worsening their symptoms and overall quality of life. The number of lives lost that were indirectly due to the pandemic are hard to quantify, but may match the lives lost that were directly due to COVID-19 infection. Therefore, SARS-CoV-2 is also associated with indirect morbidity and mortality, that could have been prevented in the case of advanced preparation or the implementation of better non-pharmaceutical interventions (NPIs) (COVIDsurg Collaborative, 2020).

Further to the indirect effects of the pandemic, studies have assessed recovered COVID-19 patients to determine the origin and understand the occurrence of 'long COVID'. A study by Sykes (2021) evaluated a cohort of 134 discharged COVID-19 patients for residual symptoms, 113 days post-discharge. Eighty-six percent of patients reported at least 1 residual symptom upon follow up, however symptoms reported were largely biopsychosocial effects of the infection, such as anxiety and fatigue. Carfi (2020) also performed research assessing persistent symptoms experienced by recovered COVID-19 patients. From a cohort of 143 patients that were evaluated 60 days post COVID-19 onset, 12.6% showed no symptoms, 32% had 1 or 2 symptoms, and 55% had 3 or more symptoms. In this instance, the symptoms reported appeared more pathological, some of which included joint pain, chest pain and dyspnoea.

In addition to physical health, the SARS CoV-2 pandemic has negatively impacted upon the mental health and well-being of many. Studies have shown that young children, university students, health-care workers and the elderly were most affected, and more likely to develop anxiety, depression, and PTSD as a result (Saladino, 2020). This may have been due to mitigation measures such as isolation and social distancing, resulting in loneliness and the inability to connect with others physically and emotionally. In accordance with this, research by Orgilés (2020) and Lee (2020) found that children and students were more likely to experience elevated stress levels, difficulties concentrating and nervousness, during the pandemic.

As well as health related outcomes, the SARS-CoV-2 pandemic has caused major economic crises, in terms of losses to the financial market, huge imbalances between supply and demand and devastating declines in productivity (Shretta, 2020). By April 2020, 32% of businesses were forced to temporarily relieve staff, causing detrimental drops in employment rates (Shretta, 2020). This statistic has shown direct correlation with the 7.4% reduction of GDP in Europe in 2020, as a consequence of government-enforced isolation (Richards, 2022). Over £55.2bn of the £84.3bn NHS budget for healthcare has been spent on the diagnosis, treatment, and mitigation of COVID-19 (Appleby, 2022). Additionally, the pandemic has caused a halt in scientific research and development for non-COVID-19 related treatments and vaccines. The number of publications in scientific research, unrelated to COVID-19, have decreased by 10-12%, potentially due to the diversion of funding and grants

towards SARS-CoV-2 and away from other divisions of research (Riccaboni and Verginer, 2022). Additionally, in July 2020, just 4 months post-lockdown, approximately 1,200 clinical trials were suspended or cancelled, due to the pandemic (Balfour, 2021). It is therefore essential that novel NPI's are developed, not only to implement in our current climate, but also to improve our preparation for any outbreaks or pandemics that occur in the future.

1.3 Electrostatic Precipitation and Ultravision™

The process of electrostatic precipitation (EP) involves the removal of suspended solid or liquid particles from gaseous or aerosol solutions, by the generation of an electric field (Calvert, 1990)(**Figure 1**). A discharge electrode is utilised to provide suspended particles with a negative charge. This electrode is often made of stainless-steel and creates a corona discharge via flow of its highly negative current into a neutrally charged space, resulting in ionisation of the surrounding air and any particles within close proximity. In addition, a return electrode, bearing a positive charge, is used to collect the negatively charged particles by electrostatic attraction, thereby precipitating particles out of suspension and onto the collection surface (Shen and Pereira, 1979). Multiple parameters govern the efficiency of particle collection, some of which include voltage, flow rate, geometric design of the electrostatic precipitator, size and concentration of ionised particles, and strength of the electric field (Pardon, 2015). Ohm's law states that an electric potential (V) is dependent on two major dimensions – the charge of the discharge electrode (Q) and the distance between the discharge and return electrodes (r), which is expressed in the following equation: V = kQ/ r, where K is equal to a constant value of 8.99 x 10^9 N 'm^2/C2 (Tenny and Keenaghan, 2021).

Electrostatic precipitation has been manipulated for a variety of commercial benefits. For example, the Tornex Inc. Indoor Air Quality Solution Company sell electronic ventilation air filters that work via EP, to collect dust and aerosolised particles. Tornex Inc. air purifiers are 95% effective at collecting particles as small as 0.3µm, in comparison to conventional mechanical filters that collect particles between 1 - 10µm with only approximately 50% efficiency (Tornex Inc, 2022). Additionally, EP filters do not clog following particle collection and are able to maintain sustainable air exchange, as opposed to mechanical filters that block easily, resulting in pressure losses of up to 50-100Pa, preventing efficient suction and

air purification (Tornex Inc, 2022). EP has also been utilised for aerosol sampling methods in hospitals and point-of-care systems, in order to rapidly diagnose patients and to precisely detect airborne pathogenic spread at a reduced cost. A study by Pardon (2015) showed that aerosol droplets from the exhaled breath of patients could be captured by EP directly onto a microfluidic lab-on-chip device, for immediate detection of bacterial or viral pathogens. This method of diagnosis could prevent the need for lung sampling procedures such as bronchoscopy, which can often be very invasive and uncomfortable for patients. In agreement with this study, Ladhani (2017) demonstrated the use of EP to detect airborne Influenza virus. As Influenza is transmissible by aerosol and remains stable and viable when travelling over large distances, it is important that we are able to detect its presence within hospital wards, care homes and other indoor areas containing individuals prone to infection. Ladhani developed a custom EP bioaerosol sampler that was able to recover undiluted aerosol samples, facilitating downstream biological assays such as qPCR. The study claimed that use of this device could reduce sampling from hours to minutes, thereby preventing viral spread much faster than currently standardised approaches.

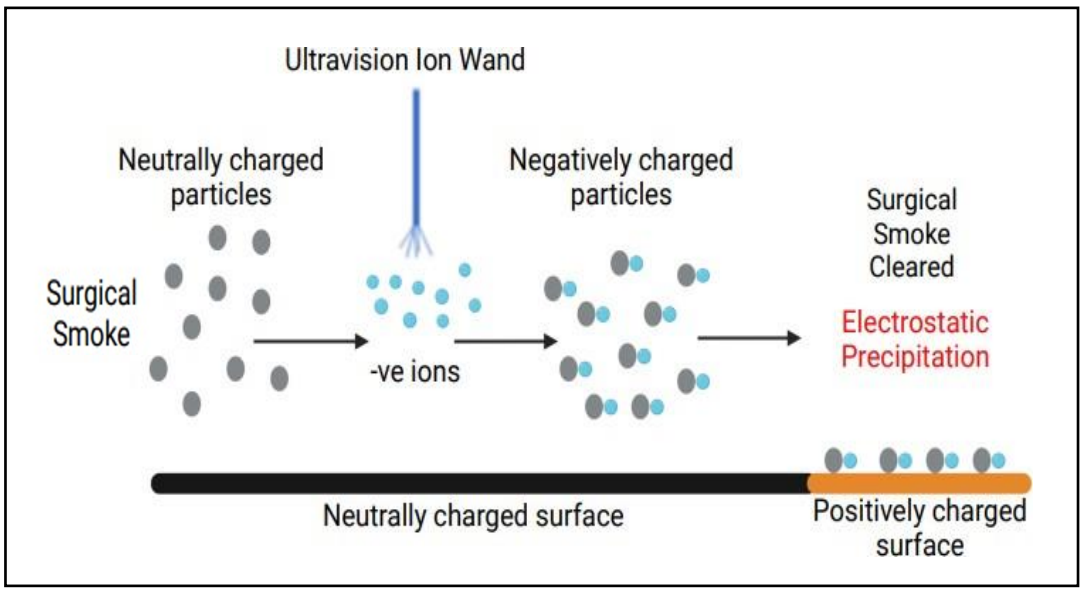

Figure 1.1. Schematic Displaying the Electrostatic Precipitation of Surgical Smoke by Ultravision™. *Surgical smoke is generated as a result of the surgical incision of tissue using electrosurgical instruments. Ultravision™ is used during laparoscopic surgery as an electrostatic precipitator, to clear surgical smoke. The Ultravision™ Ion Wand is charged with a voltage of 8kV and emits negative ions, creating a corona discharge. Particles suspended in aerosol that reach the proximity of the corona discharge become negatively charged. Additionally, a collector-plate is attached to a return electrode carrying a positive charge. Negatively charged particles are precipitated onto the positively charged collector plate via electrostatic attraction, clearing the surgical smoke (Alesi Surgical Ltd. 2022).*

EP is also manipulated during medical procedures, such as laparoscopic surgery, to clear bioaerosols that are released during the surgical incision of tissue with electrosurgical instruments (Ansell, 2014). Surgical smoke that is produced during operations can obscure the surgeon's field of view, thereby causing safety implications. Furthermore, surgical smoke consists of 95% water vapor and 5% cellular debris, which is vented into the operating theatre, therefore placing healthcare staff at risk of bacterial and viral infections (Chuang, 2012). Presently, there is no evidence that SARS-CoV-2 is transmissible via surgical smoke, however close contact with infected patients during surgical procedures can increase the risk of infection. In contrast, previous studies have identified the presence and transmission of other viruses in surgical smoke, for example HIV and HPV (Gloster and Roenigk, 1995. Johnson and Robinson, 1991). In addition, there are >20 common pathogens that spread by airborne transmission, including the Adenovirus, which too can be aerosolised during hospital procedures (Ather, 2022). For example, Adenovirus serotypes 40 and 41 natively infect the gastrointestinal system, resulting in gastroenteritis (Lu, 2008). During laparoscopic surgery, aerosolisation of gastrointestinal tissue has the capacity to release infectious Adenovirus particles into the operating theatre, placing healthcare professionals at risk of disease. Therefore, it is crucial to minimise the release of surgical smoke during closed and open surgeries. Ultravision^{TM} is a commercialised electrostatic precipitation device used to clear bioaerosols during laparoscopy (**Figure 1.1**). A study of 30 patients undergoing laparoscopy found that 94% of surgeries performed without Ultravision^{TM} were paused to allow for smoke clearance, whilst only 23% of procedures using Ultravision^{TM} were paused. In addition, 65% of surgeries performed without Ultravision^{TM} required camera cleaning, compared to a mere 15% of surgeries that used Ultravision^{TM} (Ansell, 2014). As well as this, Ultravision^{TM} is capable of precipitating particles down to 7nm in size, suggesting it may be capable of capturing and potentially inactivating virus particles (Alesi Surgical Ltd, 2022).

A small number of studies have assessed the ability of EP to capture and/or inactivate aerosolised viral and bacterial particles. For example, Kettleson (2009) evaluated the effects of EP on two aerosolised bacteriophages, T3 and MS2. The bacteriophages were aerosolised for 60 seconds and exposed to EP under various operating conditions. The resulting samples were analysed for phage presence and activity via qPCR and plaque assays. The study

identified “log reductions of 6.8 and 6.3 for the plaque assay and 4.2 and 3.5 for the qPCR assay at -10 kV for T3 and MS2, respectively” (Kettleson, 2009). It was therefore suggested that EP successfully inactivated high quantities of aerosolised bacteriophage. However, EP did not physically capture particles to the same extent, as highlighted by inconsistencies between the plaque assay and qPCR results. The paper hypothesised that the corona discharge may have generated reactive species such as O·, N· and OH·, in turn inactivating or degrading the phage and its structural components. Although the bacteriophages were inactivated, they were not collected on the return electrode in their entirety, implying that the EP device used was incapable of capturing intact bacteriophage particles via electrostatic precipitation. Further studies were therefore required to assess whether EP can both capture and inactivate virus particles from bioaerosols. It is also important to assess whether EP has the same effect on enveloped and non-enveloped viruses, which Kettleson (2009) did not address. Gaining a deeper understanding of how EP influences airborne viruses will aid our ability to manipulate devices like Ultravision^{TM} in the future, to prevent the spread and transmission of respiratory pathogens.

With the SARS CoV-2 pandemic continuing to cause global devastation, and the possibility of novel pathogenic outbreaks in the future, it is vital that non-pharmaceutical interventions are developed to reduce airborne pathogen transmission. The implementation of efficient NPI’s could prevent the delay and cancellation of medical procedures, reduce socio-economic pressures of viral outbreaks, enable the safe continuation of surgeries during future pandemics, and ultimately save lives.

1.4. Project Aims & Hypotheses

The overarching aim of this study was to evaluate whether electrostatic precipitation could capture and inactivate viral particles released in bioaerosols. Ultravision^{TM} was utilised as the electrostatic precipitator in all experiments, due to its approved use and safety during surgery. The first aim of this study was to design and construct closed and open model systems, to mimic the release of bioaerosols that occurs in real-life scenarios such as laparoscopic surgery (closed-system), open-surgery (open-system), and within indoor hospital environments (open-system). The second aim of this study was to evaluate whether Ultravision^{TM} could successfully capture and/or inactivate aerosolised enveloped and non-enveloped virus particles. The final aim was to optimise the parameters governing the

efficiency of EP and assess the resulting capture and inactivation of aerosolised virus particles. The purpose of this was to identify ideal conditions for the most efficient use of Ultravision^{TM}. In summary, this study aimed to understand and conclude the safety, efficiency, and feasibility of using Ultravision^{TM} to prevent the transmission of airborne viruses during surgical procedures.

Hypotheses of this study are listed below:

1. Ultravision^{TM} will successfully and significantly capture aerosolised viral particles.
2. Ultravision^{TM} will successfully and significantly inactivate aerosolised viral particles.
3. Ultravision^{TM} will capture and inactivate aerosolised viral particles in both the 'closed' and the 'open' system models.
4. Ultravision^{TM} will successfully capture and inactivate both enveloped and non-enveloped aerosolised viral particles to the same extent.

Chapter 2: Methods and Materials

2.1. Cell Culture

Four cell lines were predominantly used throughout this study - T-REx-293 (Human Embryonic Kidney cells, expressing the Tetracycline (Tet) repressor) and HEK-293 (Human Embryonic Kidney cells), which were sourced from the American Type Culture Collection (ATCC), CHO-CAR (Chinese Hamster Ovarian cells, transfected to express Human CAR), which were gifted from Professor Andrew Baker (University of Edinburgh), and CHO-ACE2-TMPRSS2 (Chinese Hamster Ovarian cells, transfected to express Human ACE2 and TMPRSS2) which were provided by collaborators from the Medway School of Pharmacy. T-REx-293 and HEK-293 cells were cultured in DMEM media (Dulbecco's Modified Eagle's Medium; Sigma-Aldrich, Gillingham, UK #D5796), whilst CHO-CAR and CHO-ACE2-TMPRSS2 cells were cultured in DMEM F12 media (Dulbecco's Modified Eagle's Medium/Nutrient Mixture F-12 Ham; Sigma-Aldrich, Gillingham, UK #D0697), all of which were supplemented with 10% Foetal Bovine Serum (FBS; Gibco, Paisley, UK #10500-064), 2% Penicillin and Streptomycin (Gibco, Paisley, UK #15070-063) and 1% L-Glutamine (stock 200 mM; Gibco, Paisley, UK #25030-024). Additionally, CHO-ACE2 cells were passaged with 2 ug/mL puromycin and 100 ug/mL Hygromycin once a week, to maintain stable expression of ACE2 and TMPRRS2. Cells were incubated in a certified cell culture incubator (HERA Cell, ThermoFisher Scientific) at 5% CO_2 at 37°C.

Cells were sub-cultured to approximately 80% confluency for maintenance. Sub-culturing was performed in a Class II laminar flow hood and all materials and reagents used were sterilised with 70% Industrialised Methylated Spirit (IMS). When passaging cells, media was removed and discarded and the cells were washed with 10ml PBS (Dulbecco's Phosphate Buffered Saline, Sigma-Aldrich, Gillingham, UK #D8537). PBS was then removed and 5ml of 0.05% Trypsin/EDTA (Sigma-Aldrich, Gillingham, UK #T3924) was added, detaching adherent cells from the flask. The cells were incubated with trypsin for approximately 5 minutes at 37° C and monitored visually for cell mobility. Next, 5ml of cell-specific media was added to the flask to neutralise the detached cells. The cells were transferred to a 15ml falcon and centrifuged at 428 RCF for 3 minutes to obtain a cell pellet. The supernatant was

discarded, and the cell pellet was resuspended in 10ml cell-specific media. Finally, 2ml of the resuspended cells were added to a fresh flask, containing 18ml media (1:10 split), and culturing was continued at 37°C.

2.2. Characterisation of the CHO-CAR and CHO-ACE2-TMPRSS2 Cell Lines

Antibody staining and flow cytometry were performed to ensure that the CHO-CAR and CHO-ACE2-TMPRSS2 cells highly expressed the Coxsackie Adenovirus Receptor (CAR) and the human Angiotensin-Converting Enzyme 2 (ACE2).

Cells were grown to approximately 70% confluency, harvested and centrifuged at 373 RCF for 3 minutes. The supernatant was discarded and the cell pellet was resuspended in 5ml of FACS buffer (5% FBS in in 50ml PBS). The average cell count (cells/ml) was measured using an automated CellDrop^{TM} cell counter. Cells were seeded into a 96-well plate, at 2 x 10^4 cells per well, and incubated at 37°C overnight (or until 70% confluent). Once confluent, cell media was discarded and the cells were washed with 200µl of PBS. Trypsin (50µl) was added to the cells and incubated at 37°C for approximately 3 minutes. FACS buffer (150µl) was added to the cells and pipetted up and down, resuspending the cells. The harvested cells were transferred into a V-shaped-bottom 96-well plate and centrifuged at 428 RCF at 4°C for 5 minutes. The supernatant was discarded and 100µl of primary antibody (for ACE2 staining (1:20) – Human ACE2 Antibody, R&D Systems, Minnesota, US, #MAB10826) (for CAR staining (1:500) - Anti-CAR Antibody, Sigma-Aldrich, Gillingham, UK, #05-644) was added to each well. To provide negative controls, a subset of cells were stained with 100µl mouse Immunoglobulin G antibody (1:500) (Normal Mouse IgG, Sigma-Aldrich, Gillingham, UK #NI03) and a subset of cells were left unstained. The cells were then incubated on ice for 1 hour. The cells were centrifuged again, at 428 RCF for 3 minutes, the supernatant was discarded, and the cells were washed twice with 100µl FACs buffer. Next, 100µl of the secondary antibody (ACE2 staining – (1:50) Rabbit anti-Goat IgG (H+L) Secondary Antibody, FITC, Invitrogen, #31509) (CAR staining - (1:100) F(ab')2-Goat anti-Mouse IgG (H+L) Cross-Adsorbed Secondary Antibody, Alexa Fluor 647, Invitrogen, #A21237) was added to each well and incubated on ice for an additional hour. The cells were centrifuged at 428 RCF for 3 minutes, the supernatant discarded, and were washed three times with 100µl FACs buffer. Following this, 200µl of 4% Paraformaldehyde was added to each well and refrigerated for 10 minutes to allow fixing. Finally, an additional 100µl of FACs buffer was added to each well.

The cells were centrifuged at 428 RCF for 3 minutes, the supernatant was discarded and the cells were washed three times with FACs buffer. All supernatant was removed and 100µl of PBS was added to resuspend the cells. The plate was then covered in foil and stored at 4° C, in preparation for flow cytometry.

Prior to use, the Accuri (BD Accuri C6 v.1.0.264.21) was flushed with sterile H_20 for 2 minutes on a 'FAST' speed setting. Cells were resuspended by pipetting up and down. The unstained controls were run first, for 2 minutes on a 'SLOW/MEDIUM' speed setting and the threshold was set to a limit of 10,000 events. Areas of high cell density were gated, removing areas of debris and 'random scatter'. The IgG controls and the stained samples were run for 2 minutes on a 'FAST' speed and the threshold was limited to 5,000 events. The FL4-A channel was chosen to gate all single-cell events, due to its compatibility with the AlexaFluor 647 antibody stain. Once all data was collected, the full programme version of FlowJo™v10 software was used to analyse the data.

2.3. Virus Purification using Caesium Chloride (CsCl) Gradients

CsCl virus purification was used to obtain stocks of Ad5.GFP. T-REx 293 cells were seeded into 10 T150 flasks (Corning® CellBIND® Surface cell culture flasks, Sigma-Aldrich, Gillingham, UK #CLS3292) and grown to 80% confluency. Purified Ad5.GFP was added to the cells at 10vp/cell. Cells were monitored daily until there was a noticeable change in the cell monolayer, indicating active cytopathic effect (CPE). The cells were harvested, transferred into a sterile falcon, and centrifuged at 428 RCF for 3 minutes. All supernatant was discarded and the resulting infected cell pellet was stored at -80°C.

The infected cell pellet was thawed in a water bath and centrifuged at 428 RCF for 3 minutes. The supernatant was discarded and the pellet was resuspended in 6ml PBS. Next, 6ml of tetrachloroethylene was added, causing cell lysis, and mixed vigorously for 30 seconds. The virus was then centrifuged at 59,522 RCF for 20 minutes, separating the mixture into layers of different densities. The top layer (containing virus) was removed and transferred to a 15ml falcon. An ultracentrifuge tube was acquired and 2.5ml of room temperature 1.40g/ml CsCl was added. Following this, 2.5ml of 1.25g/ml CsCl was carefully added on top, preventing mixing of the two layers. The virus was added above the two CsCl layers. Ultracentrifuge tubes were weighed and equally balanced by adding PBS, prior to spinning.

The tubes were centrifuged at 155,860 RCF for 1.5 hours at 18°C. The virus band was extracted (1ml) using a 21-gauge needle that penetrated the ultracentrifuge tube and was transferred into a sterile 15ml falcon. A second ultracentrifuge tube was acquired and 5ml of 1.34g/ml CsCl was added. The extracted virus band was transferred onto the CsCl layer and was centrifuged again at 155,860 RCF for 18 hours at 18°C. 5L of dialysis buffer was prepared (50ml 1M Tris-HCl, 39.5g NaCl, 1.02g $MgCl_2$ $(H_2O)_6$, 500ml glycerol and distilled H_20). The virus band was extracted as performed above and transferred to a sterile 15ml falcon. Slide- A-Lyzer dialysis cassettes (ThermoFisher Scientific, UK, Slide-A-Lyzer™ Dialysis Cassettes) were placed in dialysis buffer, wetting the membrane, prior to inserting the extracted virus. Once inserted, the cassette was left to dialyse in 500ml of dialysis buffer, and was continuously stirred by a magnetic stirring bar, at 4°C for approximately 7 hours. The cassette was transferred into 500ml of fresh dialysis buffer and left to stir overnight. Finally, the purified virus was extracted from the cassette, aliquoted into autoclaved eppendorfs and stored at -80°C.

A 15ml stock of purified SARS PV was obtained from collaborators at the Medway School of Pharmacy. The vectors were produced by co-transfecting HEK-293 cells with genome and packaging plasmids using Polyplus (PEIpro®). The SARS PV stocks were then purified via anion exchange chromatography and tangential flow filtration (Du, et al. 2022). Collaborators determined the physical and functional titers of the stock via a P24 immunoassay and a transduction assay in HEK-293 cells, respectively (Du, et al. 2022).

2.4. Virus Titer Determination by MicroBCA Assay

The physical titer of the Ad5.GFP stock was determined using a MicroBCA protein assay kit (Pierce Biotechnology, ThermoFisher Scientific, UK, #23235). A set of bovine serum albumin (BSA) standards were prepared at 0.5, 1.0, 2.5, 5, 10, 20, 40 and 200µg/ml, as per the manufacturer's instructions. Firstly, 150µl of each standard was added to a flat-bottomed 96-well plate in duplicate. Next, 1µl, 3µl and 5µl of purified Ad5.GFP was added to the 96-well plate in triplicate and made up to a total volume of 150µl with PBS. BCA working reagent was prepared by mixing microBCA reagents A, B and C, in a ratio of 25:24:1. Finally, 150µl of the working reagent was added to each well, and the plate was incubated for 2 hours at 37°C. A microplate reader (BioTek Cytation Multimode Reader, Agilent, US) was used to measure the absorbance of each well at λ570nm. The data obtained was analysed and compared

against the BSA standards using excel software. Protein concentrations were converted to virus particles/ml using the following formula: 1µg protein = 4 x 10^9vp.

To provide a sufficient amount of virus to use experimentally throughout this study, two stocks of Ad5.GFP were produced, and are therefore referred to as 'V1' and 'V2'. **Figure 2.1** displays the raw absorbance values measured from the BSA standard dilutions and the Ad5.GFP samples. Absorbance values taken from the BSA standards were used to produce a standard curve (**Figure 2.2**). The standard curve enabled total protein quantification of the purified Ad5.GFP stocks. The calculated physical titer for each virus stock is displayed in **Table 2.1.**

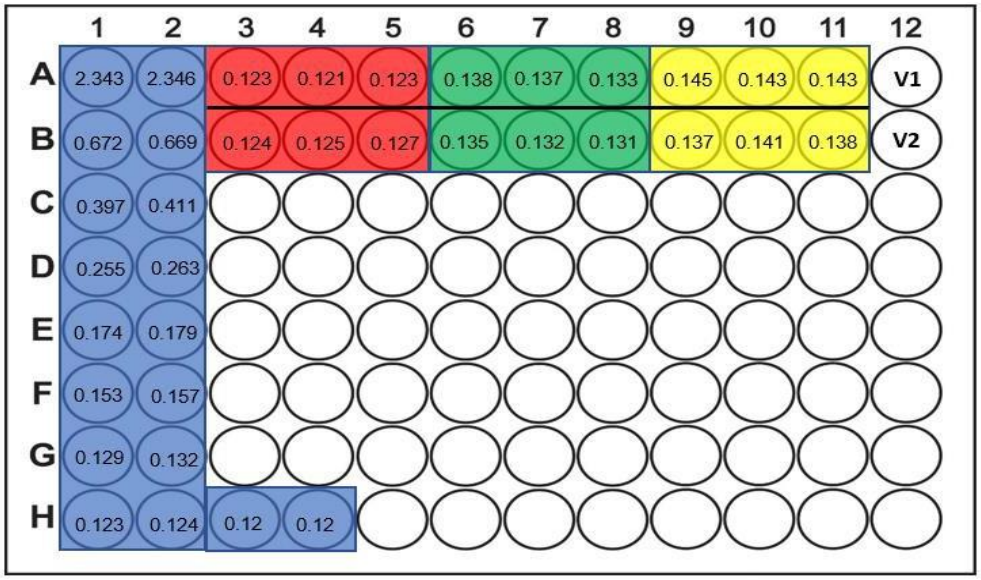

Figure 2.1. A Schematic 96-well Plate, Highlighting Absorbance Values Measured via a MicroBCA Assay in Wells Containing BSA Standard Dilutions and Dilutions of Ad5.GFP*. BSA standard dilutions (blue) were plated in duplicate (columns 1 and 2) and descend from row A-H with decreasing concentration as follows: 200, 40, 20, 10, 5, 2.5, 1.0, 0.5µg/ml, blank PBS. Virus dilutions at 1:150 (red), 1:50 (green) and 1:30 (yellow) were plated in triplicate. Row A and B highlight the absorbance values from Ad5.GFP V1 and V2 stocks respectively. Mean absorbance values were compared to the standard curve and used to determine virus titer.*

A

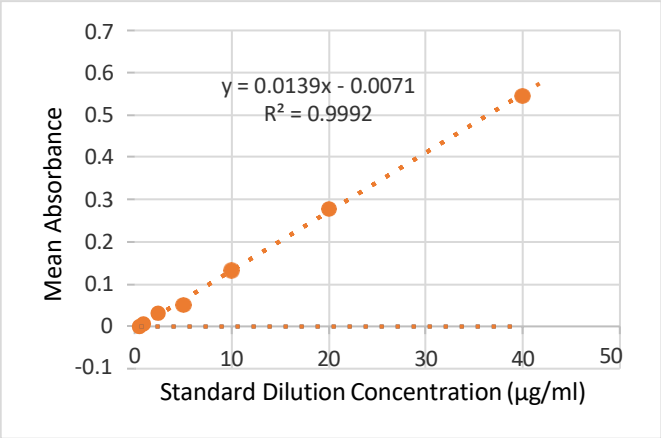

B

Sample ID/Virus		Ad5.GFP	Ad5.GFP
1µl	Rep 1	0.077	0.078
	Rep 2	0.075	0.079
	Rep 3	0.077	0.081
	Mean	0.076	0.079
	X-value	7.51	7.81
	Dilution (x150)	1126.238	1170.792
	Virus correction	**4.50495E+12**	**4.68317E+12**
	Std. Dev. (P)	0.0009	0.001
3µl	Rep 1	0.095	0.089
	Rep 2	0.091	0.086
	Rep 3	0.087	0.085
	Mean	**0.091**	**0.086**
	X-value	8.98	8.531
	Dilution (x50)	449.01	426.568
	Virus correction	**1.79604E+12**	**1.70627E+12**
	Std. Dev. (P)	0.004	0.002
5µl	Rep 1	0.099	0.091
	Rep 2	0.097	0.095
	Rep 3	0.097	0.092
	Mean	**0.097**	**0.092**
	X-value	9.62	9.125
	Dilution (x30)	288.614	273.762
	Virus correction	**1.15446E+12**	**1.09505E+12**
	Std. Dev. (P)	0.001	0.002

	3ul (1:50 dilution)	Ad5.GFP	Ad5.GFP
	Final titre (VP/ml)	1.80E+12	1.71E+12

Figure 2.2. Raw Data and Calculations used to Determine Physical Virus Titers by MicroBCA. A) *The standard curve produced from the MicroBCA assay, created using absorbance values measured from the BSA standard dilutions. The curve was used as a reference point to quantify physical virus titers.* ***B)*** *Protein quantities detected from 1, 3 and 5µl of Ad5.GFP stocks. Calculations used to determine the physical titers of the virus stocks are displayed.*

Table 2.1. Physical Titers of Virus Stocks Calculated by MicroBCA

Virus Sample	Physical Titer (Virus Particles/ml)
Ad5.GFP (V1)	1.80×10^{12}vp/ml
Ad5.GFP (V2)	1.71×10^{12}vp/ml

2.5. Virus Titer Determination by Plaque Assay

To determine the infectious titer of Ad5.GFP and SARS PV stocks, plaque assays were performed. T-REx 293 and HEK-293 cells were seeded into a flat-bottomed 12-well plate, at 1×10^5 cells per well and were left to incubate at 37°C overnight. The following serial dilutions of Ad5.GFP were prepared: 1×10^{-2}, 1×10^{-4} and 1×10^{-5}, however, SARS PV was added to the cells undiluted. Next, 1ml of each virus dilution was added to their respective cell lines in duplicate. Two wells of each cell line remained uninfected, and were supplemented with fresh media, serving as negative controls. The plates were incubated at 37°C for a further 48 hours. The cells were analysed using EVOS imaging (EVOS M7000, Invitrogen,

ThermoFisher Scientific, #AMF7000) enabling manual counting of the number of GFP-fluorescing (infected) cells per well. The plaque-forming units per ml (Pfu/ml) was calculated using the following equation:

Objective Lens	Fields/Well (12-well plate)
4 X	19
5 X	30
10 X	150
20 X	594

$$\left(\frac{(\text{Average number of plaques per well}) \times (\text{Fields per well})}{(\text{Volume of virus in } \mu\text{l}) \times (\text{dilution factor})} \right) \times 1000$$

The pfu/ml is representative of the number of infectious particles within a sample, thereby differing from the physical titer. Both vectors expressed GFP, therefore infected cells were easily identified using fluorescent EVOS imaging. Objective lenses at both x10 and x20 were used to compensate for fields containing immeasurable plaques, facilitating manual counting. **Figure 2.3** displays images gathered from both the Ad5.GFP and the SARS PV plaque assays. The negative controls displayed no green fluorescence, as expected. CPE and cell death was observed in all infected cells. Wells infected with higher concentrations of virus displayed a higher percentage of fluorescent cells. The number of fluorescent cells that were counted in each field of view were used to determine the pfu/ml values of each virus stock. The functional titers of each virus stock are displayed in **Table 2.2.**

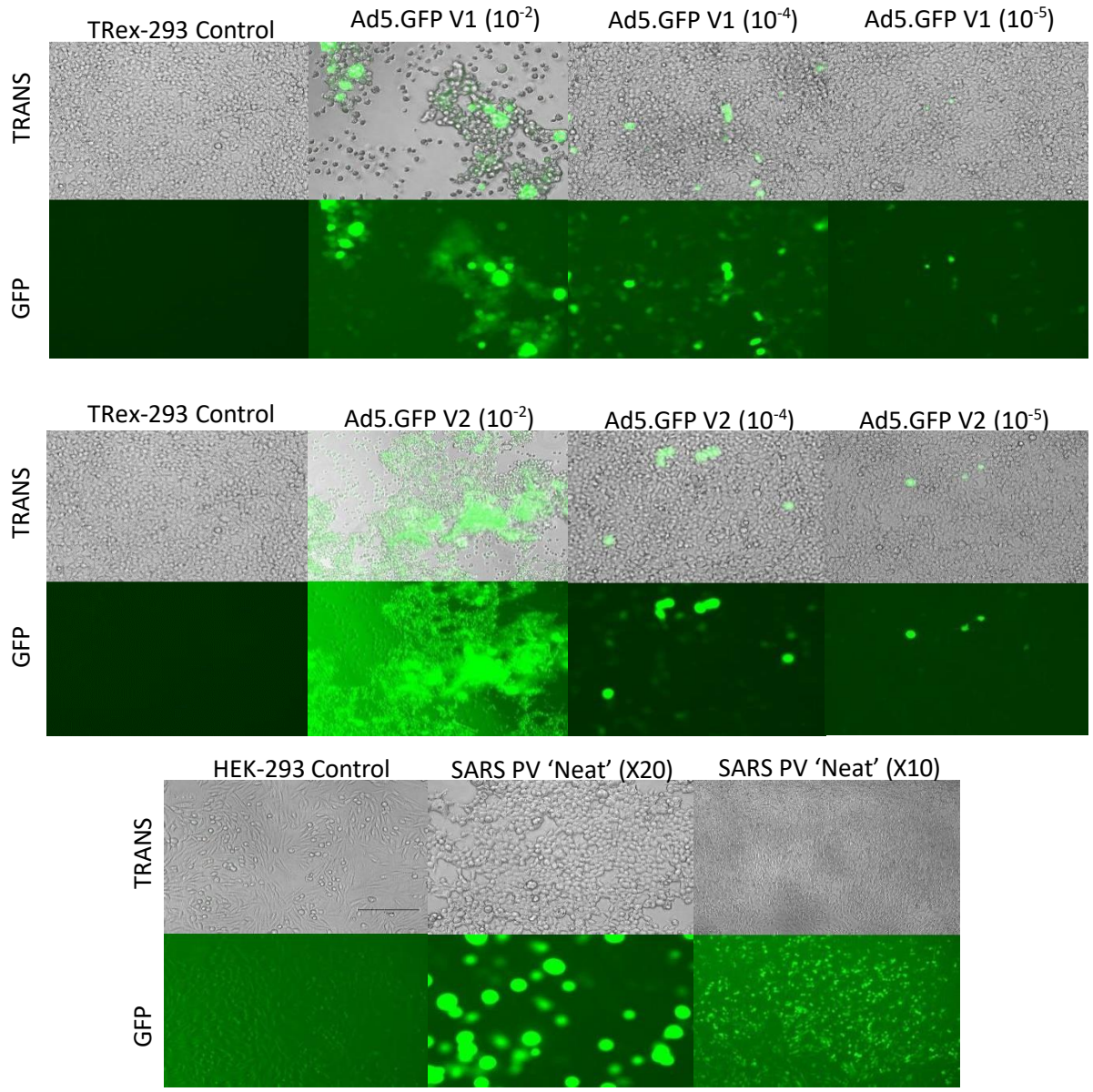

Figure 2.3. EVOS M7000 Imaging of Cells Infected with Purified Stocks of Ad5.GFP and SARS PV*. Top panels (TRANS) were imaged using transmitted light (brightfield). Bottoms panels (GFP) were imaged using the GFP light source. TRex-293 cells were imaged at objective x20 only, whereas HEK-293 cells were imaged at objective x10 and x20. No fluorescence was detected in the negative controls (uninfected cells). As the dilution of Ad5.GFP increased, the percentage of fluorescent CHO-CAR cells decreased, as expected. HEK-293 cells were infected with 'neat' SARS PV, due to the stock baring a lower physical titer. Manual counting of fluorescent cells enabled the determination of pfu/ml values for each virus stock.*

Table 2.2. Functional Titers (pfu/ml) of Virus Stocks Calculated by Plaque Assay

Virus Sample	Titer (pfu/ml)
Ad5.GFP (V1)	3.74×10^8pfu/ml
Ad5.GFP (V2)	2.55×10^8pfu/ml
SARS PV	3.3×10^7pfu/ml

Additionally, plaque assays were performed in chapters 4, 5 and 6, to determine the functional titers of the collected virus samples that had been exposed to Ultravision^{TM}. Such plaque assays were performed as outlined above, however the collected samples were added to the seeded cells neat (undiluted), as well as diluted, as the viral contents of each sample was unknown.

2.6. NanoSight Nanoparticle Analysis of Purified Virus Stocks

A NanoSight NS300 was used to analyse particle size, purity, and the concentration of each virus stock. The NanoSight is equipped with high-resolution nanoparticle tracking and fast video capture software. The size of a particle determines how fast it diffuses through a solution due to 'Brownian motion'. The NanoSight analysed the Brownian motion of the virus particles, as well as the resulting scatter of light, to deduce physical titers of each stock. The NanoSight was assembled as per the manufacturer's instructions, and 1ml of sterile PBS was slowly infused through the cell for 60 seconds, as a negative control. The cell was cleaned prior to each sample infusion. Virus stocks were diluted to 1:1000 and 1:500 using PBS and infused through the cell for 60 seconds. Particle size and concentration were measured in comparison to the negative PBS control. **Figure 2.4** displays the measurements obtained from the NanoSight. As expected, both Ad5.GFP stocks contained particles with a mean size of 95.7-95.7nm. This data was consistent with the fact that Ad5 particles are approximately 90-100nm in diameter. The mean size of particles in the SARS PV stock was 138nm and once again, this was consistent with the fact that HIV viruses are approximately 100-200nm in diameter. Additionally, the NanoSight determined the concentration of each virus stock, as displayed in **Table 2.3.**

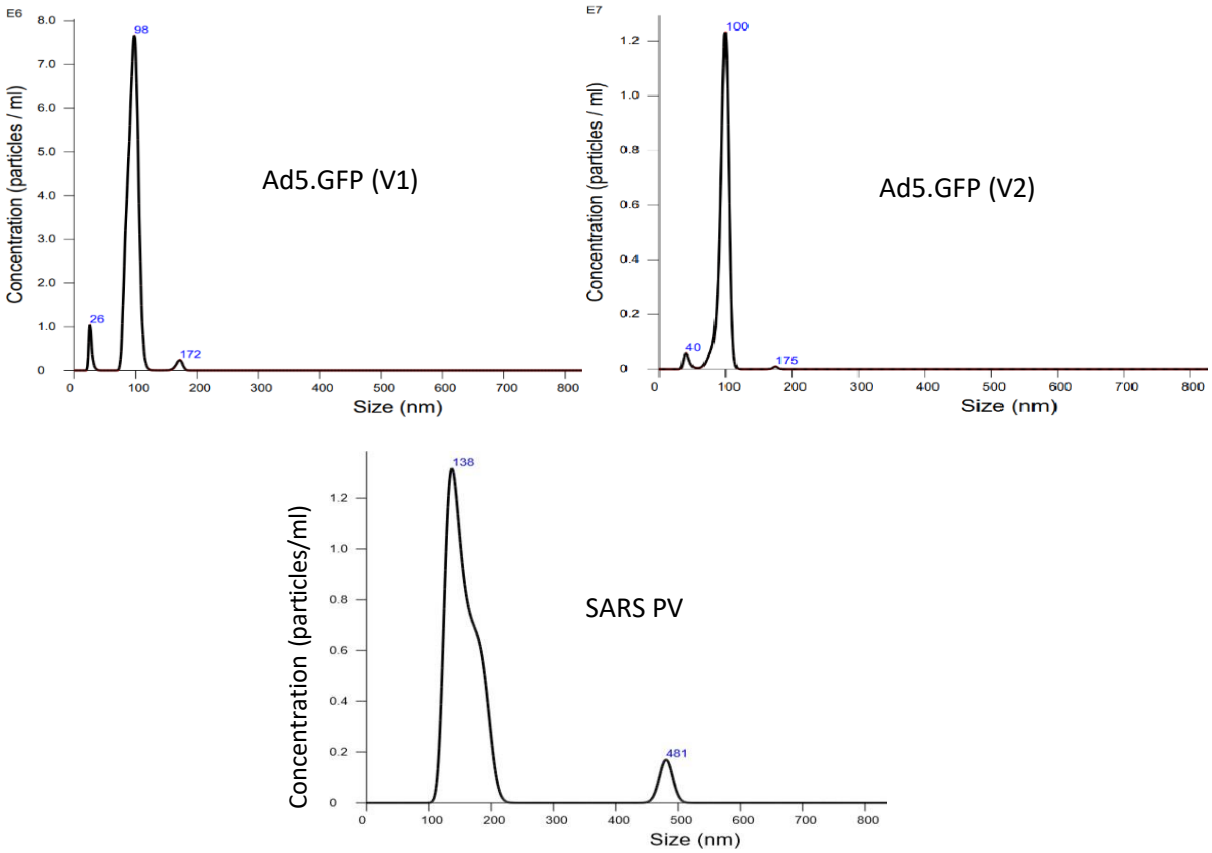

Figure 2.4. NanoSight NS300 Analysis of Purified Ad5.GFP and SARS PV Stocks*. Ad5.GFP samples were diluted by 1:1000, whilst SARS PV samples were diluted by 1:500. All samples were infused through the NanoSight cell for 60 seconds. The mean particle size for Ad5.GFP (V1) was 95.8nm. The mean particle size for Ad5.GFP (V2) was 95.7nm. The mean particle size for SARS PV was 138nm. The particle concentration estimated by the NanoSight was multiplied by the dilution factor (x1000 or x500), achieving particles/ml.*

Table 2.3. Physical Titers of Virus Stocks Calculated by NanoSight Analysis

Virus Sample	Concentration (particles/ml)
Ad5.GFP (V1)	1.66 x10^{11} particles/ml
Ad5.GFP (V2)	1.97 x 10^{11} particles/ml
SARS PV	3.7 x 10^{11} particles/ml

2.7. Western Blotting to Detect Ad5-Specific Proteins in Purified Stocks of Ad5.GFP

Western blotting was performed to validate the production of purified Ad5.GFP. Ad5.GFP was diluted (1:4 and 1:10) using RIPA buffer (RIPA Lysis Buffer 10X, Sigma, Gillingham, UK #20-188) and made up to a total volume of 20µl. Next, 5µl of LDS loading dye (NuPAGE™ LDS Sample Buffer (4X), Invitrogen™, ThermoFisher Scientific, #NP0007) and 1µl of DTT (50mM) (1,4-Dithiothreitol, Sigma-Aldrich, #3483-12-3) was added to each diluted sample, to denature and reduce the viral proteins. The samples were boiled at 70°C for 10 minutes, denaturing the proteins. MOPS running buffer (NuPAGE™ MOPS SDS Running Buffer 20X, Invitrogen, ThermoFisher Scientific, #NP0001) was prepared by adding 50ml MOPS buffer to 950ml double-distilled H_20. The gel (NuPAGE™ 4 to 12%, Bis-Tris, 1.0 mm, Mini Protein Gel, Invitrogen™, ThermoFisher Scientific, #NP0321BOX) was also washed with MOPS buffer and inserted into the gel tank (XCell SureLock™ Mini-Cell, Invitrogen™, ThermoFisher Scientific, #EI0001). The gel tank was filled with approximately 200ml of MOPS running buffer and 500µl of antioxidant (NuPAGE Antioxidant, Invitrogen, ThermoFisher Scientific, #NP0005). 10µl of the Magic Mark ladder (MagicMark™ XP Western Protein Standard, Invitrogen, ThermoFisher Scientific, #LC5602) and 20µl of each protein sample was loaded into the gel and run at 150V for approximately 1 hour. To prepare for blotting, the PVDF transfer membrane was soaked in methanol for 10 minutes. Transfer buffer was prepared by adding 50ml NuPage transfer buffer (NuPAGE™ Transfer Buffer (20X), Invitrogen™, ThermoFisher Scientific, #NP0006) to 50ml methanol and 400ml double-distilled H_20. Both the blotting membrane and the filter paper were then soaked in transfer buffer, until the membrane was no longer shiny. Once the gel had finished running, the gel was rinsed in transfer buffer and the blotting stack was assembled as follows: (bottom anode) sponge pad, filter paper, gel, membrane, filter paper, sponge pad (top cathode). A mini roller was used to remove air bubbles from the stack and additional transfer buffer was poured over the stack to prevent drying. The stack was placed back in the gel tank, filled to the top with transfer buffer and run at 20V for 1 hour. PBST was prepared by adding 1L of PBS to 1ml of Tween (Tween™ 20, Fisher BioReagents™ BP337-500, #10113103). To prepare the blocking buffer (5%), 50ml PBST was used to dissolve 2.5g of milk powder. Following transfer, the membrane was submerged in blocking buffer and left on a rocker at room temperature for 1 hour. The primary antibody (Anti-Adenovirus type 1 hexon E11 Mouse Monoclonal Antibody [clone: 1-

M-13], Abcam, VWR, #ABCAAB2596-100) was diluted to 1:1000 using 1% blocking buffer as a diluent. The membrane was submerged in the primary antibody dilution and left on a rocker at room temperature for an hour. Following this, the membrane was washed 3 times in PBST for 15 minutes. The secondary antibody (Peroxidase-conjugated Goat Anti-Mouse IgG (H+L), Jackson ImmunoResearch, #115-035-003) was diluted to 1:5000. The membrane was submerged in the secondary antibody dilution and placed on a rocker at room temperature overnight. The membrane was washed 3 times in PBST for 15 minutes. ECL detection reagent (Pierce™ ECL Western Blotting Substrate, ThermoFisher Scientific, #32106) was prepared by adding 1ml of reagent 1 to 1ml of reagent 2 and was used to soak the membrane for 5 minutes. The gel was placed in a Gel-Doc and imaged using GeneSys software.

2.8. DNA Extraction and qPCR Optimisation

Viral DNA was extracted from the purified virus stocks using a QIAamp MinElute Virus Kit (Qiagen, #57704). All reagents used during DNA extraction were prepared as per the manufacturer's instructions. In a 1.5ml sterile eppendorf, 200µl of purified virus stock was added to 25µl Qiagen protease, 220µl Buffer AL and 6.2µl cRNA (28 µg/ml). The eppendorf was vortexed for 15 seconds, ensuring efficient mixing and lysis and then incubated at 56°C for 15 minutes. 250µl of 90% ethanol was then added to the sample. The eppendorf was vortexed for 15 seconds and left to incubate at room temperature for 5 minutes. The solution was centrifuged for 1 minute and the lysate was carefully added to the QIAamp MinElute column. The eppendorf was centrifuged at 716 RCF for 1 minute and the column was placed into a fresh collection tube. To denature proteins within the sample, enabling biomolecules to pass through the filter, 500µl of buffer AW1 was added to the column and centrifuged at 716 RCF for 1 minute. The column was then placed into a new collection tube and 500µl buffer AW2 was added to remove salts. The column was centrifuged again at 716 RCF for 1 minute and then placed into a fresh collection tube. Next, 500µl of 90% ethanol was added to the column and centrifuged at 716 RCF for 1 minute. The column was placed into a fresh collection tube and centrifuged at 2,191 RCF for 3 minutes, drying the membrane. The collection tube was replaced, and the column was incubated at 56°C for 3 minutes, to ensure drying. The collection tube was replaced with a 1.5ml eppendorf and 50µl of ultra-pure water (UltraPure™ DNase/RNase-Free Distilled Water, Invitrogen™,

ThermoFisher Scientific, #11538646) was added to the centre of the membrane, eluting the DNA. This was incubated at room temperature for 1 minute and then centrifuged at 2,191 RCF for 1 minute. The column was discarded and the eppendorf containing the DNA was stored at -20°C. The purity and concentration of extracted DNA was measured using a NanoDrop™ 1000 Spectrophotometer.

Viral DNA, mastermix and primers were kept on ice during qPCR preparation. Viral DNA was diluted to 200ng/µl, using ultra-pure water as a diluent. RNAse and DNAse free eppendorfs were used to prevent contamination. Serial dilutions (1:10) of viral DNA were made as follows: undiluted (200ng/µl), 10^{-1}, 10^{-2}, 10^{-3}, 10^{-4}, 10^{-5} and 10^{-6}. The primers used (Ad5 Forward: CCTGCTTACCCCCAACGAGTTTGA, Ad5 Reverse: GGAGTACATGCGGTCCTTGTAGCTC, P24 Capsid Forward: GGCTTTCAGCCCAGAAGTGATACC, P24 Capsid Reverse: GGGTCCTCCTACTCCCTGACATG) were diluted to 10Mm. The SYBR Green Mastermix (PowerUp™ SYBR™ Green Master Mix, Applied Biosystems™, ThermoFisher Scientific, #A25741) was prepared according to manufacturer's recommendations. Firstly, 15µl of the mastermix was added to each well of the qPCR plate, followed by 5µl of the viral DNA. The plate was sealed and centrifuged to remove bubbles. QuantStudio™ software was used to set the thermal cycling conditions (**Figure 2.5**). The plate was loaded into the qPCR machine (Pharmaceutical Analytics QuantStudio™ 5 Real-Time PCR System, AppliedBiosystems™, ThermoFisher Scientific, #A31670) and run.

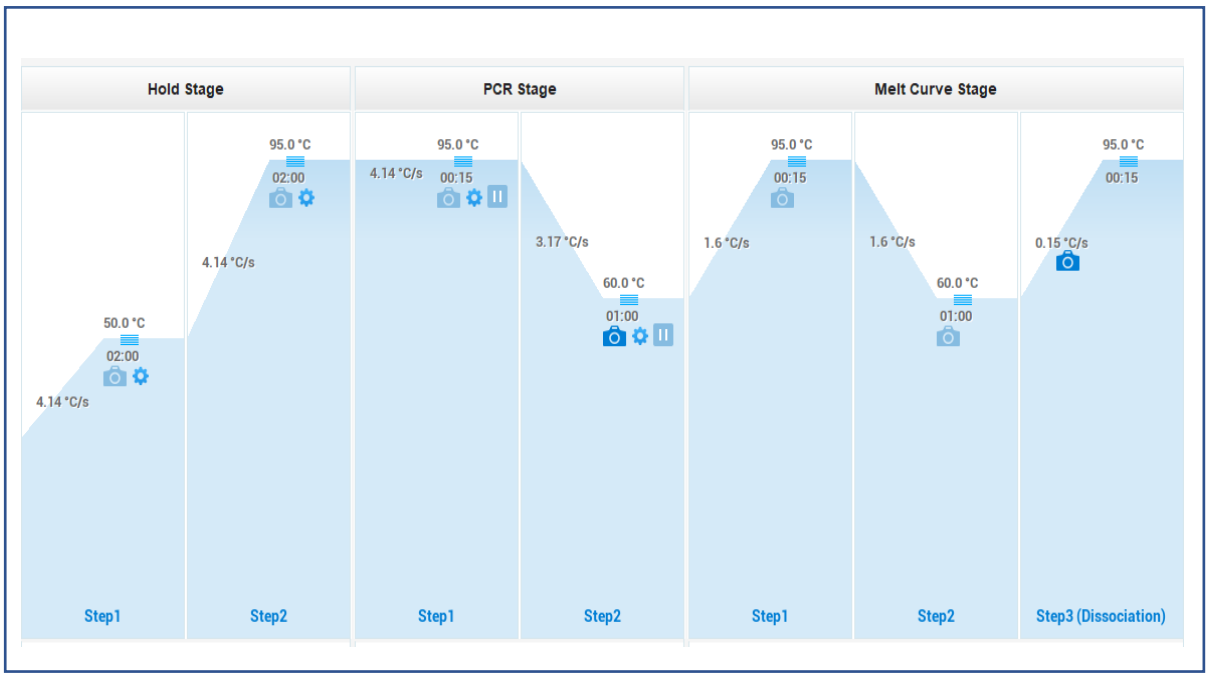

Figure 2.5. Thermal Cycling Conditions for qPCR of Viral DNA*. Conditions designed using QuantStudio™ and AppliedBiosystems PowerUp™ SYBR Green protocol guidelines.*

qPCRs were performed to amplify serial dilutions of Ad5.GFP and SARS PV DNA, to generate standard curves and optimise experimental efficiency. Primers spanning the Ad5 L3 Hexon sequence and the P24 capsid sequence (conserved across lentiviruses) were used to amplify Ad5-specific and Lentiviral-specific DNA respectively. **Figure 2.6** displays the amplification plots acquired. The amplification threshold is the level of fluorescent signal emitted from samples undergoing amplification, which significantly differs to that of the baseline signal. All fluorescent signals below the threshold represent the baseline and are thereby regarded as 'background noise'. Fluorescent signals above the threshold are statistically significant and reflect DNA template amplification. The Ct values represent the number of replication cycles at which the template produced a significant fluorescent signal, thereby crossing the threshold. Ct values can be used to calculate the DNA concentration of an 'unknown' DNA sample, as Ct values are inversely proportional to the concentration of DNA. The standard dilutions of each virus stock and their respective Ct values were used to establish standard curves (**Figure 2.7**). Evaluation of the standard curves was performed to analyse and optimise qPCR efficiency. Additionally, the standard curves were used in subsequent experiments to calculate concentrations of viral DNA from 'unknown' samples, that had been collected following virus sample aerosolisation and exposure to Ultravision™.

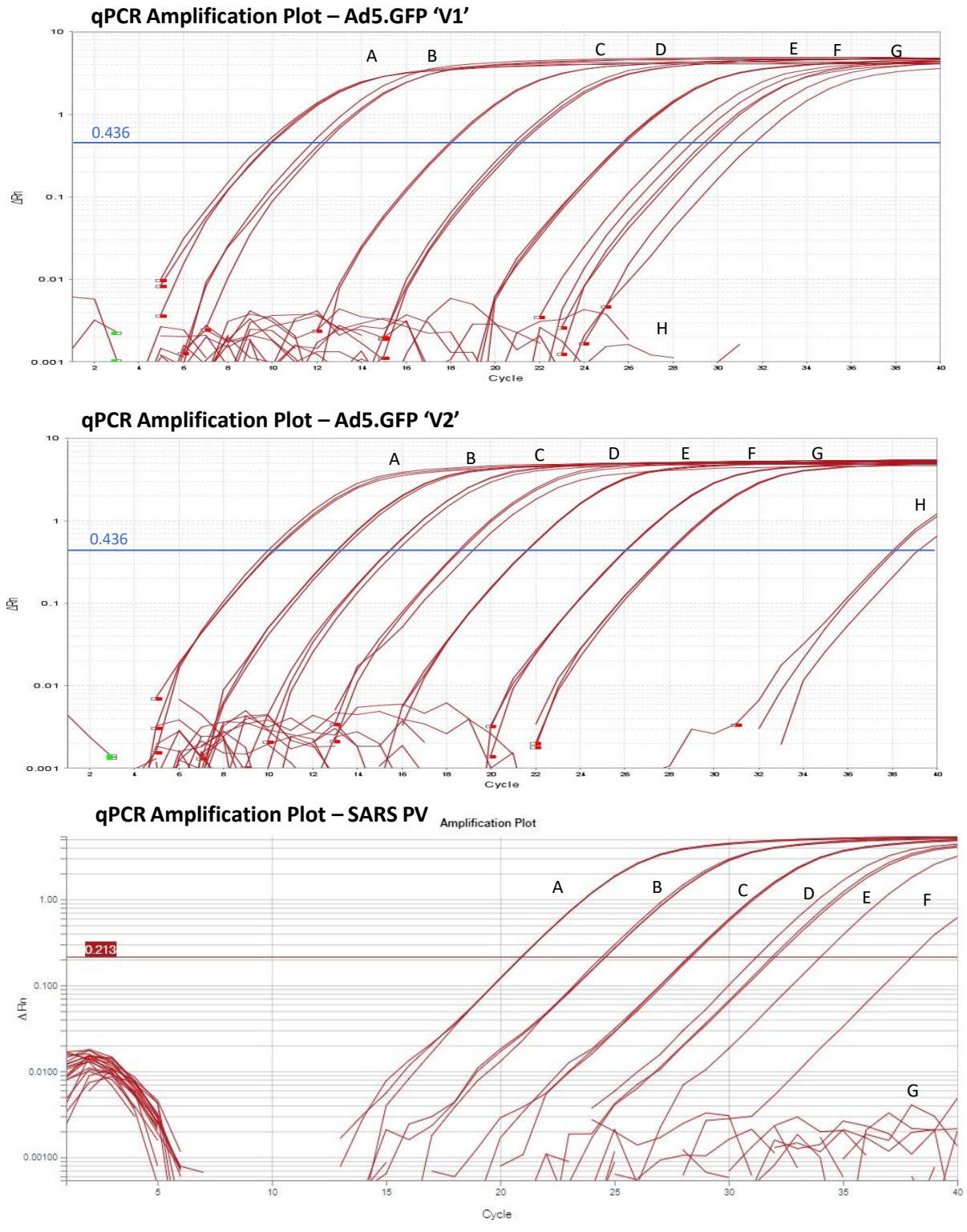

Figure 2.6. Amplification Plots Measured from qPCR of Serial Dilutions of Ad5.GFP and SARS PV*. ⊿Rn (change in fluorescent signal) on the Y-axis is measured against PCR cycle number on the x-axis. Straight blue/red line represents the threshold value – 0.436/0.213. Signals below the threshold are regarded as 'background noise'. Signals above the threshold represent statistically significant and relevant DNA template amplification. Higher DNA template concentrations show significant amplification at lower cycle numbers (Ct). A: Undiluted, B: 10^{-1}, C: 10^{-2}, D: 10^{-3}, E: 10^{-4}, F: 10^{-5}, G: 10^{-6}, H: NTC.*

Standard Curve – Ad5.GFP ‘V1’

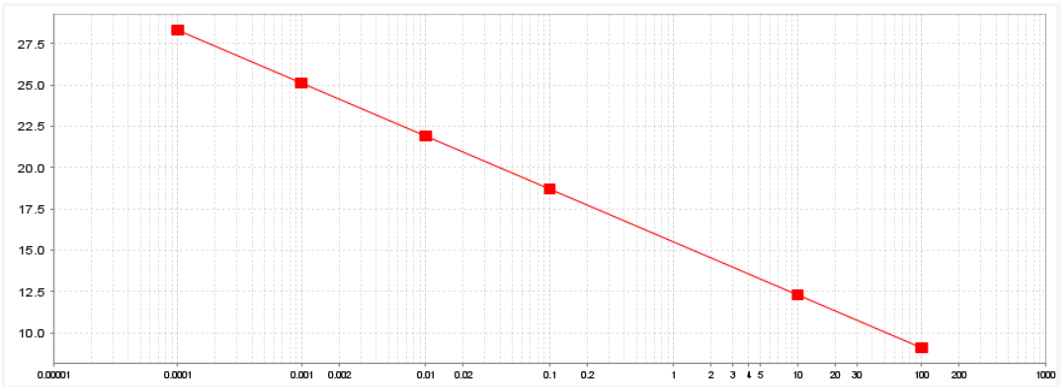

Reporter	Target	Slope	Y-Intercept	R^2	Efficiency(%)
SYBR	Target 1	-3.209	15.504	0.990	104.938

Standard Curve – Ad5.GFP ‘V2’

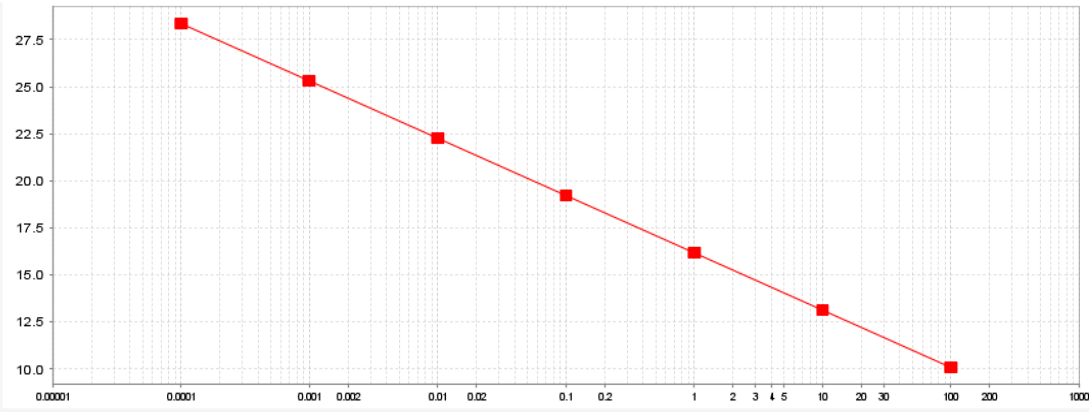

Reporter	Target	Slope	Y-Intercept	R^2	Efficiency(%)
SYBR	Target 1	-3.050	16.176	0.994	112.739

Standard Curve – SARS PV

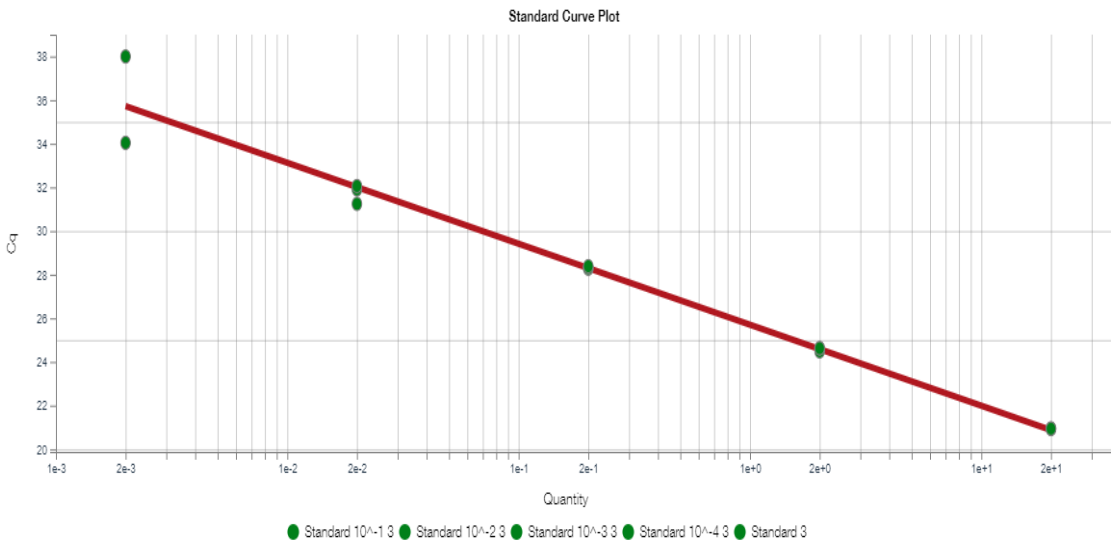

Target: Target 1 Slop: -3.712 R^2: 0.976 Y-Inter: 25.706 Eff%: 85.953 Error: 0.167

Figure 2.7. Standard Curves Produced from qPCR Amplification of Ad5.GFP and SARS PV Serial Dilutions. *Ct values are measured on the y-axis against log DNA dilutions on the x-axis. Slope, Y-intercept, R^2 and efficiency (%) values are stated below each standard curve. The Ct value from sample 'Ad5.GFP 'V1' diluted by 10^{-2}' was not included in the standard curve, as the value lied significantly outside of the trend line and was thereby regarded as an 'experimental error'. The Ct values from SARS PV samples '10^{-5} and 10^{-6}' were not included in the standard curve, as the DNA concentrations were too low and therefore could not be detected. The concentrations chosen to produce the standard curves encompassed the 'expected' concentrations of the 'unknown' experimental DNA samples (samples post-Ultravision™ exposure).*

Figure 2.7 displays the Y-intercept, slope, R^2 and efficiency (%) values for each standard curve. A slope of the log-linear phase of amplification can measure qPCR efficiency. A slope of -3.32 is equivalent to 100% efficiency, therefore values between -3.58 and -3.10 correspond to approximately 90-110% efficiency. The slopes measured from the standard curves in **figure 2.7** indicate fairly high reaction efficiency. Ideally, the efficiency of each standard curve should be 100%, in the case of perfect exponential amplification. However, the efficiency of each standard curve in **figure 2.7** varies between a range of 85% - 115%. Factors such as DNA length, GC content, enzyme quality and use of reagents containing PCR inhibitors can affect qPCR efficiency. The Y-intercept corresponds to the limit of detection of the reaction (Ct value), and providing these values remain the same in consequent qPCRs amplifying the same template DNA, the data obtained should be reliable. Finally, the correlation coefficient (R^2) reflects how well the data fits the regression line, thereby is a measure of linearity. An R^2 of 0.90-0.99 is ideal. The R^2 values in **figure 2.7** all display ideal linearity.

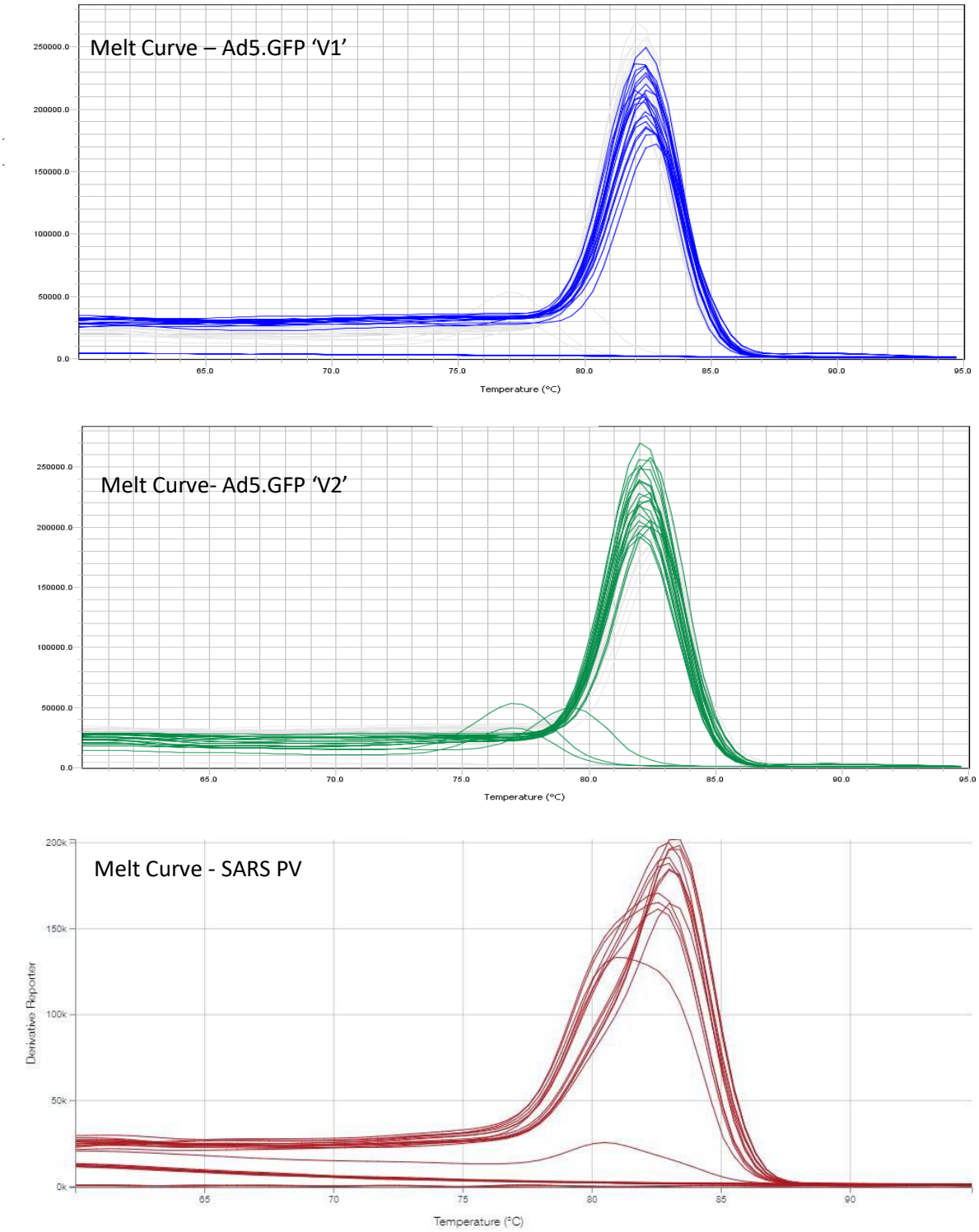

Figure 2.8. Melt Curves Produced Following qPCR Amplification of Ad5.GFP and SARS PV DNA. *-ΔF/ΔT (change in fluorescence/change in temperature) is plotted on the Y-axis against temperature plotted on the X-axis. Peaks represent dissociation of double stranded DNA at specific temperatures, resembling the Tm of the DNA sequence amplified. Singular peaks represent reaction specificity.*

To determine reaction specificity, melt curves were produced (**Figure 2.8**). As temperature increases during qPCR, double-stranded DNA dissociates into single-stranded DNA. This dissociation of DNA is displayed as a 'peak' in the melt curve. The temperature at which this occurs is termed the 'melting point' (Tm). When SYBR green dye is bound to double-stranded DNA, fluorescence is detected. However, when the DNA reaches its Tm and dissociates, the dye is released, causing a sudden drop in fluorescence. This drop in fluorescence following increased temperature (-ΔF/ΔT) creates a melt curve. Singular 'peaks' were generated in each melt curve (**figure 2.8)**, as the standards amplified all contained the same DNA template – therefore implying that all reactions were highly specific and that no primer dimerisation or DNA contamination occurred. Two small peaks at 77-80°C were observed in the melt curve obtained from the amplification of Ad5.GFP 'V2' DNA. This may have been due to high sensitivity of the PCR, or the presence of artifacts in the samples.

2.9. Transduction Efficiency of Ad5.GFP

To confirm the ability of Ad5.GFP to transduce CHO-CAR cells, a transduction assay was performed. Transduced cells were sorted by flow cytometry, to quantify the number of GFP-positive cells post infection with Ad5.GFP. This determined the number of infectious virus particles within each of the purified stocks.

Cells were grown to 80% confluency and seeded into a 96-well plate in total media, at 2 x 10^4 cells/well. The cells were incubated at 37°C overnight, until approximately 70% confluent. Serial dilutions of Ad5.GFP were prepared as follows: 1,000vp/cell, 5,000vp/cell and 10,000vp/cell. CHO-CAR cells were transduced with 100µl of each Ad5.GFP dilution and left to incubate at 37°C for 3 hours. Cells were washed twice with PBS and replenished with 200µl of total media. Transduced cells were then incubated at 37°C for 48 hours. Media was discarded and the cells were washed twice with 200µl PBS. Next, 50µl Trypsin was added to the cells and incubated at 37°C for 3 minutes. Finally, 150µl of FACS buffer was added to resuspend the cells. The harvested cells were transferred to a V-shaped-bottom 96-well plate and centrifuged at 428 RCF for 5 minutes. Supernatant was discarded and 100µl of 4% Paraformaldehyde was added to resuspend the cells. The cells were incubated at 4°C for 10 minutes to ensure fixing. The plate was centrifuged at 428 RCF for 5 minutes, the

supernatant discarded and 150µl PBS was added to each well. The plate was covered in foil and stored at 4°C.

Flow cytometry was performed using the Accuri, as outlined in **section 2.2**; however, the FLA-1 channel was used to gate GFP-positive cells, rather than the FLA-4 channel.

In addition, transduction assays were performed in chapters 4, 5 and 6, to evaluate the concentration of active virus samples in the collected samples that had been aerosolised and exposed to Ultravision^{TM}. Such transduction assays were performed as outlined above, however, the collected samples were added to the seeded cells neat (undiluted), as opposed to in a series of dilutions.

2.10. Experimental Setup of the Prototype Closed-System Model

The experimental setup of the closed-system prototype model is displayed in **figure 2.9**. A portable nebuliser (Mesh Nebuliser YS31, Changzhou Zhengyuan Medical Technology Co. Ltd) was used to aerosolise each virus sample through the closed system. The nebuliser nozzle was attached to PVC tubing, which was inserted into a plastic syringe (Disposable Syringe 50ml, Safety First Aid, Zoro, 99038). An Ultravision^{TM} power unit (Ultravision^{TM} Generator, BOWA Medial UK, Newton Abbot, DAD-001-015) was used to supply energy (approximately 8kV) to the Ion Wand discharge electrode (Ion Wand^{TM}, BOWA Medial UK, Newton Abbot, DAD-001-003) and to the return electrode (Euro adapter, BOWA Medial UK, Newton Abbot, DAD-001-031). The Ion Wand was inserted into the middle of the syringe, emitting negative ions upon activation. A copper coil was inserted into the bottom of the syringe, and attached to the return electrode, providing the copper with a positive electrical charge. An additional piece of PVC tubing was attached to the end of the syringe and connected to an autoclaved 50ml glass beaker, serving as a collection pot for condensed aerosol samples. Also attached to the glass beaker was a portable suction unit (Duet Flat-Back Aspirator, SSCOR, US, 2314B), powered at 525mmHg, to ensure the unidirectional flow of aerosol samples through the system. All experimentation was conducted in a Class II laminar flow hood, and all materials were autoclaved (glassware) or sterilised with 70% Industrialised Methylated Spirit (IMS) before and after use. Following aerosolisation of the virus samples, all disposable materials were bleached prior to disposal, and reusable equipment was sterilised with IMS and Virkon, prior to autoclaving.

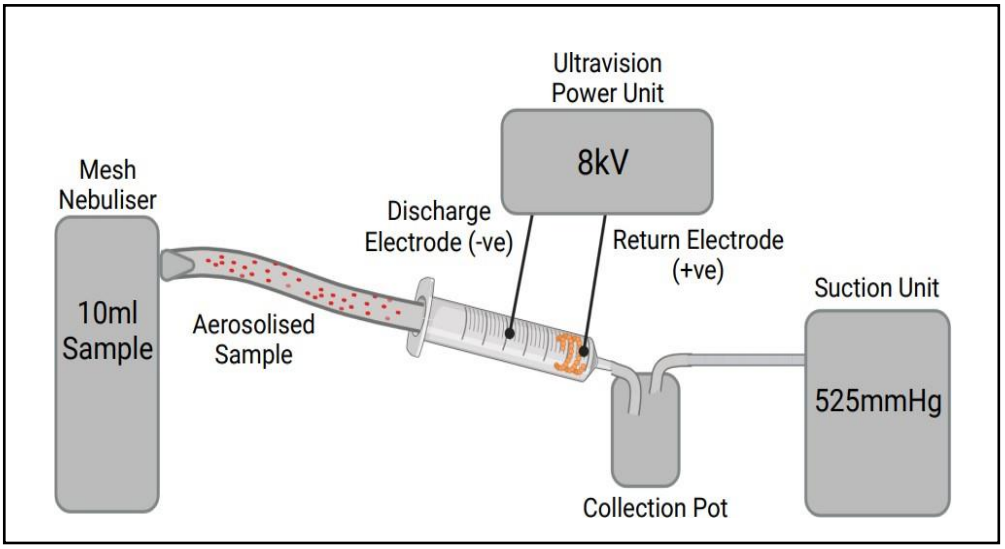

Figure 2.9. ***A Schematic Displaying the Experimental Setup of the Prototype Closed-System Model***. *Virus samples were aerosolised in a unidirectional flow through the system, exposed to Ultravision™ (active/inactive), condensed into a collection pot and stored at -80°C, prior to experimental analysis.*

2.11. Experimental Protocol using the Prototype Closed-System Model

All samples that were aerosolised and exposed to the prototype system are displayed in **Table 2.4.** Serum free media (Dulbecco's Modified Eagle's Medium; Sigma-Aldrich, Gillingham, UK #D5796) was used as a negative control. Four dilutions of Ad5.GFP were prepared, using serum free DMEM as a diluent, to a total volume of 20ml per sample. The dilutions were as follows: 1 x 10^8, 10^9, 10^{10} and 10^{11} vp/ml. For each run, 10ml of the virus sample was aerosolised through the system and exposed to either inactive Ultravision™ (UV OFF), or active Ultravision™ (UV ON). PVC tubing and glassware were sanitised with 70% IMS and flushed with aerosolised ddH_2O in between each experimental run. Following complete aerosolisation, samples were obtained from the collection pot and stored at -80°C in preparation for experimental analysis. Samples were analysed for the presence of viral genomes by qPCR and for viral activity by transduction and plaque assays.

Table 2.4. A List of all Samples Aerosolised through the Prototype System and Exposed to Ultravision™. . *Ultravision™ status is displayed for each sample as active or inactive. The time taken for each sample to undergo complete aerosolisation is stated in minutes. The volumes of the samples that were collected post-aerosolisation were significantly lower than the starting volumes of each sample and are therefore also detailed within this table.*

Sample	**Ultravision™ Status**	**Aerosolisation Time (minutes)**	**Volume Collected**
10ml Serum Free Media	Inactive	13.47	5ml
10ml Serum Free Media	Active	16.30	3.5ml
2ml Serum Free Media	-	-	2ml
10ml Ad5.GFP 10^8vp/ml	Inactive	14.32	4ml
10ml Ad5.GFP 10^8vp/ml	Active	18.32	5ml
10ml Ad5.GFP 10^9vp/ml	Inactive	13.11	5.5ml
10ml Ad5.GFP 10^9vp/ml	Active	16.10	5.5ml
10ml Ad5.GFP 10^{10}vp/ml	Inactive	14.14	5.5ml
10ml Ad5.GFP 10^{10}vp/ml	Active	16.34	5ml
10ml Ad5.GFP 10^{11}vp/ml	Inactive	13.17	5ml
10ml Ad5.GFP 10^{11}vp/ml	Active	16.42	4ml

2.12. Experimental Setup of the Refined Closed-System Model

The experimental setup of the refined closed-system model is shown in **figure 2.10**. A medical grade nebuliser (Aerogen® Solo Starter Kit, Aerogen Ltd, Galway, AG-A53000-XX) was used to aerosolise 10ml of each sample into a 3L reaction kettle (QuickFit™ Wide Neck Flask Reaction 3L, Scientific Laboratory Supplies Ltd, UK, QFR3LF). The reaction kettle was fitted with a lid containing multiple culture vessels (QuickFit™ Borosilicate Glass Flange Lid, Fisher Scientific, Leicestershire, MAF3/52), enabling the insertion of samples and materials into the kettle, whilst maintaining an air-tight system. The negatively charged Ultravision™ Ion Wand was inserted into the reaction kettle through a suba-seal, 15cm from the bottom of the reaction kettle and 7cm from either side of the reaction kettle. The Ultravision™ return electrode was attached to copper tape that covered the inside of the reaction kettle, serving as a positively charged collector plate. Stopcock adapters (QuickFit™ Borosilicate Glass Stopcock Adaptors with Sockets, Fisher Scientific, Leicestershire, MF14/3/SC) were placed throughout the system to ensure unidirectional flow of the aerosol. A suction unit

(**section 2.10**) was used to pull the aerosol through the system and into a BioSampler (BioSampler®, SKC Ltd, Dorset, 225-9595) for sample collection. The BioSampler was assembled as per the manufacturer's instructions, containing 2ml sterile serum-free media to capture the aerosol samples. To prevent viral contamination of the suction unit, a cold-trap (QuickFit™ Cold-trap, VWR, Pennsylvania, 201-3052) was fitted between the BioSampler and the suction unit. All experimentation was conducted in a Class II laminar flow hood, and all materials were autoclaved (glassware) or sterilised with 70% Industrialised Methylated Spirit (IMS) before and after use. Following aerosolisation of the virus samples, all disposable materials were bleached prior to disposal, and reusable equipment was sterilised with IMS and Virkon, prior to autoclaving.

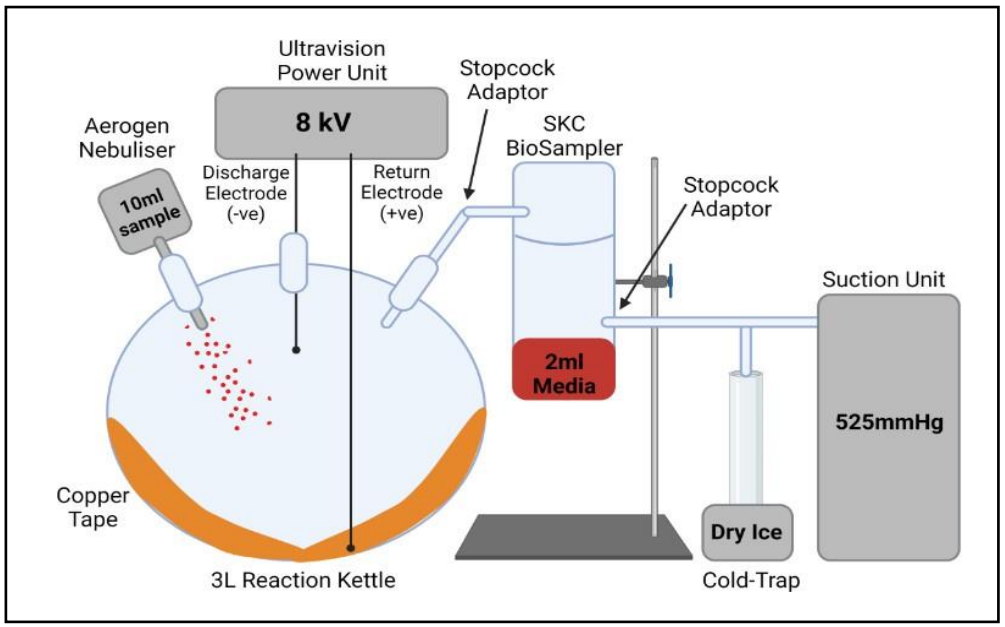

Figure 2.10. A Schematic Depicting the Experimental Setup of the Refined Closed-System Ultravision™ Model. *All samples were aerosolised into the air-tight reaction kettle, exposed to Ultravision™ (active/inactive) and suctioned into an SKC BioSampler for collection. Collected samples were stored at -80°C prior to experimental analysis.*

2.13. Experimental Protocols using the Refined Closed-System Model

The refined closed-system was used for multiple experiments to analyse the effects of different independent variables on the capture and inactivation of aerosolised virus particles. A range of variables were tested to accurately mimic the physical inconsistencies faced during the release of bioaerosols in surgical procedures. Additionally, parameters effecting the efficiency of electrostatic precipitation were evaluated to identify optimal

conditions for the use of Ultravision^{TM}. Each experimental run that was performed is detailed in **Table 2.5** below.

The first experimental run (Run #1) was performed to compare the refined closed-system with the prototype system. Data obtained from run #1 also served as a point of reference, to compare with subsequential experiments using the refined closed-system that included additional independent variables. **Figure 2.10** highlights the standardised setup used in run #1. Firstly, serum free media (Dulbecco's Modified Eagle's Medium; Sigma-Aldrich, Gillingham, UK #D5796) was aerosolised through the system. One 10ml sample of media was exposed to inactive Ultravision^{TM}, whilst another 10ml sample of media was exposed to active Ultravision^{TM} (8kV), both of which functioned as negative controls. Following this, Ad5.GFP was diluted to 1 x 10^{10}vp/ml and 10ml was aerosolised through the system and exposed to inactive Ultravision^{TM}, whilst another 10ml was exposed to active Ultravision^{TM} (8kV). Following complete aerosolisation of each sample, the condensate collected in the BioSampler was transferred into a sterile falcon and stored at -80°C, in preparation for analysis. Additionally, 2ml of serum free media and 2ml of Ad5.GFP were kept aside, and not exposed to the system. These samples were immediately stored at -80°C, serving as additional controls. Unfortunately, despite improvements to the system, slight premature condensation of the aerosolised samples was still observed in the refined model. Liquid containing active virus particles therefore accumulated in the bottom of the reaction kettle following each experimental run. This liquid was also collected following each run and stored at -80°C, in preparation for analysis. Finally, following complete aerosolisation of each sample, swabs were taken from 4 randomised regions of the copper return, using a cotton-tipped plastic swab, and inoculated in 2ml PBS for approximately 2 minutes. The PBS was then stored at -80°C, in preparation for experimental analysis.

To evaluate the effects of different independent variables on virus capture and inactivation, runs #2 - #7 were also performed. The independent variables tested and the rationale for each is highlighted in **Table 2.5.** Aside from the independent variable tested, all other dependent variables displayed in run #1, remained constant. Samples that were collected following each experimental run were analysed for the presence of viral genomes by qPCR and for viral activity by transduction and plaque assays.

Table 2.5. Experimental Runs and Independent Variables Tested Using the Refined Closed- System. *Run #1 was performed as the initial standard run, lacking optimisation, serving as a point of reference for each subsequential run.*

Experiment number	Independent Variable	Rationale	Sample Collection
Run #1	Standard Setup	To compare with results gathered from experimentation with the 'prototype' closed-system. To serve as a point of reference for subsequential experiments.	- BioSampler - Swabs of return electrode - Prematurely condensed samples within reaction kettle (RK)
Run #2	Virus sample concentration – Ad5.GFP at 1 x 10^7vp/ml and Ad5.GFP at 1 x 10^8vp/ml	To identify the optimal concentration of virus to aerosolise when evaluating the efficiency of Ultravision™ to capture and inactivate virus particles, whilst maintaining sufficient sensitivity and detectability in experimental assays.	- BioSampler - Prematurely condensed samples within reaction kettle (RK)
Run #3	Ion Wand Voltage – Comparisons between 6kV, 8kV and 10kV	To compare the effects of different Ion Wand voltages on the capture and inactivation of aerosolised virus particles.	- BioSampler
Run #4	Temperature of reaction kettle - 37°C	To maintain aerosolisation of the virus sample within the reaction kettle and prevent premature condensation. To ensure that 37°C heat does not affect virus stability or viability.	- BioSampler - Prematurely condensed samples within reaction kettle (RK)
Run #5	Number of Ion Wands – Comparisons between 1 Ion Wand and 2 Ion Wands	To analyse the synergistic capabilities of multiple Ion Wands to capture and inactivate aerosolised virus particles.	- BioSampler - Prematurely condensed samples within reaction kettle (RK)
Run #6	Material of Return Electrode – Comparisons between Copper and Stainless Steel	To determine whether viral inactivation was caused by the virucidal copper return electrode, or by Ultravision™ itself, using an inert metal as the collector plate for comparison.	- BioSampler - Swabs of Return Electrode

Run #7	Virus sample – Comparisons between SARS PV and Ad5.GFP	To evaluate the ability of Ultravision™ to capture and inactivate aerosolised enveloped and non-enveloped virus particles.	- BioSampler - Prematurely condensed samples within reaction kettle (RK)

2.14. Experimental Setup of the Prototype Open-System Model

The open-system setup is displayed in **Figure 2.11**. A medical grade nebuliser (Aerogen® Solo Starter Kit, Aerogen Ltd, Galway, AG-A53000-XX) was used to aerosolise 10ml of either serum-free DMEM media or Ad5.GFP at 1 x 10^{10}vp/ml into an enclosed 84L plastic box. The bottom of the plastic box was covered with copper tape, which was attached to the Ultravision™ return electrode (Euro adapter, BOWA Medial UK, Newton Abbot, DAD-001-031), providing it with a positive charge. Three stainless-steel sheets, each exactly 3 inches x 3 inches, were attached to the copper tape, carrying a positive charge. The stainless-steel sheets served as collector plates for precipitated virus particles. Sheet A was placed directly under the Ultravision™ Ion Wand (Ion Wand™, BOWA Medial UK, Newton Abbot, DAD-001-003). Sheet B was placed 2 inches from sheet A, and sheet C was placed 2 inches from sheet B. The Ultravision™ Ion Wand was placed 4 inches above the positively charged collector plate (sheet A), and 3.5 inches away from the Aerogen Nebuliser nozzle. It was important to maintain constant distances between the discharge electrode, the return electrode and the region of sample aerosolisation, to ensure experimental repeatability and to accurately calculate the Ion Wand voltage, according to Ohm's law. The BioSampler (BioSampler®, SKC Ltd, Dorset, 225-9595) was assembled as per the manufacturer's instructions, and filled with 2ml of fresh serum-free media prior to each run. The BioSampler was connected to the plastic box via a stopcock adaptor (QuickFit™ Borosilicate Glass Stopcock Adaptors with Sockets, Fisher Scientific, Leicestershire, MF14/3/SC) to enable sampling of the air within the plastic box. The vacuum unit (Duet Flat-Back Aspirator, SSCOR, US, 2314B) was attached to the opposite end of the BioSampler and switched on at 525mmHg, to facilitate movement of the aerosol through the plastic box and towards the BioSampler. All experiments were conducted in a Class II laminar flow hood, and all materials were autoclaved (glassware) or sterilised with 70% Industrialised Methylated Spirit (IMS) before and after use. Following aerosolisation of virus samples, all disposable materials were bleached prior to disposal, and reusable equipment was sterilised with IMS and Virkon, prior to autoclaving.

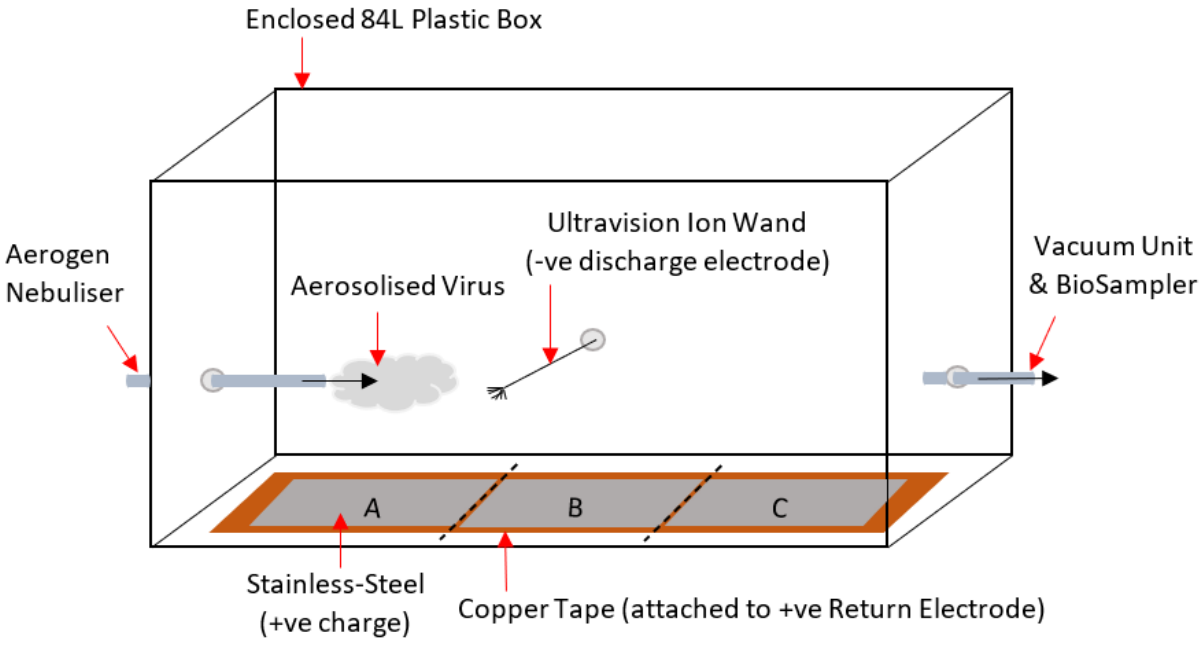

Figure 2.11. A Schematic Displaying the Experimental Setup of the Prototype Open-System Model. *The Ultravision™ Ion Wand was connected to the discharge electrode, thereby emitting negatively charged ions. The copper tape and stainless-steel sheets were connected to the Ultravision™ return electrode, thereby carrying a positive charge. All samples (SF media or Ad5.GFP) were aerosolised into the 84L plastic box, exposed to Ultravision™ (active/inactive) and suctioned via a vacuum unit into the SKC BioSampler for collection. Additionally, stainless-steel sheets were washed with 2ml SF media, post sample aerosolisation and exposure to Ultravision™, to evaluate the presence of active virus particles. All collected samples were stored at -80°C prior to experimental analysis.*

2.15. Experimental Protocol using the Prototype Open-System Model

Firstly, 20ml of Ad5.GFP at 1 x 10^{10}vp/ml was prepared, prior to aerosolisation. For control purposes, 20ml of serum-free media (Dulbecco's Modified Eagle's Medium; Sigma-Aldrich, Gillingham, UK #D5796) was also prepared for aerosolisation. Next, 10ml of each sample was aerosolised into the 84L plastic box and exposed to either active Ultravision™ (8kV) or inactive Ultravision™. Following complete sample aerosolisation, media was collected from the BioSampler and stored at -80°C. Additionally, the three stainless-steel sheets were individually washed with 2ml serum-free media, to obtain virus particles that had passively or actively precipitated onto the sheets. The resulting media solutions were also stored at -80°C in preparation for experimental analysis. All dependent variables such as temperature,

voltage, Ion Wand number, sample concentration and return-electrode material remained constant for each experimental run. Collected samples were analysed for the presence of viral genomes by qPCR and for viral activity by transduction and plaque assays.

Chapter 3: Characterisation of Viruses and Relevant Cell Lines

3.1. Introduction

To analyse the efficiency of Ultravision^{TM} to capture and inactivate aerosolised virus particles, viral vectors were generated, purified, and characterised. Although there is currently a particular focus regarding SARS-CoV-2, this study predominantly utilised the Adenovirus to evaluate the capabilities of Ultravision^{TM}. There are currently 67 reported serotypes of Adenovirus, each of which are classified into one of 8 groups, A-G (Robinson, 2013). The following experiments used Adenovirus serotype 5 (Ad5), belonging to group C (Wigand, 1982). Additionally, to represent and mimic the effects of Ultravision^{TM} on airborne SARS-CoV-2, a SARS-Lentiviral pseudotype vector (SARS PV), provided by collaborators from the Medway School of Pharmacy, was utilised. This pseudovirus comprised of a recombinant HIV1 core, with Wuhan strain SARS-CoV2 spike proteins (GenBank Accession: 43740568) inserted into its lipid envelope (Du. 2022).

Ad5 is a non-enveloped virus, approximately 90nm in diameter, with an icosahedral-shaped capsid, containing double-stranded DNA (**Figure 3.1**). The capsid is comprised of 240 hexons and 12 pentons at each vertex. Fiber shafts containing trimeric fiber knob proteins protrude from each vertex, functioning to attach the virus to its respective host cells (Russel. 2009). Ad5 fiber knob proteins recognise and bind to specific host cell receptors, the major and most commonly studied being the coxsackie adenovirus receptor (CAR). CAR is expressed at tight junctions between epithelial cells, resulting in Ad5 tropism towards epithelial cells located in the respiratory and gastrointestinal tract (Stepanenko and Chekhonin. 2018). Interactions between the Ad5 fiber knob protein and CAR enables cellular binding, whilst virus internalisation occurs following a secondary interaction between the viral penton base protein and αvβ3/5 integrins, enabling entry via a process termed endosome acidification (Wickham, 1993).

Similarly, a mature HIV1 particle is approximately 100nm – 200nm in diameter (Gürtler, 2016. Sun, 2019), however, unlike Ad5, the HIV core of SARS PV contains single stranded RNA (**Figure 3.1**). Being a retrovirus, HIV contains the enzyme Reverse Transcriptase, enabling the conversion of RNA into DNA upon host-cell infection, enabling viral replication

(Sarafianos, 2009). In contrast to Ad5, HIV is an enveloped virus, meaning that all of its genetic material is contained within a capsid (Melikyan, 2014.). In order to mimic SARS-CoV-2, the pseudovirus used throughout this project expressed homo-trimeric SARS spike glycoproteins, which extended outwards from the envelope, enabling attachment to host cells. These spike proteins are vital for cellular entry and do so by binding complementary receptors on host cell surfaces, such as Angiotensin-Converting Enzyme 2 (ACE2), which is commonly expressed on epithelial cells of the human respiratory and gastrointestinal tract (Astuti and Ysrafil. 2020). Analogous with Ad5, this protein-receptor binding aids virus internalisation and replication within host cells.

The safety profile, ease of genetic modification, mechanism of infection, size and structure of both vectors provides a clear rationale for their use in this research project.

3.1.2. Rationale for Using Ad5 and SARS PV to Evaluate the Virucidal Capabilities of Ultravision™

It was important to analyse the effects of Ultravision™ on both enveloped and non-enveloped viruses, as the electric charge and structure of the lipid envelope was thought to affect the efficiency of electrostatic precipitation. Although Ad5 and SARS PV differ, they appear similar in terms of their size, structure, and mechanism of infection.

In addition to their physical similarities, both Ad5 and SARS PV have well-established safety profiles and can be used in Category 2 laboratories, compared to wild-type SARS-CoV-2, which must be handled in a Category 3 workspace. To further enhance the safety of their use, both vectors were rendered replication deficient via genetic modification, and it is arguable that replication deficient viral vectors can be used in Category 1 workspaces. Adenoviral replication occurs in two main phases – the early phase and the late phase. In the early phase, early genes (E1-E3) are transcribed and translated, encoding proteins for viral DNA replication. In the late phase, structural proteins are transcribed and translated, enabling the assembly of mature virions (Hoeben and Uil. 2013). The Ad5 vector used in-house contains deletions in the E1-E3 genes, thereby preventing its replication. As a result, Ad5 vectors must be propagated in T-REx-293 cell lines, as these cells contain the essential E1 gene products, required for viral replication in trans. Furthermore, Ad5 has a high seroprevalence in the human population, meaning that many healthy adults' harbour

neutralising antibodies against the virus, thereby reducing the risks of its experimental use (Yu, et al. 2012). Of course, not all of the population harbour neutralising antibodies and the percentage of those that do differs geographically. For example, seroprevalence against Ad5 is much higher in Asia and Africa than it is in Europe (Yu, 2012).

To enable detection of Ad5 and SARS PV in biological assays, the GFP (green fluorescent protein) transgene was inserted into their genomes. GFP was inserted into the Ad5 genome in-house, prior to this study, via rapid AdZ recombineering (Stanton, et al. 2008). Additionally, the recombinant HIV1 core of SARS PV included a CMV transgene promoter and eGFP cDNA (Du, et al. 2022). GFP enables visualisation of virally transduced cells, further adding to the beneficial uses of these vectors throughout this study.

Finally, wild-type Ad5 is transmissible via aerosol (Kutter, et al. 2018). As this study aimed to evaluate the ability of Ultravision^{TM} to capture and inactivate virus particles released in bioaerosols, it was important to use a vector that could accurately mimic properties and characteristics of an authentic airborne virus. Therefore, in summary, Ad5 and SARS PV served as ideal candidates for the experimental testing of Ultravision^{TM}.

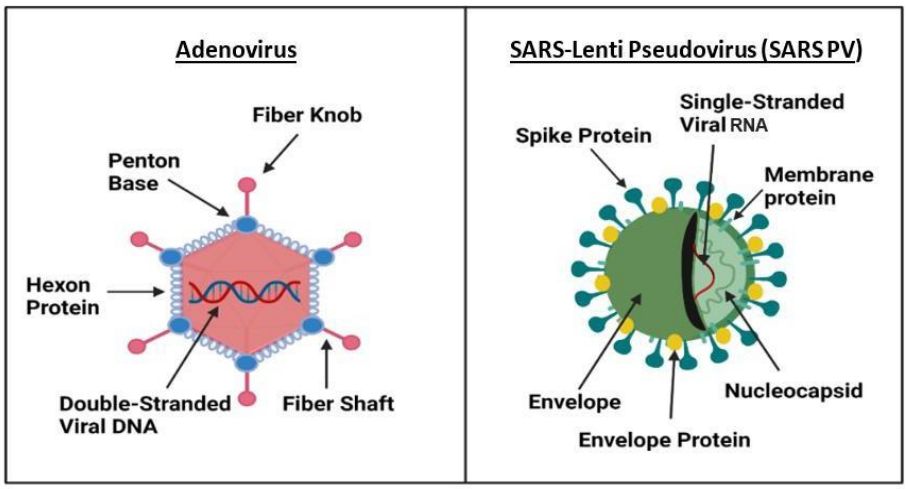

***Figure 3.1*. A Schematic Comparing the Structural Differences Between the Adenovirus and the SARS-Lenti Pseudovirus (SARS PV).** *The Adenovirus is non-enveloped, contains double-stranded DNA, and maintains an icosahedral structure. Its capsid consists of 240 hexon proteins and 12 penton bases. Fiber shafts, containing fiber knobs protrude from each penton base. SARS PV is an enveloped viral vector, containing single-stranded RNA (HIV core), which is enclosed within a nucleocapsid. The envelope consists of membrane proteins, envelope proteins and SARS CoV-2 spike proteins. (Own Figure, adapted from Russel, 2009 and Du, 2022)*

3.1.3. Chapter Aims and Hypothesis

Large stocks of purified Ad5.GFP and SARS PV were required to evaluate the ability of Ultravision^{TM} to capture and inactivate aerosolised enveloped and non-enveloped viral particles. As Ad5 and SARS PV bind to different receptors to gain cellular entry, 2 different cell lines were used throughout this project. CHO-CAR cells were used for infections with Ad5 samples, whilst CHO-ACE2-TMPRSS2 cells were used for infections with SARS PV samples. Therefore, the first aim of this chapter was to characterise the two cell lines, to ensure that each cell line highly expressed the desired receptors – CAR and ACE2. Antibody staining and flow cytometry was performed to quantify the percentage of cells expressing the desired receptors within each cell line. The second aim of this chapter was to validate the purified virus stocks by detecting virus-specific proteins via western blotting. This was important to perform, prior to using the virus stocks experimentally. The final aim of this chapter was to measure the infectivity status of Ad5. This was achieved by carrying out transduction assays in CHO-CAR cells, using various dilutions of the purified virus stocks. As the Ad5 vector expressed the GFP transgene, cells that had been successfully transduced by virus particles were fluorescent. Fluorescent cells were identified and quantified via Fluorescence-Activated Cell Sorting analysis, to determine the number of active virus particles within each stock. It was important to confirm the initial infectivity of Ad5 prior to aerosolising the virus samples under experimental conditions and exposing them to Ultravision^{TM}. As the stock of SARS PV was obtained from collaborators from the Medway School of Pharmacy, it was already titerd and therefore the initial infectivity of the viral particles was predetermined, prior to experimentation with Ultravision^{TM}.

3.2 Results

3.2.1. Characterisation of CHO-CAR and CHO-ACE2-TMPRSS2 Cells by Flow Cytometry

Flow cytometry was performed to confirm the expression of the Coxsackie Adenovirus Receptor (CAR) and the Angiotensin-Converting Enzyme 2 in CHO-CAR and CHO-ACE2-TMPRSS2 cell lines respectively. The percentage of CHO-CAR cells expressing CAR (**Figure 3.2A**) and CHO-ACE2-TMPRSS2 cells expressing ACE2 (**Figure 3.2B**) were compared to unstained and IgG-stained negative control samples. Results indicated that 97.63% of CHO-CAR cells expressed CAR, whilst 97.8% of CHO-ACE2-TMPRSS2 cells expressed ACE2.

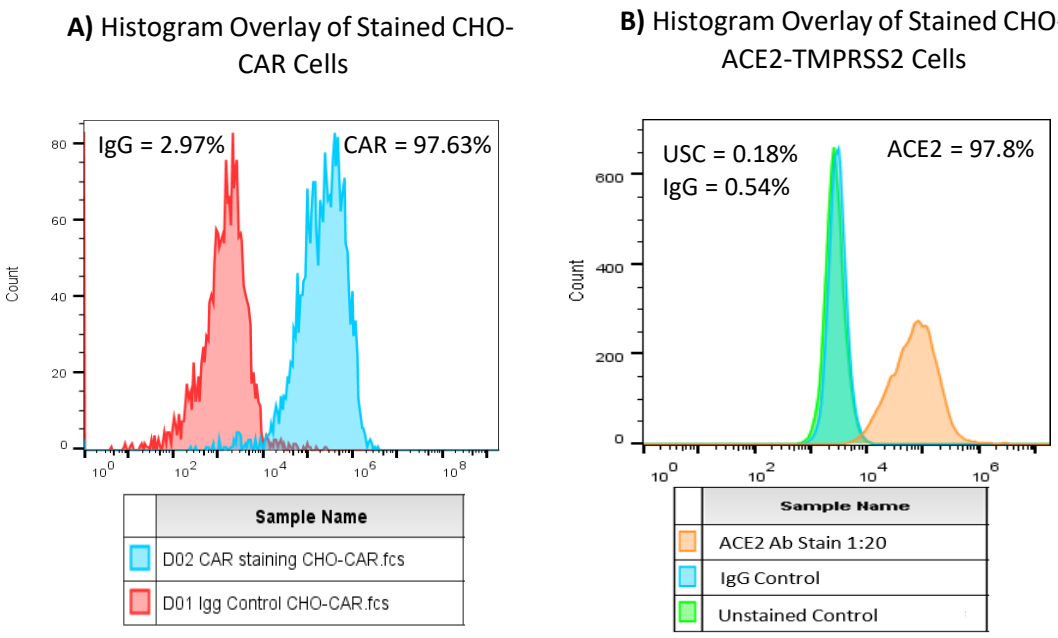

Figure 3.2. Cell-Surface Receptor Expression of CHO-CAR and CHO-ACE2-TMPRSS2 Cells, Determined by Flow Cytometry. A*) Histogram overlay of CHO-CAR cells stained with IgG control and the anti-CAR antibody. Peaks to the right indicate positive staining for CAR.* ***B****) Histogram overlay of CHO-ACE2-TMPRSS2 cells stained with IgG control, the anti-ACE2 antibody or left unstained. Peaks to the right indicate a positive staining for ACE2. USC (Unstained control), IgG (Immunoglobulin G Control), CAR (Coxsackie Adenovirus Receptor), ACE2 (Angiotensin Converting Enzyme2).*

3.2.2. Ad5 Hexon Protein Detection in Purified Stocks of Ad5.GFP by Western Blotting

To verify the presence of Ad5-specific proteins, a western blot was performed using monoclonal antibodies that recognised and bound to the hexon protein located on the Adenovirus capsid. The Adenovirus hexon protein is 110KDa, therefore bands at this molecular weight validate the presence of Adenovirus (**Figure 3.3**). Bands at 110KDa were present in all 4 Ad5.GFP protein samples. This indicated the presence of monomeric hexon protein, as expected. Samples that contained more protein (4µl compared to 2µl) displayed clearer, brighter bands. However, in general, the strength of all the bands that appeared on the gel were fairly weak. This may have been due to incomplete transfer or potential loss of protein during the washing steps.

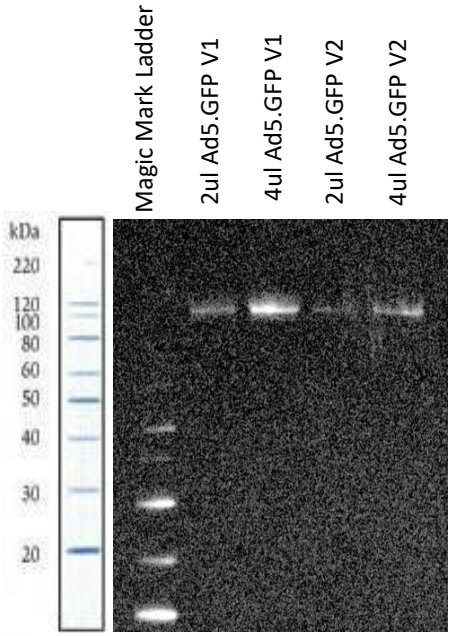

Figure 3.3. Detection of the Ad5 Hexon Protein in Purified Stocks of Ad5.GFP, Determined by Western Blotting. *Bands at 110KDa correspond to the Ad5 hexon protein. Protein was extracted from the 2 virus stocks and was loaded into the gel in 2µl and 4µl increments, to aid protein detection.*

3.2.3. Transduction Efficiency of the Ad5.GFP Purified Stock

To determine the infectivity status of the purified virus stocks, CHO-CAR cells were transduced with various dilutions of Ad5.GFP and analysed by flow cytometry. The percentage of GFP positive cells within the CHO-CAR cell samples were quantified **(Figure 3.4A)**. Additionally, the fluorescence intensity of each sample was measured **(Figure 3.4B)**. Cell populations that were transduced with higher concentrations of Ad5.GFP displayed higher percentages of GFP positive cells and correspondingly higher fluorescence intensity. Negative controls that were uninfected did not express GFP nor emit fluorescence. Due to the limited stock and low titer of SARS PV, transduction assays were not performed to analyse its initial infectivity. However, SARS PV activity was previously highlighted in plaque assays, when calculating functional titers of the stock (**Figure 2.3**).

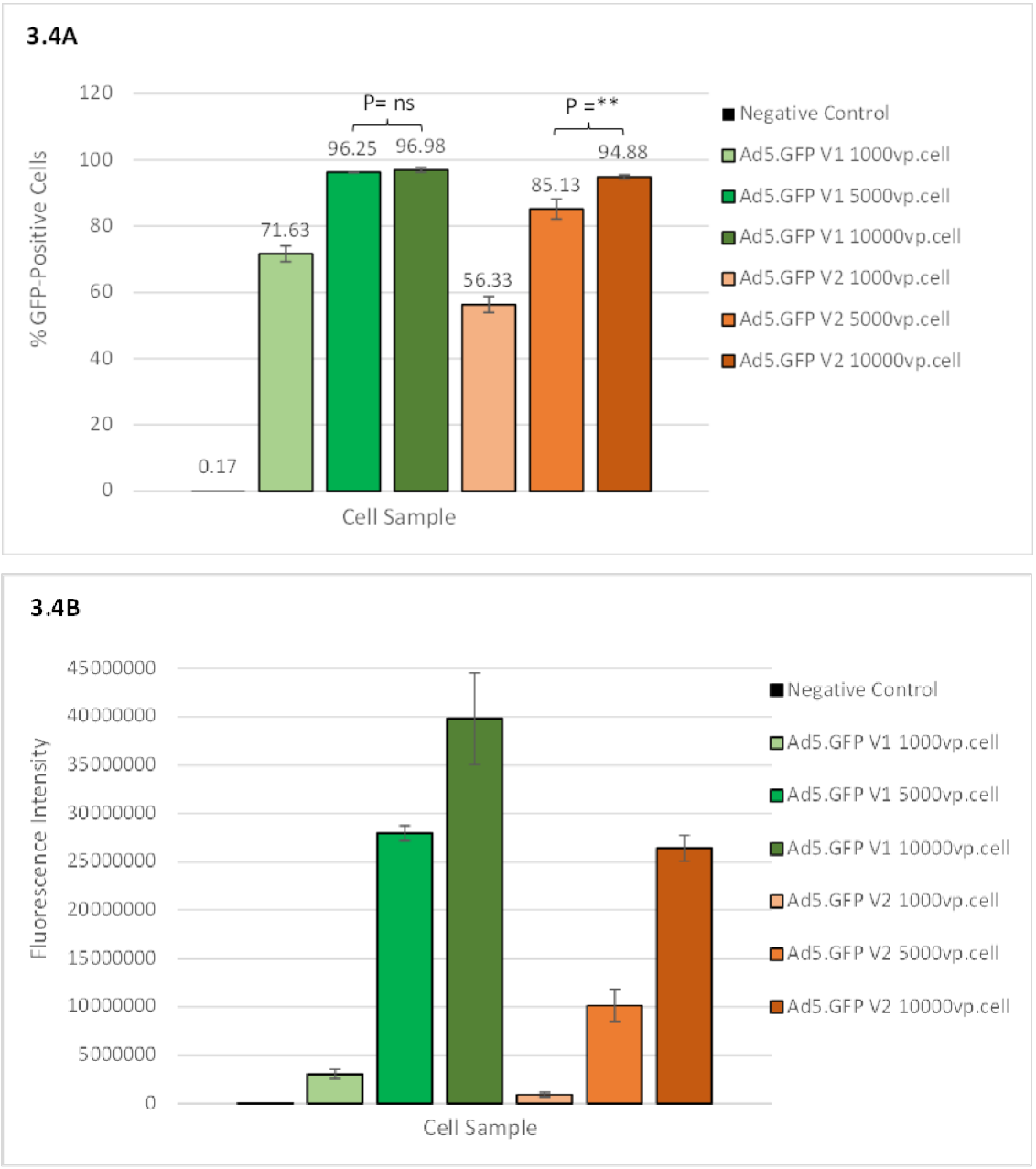

***Figure 3.4**. **A Transduction Assay Measuring GFP Expression in CHO-CAR Cells that had been Transduced with Dilutions of the Ad5.GFP Stocks. A)** Mean percentages of GFP-positive cells in transduced cell samples, compared to uninfected controls. **B)** Mean values of fluorescence intensity per transduced cell sample, compared to uninfected controls. Assay performed in triplicate - graph displays mean values and SD +/-. The Student's T-test was performed to statistically analyse and compare data sets. P = ns (No significant difference). ** = 0.0043 (Statistically significant difference).*

3.3. Discussion

A large stock of Ad5.GFP was successfully purified, titerd and characterised. Three experimental methods were chosen to titer the virus stocks: MicroBCA, plaque assay and NanoSight analysis. The titers obtained are highlighted in **Table 3.1**.

Table 3.1. Physical and Functional Titers of Purified Stocks of Ad5.GFP. Table 3.1. *Titers of Ad5.GFP calculated via MicroBCA, plaque assay and NanoSight analysis.*

Virus Stock	MicroBCA Titer	Plaque Assay Titer	NanoSight Titer
Ad5.GFP (V1)	1.80×10^{12}vp/ml	3.74×10^{8}pfu/ml	1.66×10^{11}vp/ml
Ad5.GFP (V2)	1.71×10^{12}vp/ml	2.55×10^{8}pfu/ml	1.97×10^{11}vp/ml

MicroBCA assays measured the total protein content within each sample, which is the most common method used to quantify virus within our laboratory and was therefore used as a reference point for all future experiments. In comparison, the plaque assay detected the number of infectious virus particles within each sample, which produced much lower titers than the MicroBCA, as not all particles present within the stocks were infectious. Finally, the NanoSight identified the number of intact spherical 90nm particles within each stock, however, did not account for whether the 'spheres' detected encompassed a viral genome. Therefore, the data obtained from the NanoSight was used to measure particle size and to determine stock purity, rather than to obtain an accurate stock concentration. NanoSight analysis also ensured that the virus sample was monodisperse and contained no aggregates.

As the stock of SARS PV was provided by collaborators, the physical and functional titers were already determined. However, such titers were validated in this chapter via NanoSight analysis and plaque assays.

To evaluate the ability of Ultravision^{TM} to capture and inactivate aerosolised virus particles and assess parameters that effect the efficiency of electrostatic precipitation, obtaining large stocks of Ad5.GFP and SARS PV at high titers was essential. Following exposure to Ultravision^{TM}, it was hypothesised that the concentration and activity of the virus sample would be significantly reduced. Therefore, it was important to determine initial titers and characterise infectivity of the starting virus stocks, prior to experimentation, in order to make direct comparisons with treated samples.

Chapter 4: Evaluation of Ultravision™ to Capture and Inactivate Aerosolised Virus Particles using a Prototype 'Closed-System' Model

4.1. Introduction

In order to obtain 'proof-of-concept' data determining the ability of Ultravision™ to capture and inactivate aerosolised virus particles, a preliminary study using a prototype model was performed. Small-scale, proof-of-concept experiments are important to establish the feasibility and rationale of an investigative project and help to address the risks and benefits of such experimentation. In addition, preliminary studies enable experimental optimisation and highlight areas that require improvement or alterations prior to performing more extensive studies.

A prototype model utilised in this chapter was designed and constructed by collaborators (Michael Shinkwin and Neil Warren) prior to commencement of this project (**Figure 4.1**). The closed-system model aimed to mimic the aerosol dynamics that occur during closed surgery, such as abdominal laparoscopy. Bioaerosols are released when cutting abdominal tissue using electrosurgical devices (Buggisch, 2020). The release of bioaerosols that are contaminated with viral or bacterial particles place healthcare staff and other hospitalised patients at potential risk of infection. Therefore, developing a method to prevent the escape of bioaerosols should in turn reduce disease transmission, improve the overall safety of medical procedures, and enable keyhole surgery to continue as normal during future pandemics.

The Ultravision™ device consists of a negatively charged Ion Wand (discharge electrode) and a positively charged return electrode. For this experiment, the return electrode was attached to a copper coil, where negatively charged aerosol particles could precipitate onto via electrostatic attraction. For the purpose of this preliminary study, four samples of Ad5.GFP at various concentrations were aerosolised through the prototype closed-system. Each sample was prepared in duplicate, enabling exposure of each virus dilution to inactive Ultravision™ (turned off), as well as active Ultravision™ (turned on), in separate experimental runs. To ensure unidirectional travel of the aerosol towards the Ultravision™ Ion Wand, a suction pump was attached to the collection pot, essentially pulling the sample through the entire system. Following complete aerosolisation of each sample, the aerosol

was condensed back into a liquid, facilitating collection. All samples obtained from the collection pot were stored at -80° in preparation for experimental analysis.

To determine whether Ultravision^{TM} had efficiently captured aerosolised Ad5.GFP particles via electrostatic precipitation, the collected samples were analysed by qPCR (to detect viral genomes) and using the NanoSight (to detect intact virus particles). However, NanoSight particle detection is not entirely specific to Ad5, and results can be skewed following sample contamination with particles of similar diameters. Such contamination was observed in this study, when passing the virus samples through the system. Therefore, data obtained from the NanoSight in this chapter provided a rationale for the discontinuation of NanoSight use in subsequential Ultravision^{TM} experiments. In addition, to evaluate whether Ultravision^{TM} had efficiently inactivated aerosolised Ad5.GFP particles, transduction assays and plaque assays were performed.

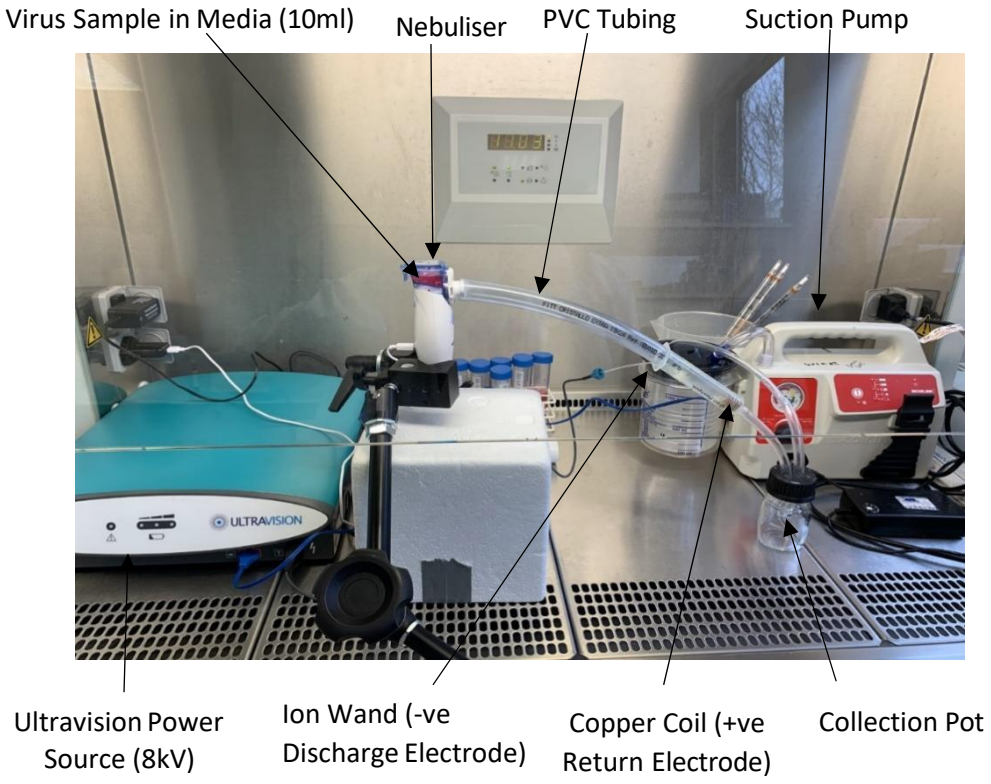

Figure 4.1. Experimental Setup of the Prototype Closed-System Model*. For each run, 10ml of diluted Ad5.GFP was loaded into the nebuliser, aerosolised through the PVC tubing and exposed to the Ultravision^{TM} Ion Wand (8kV). The Ion Wand emitted negatively charged ions, thereby negatively charging aerosolised virus particles. A copper coil was attached to the positively charged return e lectrode. The copper coil was therefore utilised as a collector plate, whereby negatively charged pa rticles were precipitated. A vacuum device was used to suction the sample through the system, maintaining a unidirectional flow of the aerosol. Following exposure to Ultravision^{TM}, the aerosol sample was condensed into a sterile collection pot. Each collected sample was immediately transferred into a sterile falcon and stored at -80°C, prior to experimental analysis.*

4.1.2. Chapter Aims and Hypothesis

The overarching aim of this chapter was to undertake preliminary experiments to obtain evidence supporting the research theory and justifying the overall project proposition. The first aim was to successfully perform experimental runs using the prototype closed-system, in a safe and repeatable manner. The second aim was to prove that Ultravision^{TM} could capture and inactivate aerosolised virus particles via electrostatic precipitation, in the constructed closed system. The final aim was to identify limitations of the prototype system and to determine variables that affected the efficiency of Ultravision^{TM}. This would enable the generation of a refined, more representative model that could be used in future studies to gather publishable and conclusive results. Following extensive reviews of relevant literature, it was hypothesised that active Ultravision^{TM} would successfully precipitate the aerosolised Ad5.GFP onto the copper coil, thereby capturing and potentially inactivating the virus particles. This result would be highlighted by the collection of uncontaminated media following the aerosolisation of Ad5.GFP and exposure to active Ultravision^{TM}. In comparison, it was conjectured that exposing aerosolised Ad5.GFP to inactive Ultravision^{TM} would result in the collection of contaminated media, containing a highly active viral load, equivalent to the starting pre-exposed sample.

4.2. Results

4.2.2. Capture of Ad5.GFP by Ultravision™ within the Prototype Closed-System, Determined by qPCR Analysis

qPCR was performed to evaluate the ability of Ultravision™ to capture aerosolised Ad5.GFP particles via electrostatic precipitation. The concentration (ng/µl) of Ad5 genomes present within each of the collected samples, post exposure to active/inactive Ultravision™, was determined (**Figure 4.2).**

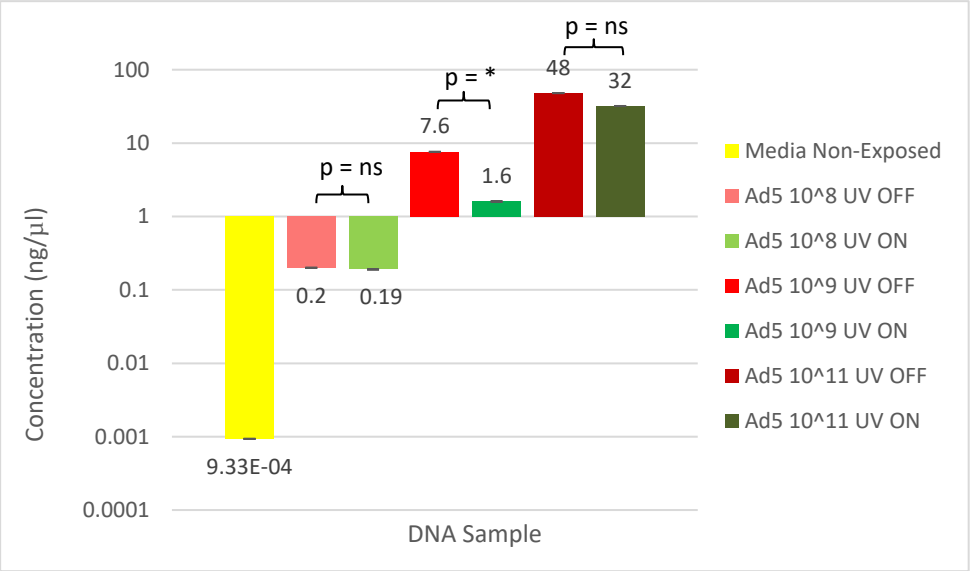

Figure 4.2. Average DNA Concentrations Obtained from qPCR Amplification of Ad5 Genomes in Samples that had been Exposed to Ultravision™ – Prototype Closed-System Run. *Yellow Bar: SF media, non-exposed to Ultravision™ (negative control). Green Bars: Ad5.GFP dilutions, exposed to active Ultravision™. Red Bars: Ad5.GFP dilutions, exposed to inactive Ultravision™. Assay performed in triplicate - graphs display mean values and SD +/-. The Student's T-test was performed to statistically analyse and compare data sets. * = 0.0195 (statistically significant), ns = no significant difference.*

The serum-free media control contained no viral DNA, thereby serving as a functional negative control. As expected, aerosolisation of higher concentrations of Ad5.GFP resulted in the collection of higher concentrations of viral DNA. This indicated that aerosolisation of Ad5.GFP through the prototype system did not affect the stability of viral DNA. A statistically significant difference in the number of Ad5 genomes was observed between samples exposed to active and inactive Ultravision™, following aerosolisation of Ad5.GFP at 10^9vp/ml. Although this difference was slight, it showed that Ultravision™ was somewhat capable of virus particle capture. No significant difference in the number of Ad5 genomes

was observed between samples exposed to inactive and active Ultravision^{TM}, following aerosolisation of Ad5.GFP at 1 x 10^{8}vp/ml and 1 x 10^{11}vp/ml. This discrepancy indicated that Ultravision^{TM} did not efficiently precipitate intact virus particles from the aerosolised samples within the prototype system setup.

4.2.3. Capture of Ad5.GFP by Ultravision^{TM} within the Prototype Closed-System, Determined by NanoSight Analysis

To determine the ability of Ultravision^{TM} to capture aerosolised viral particles, NanoSight analysis was performed to detect the number of intact Ad5.GFP particles within the collected samples. As the NanoSight is capable of visually detecting virus-sized particles, it appeared a more appropriate method of sample analysis than qPCR. Particle numbers and sizes were measured in each of the collected samples (**Figure 4.3**). Particles between 80-100nm were considered intact Ad5.GFP. Particles below this size were considered debris or artifacts, whilst above this size were thought to be bubbles, particle clumps or contamination by larger debris.

In comparison with qPCR results, NanoSight analysis detected a low level of virus-sized particles within the serum-free media controls. The NanoSight also detected non-virus-sized particles, in each of the collected samples. This indicated that the samples were contaminated with debris and artifact following aerosolisation and exposure to the prototype system. As the NanoSight is highly sensitive at detecting nano-particles of all diameters, we decided to discontinue its use to analyse collected samples going forward. Therefore, qPCR was the chosen method of determining viral capture by Ultravision^{TM} in all subsequential experiments succeeding Chapter 4.

A

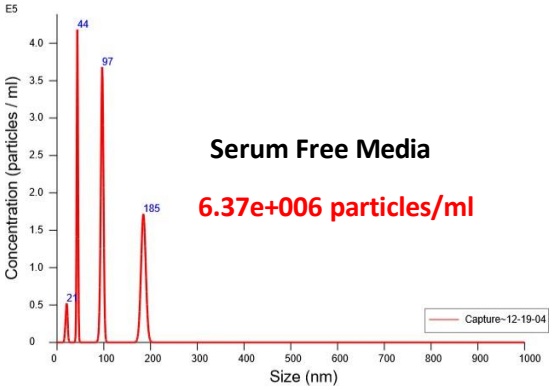

Serum Free Media

6.37e+006 particles/ml

B

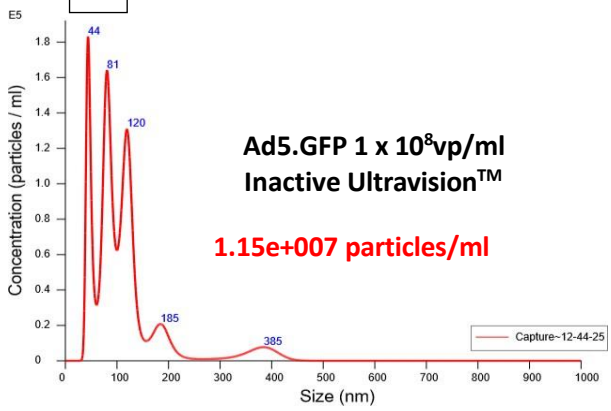

Ad5.GFP 1 x 10^8vp/ml
Inactive Ultravision™

1.15e+007 particles/ml

C

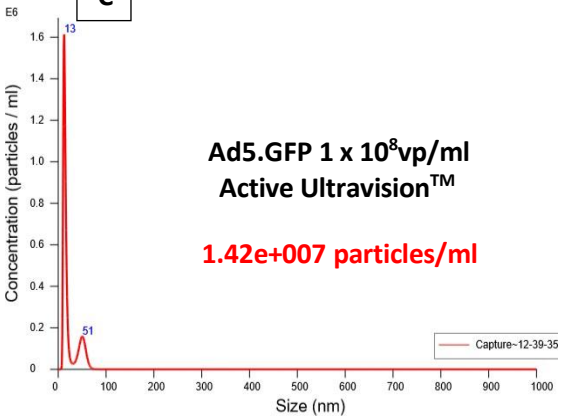

Ad5.GFP 1 x 10^8vp/ml
Active Ultravision™

1.42e+007 particles/ml

D

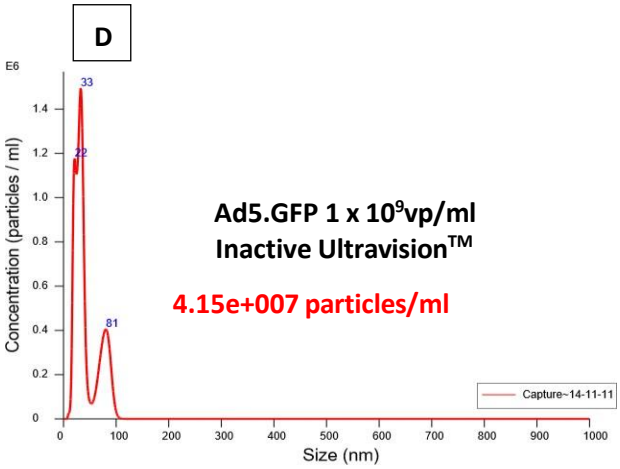

Ad5.GFP 1 x 10^9vp/ml
Inactive Ultravision™

4.15e+007 particles/ml

E

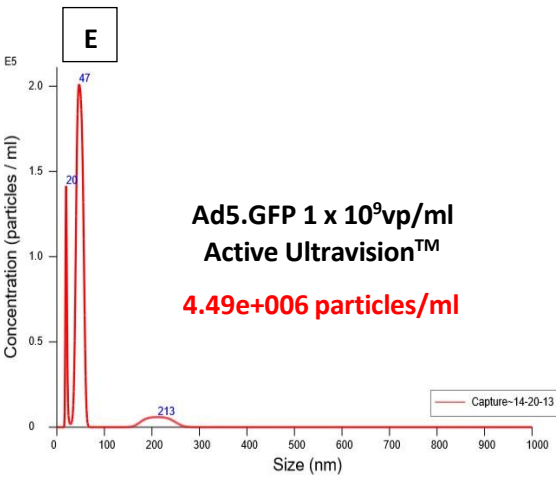

Ad5.GFP 1 x 10^9vp/ml
Active Ultravision™

4.49e+006 particles/ml

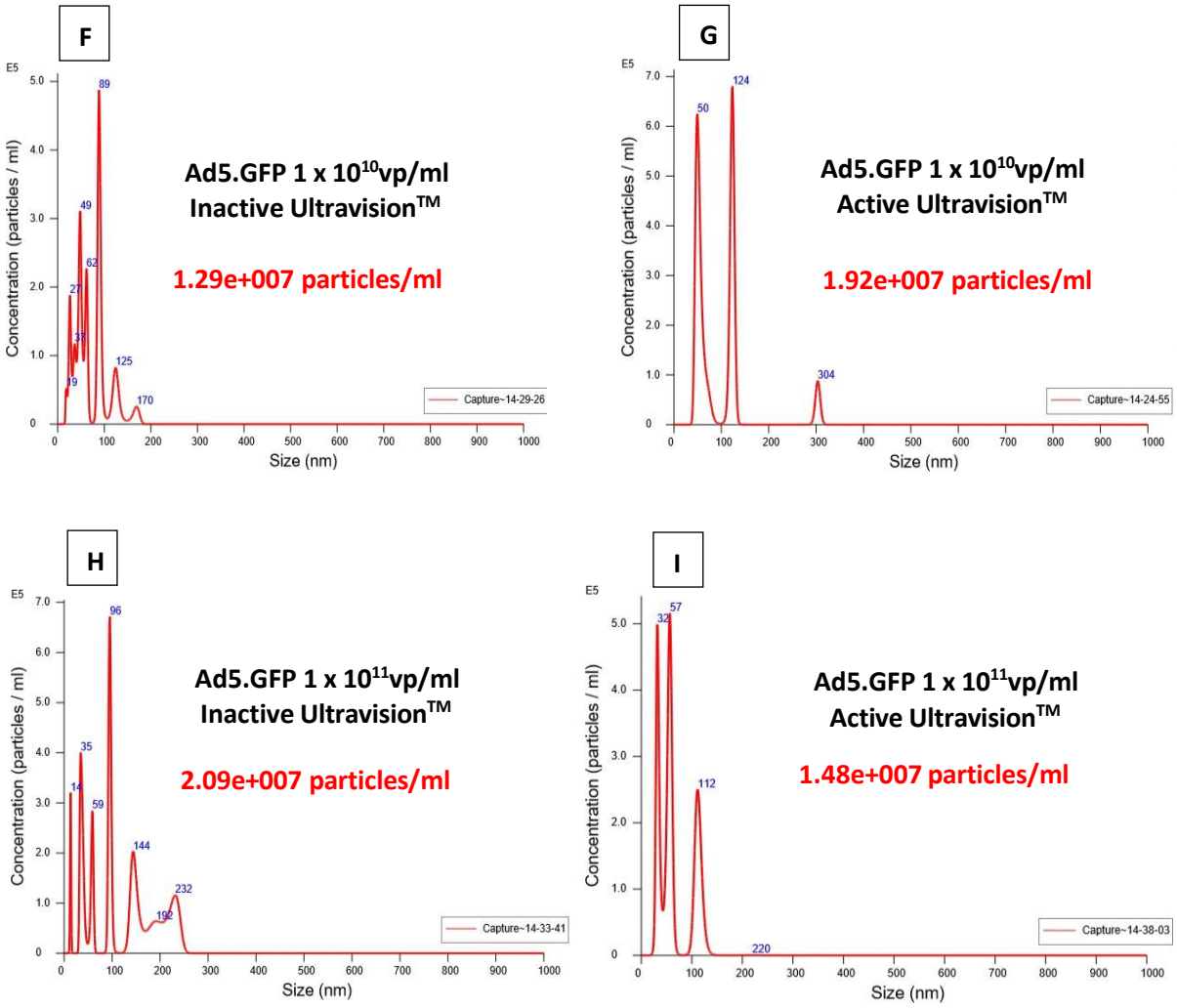

Figure 4.3. NanoSight Analysis of Ad5.GFP Samples, Following Exposure to Active/Inactive Ultravision™. *Red peaks display particle sizes and concentrations. Particles at 80-100nm were assumed as intact Ad5.GFP particles. Particles above or below this size were most likely due to contamination, clumps or bubbles within the infused sample. Starting concentrations of the samples that were aerosolised through the system are displayed in black writing. The concentrations of the collected samples, post aerosolisation, are displayed in red writing.* ***Image A*** *displays NanoSight analysis of the serum-free media negative control sample.* ***Images B – I*** *display NanoSight analysis of the Ad5.GFP samples that were exposed to active/inactive Ultravision™.*

4.2.4. Inactivation of Ad5.GFP by Ultravision™ within the Prototype Closed-System, Determined by Transduction Assay

To evaluate whether Ultravision™ successfully inactivated aerosolised Ad5.GFP, a transduction assay was performed. The percentage of GFP-positive CHO-CAR cells was used to measure the number of active Ad5.GFP particles within each of the collected samples, post-exposure to active/inactive Ultravision™ (**Figure 4.4**).

No transduction was observed in the negative control serum-free media. This demonstrated that the presence of particles within the media samples, detected by NanoSight analysis, was due to debris/artifact contamination, following sample aerosolisation through the prototype system.

The percentage of transduced CHO-CAR cells, following infection with the collected samples, was quantified by Flow Cytometry (**Figure 4.4**). For all four virus dilutions, a statistically significant reduction in transduction was observed in cells infected with samples that had been exposed to active Ultravision™ ($p < 0.2$). This confirmed that Ultravision™ was capable of inactivating aerosolised Ad5.GFP. However, the higher starting concentrations of Ad5.GFP, displayed a lower reduction in viral activity. This suggested that particle number effected the efficiency of electrostatic precipitation. It was hypothesised that slowing the aerosol flow rate, increasing the voltage of Ultravision™ or removing the spatial constraints of the prototype system would improve the efficiency of particle inactivation in samples containing higher numbers of virus particles.

In all cases, samples exposed to active Ultravision™ still contained significant levels of active Ad5.GFP, highlighting that Ultravision™ did not inactivate 100% of the virus particles. However, during experimentation, irregular volumes of the aerosol samples were prematurely condensed within the PVC tubing. Therefore, unknown volumes of active virus were deposited into the system as a liquid, avoiding exposure to Ultravision™. As Ultravision™ is unable to precipitate particles that are suspended within liquid solutions, the prematurely condensed samples contaminated the collection pot with active Ad5.GFP. This incidence provided a plausible explanation for the presence of active Ad5.GFP within the collection pot following sample exposure to active Ultravision™, thereby highlighting a limitation of the prototype system.

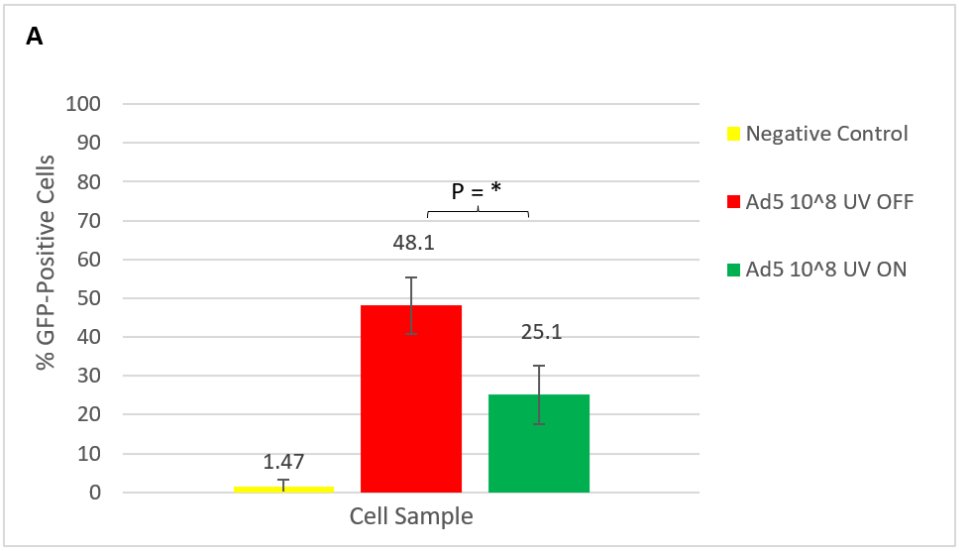
A
100
90
80
70
60
50
40
30
20
10
0
% GFP-Positive Cells
P = *
48.1
25.1
1.47
Cell Sample
Negative Control
Ad5 10^8 UV OFF
Ad5 10^8 UV ON

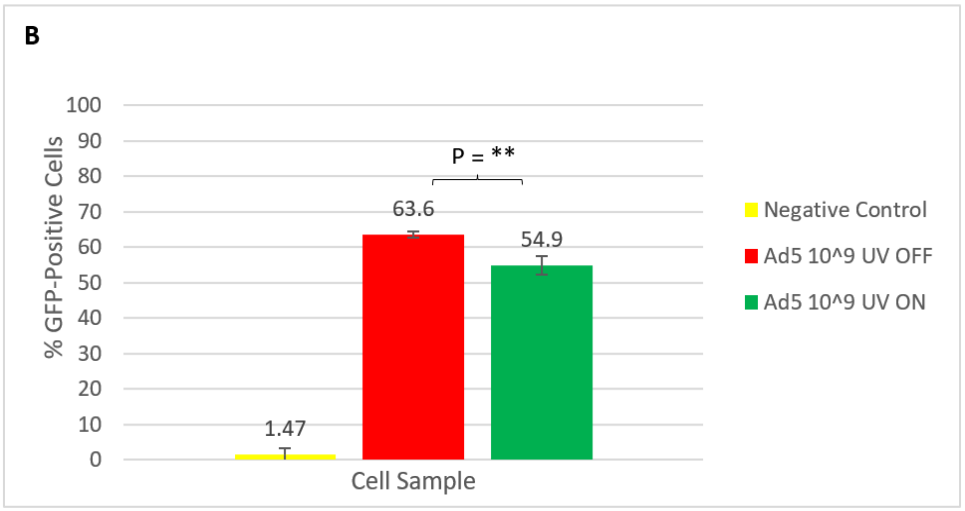
B
100
90
80
70
60
50
40
30
20
10
0
% GFP-Positive Cells
P = **
63.6
54.9
1.47
Cell Sample
Negative Control
Ad5 10^9 UV OFF
Ad5 10^9 UV ON

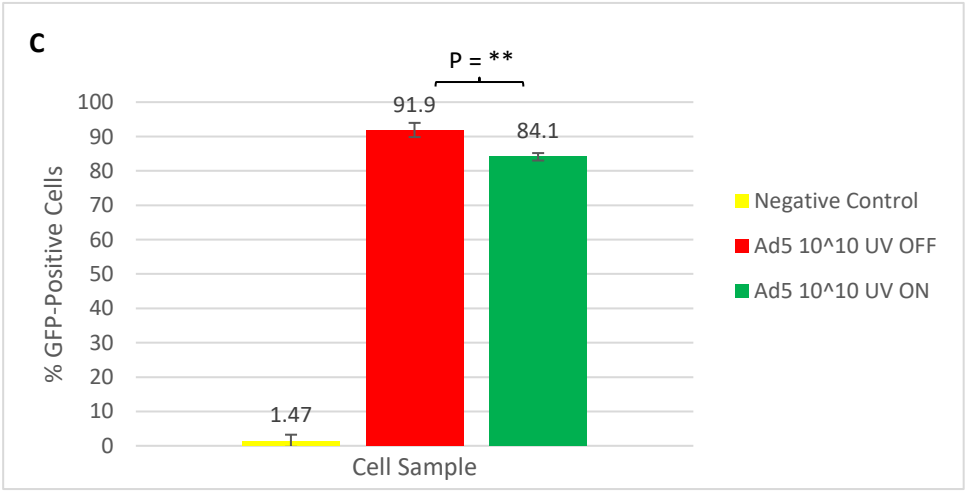
C
P = **
100
90
80
70
60
50
40
30
20
10
0
% GFP-Positive Cells
91.9
84.1
1.47
Cell Sample
Negative Control
Ad5 10^10 UV OFF
Ad5 10^10 UV ON

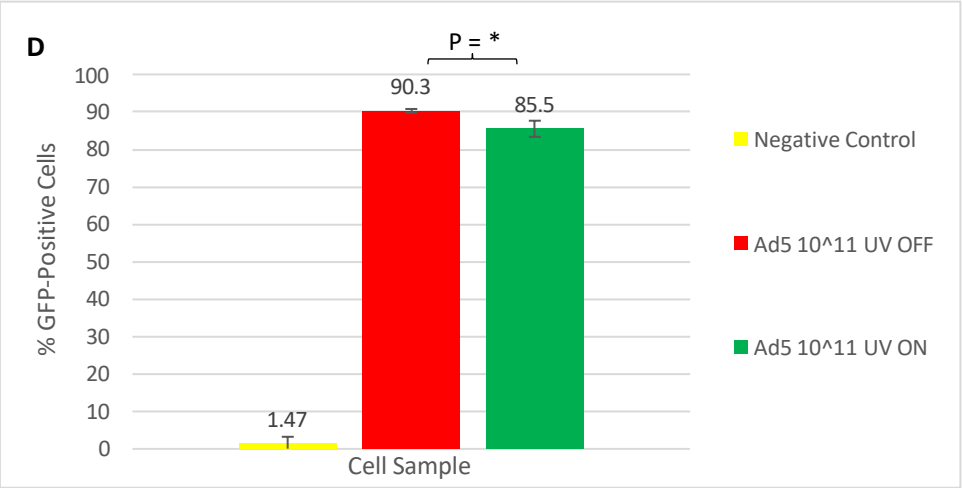

Figure 4.4. Average Percentage of CHO-CAR Cells Positive for GFP Fluorescence, Following Infection with Samples that had been Exposed to Active/Inactive Ultravision™, Determined by Flow Cytometry*. Yellow bar: CHO-CAR cells replenished with total media. Red bars: Ad5.GFP sample exposed to inactive Ultravision™. Green bars: Ad5.GFP sample exposed to active Ultravision™. Figures* ***A-D*** *display results from different starting dilutions of Ad5.GFP (10^8 - 10^{11}vp/ml). Assay performed in triplicate - graphs display mean values and SD +/-. The Student's T-test was performed to statistically analyse and compare data sets.* ***A)*** * = 0.019. **B**) ** = 0.0054. **B)** ** = 0.0043. **D**) * = 0.019.

4.2.5. Inactivation of Ad5.GFP by Ultravision™ within the Prototype Closed-System, Determined by Plaque Assay

To confirm results from the transduction assay, a plaque assay was performed (**Figure 4.5**). Wells supplemented with total media, or serum-free media that had been aerosolised through the prototype system and exposed to Ultravision™, showed no signs of fluorescence under the GFP light source. This finding supported the transduction assay results, indicating an absence of viable Ad5.GFP in the negative control. As expected, virus samples that had been exposed to inactive Ultravision™ remained highly active, resulting in observable green fluorescence. Higher starting concentrations of Ad5.GFP produced more fluorescence compared to the lower starting concentrations of Ad5.GFP, as predicted. Samples exposed to active Ultravision™ produced a significantly reduced number of fluorescent cells, once again confirming the transduction assay results and demonstrating that Ultravision™ successfully inactivated the aerosolised virus particles. The amount of fluorescence in wells that were infected with Ad5.GFP samples starting at 1 x 10^{11}vp/ml, that had been exposed to either active or inactive Ultravision™, did not significantly differ. This indicated that Ultravision™ was only capable of inactivating Ad5.GFP at concentrations below 1 x 10^{11}vp/ml within the prototype system. It is likely that the Ultravision™ Ion Wand

or the return electrode became fully saturated when exposed to higher concentrations of virus particles, reducing its efficiency and ability to capture and inactivate viral particles.

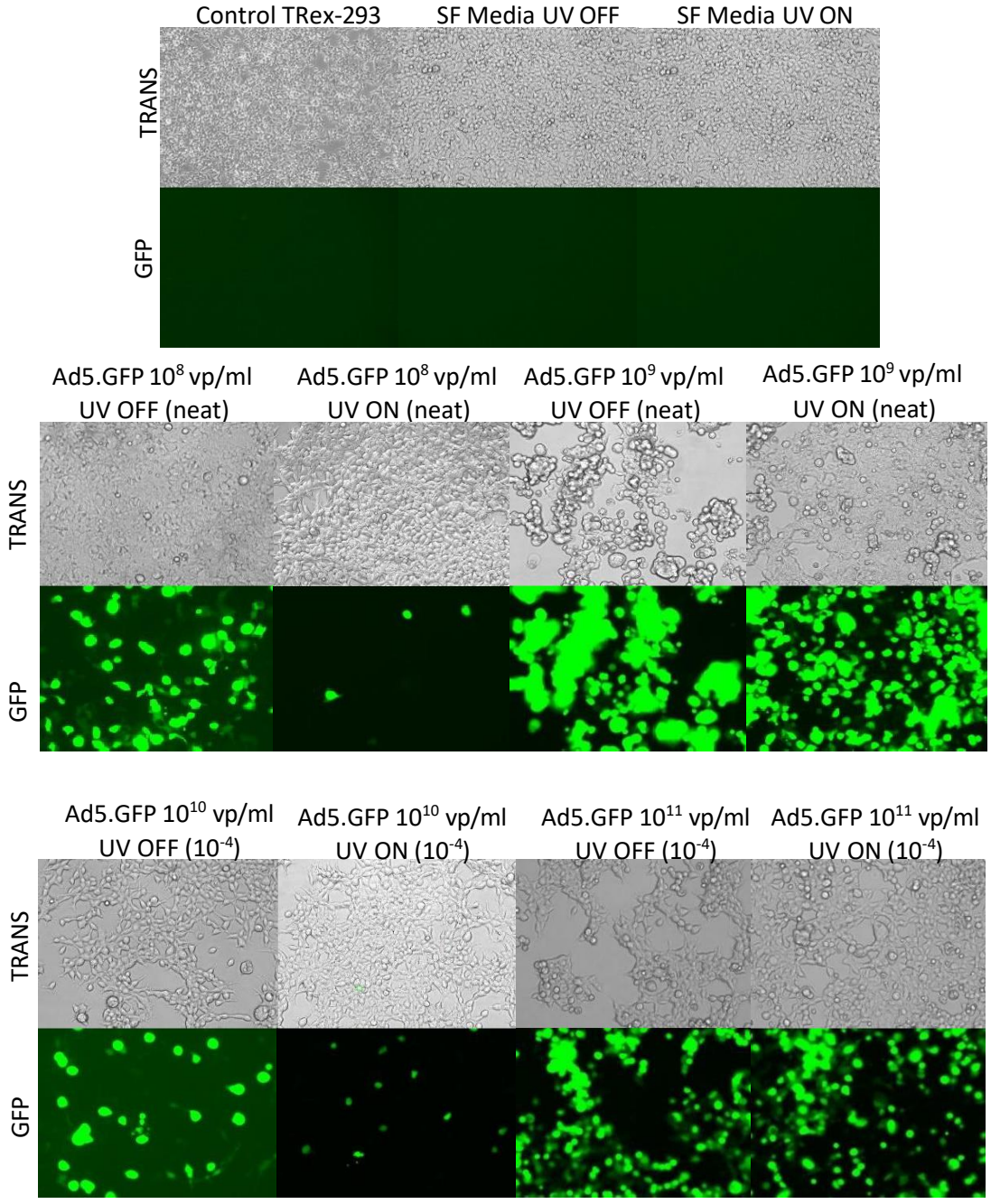

Figure 4.5. EVOS Imaging of TRex-293 Cells Infected with Samples that had been Exposed to Active/Inactive Ultravision™. *Top panels (TRANS) were imaged using transmitted light (brightfield). Bottoms panels (GFP) were imaged using the GFP light source. All wells were imaged using a x20 objective lens. Cells infected with Ad5.GFP exposed to active Ultravision™ were compared with those infected with Ad5.GFP exposed to inactive Ultravision™. Samples collected following aerosolisation of Ad5.GFP starting at 1 x10^8 and 1 x 10^{9}vp/ml were added to the cells neat, however samples collected following aerosolisation of Ad5.GFP at 1 x 10^{10} and 1 x 10^{11}vp/ml were diluted by 10^{-4} (1:10000). Numeration of fluorescent cells per well was used to calculate pfu/ml values for each collected sample.*

***Table 4.1. Functional Titers (pfu/ml Determined by Plaque Assay Analysis**. Functional Titers (pfu/ml) of Each Sample Collected from the Collection Pot, Following Ad5.GFP Exposure to Inactive/Active Ultravision™, Determined by Plaque Assay. Ad5.GFP that was aerosolised at 10^{11}vp/ml produced an immeasurable number of fluorescent cells, therefore the functional titer of such samples were undetermined, but assumed to be >10^8pfu/ml.*

Sample	Functional Titer
Ad5.GFP at 1 x 10^8vp/ml: UV OFF	4.2 x 10^5 pfu/ml
Ad5.GFP at 1 x 10^8vp/ml: UV ON	1.8 x 10^4 pfu/ml
Ad5.GFP at 1 x 10^9vp/ml: UV OFF	1.5 x 10^6 pfu/ml
Ad5.GFP at 1 x 10^9vp/ml: UV ON	1.2 x 10^5 pfu/ml
Ad5.GFP at 1 x 10^{10}vp/ml: UV OFF	3.3 x 10^8 pfu/ml
Ad5.GFP at 1 x 10^{10}vp/ml: UV ON	7.1 x 10^7 pfu/ml
Ad5.GFP at 1 x 10^{11}vp/ml: UV OFF	Undetermined, >10^8 pfu/ml
Ad5.GFP at 1 x 10^{11}vp/ml: UV ON	Undetermined, >10^8 pfu/ml

4.3. Discussion

In summary, this chapter highlighted valuable proof-of-concept preliminary data, supporting the hypothesis that Ultravision™ can capture and inactivate aerosolised virus particles, albeit to an inefficient extent. These data indicate the feasibility of aerosolising and recovering various dilutions of Ad5.GFP through the prototype closed-system, whilst maintaining viral viability and structural integrity. This was important to note prior to advancing with subsequent studies.

Although the prototype model was satisfactory for performing preliminary studies, several limitations were identified which rendered it incapable of producing accurate and reliable data. Although experiments were run in order of using the weakest to most concentrated Ad5 dilutions, to minimise contamination, it appeared that the PVC tubing, plastic syringe and other components of the system were contaminated nonetheless, therefore skewing qPCR and NanoSight results. Autoclavable glassware was required to replace all plastic materials used within the prototype model system, to ensure complete decontamination

between experimental runs. Secondly, premature condensation of the aerosol samples resulted in the accumulation of liquid within the system, which contained active virus particles (**figure 4.6**). This was problematic, as Ultravision^{TM} is only capable of ionising and precipitating particles that are suspended within aerosol solutions. Unknown volumes of prematurely condensed aerosol samples directly entered the collection pot, avoiding exposure to Ultravision^{TM}, thereby tainting the collected samples with active Ad5.GFP. This resulted in misleading plaque assay and transduction assay results, which displayed much higher concentrations of active virus particles than previously predicted. It was hypothesised that heating the model system to approximately 37°C in future studies would maintain sample aerosolisation, without affecting virus viability. Thirdly, issues were observed with the mesh nebuliser (**figure 4.7**). Gaps in the side of the nebuliser permitted the escape of small volumes of aerosolised samples, perhaps explaining the decreased volume of samples collected within the collection pot. Not only did this limit the amount of virus exposed to Ultravision^{TM}, but it also represented a potential safety hazard, as the system was unable to retain and enclose the aerosolised virus samples.

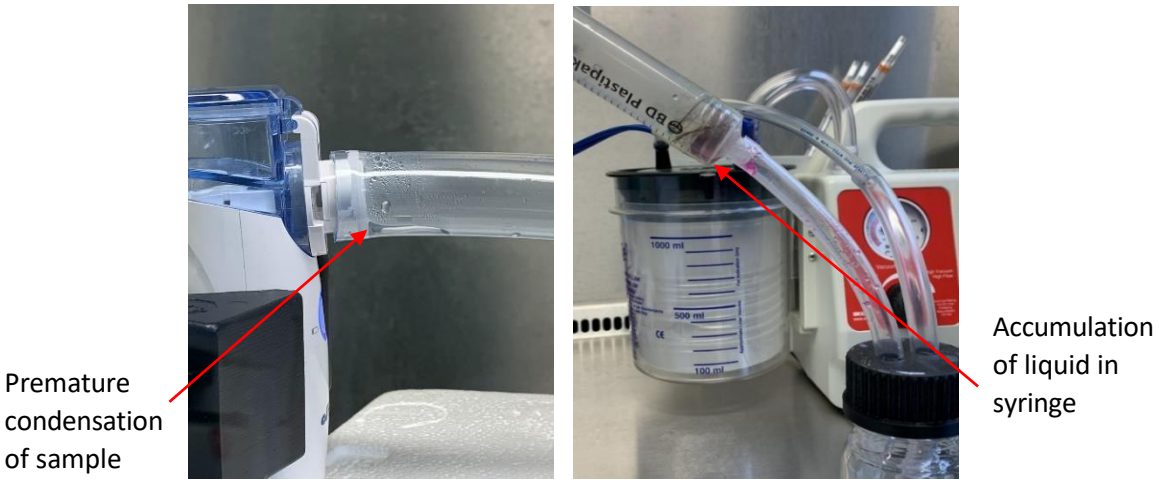

Figure 4.6*. *Images of the Prototype Closed-System Model During Sample Aerosolisation. *Premature condensation of the aerosol was observed at the nozzle of the nebuliser, causing a build-up of liquid in the PVC tubing. This accumulation of liquid proceeded downwards into the plastic syringe, where it either gathered beneath the copper coil or directly entered the collection pot. The unknown volume of sample that was prematurely condensed was not exposed to Ultravision^{TM} and thereby still contained a high concentration of active virus particles.*

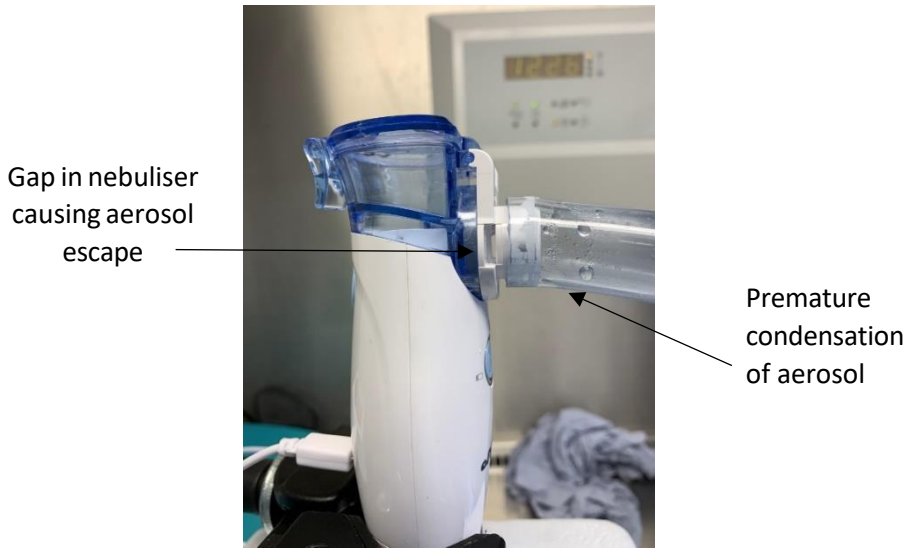

***Figure 4.7*. An Image of the Mesh Nebuliser During Sample Aerosolisation within the Prototype Closed-System Model.** *Gaps in the side of the nebuliser enabled aerosol escape, reducing the volume of sample aerosolised through the system. This image also highlights the premature condensation of the aerosol sample within the PVC tubing, prior to reaching the Ultravision™ Ion Wand.*

The data acquired from qPCR analysis suggested conflicting results (**Figure 4.2**). Virus capture was significant following exposure of Ad5.GFP at 1 x 10^9vp/ml to active Ultravision™, however virus capture was not successful upon exposure of more concentrated samples of Ad5.GFP to Ultravision™. However, the method of analysis may have been inappropriate for determining virus capture, and consequently may have led to misleading results. qPCR solely measures the contents of genetic material and does not directly quantify the number of intact virus particles within a sample. It is possible that Ultravision™ caused Ad5.GFP to degrade, thereby releasing its internal genetic material. As DNA is too small to be captured via electrostatic precipitation, it is likely that the isolated viral DNA remained suspended in aerosol and was therefore collected within the collection pot. This would explain the presence of viral DNA within the collection pot following sample exposure to active Ultravision™. Therefore, the assumption that Ultravision™ was capable of capturing virus particles was maintained, although the exact mechanism remained unknown.

A key finding of this preliminary study was that Ultravision™ successfully inactivated aerosolised non-enveloped virus particles (**Figures 4.3** and **4.4**). Although qPCR results indicated that Ultravision™ did not capture intact viral particles, transduction and plaque assay analysis indicated that Ultravision™ inactivated Ad5.GFP. It was hypothesised that

reactive species generated by the electrically charged Ion Wand caused structural degradation of the viral particles, resulting in viral inactivation. Ad5.GFP degradation may have enabled the release of viral genetic material. Further, isolated viral DNA, that is not enclosed within a viral capsid, is unable to cause infection or disease (Fenner, 1987. Gelderblom, 1996. Lentz, 2005). Therefore, regardless of the ability of Ultravision^{TM} to capture intact virus particles, its ability to inactivate aerosolised virus particles and potentially prevent airborne viral spread, was significant. However, these results encouraged additional experiments using an improved, refined closed-system to support the accuracy and reliability of the data obtained from this chapter.

Chapter 5: Evaluation of Ultravision™ to Capture and Inactivate Aerosolised Virus Particles using a Refined 'Closed-System' Model

5.1. Introduction

5.1.1. Refinement of the Closed-System Ultravision™ Model

To obtain more accurate and reliable data regarding the capability of Ultravision™ to capture and inactivate viral particles, a refined model system was required. Although the prototype system provided satisfactory proof-of-concept data, suggesting that Ultravision™ was somewhat capable of capturing and inactivating aerosolised virus particles, the extent of which remained unknown. Using information gathered from Chapter 4, a new and improved closed-system Ultravision™ model was designed and constructed in preparation for experimental analysis (**Figure 5.1**).

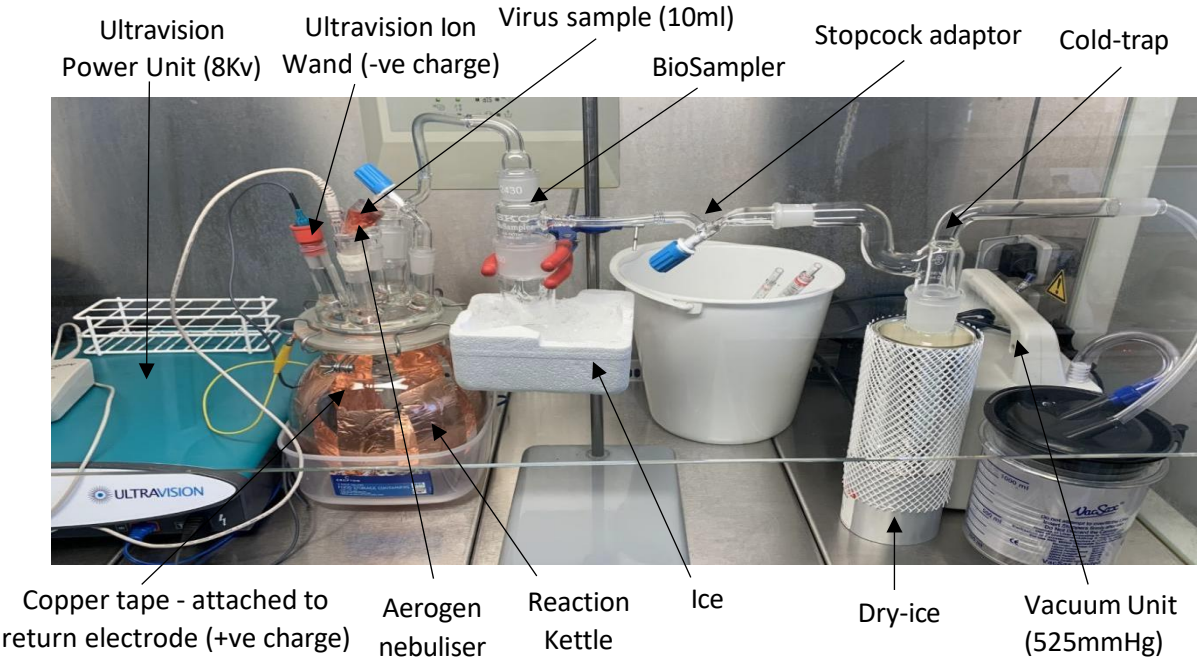

***Figure 5.1*. *Experimental Setup of the Refined Closed-System Model**. For each run, 10ml virus samples were loaded into the Aerogen nebuliser and aerosolised directly into the air-tight reaction kettle. Consequently, the aerosolised virus particles were exposed to the Ultravision™ Ion Wand. The Ion Wand emitted negatively charged ions, thereby negatively charging the aerosolised virus particles. Copper tape covering the inside of the reaction kettle was attached to the positively charged return electrode, functioning as a collector plate for precipitated particles. A vacuum unit was used to suction the sample through the system, maintaining a unidirectional flow of aerosol. Following exposure to Ultravision™, the aerosol samples were suctioned upwards into the BioSampler for sterile collection. Immediately after experimentation, collected samples were transferred into sterile falcons and stored at -80°C, in preparation for experimental analysis. A cold-trap was employed between the BioSampler and vacuum unit to prevent contamination of the vacuum.*

The prototype model used in Chapter 4 harboured many practical issues, including viral contamination, aerosol escape, inefficient sample aerosolisation and premature sample condensation, all of which made the standardisation of constant variables such as aerosol flow rate, sample volume, pressure and overall electrostatic precipitation efficiency near impossible to maintain. Therefore, the purpose of developing a refined system was to ensure repeatability and standardisation of all experimentation to produce more dependable, conclusive results. As the overarching aim of this project was to evaluate the ability of Ultravision™ to capture and inactivate aerosolised virus particles, to prevent the transmission of disease in hospital settings, it was important to use a model system that accurately represented real-life scenarios.

To mimic the authentic release of bioaerosols observed during medical procedures, the mesh nebuliser that was used to atomise particles in the prototype system was replaced with a medical grade Aerogen nebuliser (Aerogen® Solo Starter Kit, Aerogen Ltd, Galway, AG-A53000-XX). Aerogen nebulisers are used in acute care aerosol drug delivery. They enable better control of aerosolisation, without the risk of leakage or aerosol escape, and require minimal management (Dunne and Shortt, 2018). Additionally, the sample reservoir of an Aerogen nebuliser is isolated from the nebulisation circuit, thereby reducing the risk of sample contamination (Aerogen, 2022). The Aerogen nebuliser output nozzle is attached to an extended length of tubing, thus regulating the direction of the aerosol flow, reducing the risk of premature condensation and aerosol escape.

To better represent closed-surgery, a 3L glass reaction kettle was used to contain the aerosol sample, as opposed to the PVC tubing and plastic syringe used in the prototype system. The reaction kettle was chosen for three main reasons. Firstly, QuickFit glassware is autoclavable, therefore ensuring complete decontamination prior to use. Secondly, during laparoscopic surgery, the human abdomen is distended to approximately 3L in volume via CO_2 insufflation to enable surgical entry (Krishnakumar and Tambe, 2009). Efficient use of the Ultravision™ Ion Wand in 3L air spaces has therefore already been tested and approved. Additionally, the flanges attached to the reaction kettle lid enabled placement of the Ion Wand directly above the aerosol, as it would be during laparoscopic surgery. Finally, QuickFit glass stopcock-adapters were used to direct the flow of aerosol, as they are also autoclavable and adjoin to the reaction kettle to create a perfectly air-tight system.

In most experimental runs, the Ultravision^{TM} Ion Wand was charged at 8kV. However, unlike in the preliminary study, the distance between the Ion Wand and the copper return was measured. This enabled calculation of the Ion Wand's true electric charge in accordance with Ohm's law. To maintain consistency, the true electric charge of the Ion Wand remained the same in each experimental run, excluding runs that involved alterations of the Ion Wand voltage as an independent variable. Additionally, parameters thought to alter electrostatic precipitation were modified in subsequential experiments. For example, parameters such as flow rate, temperature and the number of Ion Wands present in the reaction kettle were evaluated. Such evaluation was performed to determine the optimal conditions required for Ultravision^{TM} usage, resulting in maximal capture and inactivation of aerosolised virus particles.

In comparison with the copper-coil that was connected to the return electrode in the prototype system, the refined closed-system utilised copper tape. The tape was used to cover the inside of the reaction kettle, serving as a positively charged collector plate for precipitated particles. This alteration increased the surface area of the collector plate, to improve the efficiency of electrostatic precipitation. During laparoscopic surgery, the return electrode is attached to the patient's abdominal tissue, thereby creating a large positively charged surface area for bioaerosol precipitation. Therefore, the return electrode used in the refined closed-system strived to better resemble that of the patient's abdomen during surgery. However, copper is naturally virucidal (Govind, 2021), therefore it was important to repeat experiments using an inert material such as stainless steel. This was required to determine whether Ultravision^{TM} itself or the material of the return electrode was the main cause of viral inactivation. Experimental repeats using both metals were necessary to make accurate and reliable conclusions regarding the modalities of Ultravision^{TM} and its ability to inactivate virus particles.

The final major change made to the refined closed-system was the replacement of the collection pot with an SKC BioSampler. Although the glass beaker used in the prototype system was autoclavable, it was not air-tight nor designed to sample aerosols for the presence of virus particles. The BioSampler was chosen following extensive comparisons of various bioaerosol samplers discussed within the literature (Fabian, 2009. Kutter, 2021. Li, 2018). SKC BioSamplers enable the physical collection and recovery of aerosolised virus

particles into a known volume of media, aided by aerosol suction by a vacuum unit. BioSamplers maintain virus viability and structural integrity upon collection, obtaining efficient volumes of virus particles to be experimentally analysed (Niazi, 2021). Aerosol sampling efficiency was extremely important for this study, to precisely determine the volume of infectious virus particles present post exposure to Ultravision™. Additionally, the BioSampler was placed above the reaction kettle, permitting collection of aerosol samples only. Liquid droplets were too heavy to migrate upwards, against gravity, into the BioSampler, thereby avoiding contamination by prematurely condensed samples that were not affected by Ultravision™.

5.1.2. Chapter Aims and Hypotheses

The first aim of this chapter was to develop an improved, novel closed-system model, to evaluate the capabilities of Ultravision™. System adaptations and areas requiring improvement were highlighted by preliminary studies (Chapter 4). The second aim of this chapter was to compare the ability of Ultravision™ to capture and inactivate aerosolised virus particles in the refined closed-system to that in the prototype system. Thirdly, this chapter aimed to analyse the effects of altered parameters that modified the efficiency of electrostatic precipitation. Identifying parameters that allow optimal Ultravision™ performance was a key focus of this study. Such parameters included Ion Wand voltage, temperature, return electrode material, number of Ion Wands, aerosol flow rate and virus sample concentration. Finally, this chapter aimed to compare the effects of Ultravision™ on aerosolised enveloped and non-enveloped viruses, being SARS PV and Ad5.GFP respectively.

Overall, it was hypothesised that virus capture and inactivation would be more efficient and apparent in the refined closed-system, compared to that observed within the prototype closed-system. A list of individual hypotheses, relating to specific parameters and variables, are detailed below:

1. Increasing Ion Wand voltage above 8kV will cause a corresponding increase in viral uptake and inactivation. Likewise, decreasing the voltage below 8kV will reduce the amount of viral capture and inactivation.
2. Increasing the number of Ion Wands will result in Ion Wand synergism, enhancing viral capture and inactivation.

3. Altering variables that affect sample aerosolisation, such as ambient temperature and aerosol flow rate, will affect the efficiency of electrostatic precipitation.
4. Samples containing higher concentrations of virus will be less effected by Ultravision^{TM} than samples containing lower starting concentrations of virus.
5. The copper return electrode will inactivate virus particles following direct contact, due to the virucidal properties of copper.
6. A stainless-steel return electrode will not inactivate virus particles following direct contact, as stainless-steel is an inert metal.
7. Ultravision^{TM} will successfully capture and inactivate aerosolised enveloped and non-enveloped viruses to the same extent, regardless of their structure and charge.

5.2. Results

5.2.1 Run #1 – Inactivation of Aerosolised Ad5.GFP by Ultravision™ within the Refined Closed-System Model.

Following an extensive evaluation of the prototype model, the refined closed-system model was designed and constructed. Dependent variables such as Ion Wand voltage, virus sample concentration, virus sample volume and the surface area of the return electrode were optimised and standardised. In run #1, aerosolised Ad5.GFP (1 x 10^{10}vp/ml) was exposed to active and inactive Ultravision™ (separately) and the resulting samples were collected and analysed for viral presence and activity.

To evaluate whether Ultravision™ had successfully captured Ad5.GFP particles by electrostatic precipitation, qPCR was performed (**Figure 5.2**).

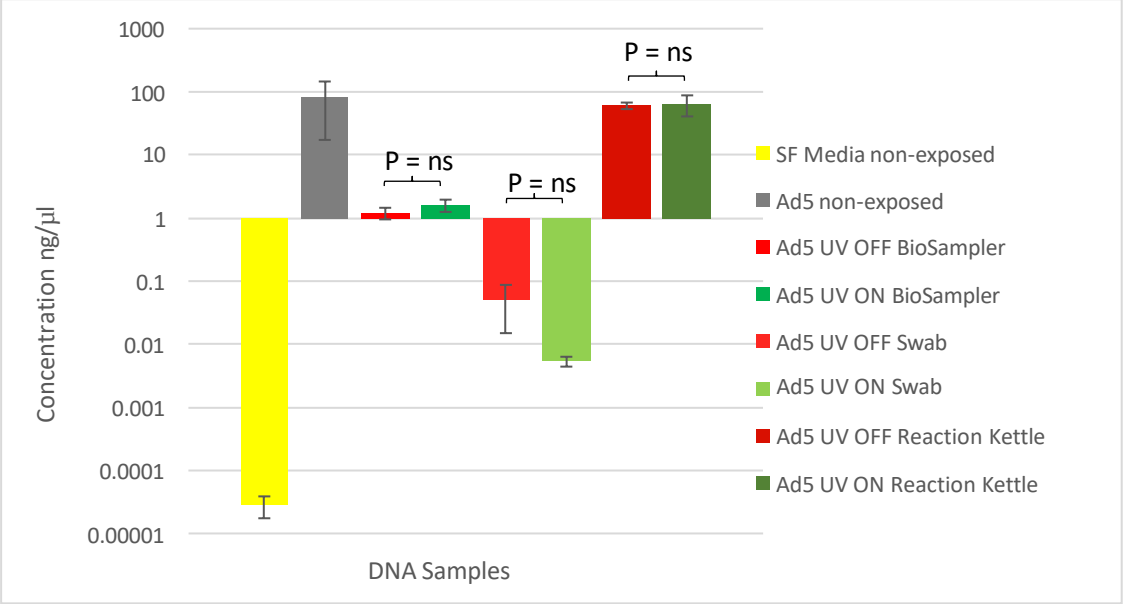

***Figure 5.2**. **Average DNA Concentrations Obtained from qPCR Amplification of Ad5 Genomes in Samples that had been Exposed to Ultravision™ – Run #1**. Samples were collected from the BioSampler, swabs of the copper return electrode and from the reaction kettle, following aerosolisation and exposure to Ultravision. Yellow bar: SF media non-aerosolised, non-exposed to Ultravision™. Grey Bars: Preparation of Ad5.GFP at 1 x 10^{10}vp/ml, non-aerosolised, non-exposed to Ultravision™. Red bars: Ad5.GFP exposed to inactive Ultravision™. Green bars: Ad5.GFP exposed to active Ultravision™. Assay performed in triplicate - graph displays mean values and SD +/-. The Student's T-test was performed to statistically analyse and compare data sets. ns = no statistically significant difference.*

The serum-free media sample contained no Ad5 genomes, thereby serving as a functional negative control. As expected, the non-exposed sample preparation of Ad5.GFP at 1 x 10^{10}vp/ml contained the highest concentration of viral DNA, serving as an adequate positive control.

Both samples collected from the BioSampler contained approximately the same number of Ad5 genomes, regardless of exposure to active or inactive Ultravision^{TM}. This indicated that Ultravision^{TM} did not successfully capture the aerosolised virus particles via electrostatic precipitation. Additionally, the concentration of Ad5 DNA in both BioSampler samples was less than that in the non-exposed preparation of Ad5.GFP, thus demonstrating a loss of virus particles following sample aerosolisation.

There was no significant difference in the number of viral genomes between the two samples collected from the reaction kettle, regardless of sample exposure to active or inactive Ultravision^{TM}. Once again, this indicated that virus capture by Ultravision^{TM} was unsuccessful. Interestingly, the number of Ad5 genomes in both reaction kettle samples was similar to that within the non-exposed preparation of Ad5.GFP. Samples collected from the reaction kettle were a result of premature aerosol condensation, thus containing virus particles that had not been aerosolised or sufficiently exposed to Ultravision^{TM}. Therefore, viral capture was unsuccessful, as the particles remained suspended within liquid solution, inhibiting electrostatic precipitation by Ultravision^{TM}.

Finally, the swab samples contained the lowest number of Ad5 genomes. This was partly due to dilution of the swab contents following inoculation in 2ml PBS. There was no significant difference in the concentration of Ad5 DNA between the swab samples obtained following Ad5.GFP exposure to active Ultravision^{TM} or inactive Ultravision^{TM}. This indicated that Ultravision^{TM} did not successfully precipitate virus particles onto the copper return electrode.

Next, a transduction assay was performed to assess viral activity within each of the collected samples (**Figure 5.3**). It was hypothesised that exposure of aerosolised Ad5.GFP to active Ultravision^{TM} would result in viral inactivation.

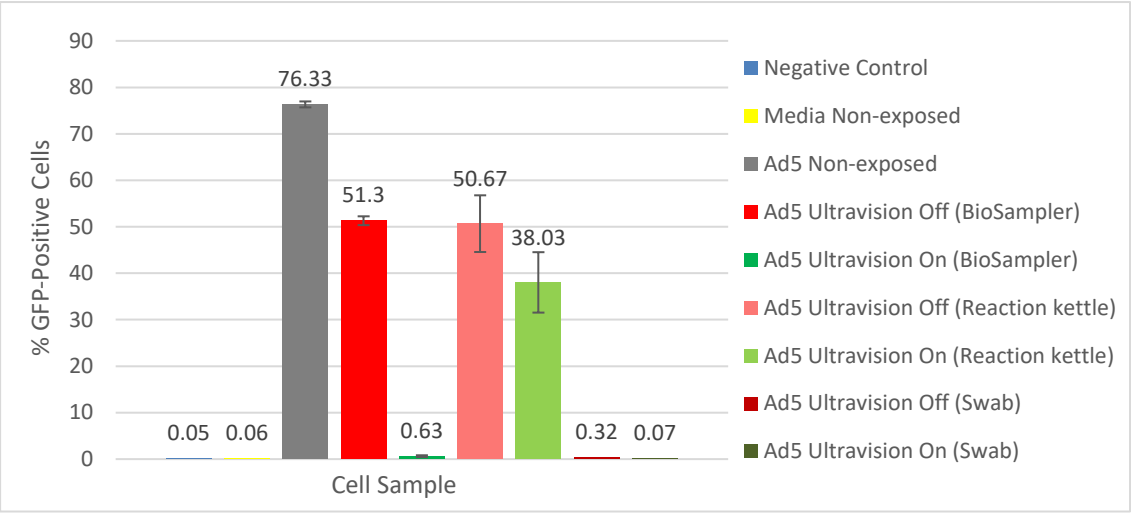

Figure 5.3. Average Percentage of CHO-CAR Cells Positive for GFP Fluorescence, Following Infection with Samples that had been Exposed to Active/Inactive Ultravision™, Determined by Flow Cytometry – Run #1*. Blue bar: CHO-CAR cells replenished with total media. Yellow bar: SF media non-aerosolised, non-exposed to Ultravision™. Grey bar: Ad5.GFP at 1 x 10^{10}vp/ml non-aerosolised, non-exposed to Ultravision™. Red bars: Ad5.GFP exposed to inactive Ultravision™. Green bars: Ad5.GFP exposed to active Ultravision™. Assay performed in triplicate - graph displays mean values and SD +/-. The Student's T-test was performed to statistically analyse and compare data sets. ** = 0.001, *** = 0.0001, * = 0.01 (statistically significant), ns = no significant difference.*

Cells exposed to SF media displayed no GFP-positive cells, thereby serving as satisfactory negative controls. Of the cells infected with the non-exposed preparation of Ad5.GFP at 1 x 10^{10}vp/ml, 76.33% were GFP-positive, thereby serving as a positive control and highlighting the initial infectivity status of the virus sample.

Of the cells infected with Ad5.GFP that had been exposed to inactive Ultravision™ and collected from the BioSampler, 51.3% were GFP-positive. This indicated that some of the virus particles were either lost or inactivated as a result of aerosolisation through the system. There was a statistically significant 81.4-fold reduction in the percentage of GFP-positive cells following infection with the Ad5.GFP sample that had been exposed to active Ultravision™ and collected from the BioSampler. This suggested that Ultravision™ was capable of efficiently inactivating aerosolised virus particles. It also implied that electrostatic precipitation was more efficient within the refined closed-system, which more closely resembled key-hole surgery, than in the prototype system.

Samples collected from the reaction kettle condensate contained high levels of active virus and did not differ statistically following exposure to active or inactive Ultravision^{TM}. This supported the hypothesis that Ultravision^{TM} was unable to influence particles that were suspended within liquid solution and could only precipitate and/or inactivate particles that were suspended within aerosols.

Finally, both swab samples, that were taken from the copper return, caused very little to no transduction in the CHO-CAR cells. Although the swab samples were diluted in 2ml PBS, viral activity should still have been apparent, relative to the concentration of viral DNA within each sample, as displayed by qPCR (**figure 5.3**). This surprising result indicated that the copper return may have inactivated the virus particles upon direct contact, regardless of the status of Ultravision^{TM}, due to its virucidal nature. Future studies using an inert metal, such as stainless-steel, rather than copper, were therefore required to deduce the exact cause of viral inactivation.

To validate results gathered from the transduction assay, a plaque assay was performed. TRex-293 cells were infected with the collected samples and analysed via EVOS imaging (**Figure 5.4**).

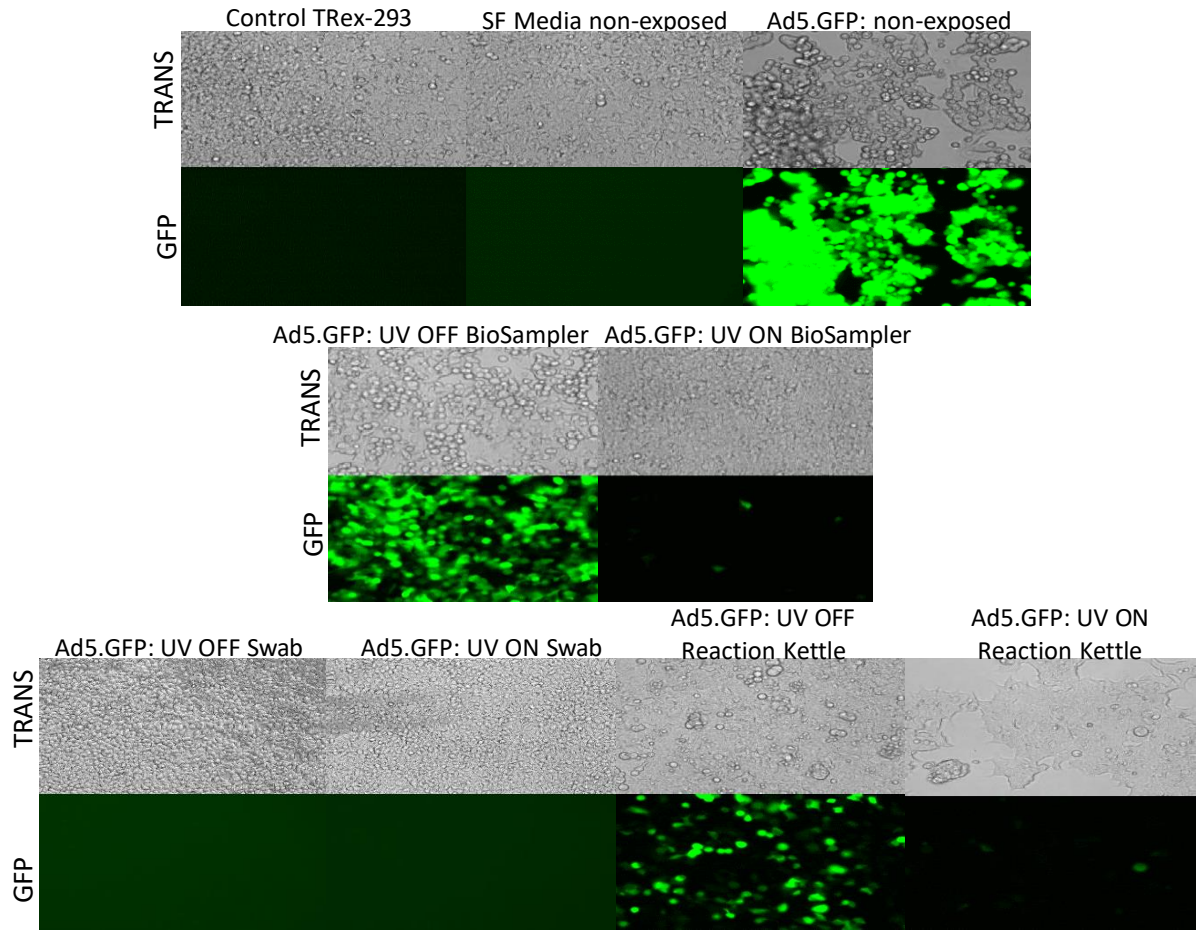

Figure 5.4. EVOS Imaging of TRex-293 Cells Infected with Ad5.GFP Samples that had been Exposed to Inactive/Active Ultravision™ – Run #1. *Top panels (TRANS) imaged using transmitted light (brightfield). Bottoms panels (GFP) imaged using the GFP light source. All wells were imaged using a x20 objective lens. Control: TRex-293 cells replenished with total media. Non-exposed: Sample non-aerosolised and non-exposed to Ultravision™. Green fluorescence under GFP light source resembles viral infection. Manual counting of fluorescent cells per field of view enabled calculation of pfu/ml per sample.*

Table 5.1. Functional Titers Determined by Plaque Assay Analysis - Run #1.

Sample	Functional Titer
Ad5.GFP: non-exposed	3 x 10^8pfu/ml
Ad5.GFP: UV OFF BioSampler	3 x 10^8pfu/ml
Ad5.GFP: UV ON BioSampler	3.6 x 10^5 pfu/ml
Ad5.GFP: UV OFF Swab	-
Ad5.GFP: UV ON Swab	-
Ad5.GFP: UV OFF Reaction Kettle	4.2 x 10^6pfu/ml
Ad5.GFP: UV ON Reaction Kettle	7.1 x 10^5pfu/ml

TRex-293 cells that were replenished with total media served as negative controls and displayed no green fluorescence under the GFP light source. Cells exposed to the SF media sample also remained uninfected, indicating the absence of active Ad5.GFP. As expected, cells infected with the non-exposed sample of Ad5.GFP generated the highest number of fluorescent cells, achieving a functional titer of approximately 3 x 10^8pfu/ml. In comparison, cells infected with the Ad5.GFP samples that had been exposed to inactive Ultravision™ and collected from the BioSampler generated a slightly lower number of fluorescent cells, albeit maintaining a high functional titer, thus mirroring the results obtained from the transduction assay. However, Ad5.GFP samples that had been exposed to active Ultravision™ and collected from the BioSampler produced a far lower number of fluorescent cells, achieving a functional titer of 3.6 x 10^5pfu/ml. This significant 833.3-fold reduction in active Ad5.GFP indicated that active Ultravision™ successfully inactivated a significant proportion of the aerosolised virus particles.

Both swab samples caused no transduction in the TRex-293 cells, as displayed by the complete absence of fluorescence. It was hypothesised that upon direct contact with the virucidal copper return, Ad5.GFP particles were inactivated, thus mirroring transduction assay results once again.

Conversely, the number of active Ad5.GFP particles within the reaction kettle samples detected via plaque assay differed to that detected via transduction assay. **Figure 5.4** shows a significant number of fluorescent cells in the TRex-293 populations that were infected with the reaction kettle samples that had been exposed to inactive Ultravision™. In comparison, cells infected with the reaction kettle samples that had been exposed to active Ultravision™ displayed a significant reduction in fluorescence, indicating successful inactivation. These results are therefore contradictory to the transduction assay results, as they demonstrate that Ultravision™ was in fact capable of inactivating virus particles that were suspended within liquid solution. Alternatively, direct contact between Ad5.GFP and the charged copper return may have altered or damaged the virus's external structure, preventing it from infecting TRex-293 cells, whilst simultaneously having no effect on its ability to bind with CAR and infect CHO-CAR cells. The reason for such conflicting results remained unknown and requires further experimental evaluation.

5.2.2. Run #2 – Capture and Inactivation of Diluted Samples of Ad5.GFP by Ultravision™ within the Refined Closed-System Model.

To better mimic the release of bioaerosols that occurs during surgery, the concentration of aerosolised Ad5.GFP was reduced from 1 x 10^{10}vp/ml in run #1, to 1 x 10^{7}vp/ml and 1 x 10^{8}vp/ml in run #2 (**Figure 5.5**). Lowering the sample concentration aimed to more accurately represent the concentrations of virus that Ultravision™ may be exposed to in real-life scenarios (Johnson, et al. 2022). Therefore, run #2 evaluated the ability of Ultravision™ to capture and inactivate Ad5.GFP from diluted aerosol samples.

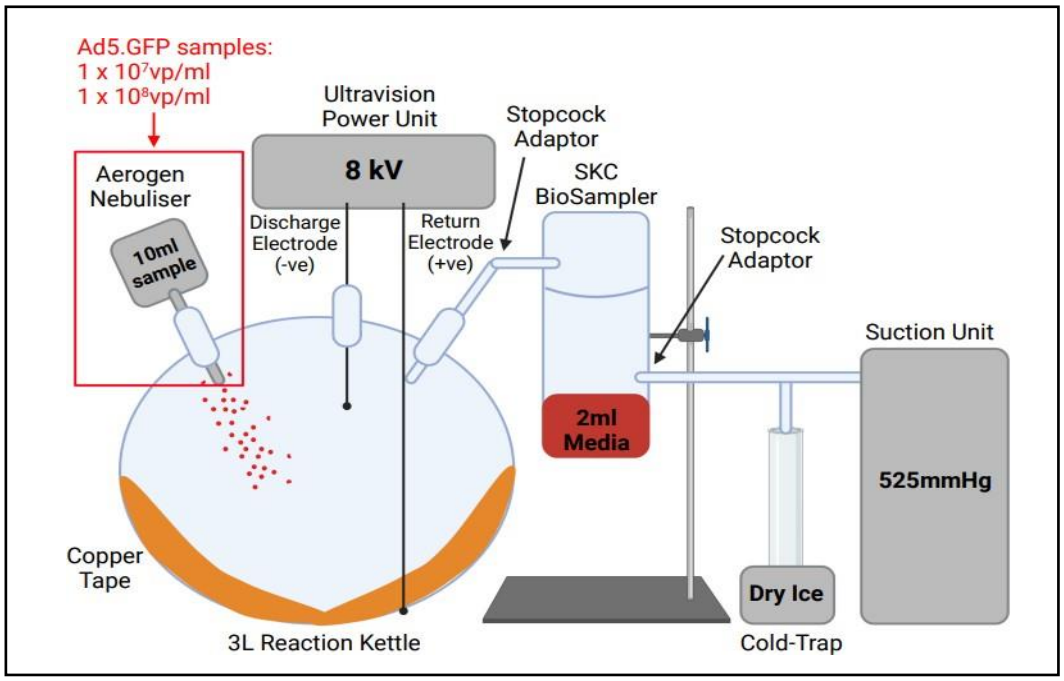

***Figure 5.5**. **A Schematic Depicting the Experimental Setup of Run #2**. The red box highlights the independent variable of run #2. The starting concentration of Ad5.GFP that was aerosolised through the system and exposed to Ultravision™ was reduced from 1 x 10^{10}vp/ml in run #1, to 1 x 10^{7}vp/ml and 1 x 10^{8}vp/ml. Therefore, four 10ml samples of Ad5.GFP were aerosolised through the system – Ad5.GFP at 1 x 10^{7}vp/ml exposed to 1) inactive Ultravision™, 2) active Ultravision™, and Ad5.GFP at 1 x 10^{8}vp/ml exposed to 1) inactive Ultravision™, 2) active Ultravision™.* Following aerosolisation, samples were collected from the BioSampler and from the reaction kettle condensate and stored at -80°C, in preparation for experimental analysis.

qPCR was performed to determine the concentration of Ad5 genomic DNA in each of the collected samples (**Figure 5.6**). This was carried out to evaluate the ability of Ultravision™ to capture Ad5.GFP particles from more dilute viral samples.

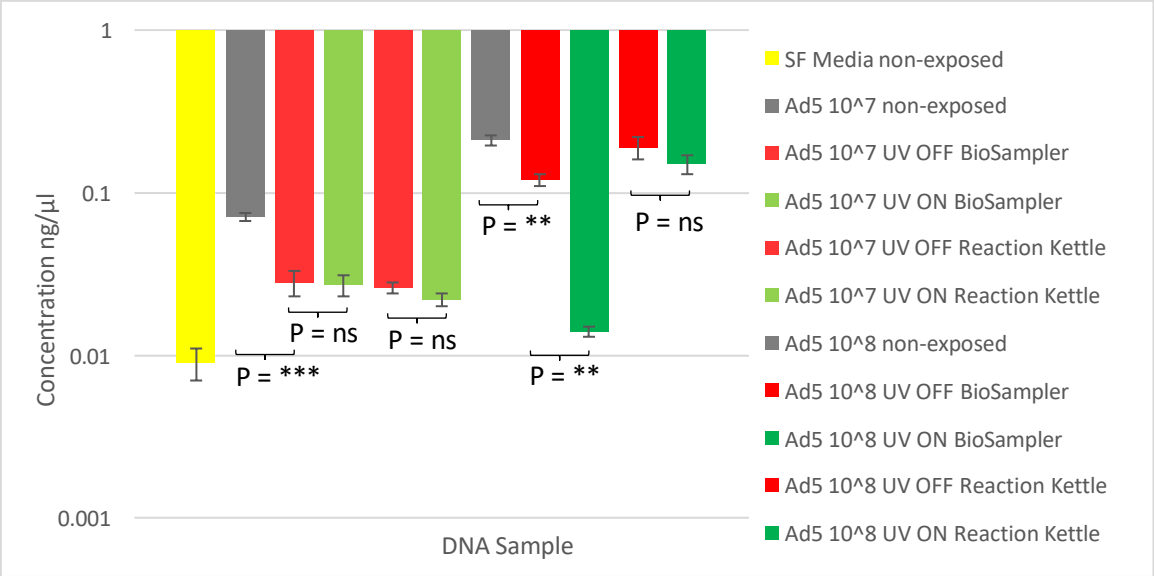

***Figure 5.6*. Average DNA Concentrations Determined by qPCR Amplification of Ad5 Genomes in Diluted Samples of Ad5.GFP that had been Exposed to Ultravision™ – Run #2**. *Yellow bar: SF media non-aerosolised, non-exposed to Ultravision™. Grey Bars: Preparations of Ad5.GFP at 1 x 10^7 and 1 x 10^8vp/ml, non-aerosolised, non-exposed to Ultravision™. Red bars: Ad5.GFP exposed to inactive Ultravision™. Green bars: Ad5.GFP exposed to active Ultravision™. Assay performed in triplicate - graph displays mean values and SD +/-. The Student's T-test was performed to statistically analyse and compare data sets. *** = 0.0004 (Ad5 10^7 non-exposed: Ad5 10^7 UV OFF BioSampler), ** = 0.0013 (Ad5 10^8 non-exposed: Ad5 10^8 UV OFF BioSampler), ** = 0.003 (statistically significant), ns = no significant difference.*

The serum-free media sample displayed a very low level (essentially zero) presence of Ad5 genomes. This contamination was considered when evaluating the data obtained from the experimental samples. Although the number of Ad5 genomes within the non-exposed preparations of Ad5.GFP was fairly low, it was proportional to the dilution factor of each sample. These qPCR results highlighted unsuccessful precipitation of virus particles following the exposure of Ad5.GFP at 1 x 10^7vp/ml to active Ultravision™. It was hypothesised that the viral concentration of the aerosolised sample was too low for accurate detection by qPCR. Therefore, following run #2, all subsequential experiments aerosolised Ad5.GFP at 1 x 10^{10}vp/ml, facilitating the detection of viral DNA within collected samples. On the other hand, Ad5.GFP at 1 x 10^8vp/ml, that was exposed to active Ultravision™, displayed a

significant decrease in the concentration of Ad5 genomic DNA. This indicated that Ultravision™ successfully captured a proportion of the aerosolised virus particles via electrostatic precipitation.

To evaluate the ability of Ultravision™ to inactivate aerosolised Ad5.GFP, a transduction assay was performed (**Figure 5.7**). CHO-CAR cells were infected with the collected samples and analysed for GFP expression by Flow Cytometry.

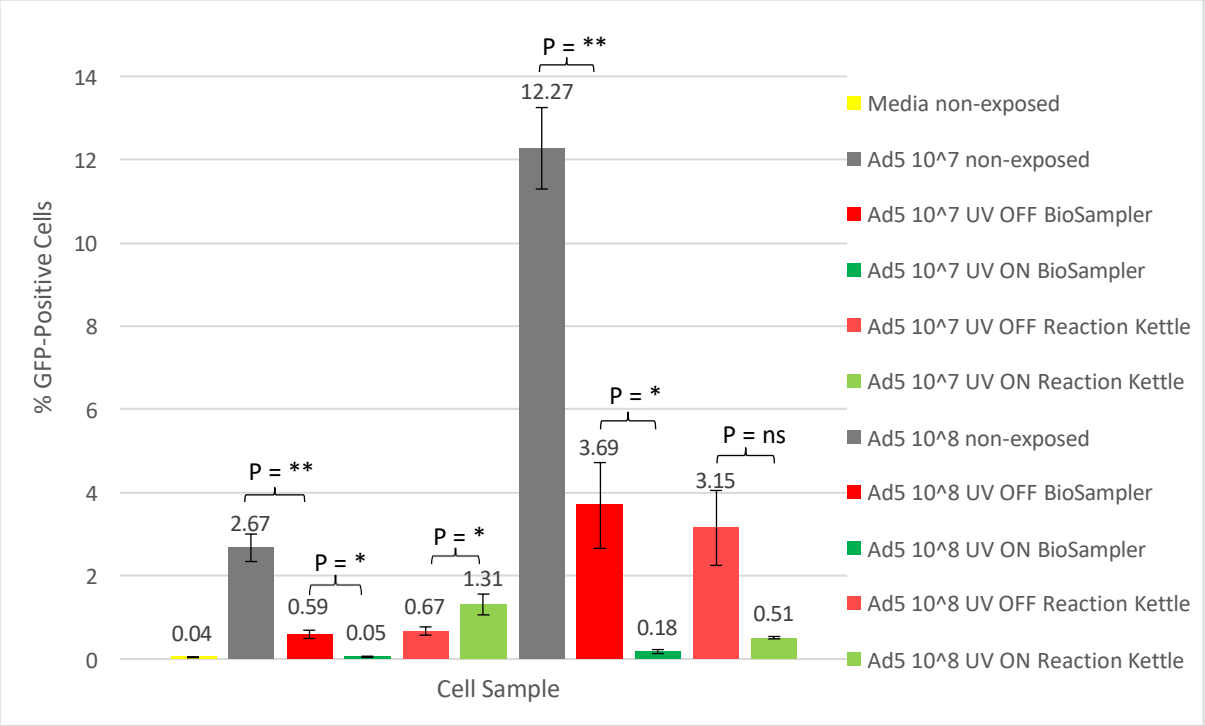

***Figure 5.7*. Average percentage of CHO-CAR Cells Positive for GFP Fluorescence, Following Infection with Diluted Samples of Ad5.GFP that had been Exposed to Inactive/Active Ultravision™, Determined by Flow Cytometry – Run #2**. *Higher GFP fluorescence correlates to a higher number of active virus particles within each sample. Yellow bar: SF media non-aerosolised, non-exposed to Ultravision™. Grey bars: Preparations of Ad5.GFP at 1 x 10^7 and 1 x 10^8vp/ml, non-aerosolised, non-exposed to Ultravision™. Red bars: Ad5.GFP exposed to inactive Ultravision™. Green bars: Ad5.GFP exposed to active Ultravision™. Assay performed in triplicate - graph displays mean values and SD +/-. The Student's T-test was performed to statistically analyse and compare data sets. ** = 0.0087 (Ad5 10^7 non-exposed: Ad5 10^7 UV OFF BioSampler), * (Ad5 10^7 UV OFF BioSampler: Ad5 10^7 UV ON BioSampler) = 0.0253, * (Ad5 10^7 UV OFF Reaction Kettle: Ad5 10^7 UV ON Reaction Kettle) = 0.0345, ** = 0.0056 (Ad5 10^8 non-exposed: Ad5 10^8 UV OFF BioSampler), * (Ad5 10^8 UV OFF BioSampler: Ad5 10^8 UV ON BioSampler) = 0.0127 (statistically significant), ns = no significant difference.*

The serum-free media caused no transduction in CHO-CAR cells, demonstrating an absence of active Ad5.GFP and serving as an efficient negative control. Non-exposed preparations of Ad5.GFP at 1 x 10^7 and 1 x 10^8vp/ml caused 2.67% and 12.27% transduction, respectively. Transduction was significantly reduced in cells that were infected with the Ad5.GFP samples that had been exposed to active Ultravision^{TM} and collected from the BioSampler. This was true for both dilutions of Ad5.GFP, indicating that Ultravision^{TM} was capable of inactivating diluted samples of aerosolised Ad5.GFP. Therefore, it was concluded that reducing the number of particles exposed to Ultravision^{TM} did not alter the efficiency of electrostatic precipitation.

Interestingly, the level of transduction was significantly reduced in cells that were infected with Ad5.GFP at 1 x 10^7vp/ml that had been exposed to active Ultravision^{TM} and collected from the reaction kettle. This was an unexpected observation, as it was previously hypothesised that Ultravision^{TM} could not inactivate or precipitate virus particles from liquid samples. In contrast, there was no significant difference in cellular transduction following infection with Ad5.GFP at 1 x 10^8vp/ml that had been exposed to active Ultravision^{TM} and collected from the reaction kettle.

To confirm data gathered from the transduction assay, a plaque assay was carried out. TRex-293 cells were infected with the samples collected from run #2 and analysed for GFP fluorescence via EVOS imaging (**Figure 5.8**).

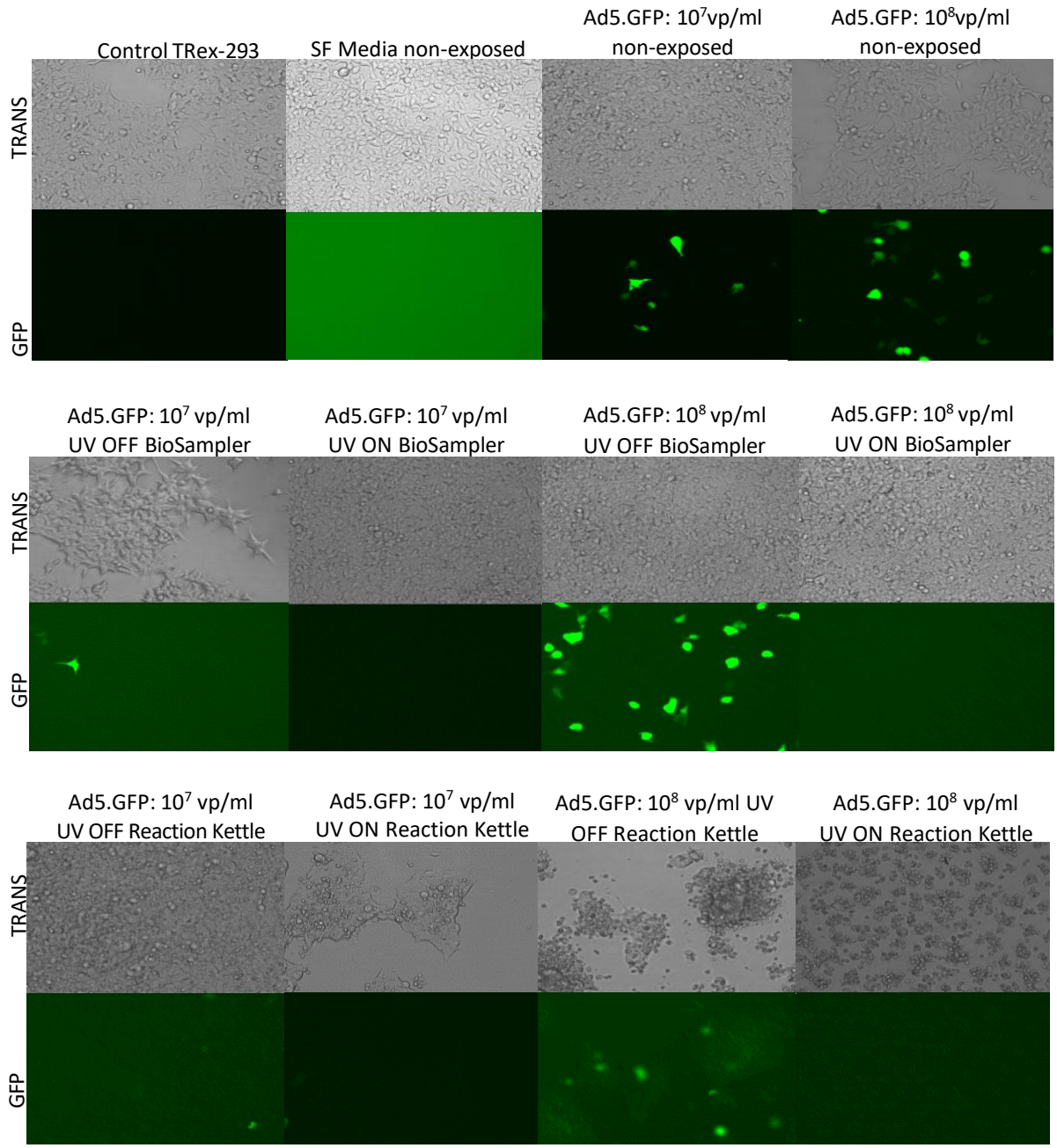

***Figure 5.8*. EVOS Imaging of TRex-293 Cells Infected with Diluted Samples of Ad5.GFP that had been Exposed to Ultravision™ – Run #2.** *Top panels (TRANS) imaged using transmitted light (brightfield). Bottoms panels (GFP) imaged using the GFP light source. All wells were imaged using a x20 objective lens. Samples collected following aerosolisation of Ad5.GFP at 1 x 10^7vp/ml and 1 x 10^8vp/ml and exposure to Ultravision. Control: TRex-293 cells replenished with total media. Non-exposed: Sample non-aerosolised and non-exposed to Ultravision™. Green fluorescence under GFP light source resembles viral infection. Manual counting of fluorescent cells per field of view enabled calculation of pfu/ml values for each sample.*

Table 5.2. Functional Titers Determined by Plaque Assay Analysis - Run #2

Sample	Functional Titer
Ad5.GFP: 10^7vp/ml non-exposed	1.6 x 10^6pfu/ml
Ad5.GFP: 10^8 vp/ml non-exposed	1 x 10^7pfu/ml
Ad5.GFP: 10^7 vp/ml UV OFF BioSampler	2.3 x 10^5 pfu/ml
Ad5.GFP: 10^7 vp/ml UV ON BioSampler	-
Ad5.GFP: 10^8 vp/ml UV OFF BioSampler	7.1 x 10^6 pfu/ml
Ad5.GFP: 10^8 vp/ml UV ON BioSampler	-
Ad5.GFP: 10^7 vp/ml UV OFF Reaction Kettle	5.9 x 10^2pfu/ml
Ad5.GFP: 10^7 vp/ml UV ON Reaction Kettle	-
Ad5.GFP: 10^8 vp/ml UV OFF Reaction Kettle	2.4 x 10^6 pfu/ml
Ad5.GFP: 10^8 vp/ml UV ON Reaction Kettle	-

Serum-free media samples displayed no signs of active Ad5.GFP. In contrast, cells infected with the non-exposed preparations of Ad5.GFP displayed fluorescence, relative to the initial dilution of each virus preparation. Cells infected with Ad5.GFP at 1 x 10^7vp/ml and 1 x 10^8vp/ml that had been exposed to active Ultravision™ and collected from the BioSampler showed no detectable infectious virus particles. This indicated that Ultravision™ successfully inactivated the diluted samples of Ad5.GFP.

Unexpectedly, samples collected from the reaction kettle displayed similar results. Samples exposed to inactive Ultravision™ resulted in cellular transduction, whilst samples exposed to active Ultravision™ produced no detectable fluorescent cells. This indicated that Ultravision™, or the virucidal activities of the electrically charged copper return, inactivated Ad5.GFP particles that were suspended within the liquid condensate. However, trans images of the cells infected with the reaction kettle samples displayed an abundance of dead cells. This implied that there may have been a level of contamination within the reaction kettle samples. Alternatively, copper ions that were dissolved into the condensate may have caused the observed cell death and potentially the inactivation of Ad5.GFP. Experimental repeats using an inert collector plate were therefore required.

5.2.3. Run #3 – Capture and Inactivation of Ad5.GFP Following Exposure to Increased Voltages of Ultravision™ within the Refined Closed-System Model.

To evaluate parameters that affect the efficiency of electrostatic precipitation, three different voltages of Ultravision™ were analysed (**Figure 5.9**). In run #1, active Ultravision™ maintained a constant voltage of 8kV. However, in this experimental run, the ability of Ultravision™ to capture and inactivate aerosolised virus particles when active at 6kV, 8kV and 10kV was compared. At current, medical procedures that manipulate electrostatic precipitation to clear surgical smoke use Ultravision™ at approximately 8kV. However, analysing different voltages helps to improve our understanding of Ultravision™ and its effects on airborne virus particles, as well as detect an optimal voltage to use during surgery, that safely and efficiently reduces the spread of disease.

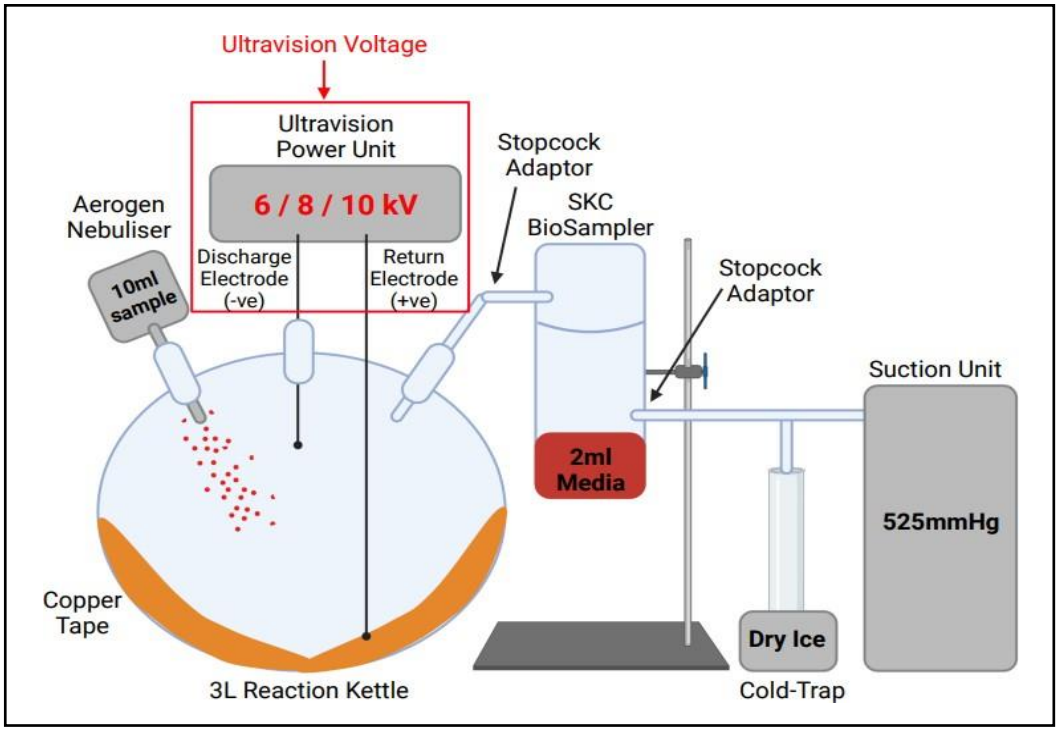

***Figure 5.9**. **A Schematic Depicting the Experimental Setup of Run #3.** The red box highlights the independent variable tested in this run. 10ml Ad5.GFP at 1 x 10^{10}vp/ml was aerosolised and exposed to inactive Ultravision™ or Ultravision™ active at 1) 6kV, 2) 8kV or 3) 10kV. Samples were collected from the BioSampler following complete sample aerosolisation and stored at -80°C, in preparation for analysis.*

qPCR was performed to determine the number of Ad5 genomes in each of the collected samples, to compare the level of virus capture by Ultravision™ at 6kV, 8kV and 10kV (**Figure 5.10**).

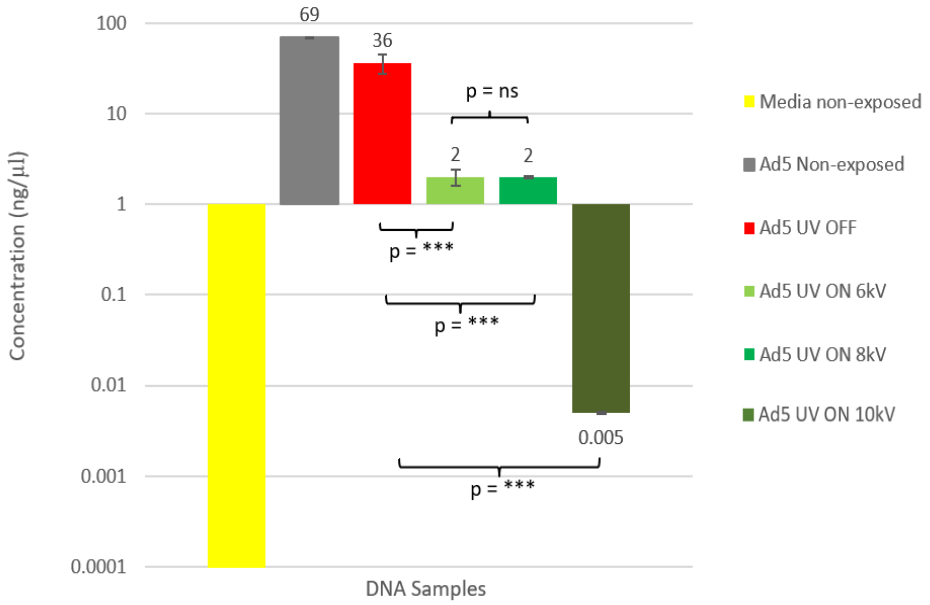

***Figure 5.10**. **Average DNA Concentrations Determined by qPCR Amplification of Ad5 Genomes in Samples of Ad5.GFP that had been Exposed to Various Voltages of Ultravision™ – Run #3**. Yellow bar: SF media non-aerosolised, non-exposed to Ultravision™. Grey bar: Preparation of Ad5.GFP at 1 x 10^{10} vp/ml, non-aerosolised, non-exposed to Ultravision™. Red bar: Ad5.GFP exposed to inactive Ultravision™. Green bars: Ad5.GFP exposed to active Ultravision™ at 6kV, 8kV and 10kV respectively. Assay performed in triplicate - graph displays mean values and SD +/-. The Student's T-test was performed to statistically analyse and compare data sets. *** (Ad5 UV OFF: Ad5 UV ON 6kV) = 0.0002, *** (Ad5 UV OFF: Ad5 UV ON 8kV) = 0.0002, *** (Ad5 UV OFF: Ad5 UV ON 10kV) = 0.0002 (statistically significant), ns = no significant difference.*

Ad5.GFP that had been aerosolised and exposed to inactive Ultravision™ displayed a high number of Ad5 genomes, albeit slightly less than the non-exposed Ad5.GFP preparation. This suggested that aerosolisation of the sample through the closed system caused a small, but significant loss of Ad5.GFP. A significant reduction in the concentration of viral DNA was observed in samples exposed to active Ultravision™ at 6kV, 8kV and 10kV. This result was surprising, as previous experimentation showed very little to no reductions in viral DNA, following sample exposure to active Ultravision™, indicating unsuccessful virus precipitation. Ultravision™ at 6kV and 8kV caused a 94.4% reduction in the number of Ad5 genomes. However, there was no significant difference in the number of Ad5 genomes between samples exposed to active Ultravision™ at 6kV and 8kV, demonstrating that a

slight reduction in voltage did not affect the efficiency of electrostatic precipitation. In contrast, samples that were exposed to active Ultravision™ at 10kV displayed a 99.9% reduction in the number of viral genomes. This indicates that 10kV is the optimum voltage of Ultravision™ to efficiently capture airborne virus particles, whilst maintaining a hospital-approved level of safety.

To compare the ability of Ultravision™ at 6kV, 8kV and 10kV to inactivate aerosolised Ad5.GFP, a transduction assay was performed (**Figure 5.11**). CHO-CAR cells were infected with samples collected from the BioSampler and analysed for GFP expression by Flow Cytometry.

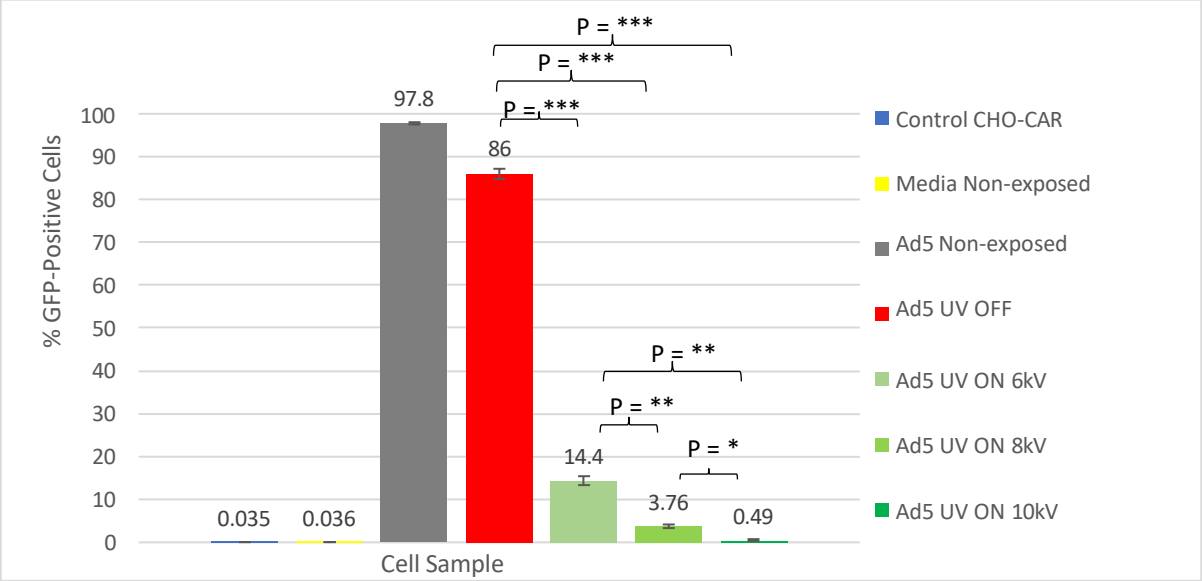

***Figure 5.11*. Inactivation of Aerosolised Ad5.GFP by Various Voltages of Ultravision™, Determined by Flow Cytometry – Run #3.** *Average percentage of GFP-positive CHO-CAR cells, following infection with samples collected from run #3. Higher GFP fluorescence correlates to a higher number of active virus particles within the sample. Blue bar: CHO-CAR cells replenished with total media. Yellow bar: SF media non-aerosolised, non-exposed to Ultravision™. Grey bar: Preparation of Ad5.GFP at 1 x 10^{10}vp/ml, non-aerosolised, non-exposed to Ultravision™. Red bar: Ad5.GFP exposed to inactive Ultravision™. Green bars: Ad5.GFP exposed to active Ultravision™ at 6kV, 8kV and 10kV. Assay performed in triplicate - graph displays mean values and SD +/-. The Student's T-test was performed to statistically analyse and compare data sets. *** = 0.0001 (Ad5 UV OFF: Ad5 UV ON 6kV/8kV/10kV), ** = 0.0056 (Ad5 UV ON 6kV: Ad5 UV ON 8kV),* ** = 0.0016 (Ad5 UV ON 6kV: Ad5 UV ON 10kV) ** = 0.0130 (Ad5 UV ON 8kV: Ad5 UV ON 10kV) (statistically significant).*

Non-exposed Ad5.GFP at 1 x 10^{10}vp/ml caused 97.8% transduction in CHO-CAR cells and therefore contained a high load of active virus particles. In comparison, Ad5.GFP that was aerosolised and exposed to inactive Ultravision™ caused 86% transduction in CHO-CAR

cells. This slight reduction in virus viability was most likely due to aerosolisation of the sample through the closed-system, resulting in loss of virus particles, thus mirroring results obtained from qPCR analysis (**Figure 5.10**). Cells infected with the virus sample that had been exposed to active Ultravision^{TM} displayed a significant reduction in the percentage of GFP-positive cells. Ad5.GFP activity was reduced by 6-fold, 22.9-fold, and 175.5-fold following exposure to active Ultravision^{TM} at 6kV, 8kV and 10kV respectively. This validated the theory that increasing the voltage of Ultravision^{TM} would increase the inactivation of viral particles.

To support data acquired from the transduction assay, a plaque assay was performed (**Figure 5.12**). TRex-293 cells were infected with the collected samples and analysed for GFP fluorescence by EVOS imaging, to quantify infectious particles.

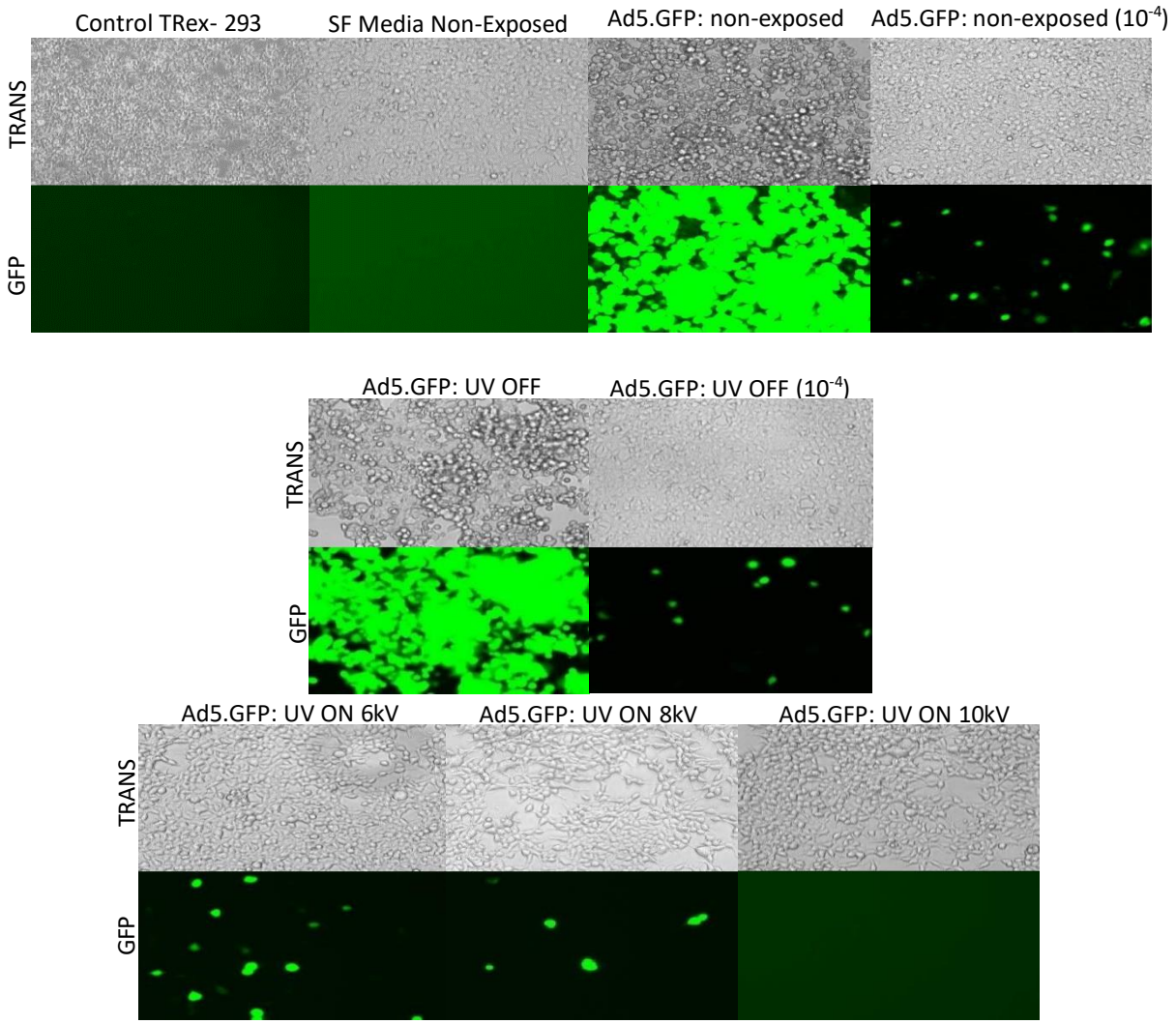

Figure 5.12. ***EVOS Imaging of TRex-293 Cells Infected with Ad5.GFP Samples that had been Exposed to Various Voltages of Ultravision™ – Run #3.*** *Top panels (TRANS) imaged using transmitted light (brightfield). Bottoms panels (GFP) imaged using the GFP light source. All wells were imaged using a x20 objective lens. Samples were collected from the BioSampler following aerosolisation of Ad5.GFP at 1 x 10^{10} vp/ml and exposure to inactive Ultravision™ or Ultravision™ active at 6kV, 8kV or 10kV. Control: TRex-293 cells replenished with total media. Non-exposed: Sample non-aerosolised and non-exposed to Ultravision. 10^{-4}: Sample diluted by 1:10,000 with SF media. Fluorescent cells under GFP light source resemble viral infection. Manual counting of fluorescent cells per field of view enabled calculation of pfu/ml values for each sample.*

Table 5.3. Functional Titers Determined by Plaque Assay Analysis - Run #3

Sample	Functional Titer
Ad5.GFP: Non-exposed	1.46 x 10^8pfu/ml
Ad5.GFP: UV OFF	1.25 x 10^8pfu/ml
Ad5.GFP: UV ON 6kV	9.6 x 10^4pfu/ml
Ad5.GFP: UV ON 8kV	2.7 x 10^4pfu/ml
Ad5.GFP: UV ON 10kV	-

Similar to the non-exposed preparation of Ad5.GFP, the functional titer of Ad5.GFP that had been exposed to inactive Ultravision™ was calculated at 1.25 x 10^8 pfu/ml. In contrast, a significant reduction in fluorescence was observed in cells infected with Ad5.GFP samples that had been exposed to active Ultravision™. The functional titer of samples exposed to active Ultravision™ at 6kV and 8kV were calculated at 9.6 x 10^4 pfu/ml and 2.7 x 10^4 pfu/ml respectively, whilst Ad5.GFP exposed to Ultravision™ active at 10kV produced no fluorescent cells. This suggested that increasing the voltage of Ultravision™ improved its efficiency to inactivate Ad5.GFP. Although voltages above 10kV are not deemed suitable for use in hospitals, usage of Ultravision™ at a maximum voltage of 10kV should theoretically inactivate all virus particles that are released in bioaerosols during surgery. However, when altering voltage, it is also important to consider the distance of the discharge electrode from the return electrode, as this too alters the electric field, in turn affecting the efficiency of electrostatic precipitation. Continuously monitoring this distance may prove difficult during closed-surgery, however for the purpose of this study, all experimentation maintained a standard distance between the Ion Wand and copper return.

5.2.4. Run #4 – Evaluating the Effects of Heating the Refined Closed-System to 37°C to Maintain Aerosolisation of Virus Samples and Enhance Sample Exposure to Ultravision™.

In all previous experimental runs, premature condensation of the aerosolised virus samples occurred within the reaction kettle. This resulted in the accumulation of Ad5.GFP particles within the bottom of the reaction kettle, of which had not been exposed to Ultravision™ and therefore remained active and viable. Additionally, premature condensation of the virus samples subsequently reduced the volume of samples collected within the BioSampler, thus affecting experimental efficiency and repeatability. Preliminary studies have suggested that

Ultravision^{TM} cannot influence particles that are suspended within liquid solutions and can only precipitate particles from aerosols. Therefore, the aim of run #4 was to prevent premature condensation of the aerosolised samples and to encourage maximal exposure of Ad5.GFP to Ultravision^{TM}. To maintain sample aerosolisation, the reaction kettle was submerged into a water bath and heated to 37°C. Thermometers were inserted into both the reaction kettle and the water bath to ensure maintenance of the temperature. Simultaneously, the BioSampler remained submerged in ice, to promote condensation of the aerosol in the collection vessel. Increased temperatures promote vaporisation and aerosolisation, compared to decreased temperatures which promote condensation (Tsang, 1990). Furthermore, following in vitro virus infection, cells are incubated at 37°C. Therefore, it was assumed that heating the aerosolised samples to 37°C would have no detrimental effects on the viability or stability of Ad5.GFP.

The experimental protocol of run #4 involved aerosolisation of Ad5.GFP at 1 x 10^{10}vp/ml through the refined closed-system, which was heated to 37°C (**Figure 5.13**). The samples were exposed to inactive/active Ultravision^{TM} (8kV) and then collected from the BioSampler for experimental analysis. Irrespective of the measures implemented to reduce sample condensation, small volumes of each sample still accumulated in the reaction kettle. These samples were also collected for experimental analysis.

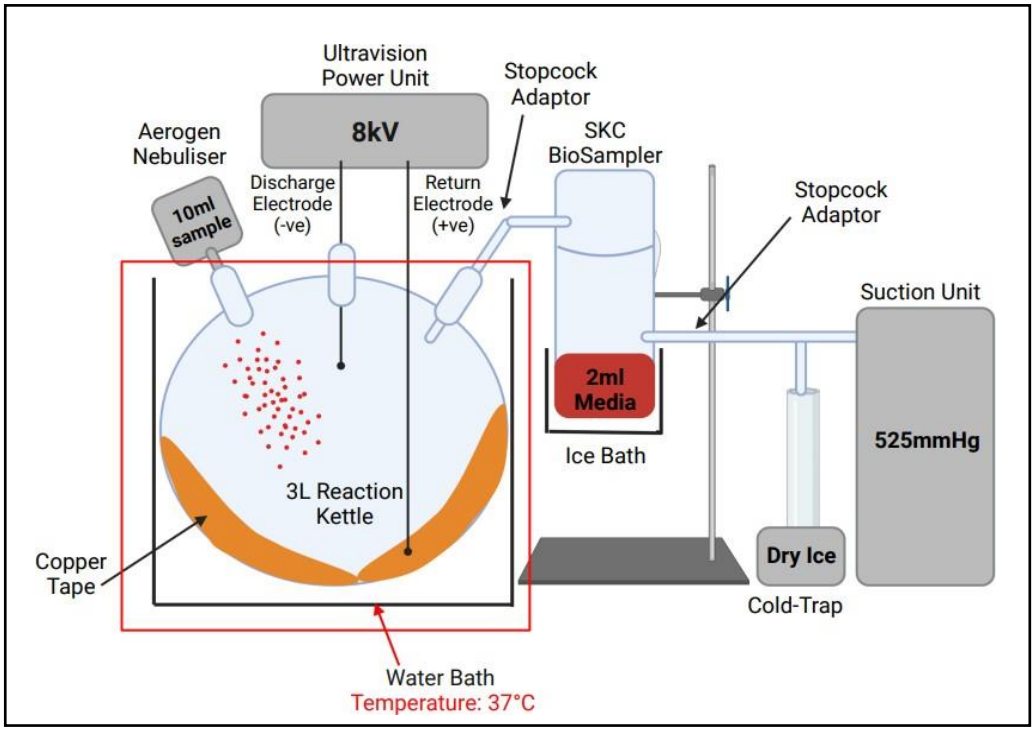

***Figure 5.13**. **A Schematic Depicting the Experimental Setup of Run #4**. The red box highlights the independent variable tested in this run. 10ml preparations of Ad5.GFP at 1 x 10^{10}vp/ml were aerosolised into the reaction kettle, which was heated to 37°C. The samples were exposed to inactive/active Ultravision™ and then collected from the BioSampler for experimental analysis. Additionally, volumes of the aerosolised samples that did condense within the reaction kettle were also collected for experimental analysis.*

To evaluate the ability of Ultravision™ to capture aerosolised Ad5.GFP in 37°C conditions, qPCR was performed (**Figure 5.14**). Additionally, the stability of viral DNA post exposure to 37°C heat was also analysed by qPCR.

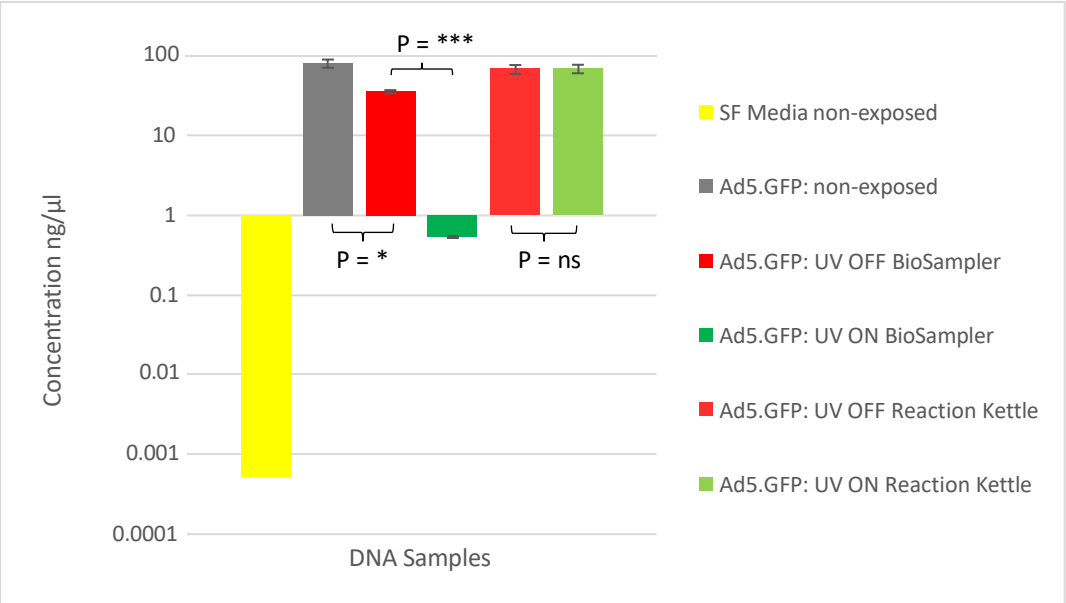

Figure 5.14. Quantification of Ad5 Genomes by qPCR in Samples Collected from the Closed System Following Aerosolisation of Ad5.GFP and Exposure to Ultravision™ at 37°C – Run #4. *Yellow bar: SF media non-aerosolised, non-exposed to Ultravision™. Grey bar: Preparation of Ad5.GFP at 1 x 10^{10} vp/ml, non-aerosolised, non-exposed to Ultravision™. Red bars: Ad5.GFP exposed to inactive Ultravision™ and 37°C heat. Green bars: Ad5.GFP exposed to active Ultravision™ and 37°C heat. Assay performed in triplicate - graph displays mean values and SD +/-. The Student's T-test was performed to statistically analyse and compare data sets. * = 0.02, *** = 0.0008 (statistically significant), ns = no significant difference.*

The non-exposed preparation of Ad5.GFP at 1 x 10^{10}vp/ml contained the highest number of viral genomes. The Ad5.GFP sample that had been exposed to inactive Ultravision™ and collected from the BioSampler also displayed a high number of Ad5 genomes. This indicated that heating the reaction kettle to 37°C had no detrimental effects on the stability of viral DNA. However, the sample that had been exposed to active Ultravision™ and collected from the BioSampler displayed a significant reduction in the concentration of Ad5 DNA. This demonstrated that Ultravision™ successfully captured Ad5.GFP particles via electrostatic precipitation.

Interestingly, the volume of condensate that accumulated in the reaction kettle, as a consequence of premature sample condensation, was significantly reduced in run #4. It was theorised that heating the reaction kettle maintained aerosolisation of the samples, thereby enhancing the exposure of virus particles to Ultravision™. However, the samples that were collected from the reaction kettle still contained high concentrations of Ad5 DNA, relative to the non-exposed virus preparation. The sample that collected within the reaction kettle occurred due to dripping of the nebuliser. Therefore, it appeared that the samples

recovered from the reaction kettle sample had not been aerosolised at all, and therefore still contained the same number of particles as the non-exposed virus preparation.

To evaluate whether enhanced aerosolisation of the virus samples improved virus inactivation upon exposure to Ultravision™, a transduction assay was performed (**Figure 5.15**). Additionally, this experimental analysis was carried out to identify whether heating the reaction kettle to 37°C affected the viability of Ad5.GFP. It was important to ensure that rising the temperature of the system did not alter the stability or viability of the virus sample, as the focal purpose of the study was to assess the ability of Ultravision™ to inactivate Ad5.GFP, and to determine optimal parameters at which electrostatic precipitation was most efficient.

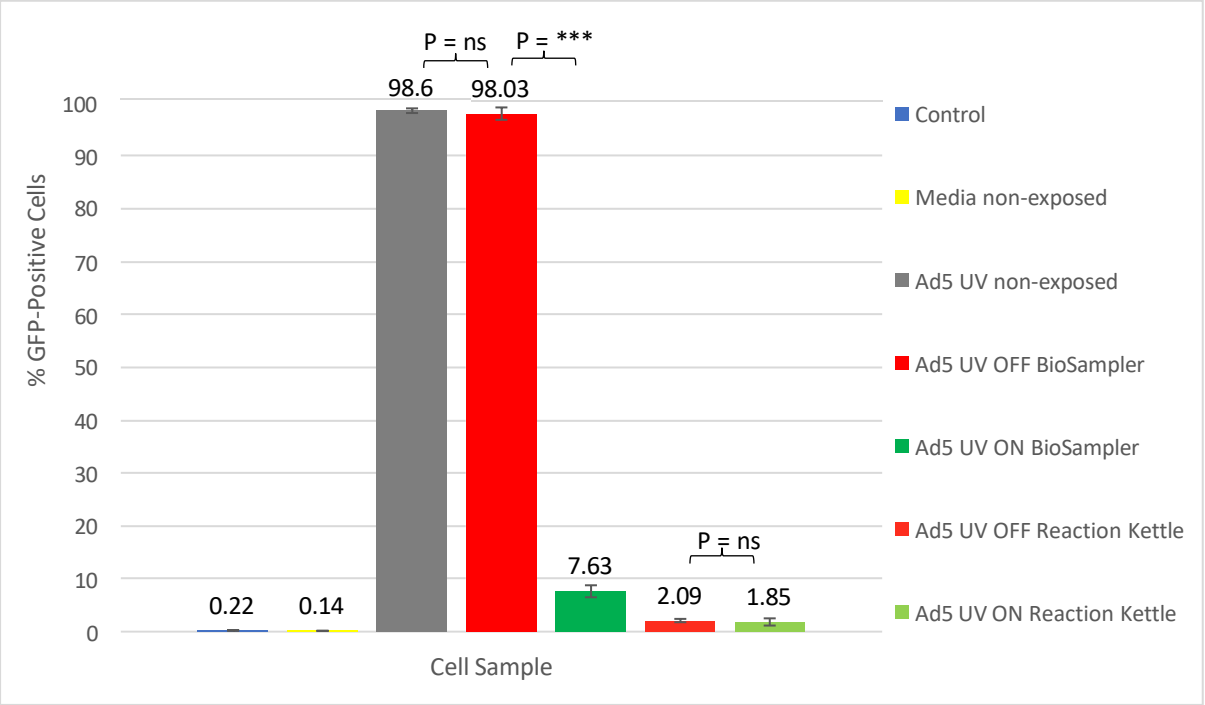

Figure 5.15. Average Percentage of GFP-positive CHO-CAR cells, Following Infection with Ad5.GFP Samples that had been Aerosolised and Exposed to Ultravision™ at 37°C - Run #4. *Higher GFP fluorescence correlates to a higher number of active virus particles within the sample. Blue bar: CHO-CAR cells replenished with total media. Yellow bar: SF media non-aerosolised, non-exposed to Ultravision™. Grey bar: Preparation of Ad5.GFP at 1 x 10^{10}vp/ml, non-aerosolised, non-exposed to Ultravision™. Red bars: Ad5.GFP aerosolised at 37°C and exposed to inactive Ultravision™. Green bars: Ad5.GFP aerosolised at 37°C and exposed to active Ultravision™. Assay performed in triplicate - graph displays mean values and SD +/-.* The *student's T-test was performed to statistically analyse and compare data sets. *** = 0.0001 (statistically significant) ns = No statistically significant difference.*

In this experiment, 98.6% of the cells were transduced by the non-exposed preparation of Ad5.GFP at 1 x 10^{10}vp/ml. Similarly, the sample of Ad5.GFP that was aerosolised through the 37°C system and exposed to inactive Ultravision™ transduced 98.03% of cells. This indicated that heating the reaction kettle to 37°C improved the viability of viral particles upon aerosolisation, in comparison to previous experimental runs. Of the cells that were infected with the Ad5.GFP sample that had been exposed to active Ultravision™, 7.63% were transduced, thus achieving a 12.8-fold reduction in virus viability. As a larger proportion of the virus sample remained aerosolised, the heated system delivered a more accurate representation of Ultravision™ during closed surgery and its ability to capture and inactivate aerosolised virus particles. Therefore, the observed log reduction in virus viability was assumed to be an accurate measurement of the capabilities of Ultravision™. Finally, samples collected from the reaction kettle, that had been exposed to active or inactive Ultravision™, caused 2.09% and 1.85% cellular transduction, respectively. It appeared that the majority of viable virus particles present within the prematurely condensed samples were inactivated by the copper return, rather than by Ultravision™ itself. This was because the volume of the condensate was far lower than that collected from previous runs, enabling the virucidal copper to directly contact a higher percentage of virus particles, resulting in viral inactivation. Therefore, heating the system was beneficial, as a higher number of Ad5.GFP particles remained aerosolised and were thereby exposed to Ultravision™.

To support data obtained from the transduction assay, a plaque assay was carried out (**Figure 5.16**). TRex-293 cells were infected with samples collected from run #4 and analysed for GFP expression via EVOS imaging.

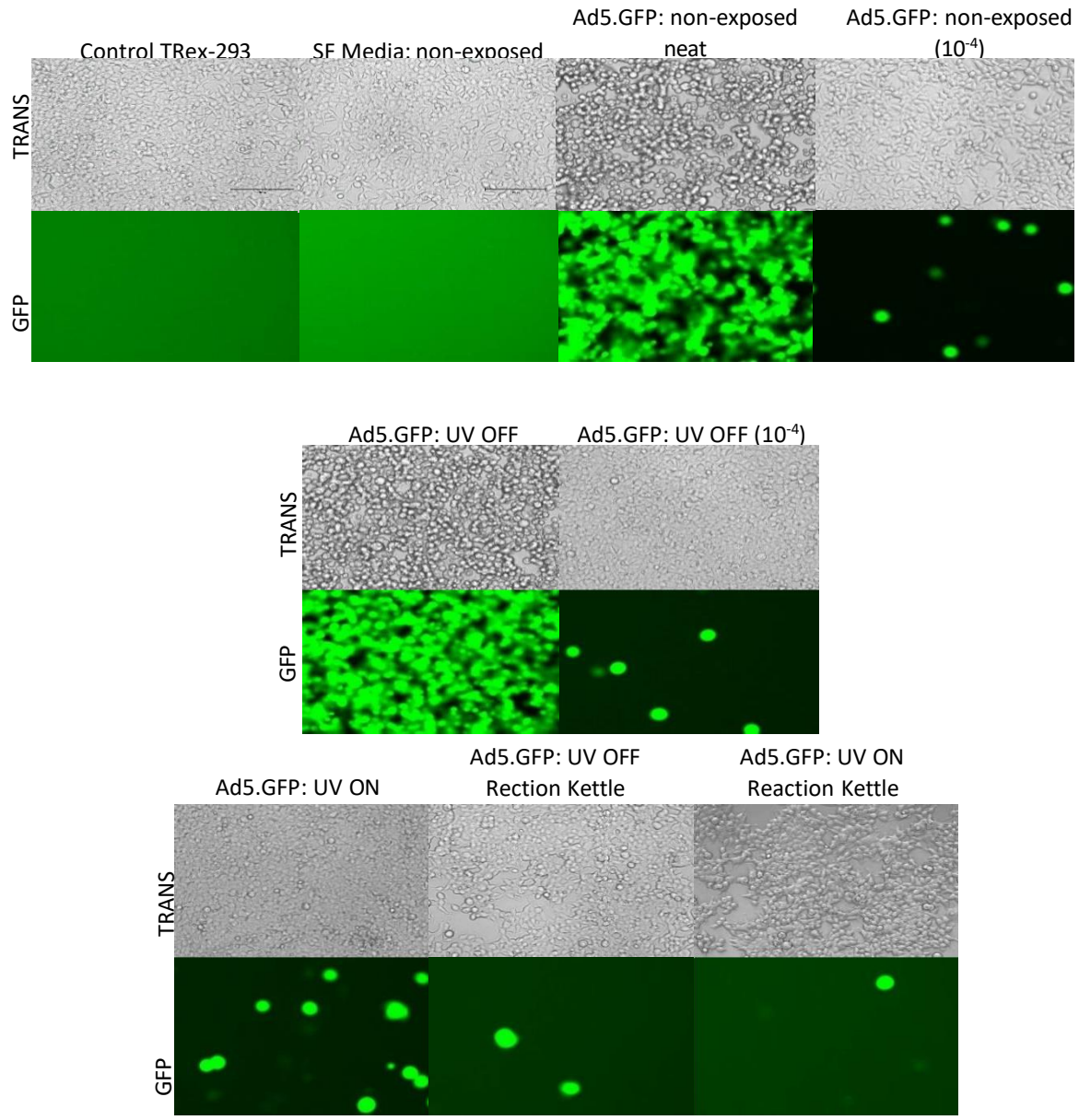

Figure 5.16. EVOS Imaging of TRex-293 Cells Infected with Ad5.GFP Samples that had been Aerosolised and Exposed to Ultravision™ at 37°C – Run #4. *Top panels (TRANS) imaged using transmitted light (brightfield). Bottoms panels (GFP) imaged using the GFP light source. All wells were imaged using a x20 objective lens. Control: TRex-293 cells replenished with total media. Non-exposed: Sample non-aerosolised and non-exposed to Ultravision™. 10^{-4}: Sample diluted by 1:10,000 with SF media. Fluorescent cells under GFP light source resemble viral infection. Manual counting of fluorescent cells per field of view enabled calculation of pfu/ml values for each sample.*

Table 5.4. Functional Titers Determined by Plaque Assay Analysis - Run #4

Sample	Functional Titer
Ad5.GFP: non-exposed	4.46 x 10^8 pfu/ml
Ad5.GFP: UV OFF BioSampler	2.7 x 10^8 pfu/ml
Ad5.GFP: UV ON BioSampler	6.83 x 10^3pfu/ml
Ad5.GFP: UV OFF Reaction Kettle	2.1 x 10^7vp/ml
Ad5.GFP: UV ON Reaction Kettle	7.1 x 10^6vp/ml

The preparation of non-exposed Ad5.GFP at 1 x 10^{10}vp/ml generated a functional titer of 4.46 x 10^8 pfu/ml. Likewise, Ad5.GFP that had been aerosolised at 37°C and exposed to inactive Ultravision™ initiated high levels of infection, obtaining a functional titer of 2.7 x 10^8 vp/ml. This demonstrated that heating the reaction kettle had no detrimental effects on the viability of Ad5.GFP. A significant reduction in fluorescence was observed in cells infected with Ad5.GFP that had been exposed to active Ultravision™ and collected from the BioSampler. The functional titer for this experimental sample was calculated at 6.83 x 10^3pfu/ml. This reduction in viral activity indicated that Ultravision™ successfully captured and/or inactivated Ad5.GFP at 37°C. Finally, samples collected from the reaction kettle showed no difference in viral viability, regardless of exposure to active/inactive Ultravision™. Such samples produced low numbers of detectable fluorescent cells, thus emulating results from the transduction assay once again. It was thereby hypothesised that heating the ambient temperature of the closed-system model reduced premature condensation of the aerosolised sample. Consequently, a larger proportion of virus particles were exposed to Ultravision™ and inactivated by the virucidal corona discharge.

5.2.5. Run #5 – Capture and Inactivation of Aerosolised Ad5.GFP by 1 Ultravision™ Ion Wand Compared to 2 Ultravision™ Ion Wands, within the Refined Closed-System.

In run #3, various voltages of Ultravision™ were exposed to aerosolised Ad5.GFP, to determine an optimal voltage that enabled maximal capture and inactivation of virus particles. Results suggested that a voltage of 10kV was the most efficient. In adherence with this study, run #5 evaluated the synergistic ability of combining 2 Ion Wands. It was proposed that using 2 Ion Wands, instead of just 1, would enhance electrostatic

precipitation, thus improving the capture and inactivation of aerosolised Ad5.GFP. The experimental protocol of run #5 involved aerosolisation of Ad5.GFP at 1 x 10^{10}vp/ml and exposure to either 1 or 2 Ion Wands, both of which were set at 8kV (**Figure 5.17).** Additionally, the reaction kettle was heated to 37°C, as performed in run #4, as this improved sample aerosolisation and virus viability. The aim of run #5 was to identify whether 2 Ion Wands (at 8kV) could cause the same level of virus capture and inactivation as 1 Ion Wand at 10kV, via Ion Wand synergism. If successful, it was hypothesised that hospitals could implement multiple Ion Wands during surgical procedures, whilst maintaining a medically approved voltage of 8kV, to remove surgical smoke whilst simultaneously preventing viral transmission.

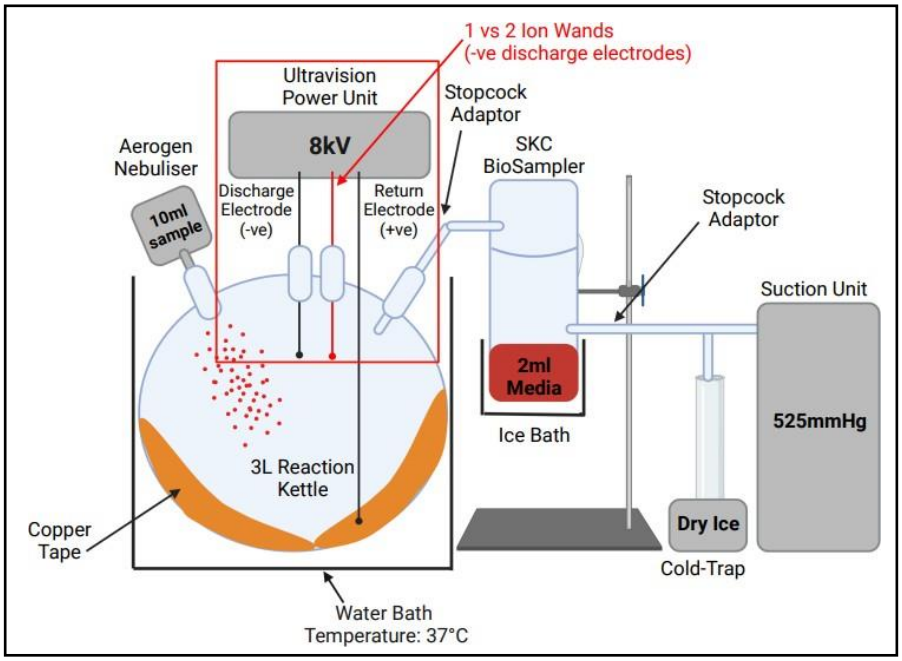

***Figure 5.17**. **A Schematic Depicting the Experimental Setup of Run #5**. The red box highlights the independent variable tested in this run. 10ml preparations of Ad5.GFP at 1 x 10^{10}vp/ml were aerosolised into the reaction kettle, which was heated to 37°C, and exposed to either 1 or 2 active/inactive Ultravision™ Ion Wands. Samples collected in the BioSampler were stored at -80°C in preparation for analysis. Additionally, any sample condensation that occurred within the reaction kettle was also collected for experimental analysis.*

To compare the ability of 1 versus 2 Ultravision™ Ion Wands to capture aerosolised Ad5.GFP, qPCR was performed (**Figure 5.18**).

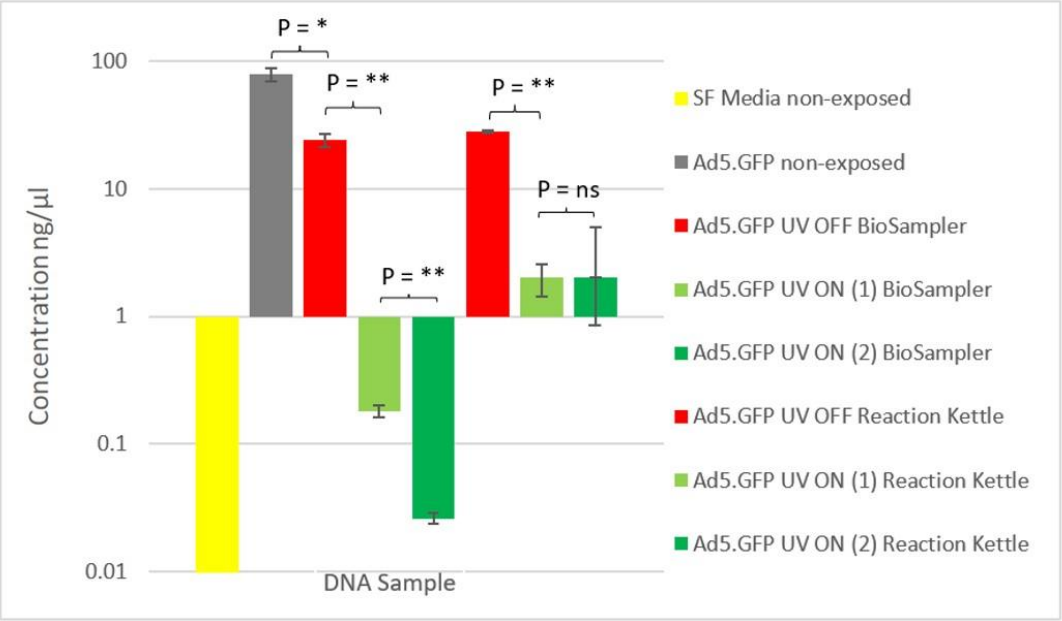

***Figure 5.18*. Average DNA Concentrations Determined by qPCR Amplification of Ad5 Genomes in Samples of Ad5.GFP that had been Exposed to 1 or 2 Ultravision™ Ion Wands at 37°C – Run #5.** *Yellow bar: SF media non-aerosolised, non-exposed to Ultravision™. Grey bar: Preparation of Ad5.GFP at 1 x 10^{10} vp/ml, non-aerosolised, non-exposed to Ultravision™. Red bars: Ad5.GFP exposed to inactive Ultravision™ at 37°C. Light Green bars: Ad5.GFP exposed to 1 active Ion Wand, at 37°C. Dark Green Bars: Ad5.GFP exposed to 2 active Ion Wands, at 37°C. Assay performed in triplicate - graph displays mean values and SD +/-. The Student's T-test was performed to statistically analyse and compare data sets. * = 0.014 (Ad5 Non-exposed: Ad5 UV OFF BioSampler), ** = 0.0053 (Ad5 UV OFF BioSampler: Ad5 UV ON (1) BioSampler), ** = 0.0050 (Ad5 UV ON (1) BioSampler: Ad5 UV ON (2) BioSampler), ** = 0.0067 (Ad5 UV OFF Reaction kettle: Ad5 UV ON (1) Reaction Kettle) (statistically significant), ns = no significant difference.*

Samples that were exposed to inactive Ultravision™ and collected from both the BioSampler and the reaction kettle contained high numbers of viral genomes. In comparison, Ad5.GFP that was exposed to 1 active Ion Wand and collected from the BioSampler displayed a 99.3% decrease in the number of Ad5 genomes. This indicated successful particle capture by Ultravision™. Additionally, Ad5.GFP that was exposed to 2 active Ion Wands and collected from the BioSampler displayed a 99.9% decrease in the number of Ad5 genomes. This therefore demonstrated that using 2 Ion Wands further enhanced viral capture. In contrast, samples that had been exposed to active Ultravision™ and collected from the reaction kettle displayed a slight but significant reduction in the concentration of viral DNA. However, increasing the number of active Ion Wands did not alter the number of Ad5 genomes within the reaction kettle samples. It was hypothesised

that these samples were not inactivated by the Ultravision™ Ion Wand itself, but rather by direct contact with the virucidal copper return electrode.

To compare the ability of 1 versus 2 Ultravision™ Ion Wands to inactivate aerosolised Ad5.GFP particles, a transduction assay was performed (**Figure 5.19**).

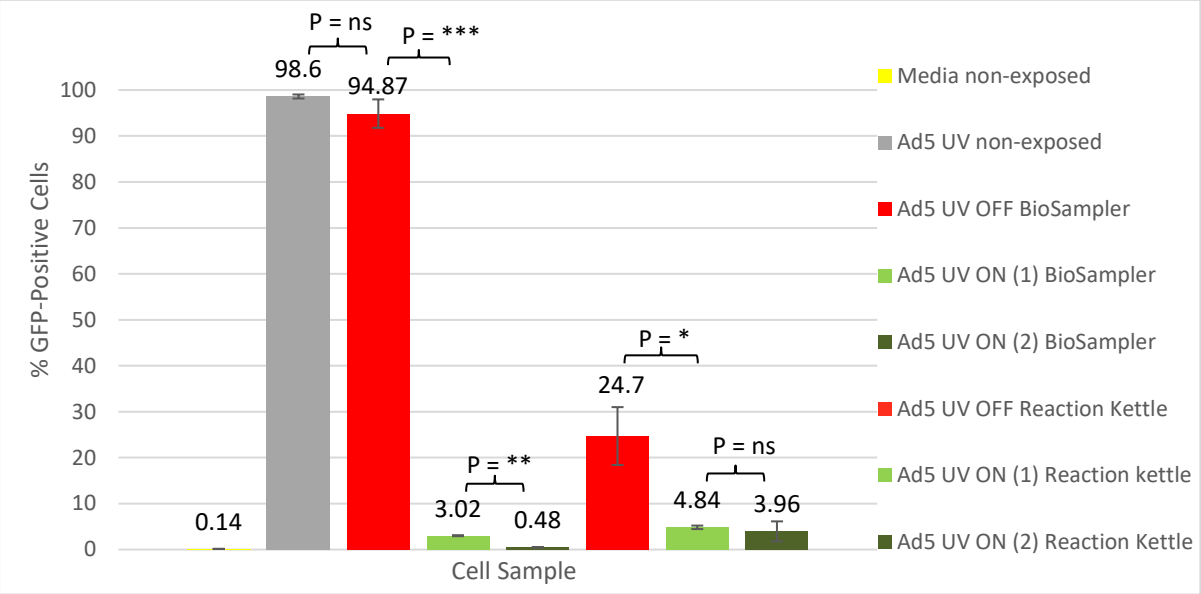

Figure 5.19. Average Percentage of GFP-Positive CHO-CAR Cells, Following Infection with Samples of Ad5.GFP that had been Exposed to 1 or 2 Ultravision™ Ion Wands, Determined by Flow Cytometry – Run #5. *Higher GFP fluorescence correlates to a higher number of active virus particles within the sample. Yellow bar: SF media non-aerosolised, non-exposed to Ultravision™. Grey bar: Preparation of Ad5.GFP at 1 x 10^{10}vp/ml, non-aerosolised, non-exposed to Ultravision™. Red bars: Ad5.GFP aerosolised at 37°C and exposed to inactive Ultravision™. Light Green bars: Ad5.GFP aerosolised at 37°C and exposed to 1 active Ion Wand. Dark Green bars: Ad5.GFP aerosolised at 37°C and exposed to 2 active Ion Wands. Assay performed in triplicate - graph displays mean values and SD +/-. The Student's T-test was performed to statistically analyse and compare data sets. *** = 0.0004, ** = 0.001, * = 0.0316 (Statistically significant), ns = No statistically significant difference.*

Infections with non-exposed preparations of Ad5.GFP at 1 x 10^{10}vp/ml produced 98.6% GFP-positive cells. Similarly, infections with Ad5.GFP that was exposed to inactive Ultravision™ and collected from the BioSampler produced 94.87% GFP-positive cells. On the other hand, only 3.02% of cells were transduced following infection with Ad5.GFP that was exposed to 1 active Ion Wand and collected from the BioSampler. 1 active Ion Wand thereby achieved a 31.4-fold reduction in virus viability. However, a 197.6-fold reduction in cellular transduction was observed in cells that were infected with Ad5.GFP that had been exposed to 2 Ion Wands and collected from the BioSampler. This level of virus inactivation mirrored that observed in run #3, whereby Ad5.GFP samples were exposed to active Ultravision™ at 10kV.

Therefore, it was assumed that the virucidal effects of 2 Ion Wands at 8kV were analogous to that of 1 Ion Wand at 10kV. Cells infected with the reaction kettle sample that had been exposed to inactive Ultravision^{TM} displayed low levels of GFP-positive cells (24.7%). This demonstrated that a small volume of the aerosolised sample still underwent premature condensation, regardless of the efforts made to maintain sample aerosolisation. Interestingly, cells that were infected with reaction kettle samples that had been exposed to active Ultravision^{TM} showed a 5-fold reduction in transduction, regardless of the number of active Ion Wands. This indicated that either Ultravision^{TM} or the electrically charged virucidal copper return was able to inactivate Ad5.GFP particles that existed within the condensed samples.

To confirm data obtained from the transduction assay, a plaque assay was carried out (**Figure 5.20**). TRex-293 cells were infected with the samples collected from run #5 and analysed for GFP fluorescence via EVOS imaging. As run #4 and run #5 were carried out simultaneously, the serum-free media negative control and the non-exposed preparations of Ad5.GFP were identical and are therefore not displayed in **Figure 5.20**.

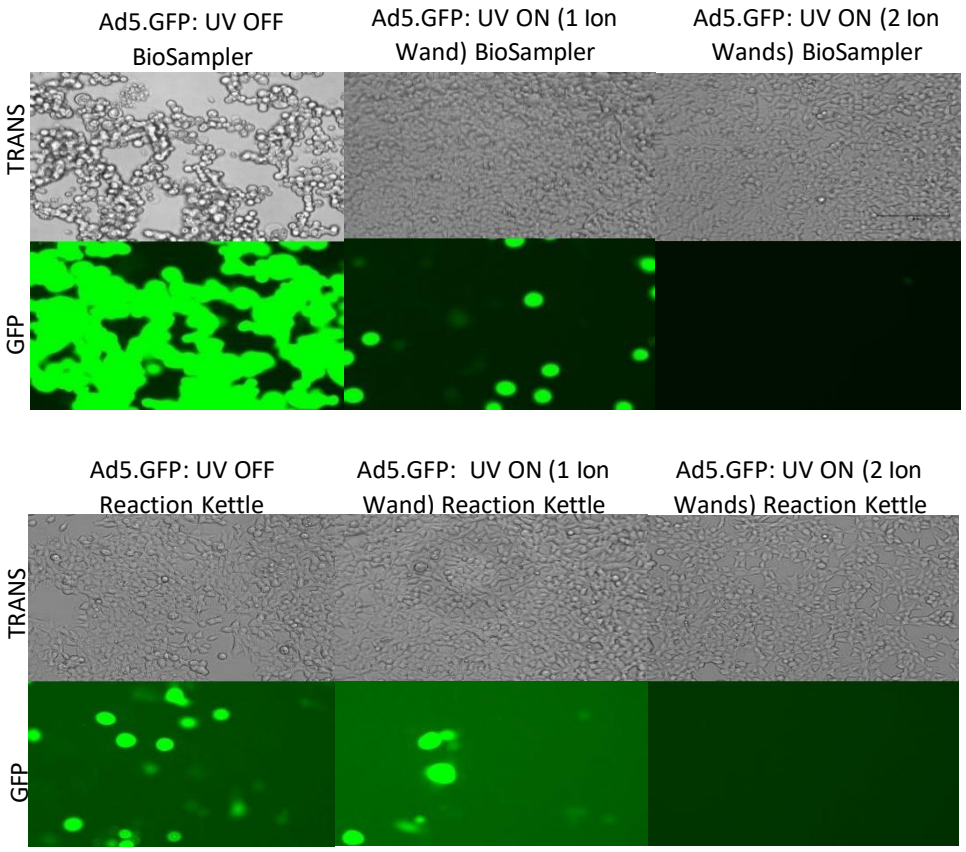

Figure 5.20. EVOS Imaging of TRex-293 Cells Infected with Ad5.GFP Samples that had been Exposed to 1 or 2 Ultravision™ Ion Wands – Run #5. *Top panels (TRANS) imaged using transmitted light (brightfield). Bottoms panels (GFP) imaged using the GFP light source. All wells were imaged using a x20 objective lens. Samples collected from the BioSampler and the reaction kettle following aerosolisation of Ad5.GFP at 1 x 10^{10} vp/ml at 37°C and exposure to 1 versus 2 Ultravision™ Ion Wands. Fluorescent cells under GFP light source resemble viral infection. Manual counting of fluorescent cells per field of view enabled calculation of pfu/ml values for each sample.*

Table 5.5. Functional Titers Determined by Plaque Assay Analysis - Run #5

Sample	Functional Titer
Ad5.GFP: UV OFF BioSampler	1.2 x 10^7vp/ml
Ad5.GFP: UV ON (1 Ion Wand) BioSampler	1.5 x 10^4vp/ml
Ad5.GFP: UV ON (2 Ion Wand) BioSampler	-
Ad5.GFP: UV OFF Reaction Kettle	1.1 x 10^6vp/ml
Ad5.GFP: UV ON (1 Ion Wand) Reaction Kettle	3.8 x 10^5vp/ml
Ad5.GFP: UV ON (2 Ion Wand) Reaction Kettle	-

A high proportion of the cells infected with the Ad5.GFP sample, that had been exposed to inactive Ultravision^{TM} and collected from the BioSampler, was successfully infected. The functional titer for this sample was calculated at 1.2 x 10^7pfu/ml. In comparison, cells infected with the Ad5.GFP sample, that had been exposed to 1 active Ion Wand and collected from the BioSampler, displayed far fewer fluorescent cells, indicating a reduction in viral activity. Further, cells infected with Ad5.GFP, that had been exposed to 2 active Ion Wands, displayed no detectable signs of cellular infection. This demonstrated that 2 Ion Wands caused complete inactivation of all Ad5.GFP particles present within the aerosolised sample. The functional titers calculated for the Ad5.GFP samples that had been exposed to 1 versus 2 active Ion Wands, were 1.5 x 10^4pfu/ml and 0 pfu/ml, respectively. This supported findings from the transduction assay, indicating that 2 Ion Wands at 8kV are equally effective at capturing and inactivating virus particles as 1 Ion Wand at 10kV.

Cells infected with the reaction kettle sample that had been exposed to inactive Ultravision^{TM} displayed a low but detectable level of infection. The volume of condensate that accumulated in the reaction was much lower than in previous runs, due to heating of the reaction kettle. This therefore explained the reduced number of virus particles present within the collected sample. On the other hand, reaction kettle samples that had been exposed to 1 active Ion Wand generated an even lower level of infection. Further, the sample that had been exposed to 2 active Ion Wands showed no detectable signs of virus activity. Contradictory to the transduction assay, this data indicated that 2 Ion Wands enhanced the level of virus inactivation within the reaction kettle sample, in comparison to 1 Ion Wand. Repeats of this study are therefore required to validate such contrasting results.

5.2.6. Run #6 – Replacing the Copper Return-Electrode with Stainless Steel, to Analyse the Level of Virus Capture and Inactivation by Ultravision™ with a Biochemically Inert Collector Plate.

In previous experimental runs, copper tape was attached to the positively charged return electrode, serving as a collector plate for the precipitation of ionised virus particles. However, studies have shown that copper is naturally virucidal and that direct contact between copper and virus particles can result in viral inactivation (Govind, 2021). Additionally, Hutasoit (2020) found that SARS-CoV-2 was efficiently inactivated following direct contact with copper-coated surfaces and revealed that 96% of the virus sample analysed was inactivated within 2 hours of exposure to copper.

The purpose of this study was to evaluate whether Ultravision™ could inactivate virus particles, as well as capture them. To ensure that the observed inactivation of Ad5.GFP was solely due to Ultravision™, as opposed to contact with virucidal copper, the return electrode in run #6 was replaced with stainless steel (**Figure 5.21**). Stainless steel is an inert, non-toxic metal (Santonen, 2010), that has been shown by Perry (2016) to allow the persistence, viability and stability of viruses such as Influenza, upon direct contact. Therefore, stainless steel does not harbour any virucidal properties, providing the rationale for its use in run #6. Following sample aerosolisation and exposure to Ultravision™, the stainless steel return was washed with 2ml serum-free media, to obtain any virus particles that had precipitated onto the metal plate. The media was then stored at -80°C, in preparation for experimental analysis. The concentration of virus particles and their status of infectivity was measured to identify the effects of steel on virus stability and viability. Between experimental runs, steel sheets were replenished with new sheets to prevent contamination. As performed in previous runs, samples were also collected from the BioSampler for analysis. Additionally, Ad5.GFP was exposed to 2 different voltages of Ultravision™ – 8kV and 10kV. Run #3 determined that increasing the Ion Wand voltage from 8kV to 10kV increased capture and inactivation of Ad5.GFP. This variable was thereby included in run #6 as an experimental control. A reduction in viral activity following an increase in Ultravision™ voltage, similar to that observed in run #3, would suggest that Ultravision™ was the sole cause of Ad5.GFP inactivation, rather than the metal attached to the return electrode.

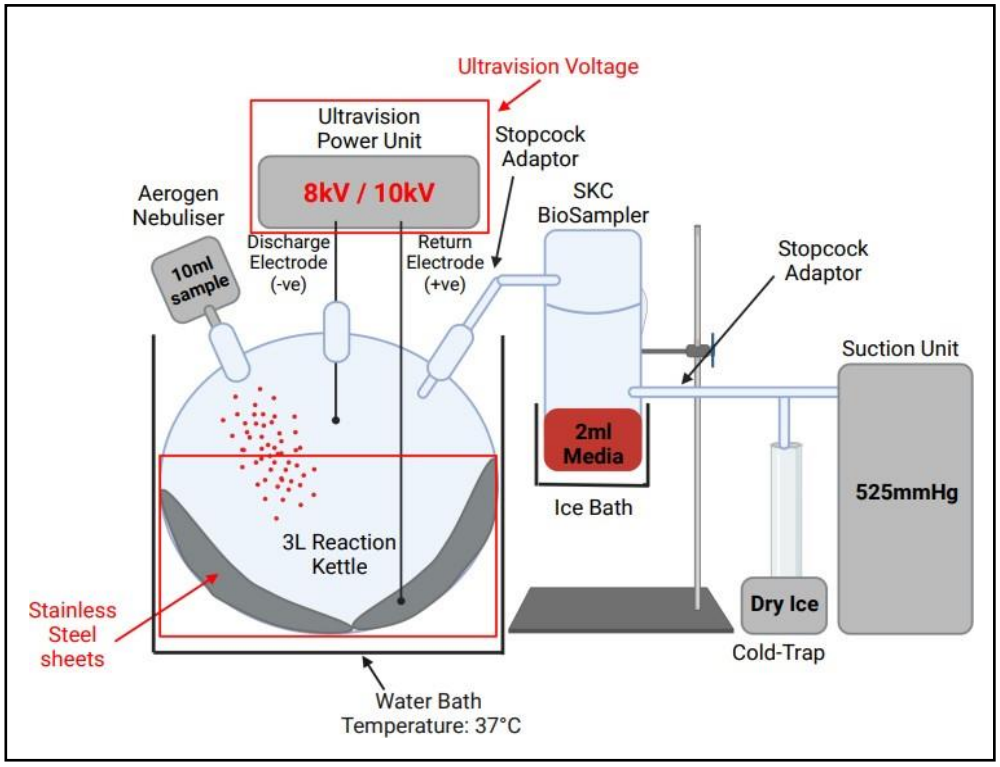

***Figure 5.21**. **A Schematic Depicting the Experimental Setup of Run #6**. The red boxes highlight the independent variables tested in this run. 10ml preparations of Ad5.GFP at 1 x 10^{10}vp/ml were aerosolised into the reaction kettle, which was heated to 37°C, and exposed to either inactive or active Ultravision™ (8kV/10kV). Following complete aerosolisation, samples were condensed and collected in the BioSampler and stored at -80°C, in preparation for analysis. Additionally, the stainless steel sheets were removed from the reaction kettle and washed with 2ml serum-free media, to analyse for viral presence and activity.*

To evaluate the ability of Ultravision™ to capture Ad5.GFP particles in run #6, qPCR was performed (**Figure 5.22**).

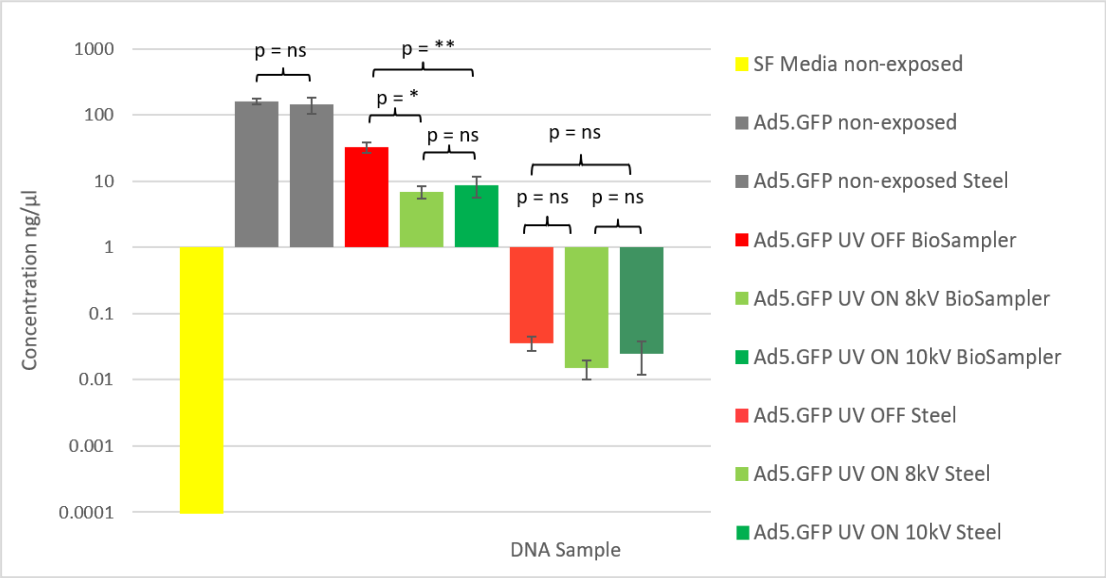

Figure 5.22. Average Concentrations of DNA in Samples that had been Exposed to Inactive/Active Ultravision™ and Stainless Steel, Determined by qPCR Amplification of Ad5 Genomes – Run #6*. Yellow bar: SF media non-aerosolised, non-exposed to Ultravision™. Grey bar: Preparation of Ad5.GFP at 1 x 10^{10} vp/ml, non-aerosolised, non-exposed to Ultravision™. Red bars: Ad5.GFP exposed to inactive Ultravision™. Green bars: Ad5.GFP exposed to active Ultravision™. Assay performed in triplicate - graph displays mean values and SD +/-. The Student's T-test was performed to statistically analyse and compare data sets. * = 0.015 (Ad5 UV OFF BioSampler: Ad5 UV ON 8kV BioSampler), ** = 0.008 (Ad5 UV OFF BioSampler: Ad5 UV ON 10kV BioSampler), (statistically significant), ns = no statistically significant difference.*

Following direct contact with stainless steel, the concentration of Ad5 DNA in the non-exposed Ad5.GFP preparation remained unchanged. This validated the theory that stainless steel is biologically inert and does not affect the stability of viral DNA. The number of viral genomes was significantly reduced in the sample that had been exposed to inactive Ultravision™ and collected from the BioSampler. This indicated that a proportion of the virus particles were lost during aerosolisation of the sample through the closed system. The sample of Ad5.GFP that had been exposed to active Ultravision™ at 8kV showed a 78% reduction in the number of viral genomes. This highlighted successful electrostatic precipitation via Ultravision™. Surprisingly, the sample exposed to Ultravision™ at 10kV and collected from the BioSampler displayed a similar percentage of reduction in the concentration of viral DNA. This was interesting, as data obtained from run #3 indicated that increasing the voltage of Ultravision™ to 10kV enhanced the level of virus capture. Nevertheless, virus capture was observed in run #6, which therefore demonstrated that Ultravision™ was the sole cause of particle precipitation. This indicated that the virucidal

copper return used in previous runs did not affect the capture of virus particles. However, perhaps the virucidal properties of copper caused viral inactivation in run #3, mimicking viral capture. This would explain why the percentage of virus capture in run #3 was higher than that observed in run #6.

All samples obtained from the stainless steel electrode contained lower numbers of Ad5 genomes, largely due to the method of sample collection. There were no significant differences in the number of Ad5 genomes between the samples obtained from the steel electrode, despite exposure to active or inactive Ultravision^{TM}. It was probable that the condensate which accumulated within the reaction kettle was a result of samples dripping from the nebuliser. The samples had therefore not been aerosolised nor sufficiently exposed to Ultravision^{TM}, allowing the concentration of virus particles to remain unchanged.

To evaluate the ability of Ultravision^{TM} to inactivate Ad5.GFP in run #6, a transduction assay was performed (**Figure 5.23**). This experiment also analysed whether stainless steel affected the viability of Ad5.GFP following direct contact.

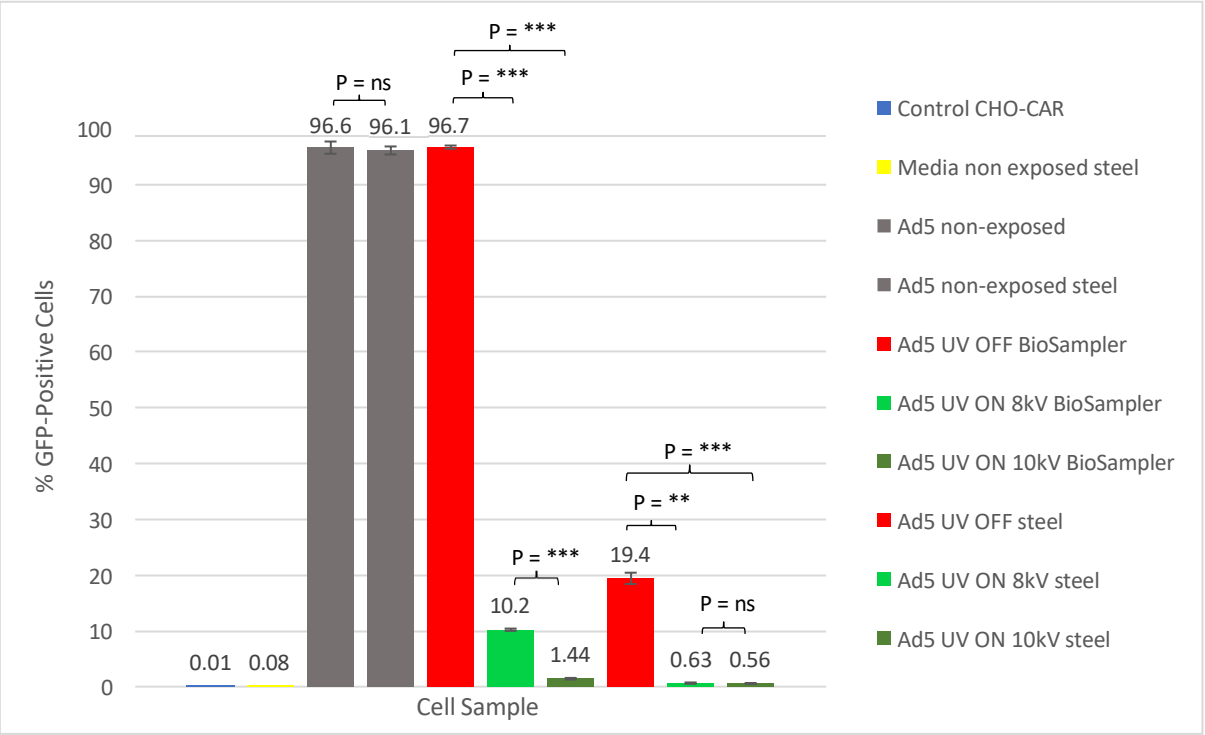

Figure 5.23. Average Percentage of GFP-Positive CHO-CAR Cells, Following Infection with Ad5.GFP Samples that had Been Exposed to Inactive/Active Ultravision™ and Stainless Steel, Determined by Flow Cytometry - Run #6. *Higher GFP fluorescence correlates to a higher number of active virus particles within the sample. Blue bar: CHO-CAR cells replenished with total media. Yellow bar: SF media non-aerosolised, non-exposed to Ultravision™. Grey bars: Preparations of Ad5.GFP at 1 x 10^{10}vp/ml, non-aerosolised, non-exposed to Ultravision™. Red bars: Ad5.GFP aerosolised and exposed to inactive Ultravision™. Light Green bars: Ad5.GFP aerosolised and exposed to active Ultravision™ at 8kV. Dark Green bars: Ad5.GFP aerosolised and exposed to active Ultravision™ at 10kV. Assay performed in triplicate - graph displays mean values and SD +/-. The Student's T-test was performed to statistically analyse and compare data sets. *** = 0.0001 (Ad5 UV OFF BioSampler: Ad5 UV ON 8kV BioSampler), *** = 0.0.0001 (Ad5 UV OFF BioSampler: Ad5 UV ON 10kV BioSampler), *** = 0.0001 (Ad5 UV ON 8kV BioSampler: Ad5 UV ON 10kV BioSampler), ** = 0.0012 (Ad5 UV OFF Steel: Ad5 UV ON 8kV Steel),* *** = 0.0008 (Ad5 UV OFF Steel: Ad5 UV ON 10kV Steel), *ns = No statistically significant difference.*

Cells infected with the non-exposed preparations of Ad5.GFP that were either non-exposed or exposed to stainless steel displayed 96.1% and 96.6% of GFP-positive cells, respectively. This indicated that stainless steel was not detrimental to virus viability. Similarly, cells infected with Ad5.GFP that had been exposed to inactivate Ultravision™ and collected from the BioSampler presented 96.7% GFP-positive cells. This indicated that sample aerosolisation and exposure to stainless steel did not alter Ad5.GFP viability. In contrast, cells infected with samples that had been exposed to active Ultravision™ at 8kV and 10kV and collected from the BioSampler, showed 9.5-fold and 67.1-fold reductions in the

percentage of GFP-positive cells, respectively. This indicated that Ad5.GFP was efficiently inactivated by Ultravision^{TM} rather than by the electrically charged metal return. There was a statistically significant difference in transduction between cells infected with samples exposed to Ultravision^{TM} at 8kV and 10kV. This mirrored results from run #3, which demonstrated that increasing the voltage of Ultravision^{TM} enhanced virus inactivation, thereby confirming the accuracy of data obtained in run #6.

Interestingly, samples that had been exposed to active Ultravision^{TM} and collected from the reaction kettle displayed a 32-fold reduction in virus viability. As stainless steel is inert, this indicated that Ultravision^{TM} alone caused the inactivation of precipitated virus particles. Therefore, the metal attached to the return electrode does not alter viral activity, and any inactivation is directly caused by Ultravision.

To further confirm these findings, a plaque assay was performed (**Figure 5.24**). TRex-293 cells were infected with the samples collected from run #6 and analysed for GFP fluorescence via EVOS imaging. Cells that were infected with the Ad5.GFP sample that had been exposed to Ultravision^{TM} at 10kV and collected from the BioSampler displayed no signs of virus activity and are therefore not included in **figure 5.24**.

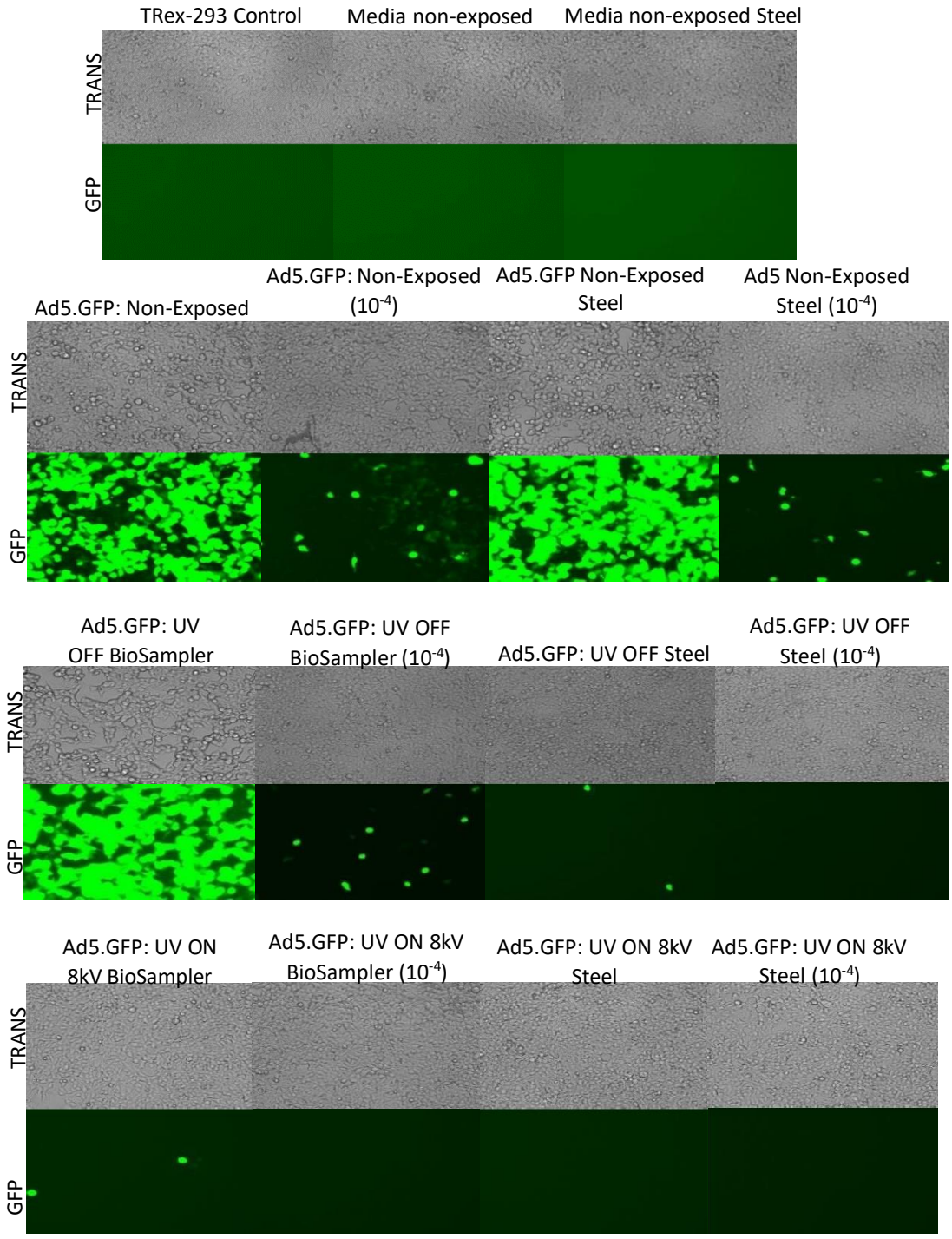

Figure 5.24. EVOS Imaging of TRex-293 Cells Infected with Ad5.GFP Samples that had been Exposed to Ultravision™ and a Stainless Steel Return Electrode – Run #6. *Top panels (TRANS) imaged using transmitted light (brightfield). Bottoms panels (GFP) imaged using the GFP light source. All wells were imaged using a x20 objective lens. Samples were collected from BioSampler and washes of the stainless-steel electrode, following aerosolisation of Ad5.GFP at 1 x 10^{10} vp/ml and exposure to Ultravision™. Control: TRex-293 cells replenished with total media. Non-exposed: Sample non-aerosolised and non-exposed to Ultravision™. Steel: Samples obtained from washes of the steel electrode with 2ml SF media. 10^{-4}: Sample diluted by 1:10,000 with SF media. Fluorescent cells under GFP light source resemble viral infection. Manual counting of fluorescent cells per field of view enabled calculation of pfu/ml values for each sample.*

Table 5.6. Functional Titers Determined by Plaque Assay Analysis - Run #6

Sample	Functional Titer
Ad5.GFP: non-exposed	1.2 x 10^8pfu/ml
Ad5.GFP: non-exposed (steel)	1.1 x 10^8pfu/ml
Ad5.GFP: UV OFF BioSampler	9.5 x 10^7pfu/ml
Ad5.GFP: UV OFF (Steel)	1.2 x 10^3pfu/ml
Ad5.GFP: UV ON 8kV BioSampler	1.1 x 10^3pfu/ml
Ad5.GFP: UV ON 8kV (Steel)	-
Ad5.GFP: UV ON 10kV BioSampler	-
Ad5.GFP: UV ON 10kV (Steel)	-

Cells infected with the samples of Ad5.GFP at 1 x 10^{10}vp/ml that were non-exposed and exposed to stainless steel displayed observable transduction, obtaining functional titers of 1.2 x 10^8pfu/ml and 1.1 x 10^8pfu/ml respectively. Once again, this demonstrated that stainless steel did not decrease the viability of Ad5.GFP upon direct contact. Correspondingly, cells infected with samples of Ad5.GFP that had been exposed to inactive Ultravision™ and collected from the BioSampler showed similar levels of transduction. The functional titer of this sample was calculated at 9.5 x 10^7pfu/ml. In comparison, Ad5.GFP samples that had been exposed to inactive Ultravision™ and collected from washes of the steel return caused much lower levels of transduction, thereby mirroring data from the transduction assay. This was most probably due to dilution of the sample following washes of the steel sheets. Unsurprisingly, Ad5.GFP samples that had been exposed to active Ultravision™ and collected from the BioSampler produced little to no detectable transduced cells. Consistent with data obtained from the transduction assay, this indicated that Ultravision™ successfully inactivated aerosolised Ad5.GFP and was the sole cause of the observed virus inactivation. Ad5.GFP samples that had been exposed to active Ultravision™ and collected from washes of the steel return displayed no signs of active Ad5.GFP. Additionally, the trans images highlight that these samples did not cause cell death, unlike samples of Ad5.GFP that were exposed to copper in previous runs. Once again, this indicated that steel did not affect virus or cell viability and that Ultravision™ alone caused virus inactivation.

5.2.7. Run #7 – Capture and Inactivation of an Aerosolised SARS-Pseudo-Virus (SARS PV) by Ultravision™ within the Refined Closed-System Model.

In runs #1 - #6, Ad5.GFP was the virus selected for aerosolisation and exposure to Ultravision™. As Ad5 is a non-enveloped virus, it was crucial to also evaluate the effects of Ultravision™ on an enveloped virus. Common viruses such as SARS-CoV-2, Influenza Virus, and Human Immunodeficiency Virus (HIV) are all examples of enveloped viruses (Virology Research Services, 2022), highlighting the importance of evaluating the ability of Ultravision™ to also capture and inactivate enveloped viruses. Lipid envelopes commonly carry a negative charge, which may affect the efficiency of electrostatic precipitation (Pekker and Shneider, 2014). Although data gathered from this study suggests that Ultravision™ can capture and inactivate non-enveloped virus particles, it cannot be simply assumed that Ultravision™ has the same effect on enveloped virus particles. Therefore, in run #7, Ad5.GFP was replaced with SARS PV – an enveloped pseudovirus (Chapter 3). Like Ad5.GFP, SARS PV is a modified viral vector that is replication deficient and expresses the GFP transgene. As the stock of SARS PV was of a lower functional titer than Ad5.GFP, SARS PV was aerosolised through the refined closed-system neat, with 5ml exposed to inactive Ultravision™ and 5ml exposed to active Ultravision™ at 8kV. As well as this, 2ml of the stock was non-aerosolised and therefore not exposed to the system or Ultravision™, serving as a positive control. Additionally, SARS PV utilises the ACE2- receptor for cellular entry upon infection, therefore all assays were performed using CHO-ACE2-TMPRSS2 cells, to ensure virus-cell compatibility. The system setup and dependent variables highlighted in run #1 remained the same. This enabled direct comparisons to be made regarding the effects of Ultravision™ on enveloped viruses versus non-enveloped viruses. Unfortunately, the stock of SARS PV provided by collaborators was limited, therefore only a single experimental run was performed using the viral vector. Further, washes of a stainless steel return electrode could not be performed in this run, due to the low starting titer of the virus sample. Samples collected from washes would have been too dilute to detect via our chosen methods of experimental analysis. Therefore, copper was used as the return electrode in run #7. Conditions achieving the most desirable outcomes, regarding enveloped viruses, may differ from those identified for non-enveloped viruses. Determining optimal Ultravision™ conditions would better inform healthcare staff or other personnel using Ultravision™, when aiming to eliminate specific pathogens and reduce disease transmission.

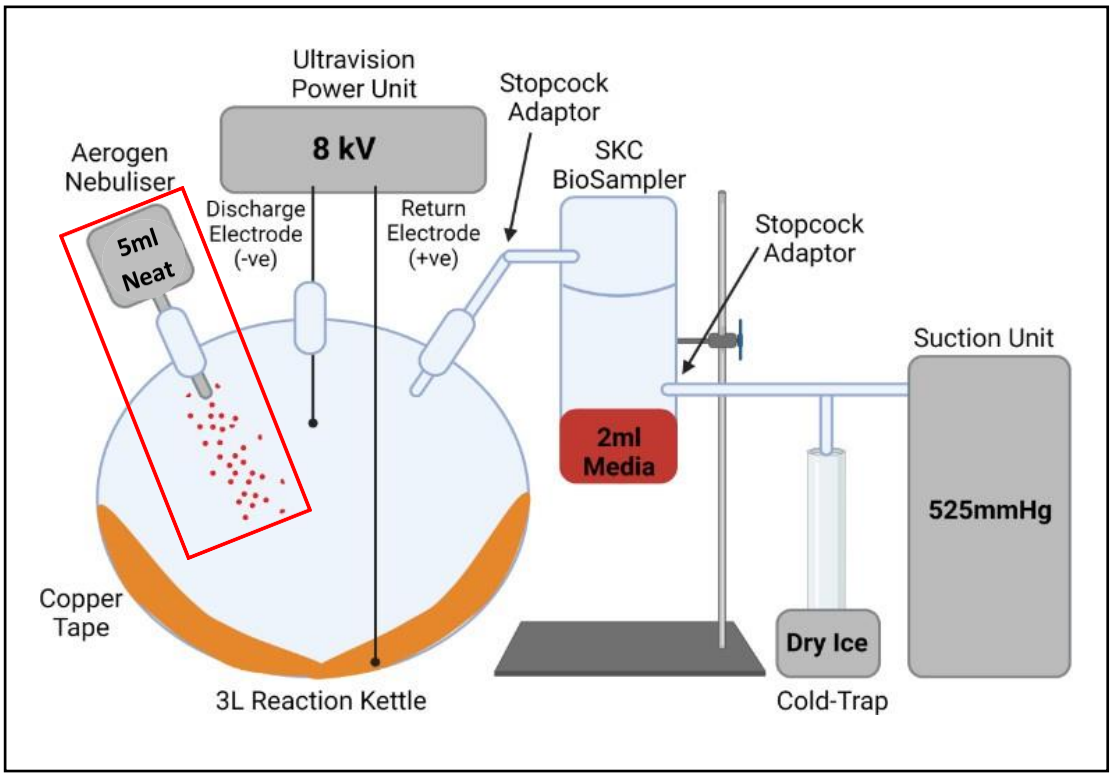

Figure 5.25. A Schematic Depicting the Experimental Setup of Run #7*. The red box highlights the independent variable. Ad5.GFP (run #1) was replaced by SARS PV (run #7). 5ml preparations of neat SARS PV were aerosolised into the reaction kettle and exposed to either inactive or active Ultravision™. Following complete sample aerosolisation, samples were condensed and collected in the BioSampler and stored at -80°C, in preparation for analysis. Additionally, premature condensation of the virus samples that accumulated in the reaction kettle were also collected and stored at -80°C for analysis.*

The number of SARS PV genomes in the collected samples were analysed by qPCR, to evaluate the ability of Ultravision™ to capture aerosolised enveloped virus particles (**Figure 5.26**). The P24 capsid sequence, which is highly conserved amongst HIV variants, and therefore expressed by SARS PV, was amplified in this experiment.

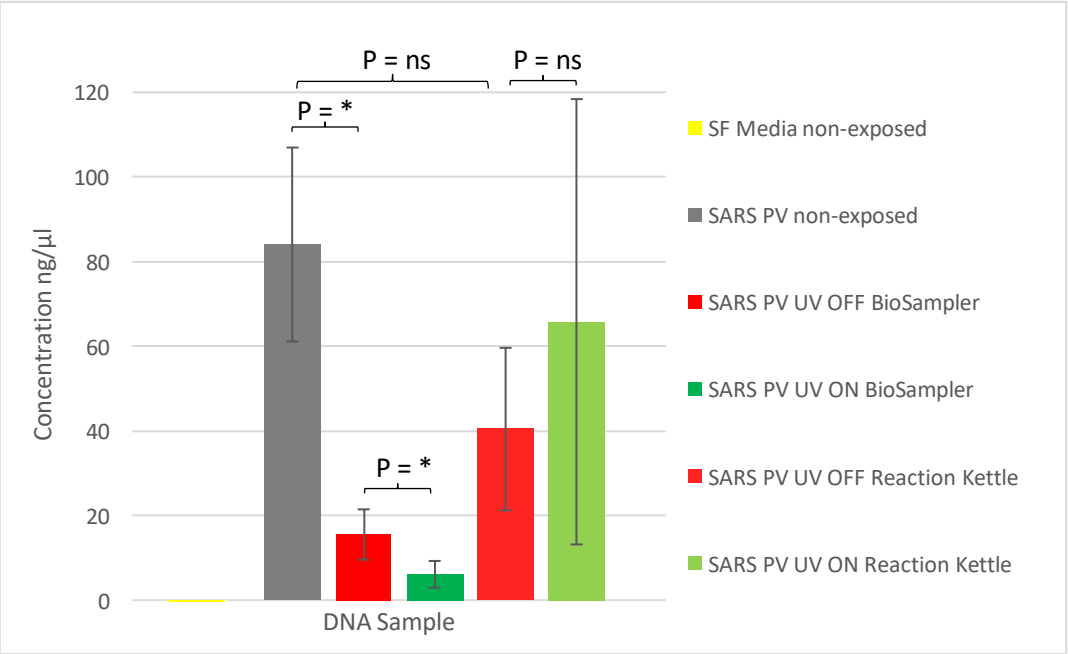

***Figure 5.26*. Average Number of SARS PV Genomes in Collected Samples of SARS PV that had been Aerosolised and Exposed to Inactive/Active Ultravision™, Determined by qPCR – Run #7.** *Yellow bar: SF media non-aerosolised, non-exposed to Ultravision™. Grey bar: Preparation of neat SARS PV, non-aerosolised, non-exposed to Ultravision™. Red bars: SARS PV exposed to inactive Ultravision™. Green bars: SARS PV exposed to active Ultravision™. Assay performed in triplicate - graph displays mean values and SD +/-. The Student's T-test was performed to statistically analyse and compare data sets. * = 0.021 (SARS PV non-exposed: SARS PV UV OFF BioSampler), * = 0.029 (SARS PV UV OFF BioSampler: SARS PV UV ON BioSampler) (statistically significant), ns = no statistically significant difference.*

The non-exposed stock of SARS PV contained the highest number of SARS PV genomes, as expected. Due to its lower titer, the SARS PV sample was run neat, as opposed to previous runs that used diluted samples of Ad5.GFP, therefore the concentration of viral RNA within the non-exposed sample was much higher. SARS PV that had been exposed to inactive Ultravision™ and collected from the BioSampler displayed an 81.6% reduction in the number of viral genomes, in comparison to the non-exposed virus sample. It was suggested that aerosolisation of the sample caused the consequential reduction. However, the sample that had been exposed to active Ultravision™ and collected from the BioSampler showed a 60.6% reduction in the number of viral genomes, in comparison to the sample exposed to inactive Ultravision™. Although a significant proportion of the sample was lost due to aerosolisation, this data demonstrated that Ultravision™ successfully captured aerosolised enveloped virus particles. This indicated that Ultravision™ is capable of precipitating non-enveloped viruses, as well as enveloped virus particles. There was no significant difference in the number of SARS PV genomes within samples obtained from the reaction kettle, that

had been exposed to active or inactive Ultravision™. This was likely due to insufficient exposure of the prematurely condensed virus particles to Ultravision™, as highlighted in previous runs.

To evaluate the ability of Ultravision™ to inactivate aerosolised SARS PV, a transduction assay was performed (**Figure 5.27**). CHO-ACE2-TMPRSS2 cells were infected with each of the collected samples and analysed for GFP expression by Flow Cytometry. As SARS PV also expresses GFP, transduced cells were GFP-positive, enabling direct quantification of the number of active virus particles within each sample.

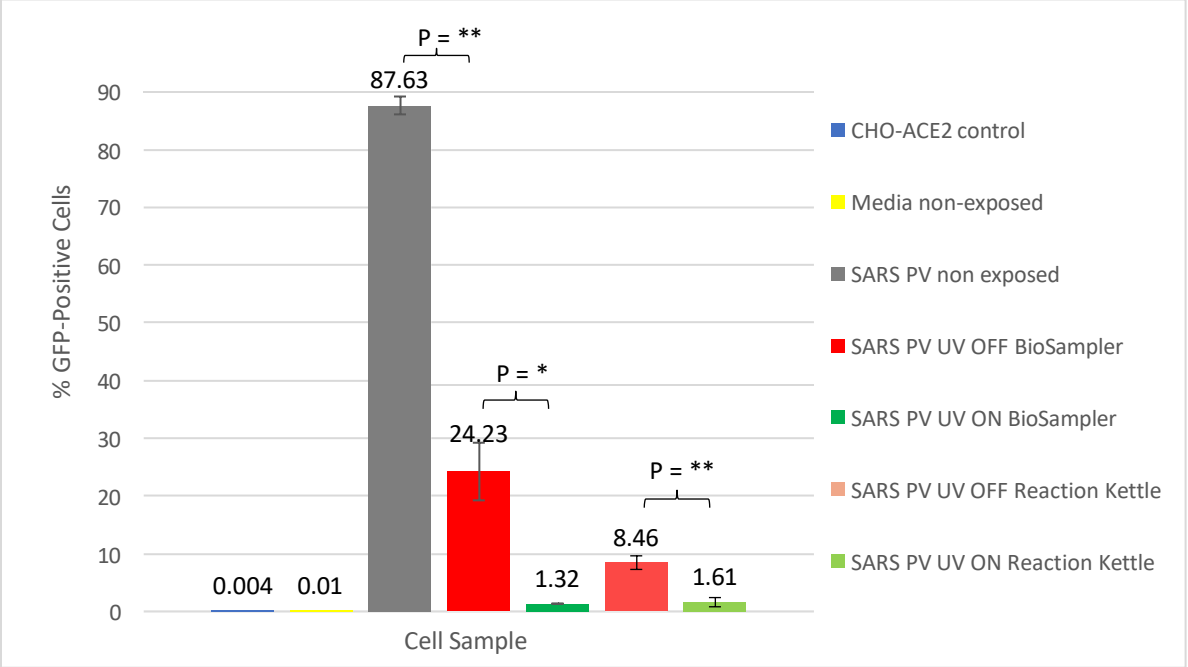

***Figure 5.27**. **Average Percentage of GFP-positive CHO-ACE2-TMPRSS2 Cells, Following Infection with SARS PV Samples that had been Aerosolized and Exposed to Inactive/Active Ultravision™, Determined by Flow Cytometry - Run #7.** Higher GFP fluorescence correlates to a higher number of active virus particles within the sample. Blue bar: CHO-ACE2-TMPRSS2 cells replenished with total media. Yellow bar: SF media non-aerosolised, non-exposed to Ultravision™. Grey bar: Neat stock of SARS PV, non-aerosolised, non-exposed to Ultravision™. Red bars: SARS PV exposed to inactive Ultravision™. Green bars: SARS PV exposed to active Ultravision™. Assay performed in triplicate - graph displays mean values and SD +/-. The Student's T-test was performed to statistically analyse and compare data sets. ** = 0.0027 (SARS PV non exposed: SARS PV UV OFF BioSampler), * = 0.02 (SARS PV UV OFF BioSampler: SARS PV UV ON BioSampler), ** = 0.002 (SARS PV UV OFF RK: SARS PV UV ON RK) (statistically significant).*

Of the cells infected with the neat stock of SARS PV, 87.63% were GFP-positive. This indicated that the stock obtained a relatively high load of active virus particles. Cells that were infected with SARS PV that had been exposed to inactive Ultravision^{TM} and collected from the BioSampler showed a significant reduction in transduction, with 24.23% cells positive for GFP expression. This indicated that aerosolisation of SARS PV through the closed-system caused viral degradation or inactivation. It was assumed that aerosolised SARS PV was less stable than Ad5.GFP. Ad5 is a respiratory virus and therefore undergoes airborne transmission, as opposed to lentiviruses, which are transmitted through bodily fluids and are not spread via aerosols (Stanford University, 2022). This may explain why SARS PV was less stable following aerosolisation, compared to Ad5.GFP. However, cells that were infected with SARS PV that had been exposed to active Ultravision^{TM} and collected from the BioSampler displayed an 18.5-fold reduction in viral activity. This showed that Ultravision^{TM} was capable of inactivating aerosolised enveloped virus particles. However, the virucidal capabilities of Ultravision^{TM} would have been better characterised if SARS PV had better withstood aerosolisation. Finally, 8.46% of cells that were infected with SARS PV that had been exposed to inactive Ultravision^{TM} and collected from the reaction kettle were GFP-positive. This demonstrated that aerosolisation and premature condensation of the SARS PV stock reduced virus viability. Additionally, virus inactivation may have been enhanced following direct contact between SARS PV and the virucidal copper return. Interestingly, 1.16% of cells that were infected with the SARS PV sample that had been exposed to active Ultravision^{TM} and collected from the reaction kettle were GFP-positive, thereby achieving a 5.3-fold reduction in virus activity. This indicated that Ultravision^{TM}, or the electrically charged copper return, contributed to the inactivation of the condensed sample of SARS PV.

To confirm data acquired from the transduction assay, a plaque assay was performed. CHO-ACE2-TMPRSS2 cells were infected with the sample collected from run #7 and analysed for GFP fluorescence via EVOS imaging (**Figure 5.28**).

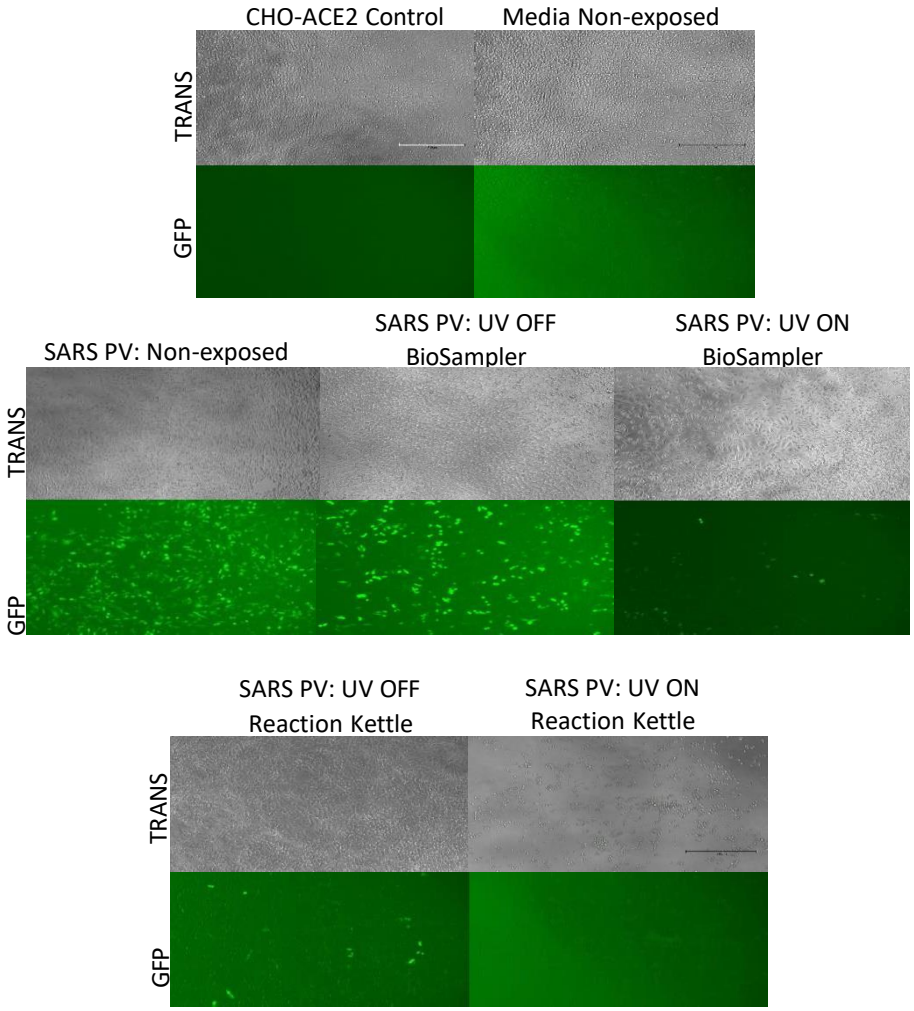

***Figure 5.28**. **EVOS Imaging of CHO-ACE2-TMPRSS2 Cells Infected with SARS PV Samples that had been Aerosolised and Exposed to Ultravision™ – Run #7.** Top panels (TRANS) imaged using transmitted light (brightfield). Bottoms panels (GFP) imaged using the GFP light source. All wells were imaged using a x10 objective lens. CHO-ACE2 Control: Cells replenished with total media. Non-exposed: Sample non-aerosolised and non-exposed to Ultravision™. Fluorescent cells under GFP light source resemble SARS PV infection. Manual counting of fluorescent cells per field of view enabled calculation of pfu/ml values for each sample.*

Table 5.7. Functional Titers Determined by Plaque Assay Analysis - Run #7

Sample	**Functional Titer**
SARS PV: non-exposed	3 x 10^7pfu/ml
SARS PV: UV OFF BioSampler	2.2 x 10^4pfu/ml
SARS PV: UV ON BioSampler	5.3 x 10^3pfu/ml
SARS PV: UV OFF Reaction Kettle	2.2 x 10^3pfu/ml
SARS PV: UV ON Reaction Kettle	-

Cells infected with the non-exposed stock of SARS PV displayed a significant level of fluorescence, and a calculated functional titer of 3 x 10^7pfu/ml. A reduction in fluorescence was observed in cells that were infected with the SARS PV sample that had been exposed to inactive Ultravision^{TM} and collected from the BioSampler. A functional titer of 2.2 x 10^4pfu/ml was calculated for this sample. This finding mirrored data obtained from the transduction assay, where 24.23% of cells were transduced following infection with the same sample. This indicated that the viability of SARS PV was significantly reduced following aerosolisation into the closed-system. As expected, cells that were infected with the SARS PV sample that had been exposed to active Ultravision^{TM} and collected from the BioSampler showed a significant reduction in fluorescence. This demonstrated that Ultravision^{TM} successfully inactivated the virus particles that survived aerosolisation. Finally, cells that were infected with samples collected from the reaction kettle emulated results acquired from the transduction assay. Cells that were infected with SARS PV that had been exposed to inactive Ultravision^{TM} and collected from the reaction kettle displayed low levels of infection. The functional titer calculated for this sample was 2.2 x 10^3pfu/ml. In comparison, cells that were infected with SARS PV that had been exposed to active Ultravision^{TM} and collected from the reaction kettle showed no detectable signs of infection, therefore indicating that Ultravision^{TM} had caused complete inactivation of SARS PV. Contradictory to experiments with Ad5.GFP, this result suggested that Ultravision^{TM} inactivated SARS PV particles that were suspended within the condensed sample. However, virus inactivation may have been enhanced by the electrically charged copper return. Such questions may be answered with repeat experiments using an inert stainless-steel return electrode.

5.3. Discussion

The overarching aim of this chapter was to evaluate the ability of Ultravision^{TM} to capture and inactivate aerosolised virus particles within a closed system. The prototype closed-system (Chapter 4) had multiple limitations. In comparison, the refined closed-system used in this chapter was more representative of closed surgery and therefore gained more reliable, conclusive results. In addition, multiple variables and physical parameters of the closed-system were altered and assessed throughout this chapter. Such independent variables included virus sample concentration, voltage, temperature, the number of Ion Wands present within the reaction kettle, the material of the return electrode and the virus sample itself. This aided the identification of optimal conditions required for maximal virus capture and inactivation by Ultravision^{TM}.

5.3.1. Virus Capture by Ultravision^{TM} within the Refined Closed-System Model

We hypothesised that Ultravision^{TM} could capture aerosolised virus particles via electrostatic precipitation. It was theorised that Ad5.GFP particles would precipitate onto the copper return electrode within the reaction kettle, preventing viral contamination of the media within the BioSampler. Data gathered from run #1 indicated that Ultravision^{TM} could not capture aerosolised virus particles. However, following system optimisations, such as increased voltage, increased number of Ion Wands and enhanced sample aerosolisation, data from runs #2 - #6 showed that Ultravision^{TM} could successfully and significantly capture aerosolised virus particles.

During surgery, human tissue is cut using electrosurgical instruments. Such cutting causes the escape of bioaerosols from the patient's body, into the surrounding environment (Göhler, 2021). Bioaerosols mainly consist of water vapour, however a small percentage consists of cellular debris and other small particles (Serban, 2020). Therefore, if the patient undergoing surgery is carrying an infectious disease, it is possible that the bioaerosols released contain infectious pathogens (Gloster and Roenigk, 1995. Johnson and Robinson, 1991). This increases the risk of disease transmission to healthcare staff and other patients during surgery. The reaction kettle used within the closed-system aimed to mimic a patient's abdomen, as Ultravision^{TM} is most commonly used to clear surgical smoke during abdominal laparoscopy. Therefore, virus samples that accumulated within the reaction kettle aimed to resemble the viral contents within the abdomen of an infectious patient

undergoing surgery. Additionally, samples collected from the BioSampler aimed to mimic the contents of bioaerosols that escape during closed surgery. The presence of virus particles that remained within the reaction kettle were of no concern, as such particles would not be released during surgery. However, virus particles that were collected within the BioSampler were of major concern, as infectious bioaerosols released from the abdomen enable disease transmission. Thus, it was hypothesised that Ultravision^{TM} would reduce the number of virus particles that entered the BioSampler, via successful electrostatic precipitation, resulting in an accumulation of virus particles within the reaction kettle. Additionally swabs and washes of the return electrode were performed in Chapter 5, to detect the number of virus particles that had precipitated onto the return as a result of electrostatic precipitation. Therefore, successful capture of aerosolised virus particles was visualised in chapter 5 as an accumulation of virus particles within the reaction kettle, and an absence of virus particles collected within the BioSampler.

To evaluate the ability of Ultravision^{TM} to capture virus particles, qPCRs were performed to determine the number of viral genomes within each of the collected samples. Surprisingly, virus capture appeared unsuccessful in run #1. The concentration of viral DNA within the BioSampler was not reduced following sample exposure to Ultravision^{TM}. This implied that the aerosolised particles were not precipitated onto the return electrode within the reaction kettle. However, independent variables were not optimised in run #1, explaining the unsuccessful capture of viral particles. On the other hand, successful virus capture was observed in runs #2 - #6, where conditions were altered and optimised to enhance electrostatic precipitation and virus capture.

In run #2, two diluted samples of Ad5.GFP were aerosolised and exposed to Ultravision^{TM}. Ad5.GFP at 1 x 10^8vp/ml was successfully captured by Ultravision^{TM}, as determined by a decrease in viral genomes within the BioSampler. However, the sample of Ad5.GFP at 1 x 10^7vp/ml was not successfully captured by Ultravision^{TM}. It was hypothesised that the starting concentration of the virus (1 x 10^7vp/ml) was too low for accurate detection by qPCR. Therefore, all subsequential runs aerosolised Ad5.GFP at 1 x 10^{10}vp/ml, to facilitate the ability to detect changes in the number of viral genomes within the collected samples via qPCR.

In run #3, various Ultravision™ voltages were compared to determine the optimum voltage at which Ultravision™ was able to capture maximal virus particles. Although virus capture appeared successful following Ad5.GFP exposure to Ultravision™ at 6kV and 8kV, exposure of Ad5.GFP to Ultravision™ at 10kV captured the highest number of virus particles. 10kV is the maximum voltage that is medically approved for Ultravision™ use during surgery. Therefore, surgeons could use Ultravision™ at 10kV when clearing surgical smoke, as this should simultaneously reduce the risk of disease transmission during surgery. Likewise, run #5 compared the ability of 1 versus 2 Ultravision™ Ion Wands to capture aerosolised Ad5.GFP. Both Ion Wands were set at 8kV, which is the standard voltage of Ultravision™ that is currently used during surgery. qPCR results indicated that using 2 Ion Wands at 8kV achieved a similar level of virus capture as 1 Ion Wand at 10kV.

Upon gaining such key findings regarding the ability of Ultravision™ to capture virus particles, additional modalities of Ultravision™ were speculated. For example, an air-purification system obtaining a series of multiple Ion Wands may enable efficient virus capture within an open setting, thereby not limiting the use of Ultravision™ to solely closed surgery. The development of a novel air-purifier that successfully captures virus particles would be extremely marketable in our current climate, as well as improve the safety conditions of hospitals and other communal environments in the case of future pandemics.

Condensation of the virus samples was observed in runs #1 - #3, resulting in the accumulation of active virus particles within the reaction kettle. To overcome this issue, 37°C heat was applied to the reaction kettle in run #4, to maintain sample aerosolisation. qPCR results from run #4 demonstrated that sustained aerosolisation of Ad5.GFP enabled better virus capture by Ultravision™. It was theorised that Ultravision™ could not efficiently influence virus particles present within the condensed, liquid solutions and thereby only precipitated particles that were suspended in aerosol. This finding was important to note for the medical use of Ultravision™, as surgeons must not presume that liquid substances released during surgery are equally decontaminated by Ultravision™ in the same way as bioaerosols.

Finally, in run #7, the ability of Ultravision™ to capture both enveloped and non-enveloped virus particles from bioaerosols was compared. It appeared that electrostatic precipitation was not only capable of capturing non-enveloped viruses (Ad5.GFP) but could also capture

enveloped viruses (SARS PV). qPCR results demonstrated that the number of SARS PV genomes collected within the BioSampler was significantly reduced (60.6% reduction) following viral exposure to active Ultravision^{TM}. This indicated that the SARS PV particles were successfully precipitated onto the return electrode within the reaction kettle. However, due to limited stocks, only one experimental run was performed using SARS PV, therefore experimental repeats are essential to acquire reliable, conclusive results. Additionally, future experimental runs should also analyse independent variables that affect the efficiency of the electrostatic precipitation to capture enveloped virus particles. Conditions that enable the optimal capture of non-enveloped virus particles may differ to those required for the capture of enveloped virus particles. Therefore, it is important to assess variables such as voltage, temperature, and aerosol flow rate, when evaluating the ability of Ultravision^{TM} to capture structurally different viruses.

In summary, experimentation using the refined closed-system demonstrated that Ultravision^{TM} can capture aerosolised non-enveloped and enveloped viral particles. Although virus capture was significant, the amount of capture was slight and differed between experimental runs. Perhaps the method of detecting viral capture during this study was limited. qPCR measures the presence and concentration of viral genomes, as opposed to the presence and concentration of intact virus particles. Therefore, it was considered that the DNA/RNA collected from the BioSampler may have been free from a viral envelope or capsid. Kettleson (2009) suggested that electrostatic precipitators generate reactive species via the corona discharge of the negative electrode. Reactive species have the potential to degrade virus particles, which theoretically, would result in the release of viral DNA/RNA. This theory provides an explanation for the collection of viral DNA/RNA within the BioSampler following viral exposure to active Ultravision^{TM}. Isolated DNA/RNA is too small to be captured by electrostatic precipitation and would therefore accumulate within the BioSampler; whilst larger structural components, such as viral envelopes or capsids, would precipitate onto the return electrode within the reaction kettle following exposure to active Ultravision^{TM}. Therefore, the amount of DNA/RNA present within the BioSampler may not correlate to the amount of viral capture or degradation occurring within the reaction kettle. Due to this, analysing the presence and concentration of viral proteins (e.g., viral envelope/capsid) via western blots, ELISAs or antibody binding assays, may be more suitable

for demonstrating the capabilities of Ultravision™ and deducing its mechanism of action. However, it is important to note that isolated viral DNA/RNA, that is not enclosed within a viral capsid, is inert and non-infectious. Therefore, its presence within bioaerosols is not harmful (Fenner, 1987. Gelderblom, 1996. Lentz, 2005). Capsids are required to deliver viral DNA/RNA to cells upon infection, therefore no infection or viral replication can take place when cells are exposed to isolated viral DNA/RNA. Additionally, it is likely that viral DNA/RNA would be degraded quickly when suspended in aerosol, further reducing the impact of its presence in bioaerosols (Fenner, 1987. Gelderblom, 1996. Lentz, 2005). Nevertheless, repeat studies of the runs performed in Chapter 5 are required to analyse virus capture caused by Ultravision™, using alternative experimental methods.

5.3.2. Virus Inactivation by Ultravision™ within the Refined Closed-System Model

Next, the ability of Ultravision™ to inactivate aerosolised virus particles was analysed. We hypothesised that Ultravision™ could inactivate aerosolised virus particles, due to the generation of reactive species from the corona discharge of the Ultravision™ Ion Wand. Overall, the data from chapter 5 demonstrated that Ultravision™ was able to significantly inactivate both enveloped and non-enveloped virus particles.

Optimal conditions for the inactivation of virus particles by Ultravision™ were determined in this chapter. Data from run #3 indicated that using Ultravision™ at 10kV, as opposed to 6kV or 8kV, enhanced virus inactivation. Additionally, run #5 highlighted that exposure of Ad5.GFP to 2 Ultravision™ Ion Wands at 8kV, as opposed to 1 Ion Wand at 8kV, also enhanced virus inactivation. Both methods of achieving significant virus inactivation maintained medically approved voltages and settings, therefore could be implemented during surgery, to reduced disease transmission.

Additional parameters effecting the efficiency of Ultravision™ were also altered in chapter 5, and the resulting level of virus inactivation was analysed. In run #4, the reaction kettle was heated to 37°C to maintain sample aerosolisation. This promoted the exposure of aerosolised virus particles to the Ultravision™ Ion Wand, improving the efficiency of virus inactivation, irrespective of the voltage or number of Ion Wands used. Another parameter that underwent alteration was the material of the positively charged return electrode. Copper tape was used in runs #1-#5 to collect precipitated particles via electrostatic

attraction. However, copper is a virucidal metal, and therefore has the capacity to inactivate virus particles (Govind, 2021). To ensure that Ultravision™ was the sole cause of virus inactivation, copper was replaced with stainless-steel in run #6. Stainless-steel is biologically inert and therefore does not affect the activity of virus particles upon direct contact. Results obtained from run #6 demonstrated that Ultravision™ was the sole cause of virus inactivation, confirming the reliability of the data gathered from runs #1-#5.

Finally, Chapter 5 aimed to deduce whether Ultravision™ could inactivate both enveloped and non-enveloped virus particles. In runs #1-#6, Ad5.GFP (non-enveloped) was exposed to Ultravision™, whilst in run #7, SARS PV (enveloped) was exposed to Ultravision™. Transduction assays and plaque assays indicated successful inactivation of both viruses, post exposure to active Ultravision™. However, aerosolisation of SARS PV alone caused a significant level of virus inactivation. SARS PV is comprised of a lentivirus capsid, surrounding a HIV core. Unlike Ad5, which is a respiratory pathogen, lentiviruses are not transmissible via aerosol. It is therefore likely that aerosolisation of SARS PV resulted in viral instability and degradation, causing inactivation. In future studies, a respiratory enveloped pathogen, such as whole SARS-CoV-2 (which would require to be run in CL3 containment levels, available in house), could be used to accurately evaluate the ability of Ultravision™ to capture and inactivate enveloped respiratory-virus particles. Lastly, as stated for the capture of enveloped virus particles, conditions that enable the optimal inactivation of enveloped virus particles may differ to those required for the inactivation of non-enveloped virus particles; therefore, additional experimental runs evaluating a multitude of independent variables are required.

Chapter 6: Evaluation of Ultravision™ to Capture and Inactivate Aerosolised Virus Particles using a Prototype 'Open-System' Model

6.1. Introduction

Chapters 4 and 5 evaluated the ability of Ultravision™ to capture and inactivate aerosolised virus particles within a closed system. The closed-system models were designed to resemble the release of bioaerosols that occurs during key-hole surgery. Since Ultravision™ is currently used to clear surgical-smoke during surgical procedures, its efficiency and safety has already been established and medically approved within closed-system environments. Data gathered from Chapters 4 and 5 indicate that Ultravision™ can efficiently inactivate aerosolised virus particles within a closed system. Due to recent advances in Ultravision™ technology, it is likely that Ultravision™ will be employed during open surgeries in the near future, to clear surgical smoke. Therefore, the final chapter of this study evaluated the ability of Ultravision™ to capture and inactivate aerosolised virus particles within an open-system environment.

As discussed in section 1.3, it has been demonstrated that bioaerosols released during surgery can contain live virus particles, capable of infecting healthcare staff and other patients (Gloster and Roenigk, 1995. Johnson and Robinson, 1991). Ultimately, this can occur during open or closed surgery. Therefore, manipulating the virucidal properties of Ultravision™ may prevent the transmission of respiratory pathogens during medical procedures. However, the release of surgical bioaerosols is not the only means of virus spread. Most disease spread within hospitals occurs via airborne or droplet transmission. When infectious patients cough, sneeze, talk and touch objects, the likelihood of virus spread is increased. This of course occurs within open, communal environments. At present, HEPA filters and air-ventilation systems are in place to reduce disease transmission, however such devices are not 100% effective. Determining the ability of Ultravision™ to capture and inactivate aerosolised virus particles within an open system may highlight a novel avenue for its use in hospitals. If successful, Ultravision™ could be implemented in the development of new and improved air-purification systems, improving the sanitisation and decontamination of air within hospitals. This is important as hospitals serve as breeding grounds for all types of infectious pathogens. Therefore, employing a better method of air-filtration would reduce the impacts of future pandemic outbreaks.

The most commonly used air-purification systems in hospitals are HEPA air filters, Ultraviolet light sterilisation and indeed electrostatic precipitator filters (Elsaid and Ahmed, 2021). Although each system is somewhat effective, all methods obtain a series of limitations, thus affecting the cleaning of indoor air.

HEPA filters are deep, bulky and use high levels of energy, as well as require regular filter changes, which can be expensive and non-economical. Only qualified personnel are permitted to change HEPA filters, as this can be hazardous. The filters can harbour live viruses and other pathogens, thereby risking the transmission of disease during changes. This raises an issue, as the efficiency of HEPA filters is drastically reduced once the filter is saturated, hence filter changes are essential and required often (Christopherson, 2020). Additionally, some viruses, including SARS-CoV-2, are too small to be trapped by HEPA filtration. Most HEPA filters can trap particles at a minimum size of 0.15µm, whereas SARS-CoV-2 is roughly 0.1µm in diameter and may therefore bypass the filtration mechanism (Bar-On, 2020. Christopherson, 2020).

Although Ultraviolet light has shown competent destruction of pathogens in an abundance of studies, its efficiency is limited to its alignment with and distance from the pathogen itself (Ramos, 2020). Additionally, the lack in standardisation of the irradiance dose and exposure time is of concern and may be hazardous when implemented in settings lacking medical professionals (Ramos, 2020).

Comparatively, electrostatic precipitators, including Ultravision^{TM}, are highly efficient at capturing particles, ranging from approximately <7nm – 10µm, therefore including SARS-CoV-2 and other small viruses (Alesi Surgical, 2022). In addition to capturing pathogens, Ultravision^{TM} has the capacity to inactivate pathogens, thus enhancing air decontamination and prohibiting device-cleaning-related risks. Further to this, electrostatic precipitators do not require filter changes, and are therefore more economical and easier to manage. Understanding these additional modalities of Ultravision^{TM} and employing it into novel air-filtration devices may prove advantageous in hospital settings. Other electrostatic precipitators are already used to sample the air within hospitals, enabling rapid and accurate diagnosis of infectious patients (Piri, 2021). Air-sampling is performed to precisely identify pathogens causing infections within hospitals, to stop the spread of disease and to treat the infected patients with pathogen-specific medication. This of course is performed in

open environments, providing a second rationale for the evaluation of Ultravision^{TM} to capture and inactivate aerosolised virus particles within an open-system. This also implies a high likelihood of success, feasibility, and practicality.

The number of published studies assessing the ability of electrostatic precipitation to capture aerosolised pathogens is limited. Even fewer studies have analysed the ability of electrostatic precipitation to inactivate pathogens. However, those that do exist have used only closed-system models. Due to the lack of studies using open-system models, this chapter aimed to fill the gap that exists within the literature. Therefore, a third Ultravision^{TM} model was designed and constructed. The model was a prototype, to gain 'proof-of-concept' data, regarding the capabilities of Ultravision^{TM} within an open environment. The setup of the prototype open-system model is displayed in **figure 6.1**.

Due to limited time and virus samples, only two experimental runs were performed using the open-system. Firstly, a control run was performed, whereby PBS was aerosolised through the system and exposed to active and inactive Ultravision^{TM}. This was carried out to ensure that the system ran correctly with no leaks and to test the practicality of sample collection from the BioSampler and from the 3 stainless-steel sheets. Secondly, an experimental run was performed, whereby a known concentration of Ad5.GFP was aerosolised through the system and exposed to active or inactive Ultravision^{TM}. In this sense, the open-system was not dissimilar from the closed-system, however the direction of air-flow was less controlled in the open-system, thereby mimicking air-flow dynamics that occur in open environments.

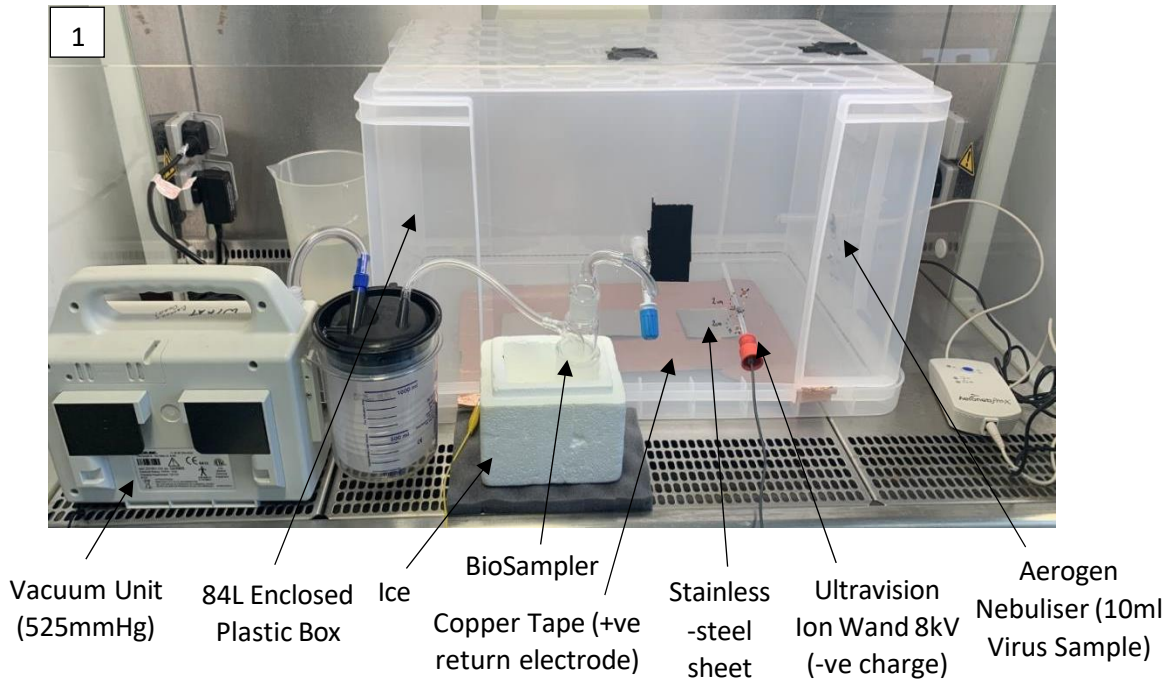

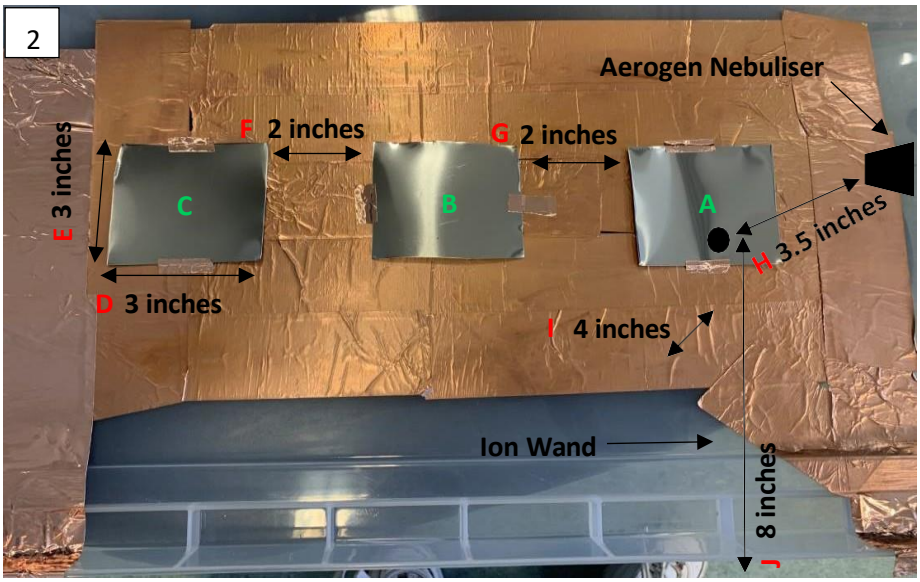

Figure 6.1. ***Experimental Setup of the Prototype Open-System Model. 1)*** *10ml virus samples were aerosolised via the Aerogen nebuliser into the 84L plastic box. The copper tape covering the bottom of the box was connected to the return electrode, thereby holding a positive charge. The 3 stainless-steel sheets attached to the copper return were utilised as collector plates, for the capture of virus particles. The flow of aerosol was passed across the Ultravision™ Ion Wand (8kV), ensuring particle exposure to the corona discharge. A vacuum device was used to suction the sample through the system, directing the flow of aerosol into the BioSampler for sample collection.* ***2)*** *The Ion Wand was placed 3.5 inches from the nebuliser, 4 inches above the copper return and directly over the first steel sheet (A). Steel sheet B was positioned 2 inches from steel sheet A and 2 inches from steel sheet C. Following complete sample aerosolisation, the steel sheets were washed with 2ml SF media to obtain any precipitated virus particles for experimental analysis. All collected samples were stored at -80°C.*

The open-system was designed to resemble that of a hospital room. At first, the enclosure of aerosolised samples within the 84L plastic box appears counterproductive, as it seems to resemble that of the closed-system model. However, in hospitals, ventilation systems circulate and filter the air within each room. Therefore, the plastic box will mimic the circulation of air within a room, yet on a much smaller scale. Additionally, the volume of air within the box was 28 times greater than that within the reaction kettle of the closed-system, thereby permitting free and randomised movement of the aerosolised particles.

In addition to airborne transmission, droplet transmission facilitates viral spread. Following natural aerosolisation of virus particles, for example as a result of coughing, virus particles deposit onto nearby surfaces and objects. When another person touches the contaminated surface, they are then prone to viral infection. The implementation of stainless-steel sheets in the open-system model was to analyse the likelihood of droplet transmission, before and after the employment of Ultravision^{TM}. It was theorised that virus particles would both passively and actively precipitate onto the steel sheets – passively, due to the nature of gravity, and actively, due to electrostatic precipitation caused by Ultravision^{TM}. Therefore, analysing the steel sheets for viral presence and activity was important, to evaluate the ability of Ultravision^{TM} to inhibit droplet transmission. The three steel sheets were strategically placed at various distances from the point of sample aerosolisation. This was performed to evaluate the distance of virus particle travel when aerosolised into an open environment and exposed to inactive or active Ultravision^{TM}. It was hypothesised that virus particles would travel a much shorter distance when exposed to active Ultravision^{TM}, as a result of electrostatic precipitation.

The preliminary study aimed to identify additional modalities of Ultravision^{TM}, that may circumvent the limitations of currently used air-purification devices, resulting in more efficient air cleaning.

6.1.2. Chapter Aims and Hypotheses

The aims of this chapter are detailed in the list below:

1. To design and construct a novel open-system model, resembling the aerosol dynamics that occur within open environments (e.g., open surgery / ventilation within a hospital room).

2. To evaluate the ability of Ultravision^{TM} to capture and inactivate aerosolised virus particles within the open-system model.

3. To compare the efficiency of Ultravision^{TM} to capture and inactivate virus particles within the open-system model to that within the closed-system model.

4. To identify limitations of the prototype open-system, to better advise the production of a more accurate, refined open-system in the case of future experimentation.

Although previous studies have assessed the use of electrostatic precipitation as a method of air-sampling and air-purification, very few studies have assessed the association between electrostatic precipitation and the removal and inactivation of virus particles. Furthermore, studies analysing virus capture and inactivation that do exist have only performed experiments within closed-system models. Therefore, hypotheses regarding the ability of Ultravision^{TM} to capture and inactivate virus particles within an open system were based on results obtained from closed-system studies, including those performed in Chapters 4 and 5. It was hypothesised that virus samples aerosolised through the open-system and exposed to inactive Ultravision^{TM} would retain a highly active viral load. In comparison, it was hypothesised that exposure of aerosolised virus samples to active Ultravision^{TM} would show significant reductions in the concentration of active virus particles. We considered that the number of active virus particles collected in the BioSampler would reduce, whilst the number of virus particles actively precipitated onto the stainless-steel sheets would increase, as a result of electrostatic precipitation. Additionally, it was believed that particles precipitated onto the stainless-steel sheets would be inactivated, due to the generation of reactive species from the corona discharge produced by the Ion Wand. Finally, we evaluated whether virus particles would passively precipitate onto all three stainless-steel sheets following exposure to inactive Ultravision^{TM}. Alternatively, we sought to assess whether virus particles would actively precipitate onto stainless-steel sheet A alone, following exposure to active Ultravision^{TM}.

6.2. Results

The prototype open-system was satisfactory for gaining preliminary data. The system functioned correctly, without leakages or premature condensation of the aerosolised samples. In addition, sample collection from both the BioSampler and stainless-steel sheets was feasible and practical, to determine the extent of electrostatic precipitation and virus inactivation caused by Ultravision™.

Although the ability of Ultravision™ to capture and inactivate aerosolised virus particles was predominantly analysed via biological assays, the effects of Ultravision™ were also observable to the naked eye. **Figure 6.2** highlights the visible effects of Ultravision™ on the flow of aerosol within the open-system. Additionally, **figure 6.3** displays the visible precipitation of aerosol particles onto the steel collector plate, following sample exposure to active Ultravision™. Both figures indicate efficient electrostatic precipitation of the aerosol particles onto the return-electrode. However, experimental analysis of samples collected from the BioSampler and the stainless-steel sheets was still required, to assess whether Ultravision™ had also influenced virus viability.

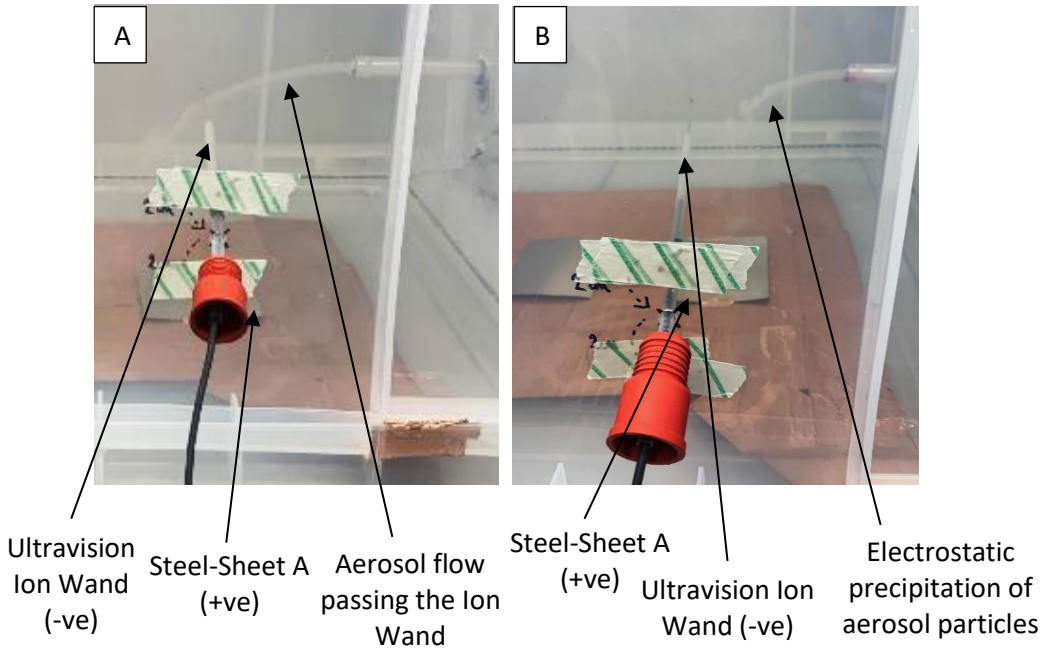

***Figure 6.2**. **Photo Images of the Aerosolisation of Virus Samples into the Open-System Model**. **Image A** displays the flow of aerosol upon exposure to inactive Ultravision™. The aerosol passed the Ion Wand and travelled across the 84L plastic box. **Image B** displays the flow of aerosol upon exposure to active Ultravision™. The flow of aerosol was prevented from passing the Ion Wand due to successful electrostatic precipitation of the aerosolised particles onto the positively charged steel-sheet. Therefore, the aerosol travelled a much shorter distance across the 84L plastic box.*

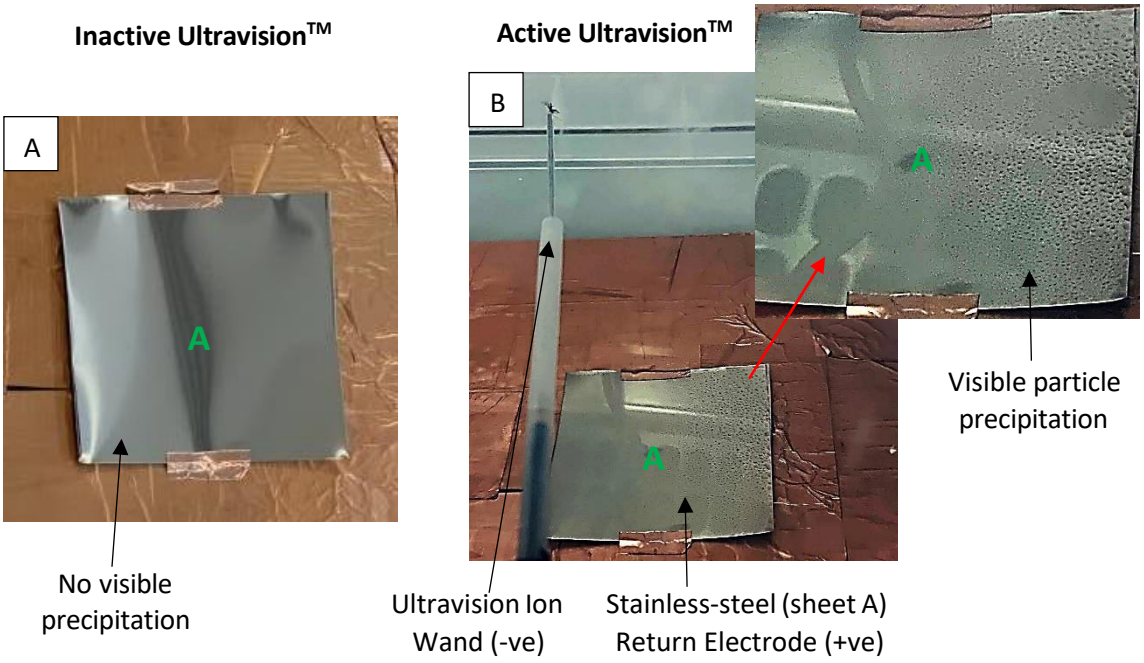

Figure 6.3. Photographs of Stainless-Steel Sheet A, Following the Exposure of Aerosolised Virus Samples to Inactive/Active Ultravision™. Image A *displays stainless-steel sheet A following sample exposure to inactive Ultravision™. No droplets of the aerosol sample were visible on sheet A, indicating no particle precipitation.* ***Image B*** *displays stainless-steel sheet A following sample exposure to active Ultravision™. Visible droplets were observed on the right-hand side of the steel sheet (in front of the Ion Wand), however, no droplets were displayed on the left-hand side of the steel sheet (passed the Ion Wand). This demonstrated successful electrostatic precipitation of the aerosolised particles onto the return electrode. Red arrow: Magnification of image B.*

6.2.2. Capture of Aerosolised Ad5.GFP by Ultravision™ within the Open-System Model.

To evaluate whether Ultravision™ had successfully captured Ad5.GFP within the open-system model, qPCR was performed (**Figure 6.4**). DNA was extracted from samples collected from the BioSampler and from samples obtained following washes of the stainless-steel sheets. Ad5 genomic DNA was quantified by qPCR in each of the collected samples, to measure the concentration of Ad5 genomes post sample exposure to inactive/active Ultravision™.

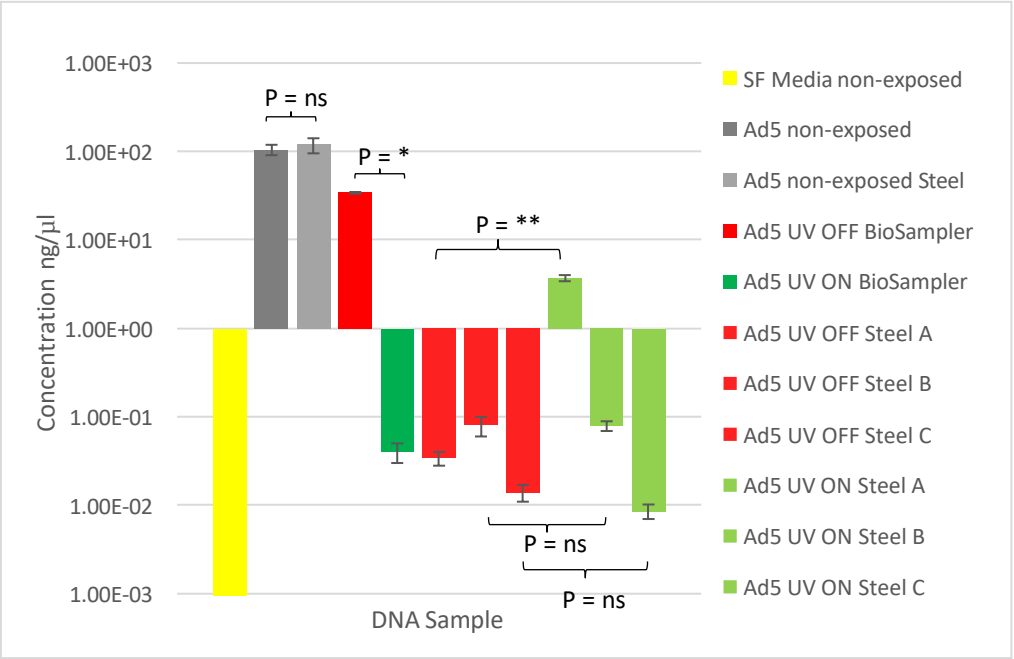

***Figure 6.4*. Average Number of Ad5 Genomes in Collected Samples of Ad5.GFP that had been Aerosolised and Exposed to Inactive/Active Ultravision™ within the Open-System, Determined by qPCR.** *Yellow bar: SF media non-aerosolised, non-exposed to Ultravision™. Grey bar: Preparation of Ad5.GFP at 1 x 10^{10}vp/ml, non-aerosolised, non-exposed to Ultravision™. Red bars: Ad5.GFP exposed to inactive Ultravision™. Green bars: Ad5.GFP exposed to active Ultravision™. (A/B/C: corresponds to the distance of the steel sheet from the Ion Wand). Assay performed in triplicate - graph displays mean values and SD +/-. The Student's T-test was performed to statistically analyse and compare data sets. * = 0.017 (Ad5 UV OFF BioSampler: Ad5 UV ON BioSampler), ** = 0.0023 (Ad5 UV OFF Steel A: Ad5 UV ON Steel A) (statistically significant), ns = no statistically significant difference.*

Direct contact between the stainless-steel and the aerosolised virus sample caused no significant difference to the number of Ad5 viral genomes within the non-exposed preparation of Ad5.GFP. This confirmed that stainless-steel is inert and does not affect the stability of viral DNA. Following aerosolisation of Ad5.GFP into the open-system and exposure to inactive Ultravision™, the concentration of Ad5 genomic DNA that was collected within the BioSampler was significantly reduced. This indicated that aerosolisation alone resulted in the loss of Ad5.GFP particles. Is it likely that aerosolising Ad5.GFP into the open-system promoted free and randomised particle movement, thereby reducing the number of particles suctioned into the BioSampler, thus explaining the reduction of Ad5 DNA. Nevertheless, a 98.8% reduction in the number of viral genomes was observed in samples that had been exposed to active Ultravision™ and collected from the BioSampler.

This data suggests that Ultravision™ is capable of capturing aerosolised virus particles within open-system environments via electrostatic precipitation.

Following the exposure of Ad5.GFP to Ultravision™, all three stainless-steel sheets were washed with 2ml serum-free media and the resulting media was stored for experimental analysis. All three stainless-steel sheets contained very low concentrations of Ad5 genomic DNA, post exposing Ad5.GFP to inactive Ultravision™. This indicated that the sample of Ad5.GFP remained aerosolised and freely circulated within the 84L plastic box. In comparison, following Ad5.GFP exposure to active Ultravision™, stainless-steel sheet A contained a significant amount of Ad5 viral genomes. This indicated that Ultravision™ successfully captured the aerosolised virus particles onto stainless-steel sheet A. However, stainless-steel sheets B and C contained very low concentrations of Ad5 genomic DNA. As the Ion Wand was placed directly above stainless-steel sheet A, the aerosolised sample actively precipitated onto this steel sheet. Therefore, fewer virus particles remained aerosolised, thus explaining the lower numbers of Ad5 genomes obtained from steel sheets B and C. This demonstrates that Ultravision™ can successfully prevent the escape of aerosolised virus particles within an open system environment, as ionised particles are unable to bypass the region of electrostatic precipitation.

6.2.3. Inactivation of Aerosolised Ad5.GFP by Ultravision™ within the Open-System.

To evaluate the ability of Ultravision™ to inactivate virus particles within the prototype open-system, a transduction assay was performed (**Figure 6.5**). CHO-CAR cells were infected with each of the collected samples and analysed for GFP expression by Flow Cytometry.

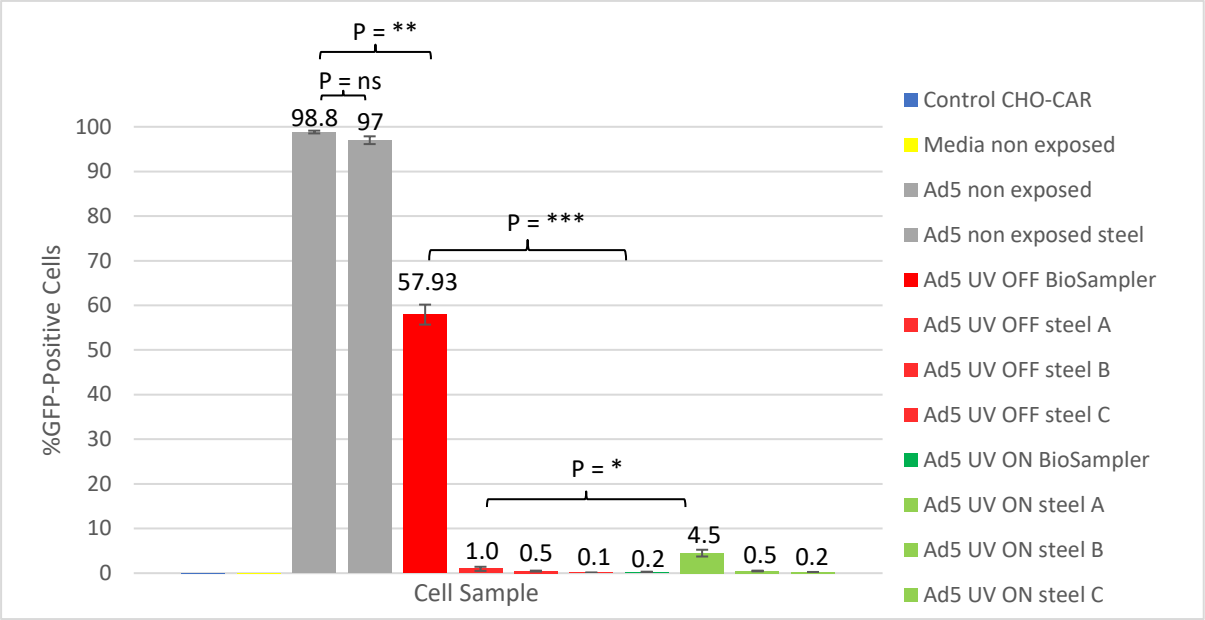

***Figure 6.5*. Average Percentage of CHO-CAR Cells Positive for GFP Expression, Following Infection with Ad5.GFP Samples that had been Aerosolised into the Open-System and Exposed to Ultravision™, Determined by Flow Cytometry.** *Blue bar: CHO-CAR cells replenished with total media. Yellow bar: SF media non-aerosolised, non-exposed to Ultravision™. Grey bars: Ad5.GFP at 1 x 10^{10}vp/ml non-aerosolised, non-exposed to Ultravision™. Red bars: Ad5.GFP exposed to inactive Ultravision™. Green bars: Ad5.GFP exposed to active Ultravision™. Steel: Sample washed from stainless-steel sheets (A/B/C: corresponds to distance from the Ion Wand). Assay performed in triplicate - graph displays mean values and SD +/-. The Student's T-test was performed to statistically analyse and compare data sets. ** = 0.001 (Ad5 non exposed: Ad5 UV OFF BioSampler), ***(Ad5 UV OFF BioSampler: Ad5 UV ON BioSampler) = 0.0005, * (Ad5 UV OFF steel A: Ad5 UV ON steel A) = 0.03 (statistically significant), ns = no significant difference.*

There was no significant difference between the percentage of GFP-positive cells in cells infected with the non-exposed preparations of Ad5.GFP that had and had not been exposed to stainless-steel. Again, this indicated that stainless-steel does not affect the viability of Ad5.GFP upon direct contact. 57.93% of cells were transduced by the Ad5.GFP sample that had been exposed to inactive Ultravision™ and collected from the BioSampler. This reduction in viral activity may have been due to the loss of virus particles within the open-system. The 84L plastic box was 28 times larger than the 3L reaction kettle that was used in the closed-system, therefore it was likely that more of the virus particles within the open-system remained aerosolised or passively deposited within the plastic box. In contrast, only 0.2% of cells were transduced by the equivalent Ad5.GFP sample exposed to active Ultravision™ and collected from the BioSampler. This 290-fold reduction in virus activity

demonstrated that Ultravision^{TM} successfully inactivated the aerosolised viral particles within the open-system.

As stainless-steel is biochemically inert, it was possible to analyse the stainless-steel sheets for the presence of active virus particles. Following the exposure of Ad5.GFP to inactive Ultravision^{TM}, all three stainless-steel sheets contained no detectable traces of viable virus particles. This indicated that the sample remained aerosolised, and was not subjected to electrostatic precipitation. Additionally, it is likely that most virus particles were either suctioned into the BioSampler via the vacuum unit, or randomly distributed across the 84L plastic box. On the other hand, following the exposure of Ad5.GFP to active Ultravision^{TM}, stainless-steel sheet A contained a low but significant number of active virus particles. In agreement with the qPCR data, this indicated that Ultravision^{TM} successfully precipitated virus particles onto stainless-steel sheet A and simultaneously inactivated the majority of captured particles. However, stainless-steel sheets B and C contained no detectable viable virus particles. This indicated that all of the virus particles were precipitated onto sheet A, due to its positioning directly beneath the Ion Wand. It was therefore concluded that Ultravision^{TM} successfully captured and inactivated aerosolised Ad5.GFP particles within the open-system, however the exact level of virus inactivation remained unclear.

To validate the results obtained from the transduction assay, a plaque assay was performed (**Figure 6.6**). TRex-293 cells were infected with samples that had been exposed to Ultravision^{TM} within the open-system and analysed for GFP fluorescence via EVOS imaging.

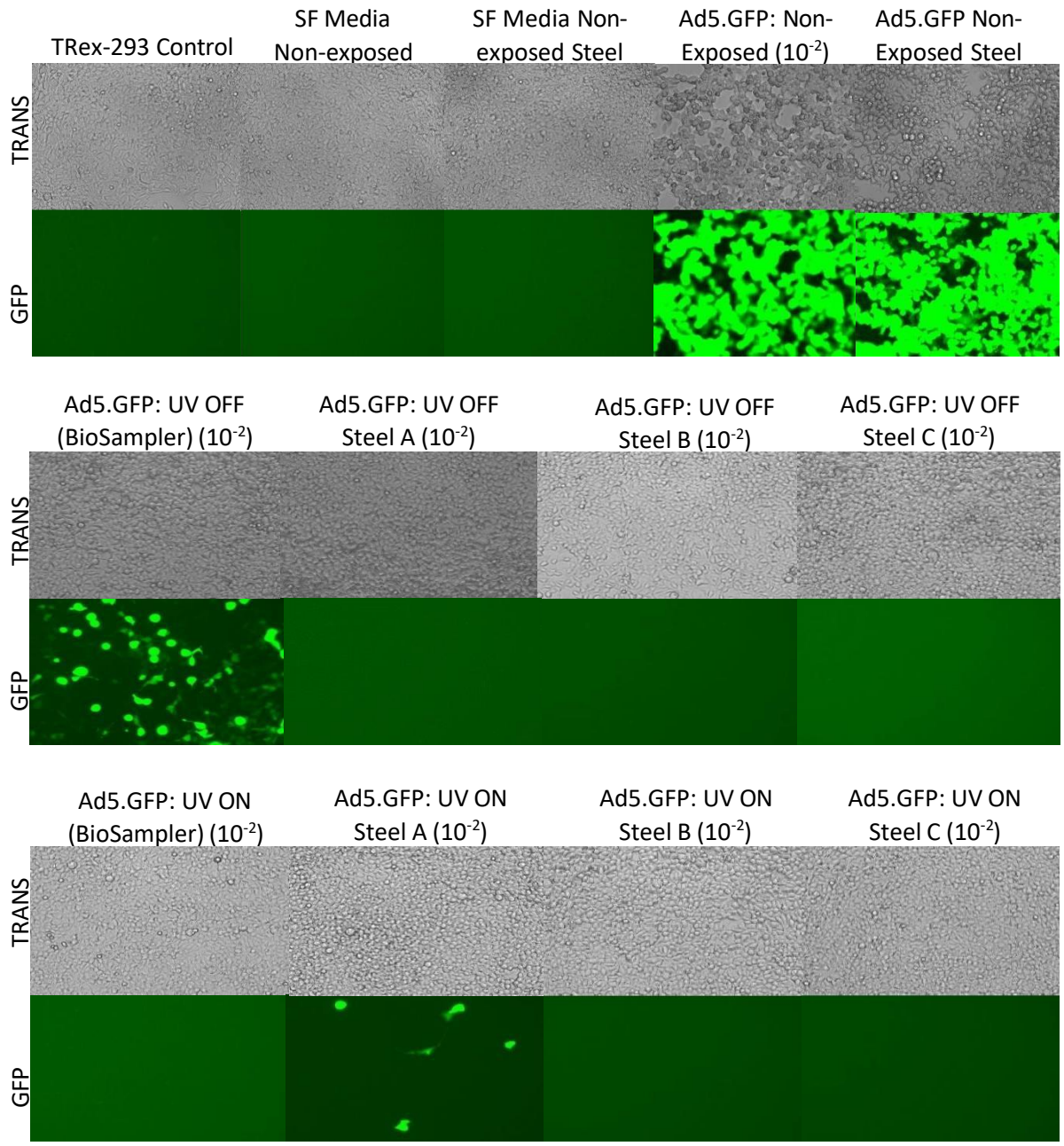

***Figure 6.6*. EVOS Imaging of TRex-293 Cells Infected with Samples of Ad5.GFP that had been Aerosolised into the Open-System and Exposed to Ultravision™.** *Top panels (TRANS) imaged using transmitted light (brightfield). Bottoms panels (GFP) imaged using the GFP light source. All wells were imaged using a x20 objective lens. Samples were collected from the BioSampler and washes of the stainless-steel sheets, following aerosolisation of Ad5.GFP at 1 x 10^{10} vp/ml into the open-system and exposure to inactive/active Ultravision™. Control: TRex-293 cells replenished with total media. Non-exposed: Sample non-aerosolised and non-exposed to Ultravision™. Steel: Sample washed from stainless-steel sheets (A/B/C: corresponds to the distance from the Ion Wand). 10^{-2}: Sample diluted by 1:100 with SF media. Fluorescent cells under GFP light source resemble viral infection. Manual counting of fluorescent cells per field of view enabled calculation of pfu/ml values for each sample.*

Table 6.1. Functional Titers Determined by Plaque Assay Analysis – Prototype Open-System

Sample	**Functional Titer**
Ad5.GFP non-exposed	1 x 10^8pfu/ml
Ad5.GFP non-exposed (steel)	1 x 10^8pfu/ml
Ad5.GFP: UV OFF BioSampler	4.2 x 10^6pfu/ml
Ad5.GFP: UV OFF (Steel A)	-
Ad5.GFP: UV OFF (Steel B)	-
Ad5.GFP: UV OFF (Steel C)	-
Ad5.GFP: UV ON BioSampler	-
Ad5.GFP: UV ON (Steel A)	3.6 x 10^5pfu/ml
Ad5.GFP: UV ON (Steel B)	-
Ad5.GFP: UV ON (Steel C)	-

Direct contact with stainless-steel made no significant difference to the pfu/ml value calculated for the non-exposed preparation of Ad5.GFP. Once again, this implied that stainless-steel alone had no adverse effects on the viability of Ad5.GFP. Cells transduced with the Ad5.GFP sample that had been exposed to inactive Ultravision^{TM} and collected from the BioSampler displayed reduced transduction relative to the non-exposed positive controls. This indicated that virus particles were lost within the open-system upon sample aerosolisation, and thus fewer viable virus particles were collected in the BioSampler. On the other hand, cells transduced with the Ad5.GFP sample that had been exposed to active Ultravision^{TM} and collected from the BioSampler displayed no detectable signs of transduction. This demonstrated that Ultravision^{TM} efficiently captured and inactivated aerosolised Ad5.GFP within the open-system model. It therefore appeared that Ultravision^{TM} could successfully inactivate aerosolised viral particles within the open-system model, similar to that within the closed-system model.

Cells transduced with the samples obtained from steel-sheets A, B and C, following Ad5.GFP exposure to inactive Ultravision^{TM}, displayed no viable virus particles. Under the TRANS light source, the cells appeared to be normal and proliferating. In comparison, cells transduced with the sample obtained from stainless-steel sheet A, following Ad5.GFP exposure to active Ultravision^{TM}, demonstrated a low but detectable level of transduction and thus low levels

of active viral particles. The functional titer of this sample was calculated at 3.6 x 10^5pfu/ml. This indicated successful electrostatic precipitation of Ad5.GFP particles onto the steel sheet, however, it also demonstrated that not all of the precipitated virus particles were successfully inactivated by Ultravision™. Furthermore, in agreement with data obtained from the transduction assay, cells infected with samples from steel-sheets B and C, following Ad5.GFP exposure to active Ultravision™, displayed no sign of active Ad5.GFP. This evidenced that particle precipitation predominantly occurred on steel-sheet A, due to the placement of the Ion wand directly above steel-sheet A. This implied that most virus particles were prohibited from passing the Ion Wand, thus indicating that Ultravision™ successfully precipitated viral particles in the open-system model.

6.3. Discussion

In summary, the key findings from Chapter 6 suggest that Ultravision™ was capable of successfully capturing and inactivating virus particles that were aerosolised within the prototype open-system. Data gathered from qPCR analysis (**Figure 6.4**) demonstrated that Ultravision™ captured Ad5.GFP particles via electrostatic precipitation onto stainless-steel sheet A, which was positioned directly beneath the Ion Wand. This was highlighted by a reduction in viral DNA collected within the BioSampler and a simultaneous increase in viral DNA collected on the surface of steel-sheet A. Additionally, visible particle precipitation was observed during experimental runs (**Figures 6.2** and **6.3)**. Indeed, particle precipitation appeared more prominent within the prototype open-system compared to that within the two closed-systems utilised in Chapters 4 and 5. This therefore suggests an exciting potential avenue for future uses of Ultravision™, in addition to its traditional use in key-hole surgery for the removal of surgical-smoke.

Results acquired from both the transduction and plaque assays (**Figures 6.5 and 6.6**) demonstrated that Ultravision™ successfully inactivated a significant amount of the aerosolised Ad5.GFP particles. The data obtained from analysis of the BioSampler samples revealed a 290-fold reduction in viral activity following virus exposure to active Ultravision™ (**Figure 6.5**). As a low level of Ad5 DNA was still detected in the BioSampler following sample exposure to active Ultravision™ (**Figure 6.4**), it appears that the small number of particles that had escaped electrostatic precipitation were still efficiently inactivated by the Ion Wand's virucidal corona discharge. It was therefore assumed that Ultravision™ has the

capacity to successfully inactivate virus particles within open-system environments. This highlights Ultravision^{TM} as a useful technology for the basis of a novel air-filtration or ventilation device. However, a small proportion of virus particles that precipitated onto steel-sheet A, following exposure to active Ultravision^{TM}, were still viable. This therefore identified a limitation of using Ultravision^{TM} as a filtration device, as cleaning of the machine could result in exposure to active virus particles. However, replacing the stainless-steel return-electrode for a material harbouring virucidal properties, such as copper, may purposefully enhance the level of virus inactivation upon electrostatic precipitation. Further studies evaluating this are therefore required.

Overall, the prototype open-system worked well as a means of obtaining 'proof-of-concept' data. The model system was able to mimic an open-air environment, albeit on a smaller scale than reality. Results gathered from this study provide a rationale for further evaluation of Ultravision^{TM} within open-systems, however, this would require an improved, refined model system to more accurately resemble the aerosol dynamics of open-air spaces.

As the open-system model used in Chapter 6 was simply a prototype, it encompassed some limitations and weaknesses. Firstly, although the model aimed to mimic an open-system, it was still essentially 'closed', due to enclosure of the aerosol sample within the 84L plastic box. Indeed, the system was much larger than the closed-system, behaving more like that of an indoor space, however future studies using larger-scale models are required for more accurate representation. As well as this, due to limited time and equipment, only one experimental run was performed using the open-system. Performing experimental repeats in future studies is therefore essential to obtain conclusive and reliable results, which will undoubtedly uncover additional findings regarding the capabilities of Ultravision^{TM} within open-systems. Data from such experimental repeats could also be used to mathematically model the effects of Ultravision^{TM} in open-systems. It is possible to develop computer simulations upscaling the original prototype system, to generate large quantities of theoretical data that may better determine the capabilities of Ultravision^{TM}. Additionally, using computer simulations would dramatically reduce the cost of consumables and time required to manually repeat experiments using larger open-system models.

Interestingly, virus capture was more efficient in the open-system compared to the closed-system, although this data was gained from a single experiment using the open system, so

requires repeating. As the BioSampler and vacuum unit were located further away from the point of sample aerosolisation in the open-system, it is likely that particles escaped suction into the BioSampler and instead passively precipitated within the 84L box, mimicking particle capture. Contrastingly, in the closed-system, the vacuum unit had a far stronger influence on the aerosol, promoting movement of particles directly into the BioSampler. As well as this, the stainless-steel sheets used in the open-system were only 3 inches x 3 inches. Particle precipitation could have also occurred on the positively charged copper tape that surrounded the steel sheets. Due to this, it is likely that samples collected from the steel-sheets did not contain all of the virus particles that had been successfully precipitated. Viral particles that precipitated onto the copper tape, rather than the stainless-steel sheets, were thereby unaccounted for. To circumvent this in future studies, the entire base of the plastic box could be covered with stainless-steel, increasing the surface area of experimental sampling.

Due to limited time and consumables, experimental repeats identifying optimal conditions for the use of Ultravision^{TM} within the open-system model were not performed. Therefore, future studies should focus on parameters of the open-system model thought to influence the efficiency of electrostatic precipitation, such as temperature, humidity, voltage, Ion Wand number, box volume and sample concentration. Optimal conditions allowing maximal virus capture and inactivation within the open-system may differ to those required within the closed-system. Therefore, it is important to identify and understand physical parameters that improve the function of Ultravision^{TM} for its use in both scenarios. As well as this, it would also be valuable to expose an enveloped respiratory virus to Ultravision^{TM} within the open-system model. This would enable comparisons to be made regarding the ability of Ultravision^{TM} to capture and inactivate both enveloped and non-enveloped viruses within an open-system.

Succeeding ‘proof-of-concept’ studies using prototype open-systems, the next natural step is to assess the abilities of Ultravision^{TM} within real-life environments, such as hospital rooms or surgical suites. It would be sensible to first aerosolise virus-like-particles, tagged with fluorescent dyes, to initially evaluate the capabilities of Ultravision^{TM} in an open room setup. However, such experimentation would only enable the analysis of virus capture and precipitation. Additional studies could attempt to test the efficiency of Ultravision^{TM} to

capture and inactivate aerosolised virus particles in a clinical setting, prior to implementing Ultravision^{TM} as a method of reducing the spread of airborne diseases during surgery. If successful, it would be possible to develop novel air-filtration and ventilation systems exploiting Ultravision^{TM} technology, to use within hospital settings.

Chapter 7. Discussion and Conclusions

7.1. Discussion

In today's climate, with the 2020 SARS CoV-2 pandemic continuing to cause global devastation, it is abundantly clear that novel mechanisms of reducing viral transmission by bioaerosols must be developed. SARS CoV-2 has caused the death and morbidity of millions worldwide, both directly and indirectly. With the pandemic placing our healthcare systems under great pressure, thousands of medical procedures have been delayed and cancelled as a result, prolonging or completely preventing the diagnosis and treatment of ill patients (Fink, 2020. Propper, 2020). However, issues do not only lie within the medical and healthcare setting, as the costs of the pandemic have been more than just deaths directly related to SARS CoV-2. The world has also experienced an economic crisis as a result of the pandemic, with financial markets dropping, businesses forced into closure, and a huge decline in the number of available jobs. Such events have affected the mental health of many, placing further strains on the NHS. Therefore, an intervention is urgently required, not only to prevent transmission of SARS CoV-2, but also to tackle the indirect effects of the pandemic and to increase our preparedness for any pathogenic outbreaks or pandemics that may occur in the future.

As the spread of airborne viruses occurs predominantly within hospitals, where the most vulnerable and at-risk individuals are situated, it was of high priority to focus research into this area first. During surgery, bioaerosols are released when cutting human tissue with electrosurgical equipment. Previous studies have shown that such bioaerosols have the capacity to carry pathogens, in particular respiratory viruses, posing hazardous towards healthcare staff, whom are thereby most at risk of infection during surgical procedures (Gloster and Roenigk, 1995. Chuang, 2012). Although there are no definitive studies evidencing the risks of SARS-CoV-2 transmission via surgical smoke, it is accepted that precautions must be taken and transmission assumed possible (Mowbray, 2020). Ultravision^{TM} is currently used during key-hole surgery to remove surgical smoke via electrostatic precipitation, improving the surgeon's field of vision. However, many studies (section 1.3) have indicated that the process of electrostatic precipitation is also capable of capturing aerosolised microorganisms, including virus particles, highlighting a potential additional modality of Ultravision^{TM}. Yet, few studies have assessed the ability of

electrostatic precipitation to also inactivate airborne virus particles. Thus, the overall premise of this research project was synthesised – to evaluate the ability of Ultravision™ to capture and inactivate virus particles released in bioaerosols. Further, it was hypothesised that if Ultravision™ proved successful within models mimicking key-hole surgery, it could also be used to prevent viral spread within open-systems, such as open-surgery or within hospital rooms as an air-filtration-like device. Therefore, the first aim of this study was to develop two model systems – a closed system, mimicking key-hole surgery and an open system, mimicking open surgery. The second aim was to aerosolise virus samples into each model system, thereby exposing virus particles to Ultravision™. Finally, the third aim was to analyse the consequential capture and inactivation of virus particles by Ultravision™ within each system.

Due to the number of experimental runs performed throughout this research project, multiple findings and conclusions were identified. Therefore, the 5 key findings of this study are individually listed and discussed below. It is important to note that for the purpose of this discussion, the key findings were predominantly made from analysis of the BioSampler samples. Samples from the BioSampler held more significance in terms of answering the research question than samples collected from the reaction kettle, swabs of the return electrode or washes of the stainless-steel sheets. This is because the BioSampler analysed the contents of the air within each system, following the exposure of virus particles to Ultravision™ and could therefore directly inform us of the efficiency of Ultravision™ to capture and inactivate aerosolised virus particles. For example, collection of a highly active and abundant viral load following sample exposure to Ultravision™ would suggest that Ultravision™ was highly inefficient. Whereas, the collection of a low number of inactive virus particles would suggest that Ultravision™ was highly efficient. Samples collected from the reaction kettle, swabs of the return-electrode and washes of stainless-steel sheets were mainly performed to gain a better understanding of the mechanisms of electrostatic precipitation, to highlight how Ultravision™ was affecting the aerosolised particles and why the virus particles were behaving the way they were. In real-life scenarios, the concentration and activity status of virus particles within the air is of main concern, as this is what increases the risk of viral transmission to healthcare staff and patients during surgery.

Therefore, the 5 key findings listed below are drawn from samples collected from the BioSampler (unless stated otherwise).

7.1.1. Ultravision™ Successfully Captured Aerosolised Ad5.GFP Particles within the Closed-System Model.

qPCR analysis was performed to evaluate the ability of Ultravision™ to capture aerosolised virus particles. In runs #2 - #6, the concentration of viral DNA within the BioSampler was significantly reduced following Ad5.GFP exposure to active Ultravision™. This finding suggested that Ad5 particles were actively precipitated onto the return electrode within the reaction kettle, suggesting that Ultravision™ could capture aerosolised virus particles. In contrast, results from run #1 implied that Ultravision™ may not be capable of capturing virus particles via electrostatic precipitation. This contradictory result may have been due to experimental error, as run #1 was the first experiment using the closed-system model with active virus samples. Such results highlight the importance of experimental repeats, as the remaining 5 runs displayed successful virus capture by Ultravision™. Alternatively, run #1 was the only run lacking optimisation, which may also explain the unsuccessful capture of virus particles.

However, virus capture was not 100% successful in any of the experimental runs. Isolated DNA (not enclosed within a capsid) is too small to be captured by electrostatic precipitation. It is therefore possible that exposing Ad5.GFP to Ultravision™ resulted in structural degradation of the virus, causing the release of viral DNA from the capsid. Kettleson (2009) suggested that the corona discharge produced by the Ion Wand generates reactive species. It is likely that exposing Ad5.GFP to reactive species caused structural degradation of the virus particles. Therefore, larger fragments, such as the virus capsid, may have precipitated onto the return electrode, whilst smaller fragments, such as the viral DNA, may have remained aerosolised and hence migrated through the system, collecting within the BioSampler. However, isolated DNA is biochemically inert and incapable of infecting cells. An intact capsid or viral vector is required for cellular entry and viral replication (Fenner, 1987. Gelderblom, 1996. Lentz, 2005). Therefore, providing that Ultravision™ is capable of structurally degrading virus particles, it is fair to assume that Ultravision™ can successfully prevent the transmission of respiratory viruses, regardless of its ability to capture intact virus particles.

As qPCR analysis was the only method of evaluating electrostatic precipitation, the exact mechanism of virus capture was not definitively established. Following use of the prototype closed-system, collected samples were analysed by the NanoSight, to determine the number of intact virus particles that had been collected within the collection pot. However, the sample was contaminated after aerosolisation through the model system and therefore the NanoSight was unable to accurately distinguish the concentration of intact Ad5.GFP particles. As qPCR only provides information regarding the concentration of viral DNA, other methods of evaluating the ability of Ultravision^{TM} to capture intact virus particles are required. In future studies, techniques that can detect and quantify intact virus particles must be employed, such as ELISA assays and western blots. This may provide further insight into theories regarding virus degradation and precipitation caused by Ultravision^{TM}. Buggisch (2020) performed a similar study, however using a water-based condensation particle counter to determine the concentration of particles captured via electrostatic precipitation. Although this method was capable of distinguishing intact virus particles based on particle size, it was not species specific, and therefore potentially gathered misleading results. Combining a multitude of methods assessing the presence of intact virus particles is therefore required to better evaluate the association between Ultravision^{TM} and virus capture in future experiments.

7.1.2. Ultravision^{TM} Successfully Inactivated Aerosolised Ad5.GFP Particles within the Closed-System Model.

Transduction assays and plaque assays were performed to evaluate the ability of Ultravision^{TM} to inactivate aerosolised Ad5.GFP within the closed-system model. Successful virus inactivation was observed in all 6 experimental runs. Not only was virus inactivation successful, but it was also highly efficient, with 90-98% of virus particles inactivated by Ultravision^{TM} following each run. Furthermore, by adjusting parameters that enhanced the efficiency of electrostatic precipitation, such as increasing the Ion Wand voltage and the number of Ion Wands present within the reaction kettle, the amount of virus inactivation increased up to almost 100%. This additional modality of Ultravision^{TM} therefore outshone its ability to capture virus particles. Therefore, it was suggested that viral transmission could be successfully prohibited by Ultravision^{TM} via particle inactivation alone.

In agreement with the study by Kettleson (2009), key findings from chapter 5 indicate that the generation of reactive species from the Ion Wand's corona discharge caused the observed inactivation of the aerosolised virus particles. In addition, a recent study by Song (2022) manipulated this phenomenon, and used pulsed corona discharge plasma to inactivate water-borne viruses. They too found that with a high voltage, the corona discharge was capable of inactivating virus particles via structural degradation. As well as this, Hyun (2017) used a carbon-fiber ioniser, which generated a corona discharge, to inactivate aerosolised bacteriophages. However, Hyun only managed to inactivate 78.8% of the bacteriophages, after 30 minutes of exposure. In comparison, the use of Ultravision^{TM} in chapter 5 managed to inactivate >90% of virus particles after < 20 minutes of exposure. This suggested that the corona discharge generated by Ultravision^{TM} is much stronger and more efficient at filtering airborne microorganisms than the carbon-fiber ioniser.

Although a number of virus particles managed to escape electrostatic precipitation within the reaction kettle, the majority of particles were inactivated by Ultravision^{TM}, therefore posing no threat of infection or transmission. Due to these 'proof-of-concept' findings, it was implied that the use of Ultravision^{TM} during key-hole surgery, to prevent the spread of respiratory viruses, should theoretically work - providing the conditions of the operating room are similar to that created within the closed-system model.

7.1.3. Optimal Conditions for the Maximal Capture and Inactivation of Ad5.GFP by Ultravision^{TM} within the Closed-System Model were Determined.

Parameters known to influence the efficiency of electrostatic precipitation were altered in a variety of experimental runs using the closed-system model. The consequential capture and inactivation of virus particles was analysed to identify which conditions enabled optimal Ultravision^{TM} productivity. Parameters that underwent alteration included Ion Wand voltage, the number of Ion Wands, system temperature and the material of the return-electrode.

In run #3, Ion Wand voltages of 6kV, 8kV and 10kV were compared. Significant virus capture was observed by Ultravision^{TM} at 6kV and 8kV, causing an approximate 94% reduction in the concentration of viral DNA (**Figure 5.10**). However, virus capture was largely enhanced when using Ultravision^{TM} at 10kV, as displayed by a 99.9% reduction in the concentration viral

DNA (**Figure 5.10**). Additionally, Ultravision^{TM} at 6kV and 8kV caused 6-fold and 22.9-fold reductions in viral activity respectively (**Figure 5.11**). Although virus inactivation was significant at 6kV and 8kV, Ultravision^{TM} worked most efficiently at 10kV, causing 175.5-fold reductions in viral activity (**Figure 5.11**). It was therefore concluded that the optimal voltage of Ultravision^{TM}, whilst remaining within a medically approved range, is 10kV. Furthermore, plaque assay analysis displayed 100% virus inactivation following virus sample exposure to Ultravision^{TM} at 10kV, validating this conclusion. Similarly, run #5 also altered parameters effecting the efficiency of electrostatic precipitation. Rather than altering Ion Wand voltage, the number of Ion Wands present within the reaction kettle was changed. Run #5 compared the effects of using 1 Ion Wand, versus 2 Ion Wands, to capture and inactivate virus particles. A 99.3% reduction in the number of viral genomes was observed using 1 Ion Wand, whilst a 99.9% reduction was achieved when using 2 Ion Wands (**Figure 5.18**). Additionally, 1 Ion Wand caused a 31.4-fold reduction in virus viability, whilst 2 Ion Wands caused a 197.6-fold reduction in viral activity (**Figure 5.19**). As well as this, 100% virus inactivation was observed following plaque assay analysis of the sample exposed to 2 Ion Wands (**Figure 5.20**). These findings demonstrated that the 2 Ion Wands worked more efficiently to capture and inactivate virus particles, as opposed to 1 Ion Wand. However, the distance between the 2 Ion Wands was considered highly important, as the distance between two electrodes effects the true voltage and strength of the electric field, according to Ohm's law. Placing the Ion Wands too close together may result in electric repulsion, whilst placing the Ion Wands too far apart may reduce their combined efficacy. It is therefore important to standardise distances when using multiple Ion Wands during surgery. Overall, these key findings from chapter 5 implied that using 1 Ion Wand at 10kV was equally efficient at capturing and inactivating virus particles as using 2 Ion Wands at 8kV.

The temperature of the closed-system model was also altered in chapter 5 to enhance electrostatic precipitation. Premature condensation of the virus samples was experienced in experimental runs #1 - #3. This resulted in the accumulation of active virus particles within the bottom of the reaction kettle, of which had not been exposed to Ultravision^{TM}. Therefore, the reaction kettle was heated to 37°C in run #4 to promote aerosolisation of the virus samples, preventing premature condensation. This resulted in greater exposure of the

virus samples to Ultravision™, thereby improving particle capture and inactivation. Due to this, it was concluded that Ultravision™ is only capable of influencing virus particles that are suspended within aerosol. This finding is important to note by medical professionals using Ultravision™, as the release of solid or liquid samples from infectious patients during surgery will not be decontaminated by Ultravision™ and should therefore be handled with caution.

Finally, the material of the return-electrode was altered in run #6. Copper was used in runs #1 - #5, however it was hypothesised that the amount of virus inactivation observed in said runs may have been skewed due to the virucidal properties of copper. Previous studies have evidenced that direct contact between microorganisms and copper surfaces can result in microorganism death or inactivation (Govind, 2021). Therefore, to deduce whether Ultravision™ was the sole cause of virus inactivation, the copper return was replaced with stainless-steel. Stainless-steel is biochemically inert and is not harmful to virus particles following direct contact (Santonen, 2010). The level of virus capture and inactivation remained consistent in run #6 with that observed in runs #1 - #5, thereby confirming the assumed capabilities of Ultravision™. However, when considering additional modalities of Ultravision™, the inclusion of a virucidal return-electrode may prove useful. Of course, Ultravision™ has shown capable of inactivating virus particles within a closed-system by itself, however if employed within an open-system, as part of a ventilation or air-filtration device, the likelihood of virus particle escape would be increased. Therefore, the addition of a virucidal return-electrode may enhance the ability of Ultravision™ to inactivate respiratory pathogens, improving the safety and efficiency of its usage. Current methods of ventilation and air-purification systems are limited by their inability to inactivate pathogenic particles following successful capture. Therefore, developing a novel device overcoming such limitations would be hugely marketable and beneficial in hospital settings.

7.1.4. Ultravision™ Successfully Captured and Inactivated Aerosolised SARS PV within the Closed-System Model.

Although Ultravision™ was capable of capturing and inactivating aerosolised Ad5.GFP, which is a non-enveloped virus, it was unknown whether Ultravision™ would have similar effects on enveloped virus particles. Therefore, in run #7, SARS PV (an enveloped pseudovirus) was aerosolised into the closed-system and exposed to Ultravision™. qPCR

results demonstrated successful capture of SARS PV by Ultravision, as displayed by a 60.6% reduction in the concentration of SARS PV RNA (**Figure 5.26**). In addition, Ultravision™ successfully inactivated aerosolised SARS PV, as highlighted by transduction assay and plaque assay analysis. SARS PV activity was reduced by 94.6%, following sample exposure to active Ultravision™ (**Figure 5.27**). Similarly, plaque assay analysis highlighted a significant, visible reduction in the number of fluorescent cells, following infection with the SARS PV sample that had been exposed to active Ultravision™ (**Figure 5.28**). The findings from run #7 therefore confirmed the theory that Ultravision™ is capable of capturing and inactivating enveloped virus particles, as well as non-enveloped virus particles.

However, aerosolisation alone caused significant reductions in the concentration and activity of SARS PV. This was displayed by a decrease in the concentration of viral RNA and virus viability, following SARS PV exposure to inactive Ultravision™ and collection from the BioSampler. The SARS pseudovirus was comprised of a HIV core that was enclosed within a lentiviral capsid. It is well established within the literature that cell-free lentiviruses are unstable and the titer of lentivirus stocks dramatically decrease within less than one hour when stored at room temperature (Rahman, 2013). Not only was the SARS PV sample used at room temperature, but it was also aerosolised into the closed-system. Unlike Adenoviruses and Coronaviruses, Lentiviruses are not respiratory viruses. Lentiviruses spread via bodily fluids, and therefore cannot remain stable when suspended within aerosol (Schlimgen, 2016). Due to this, it is possible that aerosolisation resulted in the structural instability of SARS PV, thus resulting in RNA degradation and loss of particle viability. Therefore, future studies using respiratory pathogens are required to accurately assess the ability of Ultravision™ to capture and inactivate enveloped virus particles.

A recent study by Redmann (2022) used a miniaturised electrostatic precipitator to remove SARS-CoV-2 from bioaerosols. The study identified successful capture of up to 96.9% of the virus particles. This indicates that it is possible for electrostatic precipitator devices, such as Ultravision™, to efficiently capture enveloped viruses. Such findings suggest that the choice of the enveloped virus used in this study (SARS PV) was the limiting factor and future experiments analysing the association between Ultravision™ and enveloped virus particles should only use respiratory virus samples. Additionally, Piri (2021) exposed aerosolised Coronavirus and Influenza virus samples to an electrostatic precipitator device, to analyse its

ability to accurately sample the contents of virus particles within the air. However, Piri used Absorbic Acid dissolved in PBS to collect the precipitated virus particles, as a method of counteracting particle impairment caused by the reactive species generated from the corona discharge. This increased the survivability of the virus particles during air-sampling, to precisely detect the number of particles present. Future studies analysing the ability of Ultravision^{TM} to capture both enveloped and non-enveloped particles could implement the use of Absorbic Acid to maintain virus viability during aerosolisation. Although this would achieve more reliable results regarding the capability of Ultravision^{TM} to capture virus particles, it would not deduce the ability of Ultravision^{TM} to inactivate virus particles, as viability would be protected and promoted by Absorbic Acid. Additionally, Alsved (2020) aerosolised virus particles via a bubble-bursting method and stated that this alternative method of sample aerosolisation maintained viral stability and viability. Future studies evaluating the ability of Ultravision^{TM} to capture unstable virus samples could employ such methods of sampling and aerosolisation.

Due to limited time and limited stocks of SARS PV, only one experimental run was performed using SARS PV. Experimental repeats are required to ensure reliability of the data collected and the conclusions made. In addition, parameters effecting the efficiency of electrostatic precipitation ought to be altered to assess optimal conditions for the capture and inactivation of enveloped virus particles, as conditions may vary depending on virus structure and species.

7.1.5. Ultravision^{TM} Successfully Captured and Inactivated Aerosolised Ad5.GFP Particles within the Open-System Model.

The evaluation of Ultravision^{TM} to capture and inactivate aerosolised Ad5.GFP within an open-system was performed in Chapter 6. Firstly, the influence of Ultravision^{TM} upon the flow of aerosol was visible to the naked eye (**Figures 6.2** and **6.3**). Aerosolised particles were precipitated onto the return electrode, which was placed directly beneath the Ion Wand, prohibiting particles from passing the region of corona discharge. This thereby indicated successful particle capture via electrostatic precipitation. The extent of particle capture was also evaluated by qPCR analysis. The sample of Ad5.GFP that was exposed to active Ultravision^{TM} and collected from the BioSampler displayed a 98.8% reduction in the concentration of Ad5 genomic DNA (**Figure 6.4**). In comparison, the concentration of Ad5

genomic DNA that was collected on steel-sheet A, positioned directly beneath the Ion Wand, increased following Ad5.GFP exposure to active Ultravision™. This indicated that Ultravision™ successfully captured Ad5.GFP particles onto the return electrode within the open-system model. Additionally, the ability of Ultravision™ to inactivate Ad5.GFP particles within the open system was displayed by transduction assay and plaque assay analysis. A 99.7% reduction in viral activity was observed, following Ad5.GFP exposure to active Ultravision™ (**Figure 6.5**). Furthermore, the Ad5.GFP sample that had been exposed to active Ultravision™ caused no fluorescence in TRex-293 cells, under the GFP light source (**Figure 6.6**). This demonstrated that Ultravision™ inactivated 100% of the aerosolised virus particles. Of course, it was likely that a proportion of virus particles remained aerosolised, or passively deposited within the 84L plastic box. Such virus particles were not accounted for, thereby mimicking virus capture and inactivation. Therefore, the level of virus capture and inactivation was most probably less than results from the qPCR, transduction assay and plaque assay implied. However, the purpose of Chapter 6 was to gain 'proof-of-concept' data regarding the additional modalities of Ultravision™, which was successfully achieved.

Data obtained from Chapter 6 provides a rationale for the incorporation of Ultravision™ technology into the development of a novel air-filtration device. This could be implemented in hospital rooms and surgical suites to prevent viral transmission and improve sanitation within medical environments. However, transduction assay analysis of the stainless-steel return electrodes revealed that 4.5% of captured virus particles remained viable (**Figure 6.5**). To improve the efficiency of Ultravision™ in its ability to inactivate virus particles, the stainless-steel sheets could be replaced with a virucidal material, to ensure that all captured particles are efficiently inactivated. This would overcome limitations of currently used air-filtration devices, such as HEPA filters, which harbour active pathogens upon capture.

Although this preliminary data suggests that Ultravision™ is capable of capturing and inactivating virus particles within open systems, experimental repeats are required to confirm that the data acquired is accurate and reliable. Additionally, refined open-system models, that are larger and more representative of indoor spaces, must be designed and constructed to better resemble the abilities of Ultravision™ in real-life scenarios. Aerosol dynamics are largely affected by spatial constraints, air-flow, temperature and pressure. Therefore, a larger model is required to mimic particle movement and behaviours that occur

in open system environments. As well as this, studies using enveloped viruses are also required, to ensure that Ultravision™ can efficiently capture and inactivate a range of virus particles to the same extent. In addition, studies assessing parameters such as voltage, temperature, return-electrode material, and virus sample concentrations must be performed to identify optimal conditions for the use of Ultravision™ within an open-system. Such conditions may differ to those needed for maximal Ultravision™ efficiency within a closed-system. To reduce the cost of consumables and the time taken to perform further experimentation, computer simulations of various open-systems could be developed via mathematical modelling. Doing so would allow for large quantities of data to be gathered, generating an abundance of theoretical hypotheses concerning Ultravision™ and its array of modalities.

7.2. Contributions to the Field of Research

Electrostatic precipitators already exist as methods of removing surgical smoke, sampling air and filtering air. However, little has been established regarding the ability of electrostatic precipitation to capture and inactivate virus particles. Few studies have evaluated the capture of airborne pathogens, such as bacteria and fungi, via electrostatic precipitation. However, far less have focused on the capture of respiratory viruses. Furthermore, even fewer studies have assessed the ability of electrostatic precipitation to inactivate airborne pathogens. This is most probably due to the issue of particle size, as virus particles are much smaller than bacteria and fungi and are therefore harder to successfully capture and inactivate. Currently used air-purification devices are unable to filter virus-sized particles, therefore creating a gap in the field of research. This project has identified an efficient method of capturing and inactivating respiratory virus particles, in both closed and open environments. Therefore, this study has contributed to closing the gap in this field of research.

Data acquired from this study highlights additional modalities of Ultravision™. These newly found capabilities of Ultravision™ will undoubtedly benefit consumers, such as surgeons, healthcare staff and hospital patients. Further, results uncovered from this study will also directly benefit Alesi Surgical Ltd, as the additional modalities of Ultravision™ will greatly increase its marketability. Not only can Ultravision™ be used during surgery to clear surgical smoke, but it can also be used to capture and inactivate viruses, as well as other pathogens,

released from surgical bioaerosols. Using Ultravision™ to generate a novel air-purification device could introduce the technology into an entirely new area of the market, further increasing its sales and profits.

Regarding other uses of Ultravision™, the device could also be employed when delivering aerosolised medications to patients. For example, pressurised intraperitoneal aerosol chemotherapy (PIPAC) has recently been developed as a method of treating unresectable tumours (Willaert, 2019). This use of electrostatic precipitation ensures the safe delivery of aerosolised chemotherapy to tumour sights and promotes tissue penetration of oncolytic drugs. Furthermore, on a similar note, aerosol delivery of oncolytic, tumour selective Adenoviruses, may enhance the treatment and elimination of certain tumours. Implementing Ultravision™ when delivering oncolytic virotherapies by PIPAC to patients will improve the safety of such procedures and promote therapeutic success (Tate, 2021).

7.3. Future Directions

It is vital that experimental repeats are performed using both closed and open model systems, to ensure that the results obtained from this study are accurate and reliable. A list of future directions are detailed below, to ameliorate subsequential experimentation and advance on the data obtained from this study.

1. Refine the 'Closed' and 'Open' model systems, to better resemble aerosol dynamics within 'closed' and 'open' environments.
2. Expose both enveloped and non-enveloped respiratory viruses to Ultravision™.
3. Assess physical parameters that effect electrostatic precipitation, to identify optimal conditions for the usage of Ultravision™.
4. Improve methods of sample analysis when evaluating virus capture. E.g., perform western blots, NanoSight analysis, ELISA assays or employ a physical particle counter, to detect the concentration of intact virus particles.
5. Create computer simulations of Ultravision™ in a variety of environments via mathematical modelling to obtain large quantities of theoretical data.
6. Evaluate the ability of Ultravision™ to capture and inactivate aerosolise virus particles in authentic surgical environments, prior to implementing the device during surgery.

7.4. Concluding Summary

In summary, our findings indicate that Ultravision™ can successfully capture and inactivate virus particles from surgical bioaerosols. It therefore has the potential to reduce the spread of airborne diseases during medical procedures. However, it is important that future research is focused in this area, to determine the exact capabilities of Ultravision™ in real-life surgical scenarios and to identify optimal conditions for its usage. Employing Ultravision™ in the case of future viral pandemics will undoubtedly reduce pressures on the NHS, improve the safety of medical procedures and ultimately save lives.

8. References

Aerogen. 2022. Aerosol medication administration with Aerogen Solo. Available at: https://www.aerogen.com/solo-for-aerosol-medication-administration/ [Accessed: 26/07/22]

Alesi Surgical Ltd. 2022. *Performance data*. Available at: https://www.alesi-surgical.com/performance-data/ [Accessed: 24/07/22]

Alsved, M., Widell, A., Dahlin, H., et al. 2020. Aerosolization and recovery of viable murine norovirus in an experimental setup. *Sci Rep*. **10**(1): 15941. Doi: 10.1038/s41598-020-72932-5.

Ansell, J., Warren, N., Wall, P., et al. 2014. Electrostatic precipitation is a novel way of maintaining visual field clarity during laparoscopic surgery: a prospective double-blind randomized controlled pilot study. *Surg Endosc*. **28**(7): 2057-65. doi: 10.1007/s00464-014-3427-8.

Appleby, J. 2022. The public finance cost of covid-19. *BMJ*. **376**. doi: https://doi-org.abc.cardiff.ac.uk/10.1136/bmj.o490

Astuti, I., and Ysrafil, Y. 2020. Severe Acute Respiratory Syndrome Coronavirus 2 (SARS-CoV-2): An overview of viral structure and host response. *Diabetes & Metabolic Syndrome*. **14**(4): 407-412. doi: 10.1016/j.dsx.2020.04.020

Ather, B., Mirza, T.M., and Edemekong, P.F. 2022. *Airborne Precautions*. Treasure Island. StatPearls Publishing.

Bar-On, Y.M., Flamholz, A., Phillips, R., Milo, R. 2020. SARS-CoV-2 (COVID-19) by the numbers. *eLife*. **9**: e57309. Doi: 10.7554/eLife.57309

Balfour, H. 2021. COVID's impact on cancer therapeutics: clinical trial and treatment disruptions. Available at: https://www.europeanpharmaceuticalreview.com/article/143162/covids-impact-on-cancer-therapeutics-clinical-trial-and-treatment-disruptions/ [Accessed: 24/07/22]

Calvert, J. G. 1990. Glossary of atmospheric chemistry terms (Recommendations 1990). *Pure and Applied Chemistry*. 62(11): 2167-2219. Doi: https://doi.org/10.1351/pac199062112167

Christopherson, D.A., Yao, W.C., Lu, M., Vijayakumar, R., and Sedaghat, A.R. 2020. High-Efficiency Particulate Air Filters in the Era of COVID-19: Function and Efficacy. *Otolaryngol Head Neck Surg*. **163**(6):1153-1155. Doi: 10.1177/0194599820941838.

Chuang, H., BéruBé, K., and T., Jones. 2012. A Study of the Ability of the Innervision Electrostatic Precipitator to Clear the Particulate Matter Produced by Energy-Based Surgical Instruments. Cardiff. Asalus Medical Instruments Ltd.

COVIDsurg Collaborative. 2020. Elective surgery cancellations due to the COVID-19 pandemic: global predictive modelling to inform surgical recovery plans. *The British Journal of Surgery*. **107**(11): 1440-1449. doi: 10.1002/bjs.11746.

Crenshaw, B.J., Jones, L.B., Bell, C.R., Kumar, S., Matthews, Q.L. 2019. Perspective on Adenoviruses: Epidemiology, Pathogenicity and Gene Therapy. *Biomedicines*. **7**(3): 61 doi: 10.3390/biomedicines7030061 https://www.ncbi.nlm.nih.gov/pmc/articles/PMC6784011/

Doms, R.W. 2016. Basic Concepts - A Step-by-Step Guide to Viral Infection. *Viral Pathogenesis (Third Edition)*. 29-40. Doi: https://doi.org/10.1016/B978-0-12-800964-2.00003-3

Du, Y., Miah, K. M., Habib, O., et al. 2022. Lung directed antibody gene transfer confers protection against SARS-CoV-2 infection. *BMJ Thorax*. **0**: 1–8. doi:10.1136/thoraxjnl-2021-217650

Dunne, R.B. and Shortt, Sandra. 2018. Comparison of bronchodilator administration with vibrating mesh nebulizer and standard jet nebulizer in the emergency department. *The American Journal of Emergency Medicine*. **36**(4): 641-646. Doi: https://doi.org/10.1016/j.ajem.2017.10.067

Elsaid, A.M. and Ahmed, M. S. 2021. Indoor Air Quality Strategies for Air-Conditioning and Ventilation Systems with the Spread of the Global Coronavirus (COVID-19) Epidemic: Improvements and Recommendations. *Environmental Research*. **199**: 111314. Doi: 10.1016/j.envres.2021.111314

Fabian, P., McDevitt, J.J., Houseman, E.A. and Milton, D.K. 2009. Airborne influenza virus detection with four aerosol samplers using molecular and infectivity assays: considerations for a new infectious virus aerosol sampler. *Indoor Air*. **19**(5): 433-41. doi: 10.1111/ j.1600-0668.2009.00609.x.

Fenner, F., Bchmann, P.A., Gibbs, E.P.J., et al. 1987. Structure and Composition of Viruses. *Veterinary Virology*. pp 3-19. Doi: 10.1016/B978-0-12-253055-5.50005-0

Ferguson, N., Laydon, D., Nedjati-Gilani, G., et al. 2020. Report 9: Impact of non-pharmaceutical interventions (NPIs) to reduce COVID-19 mortality and healthcare demand. Imperial College London - COVID-19 Response Team. Doi: https://doi.org/10.25561/77482

Fink, J.B., Ehrmann, S., Li, J., et al. 2020. Reducing Aerosol-Related Risk of Transmission in the Era of COVID-19: An Interim Guidance Endorsed by the International Society of Aerosols in Medicine. *Journal of Aerosol Medicine and Pulmonary Drug Delivery*. **33**(6): 300-304. Doi: https://doi-org.abc.cardiff.ac.uk/10.1089/jamp.2020.1615

Firquet, S., Beaujard, S., Lobert, P.E., et al. 2015. Survival of Enveloped and Non-Enveloped Viruses on Inanimate Surfaces. *Microbes and Environments*. **30**(2): 140–144. doi: 10.1264/jsme2.ME14145.

Gelderblom, H.R. 1996. *Medical Microbiology*. 4th Edition. Galveston. University of Texas Medical Branch at Galveston.

Gloster, H.M. and Roenigk, R.K. 1995. Risk of acquiring human papillomavirus from the plume produced by the carbon dioxide laser in the treatment of warts. *J Am Acad Dermatol*. **32**(3):436-41. doi: 10.1016/0190-9622(95)90065-9.

Göhler, Daniel., Buggisch, Jonathan., Oelschlägel, Kathrin., et al. 2021. Bioaerosol release and exposure during laparoscopic surgery and performance of bioaerosol elimination technologies. [Poster]. *European Aerosol Conference*. Birmingham. August 2021. Doi: 10.13140/RG.2.2.15771.59687.

Govind, V., Bharadwaj, S., Sai Ganesh, M.R., et al. 2021. Antiviral properties of copper and its alloys to inactivate covid-19 virus: a review. *Nature Public Health Emergency Collection*. **34**(6): 1217–1235. doi: 10.1007/s10534-021-00339-4

Gürtler, L., Aepfelbacher, M., Bauerfeind, U., et al. 2016. Human Immunodeficiency Virus (HIV). *Transfusion Medicine and Hemotherapy*. **43**:203–222. Doi: 10.1159/000445852

Hoeben, R.C., and Uil, T.G. 2013. Adenovirus DNA Replication. *Cold Spring Harbor Perspectives in Biology*. **5**(3): a013003 doi: 10.1101/cshperspect.a013003 https://www.ncbi.nlm.nih.gov/pmc/articles/PMC3578361/

Hou, Z., Tong, Y., Du, F., et al. 2021. Assessing COVID-19 Vaccine Hesitancy, Confidence, and Public Engagement: A Global Social Listening Study. *J Med Internet Res*. **223**(6):e27632. doi: 10.2196/27632.

Hutasoit, N., Kennedy, B., Hamilton, S., et al. 2020. Sars-CoV-2 (COVID-19) inactivation capability of copper-coated touch surface fabricated by cold-spray technology. *Manufacturing Letters*. **25**: 93–97. Doi: 10.1016/j.mfglet.2020.08.007

Jarvis, M.C. 2020. Aerosol Transmission of SARS-CoV-2: Physical Principles and Implications. *Frontiers in Public Health*. **8**: 590041. doi: 10.3389/fpubh.2020.590041.

Johnson, T.J., Nishida, R.T., Sonpar, A.P. et al. 2022. Viral load of SARS-CoV-2 in droplets and bioaerosols directly captured during breathing, speaking and coughing. *Sci Rep*. **12**:3484. Doi: https://doi.org/10.1038/s41598-022-07301-5

Johnson, G.K. and Robinson, W.S. 1991. Human immunodeficiency virus-1 (HIV-1) in the vapors of surgical power instruments. *J Med Virol*. **33**(1): 47-50. doi: 10.1002/jmv.1890330110.

Kettleson, E.M., Ramaswami, B., Hogan, C.J., et al. 2009. Airborne Virus Capture and Inactivation by an Electrostatic Particle Collector. *Environ Sci Technol*. **43**: 5940–5946. Doi: 10.1021/es803289w

Krishnakumar, S. and Tambe, P. 2009. Entry complications in laparoscopic surgery. *J Gynecol Endosc Surg*. **1**(1): 4-11. doi: 10.4103/0974-1216.51902.

Kutter, J.S., de Meulder, D., Bestebroer, T.M., et al. 2021. Comparison of three air samplers for the collection of four nebulized respiratory viruses - Collection of respiratory viruses from air. *Indoor Air*. **31**(6): 1874-1885. doi: 10.1111/ina.12875.

Kutter, J.S., Spronken, M.I., Fraaij, P.L., Fouchier, R.A.M., Herfst, S. 2018. Transmission routes of respiratory viruses among humans. *Current Opinion in Virology*. **28**: 142-151 doi: https://doi.org/10.1016/j.coviro.2018.01.001

Ladhani, L., Pardon, G., Meeuws, H., et al. 2017. Sampling and detection of airborne influenza virus towards point-of-care application. *PLOS ONE*. **12**(3). Doi: https://doi.org/10.1371/journal. pone.0174314

Laue, M., Kauter, A., Hoffmann, T. et al. 2021. Morphometry of SARS-CoV and SARS-CoV-2 particles in ultrathin plastic sections of infected Vero cell cultures. *Nature – Scientific Reports.* **11**: 3515 Doi: https://doi.org/10.1038/s41598-021-82852-7

Lee, B.U. 2020. Minimum Sizes of Respiratory Particles Carrying SARS-CoV-2 and the Possibility of Aerosol Generation. *International Journal of Environmental Research and Public Health.* **17**(19): 6960 Doi: 10.3390/ijerph17196960

Lee, J. 2020. Mental health effects of school closures during COVID-19. *The Lancet Child & Adolescent Health*. **4**(6): 421. Doi: https://doi.org/10.1016/S2352-4642(20)30109-7

Lentz, Y.K., Worden, L.R., Anchordoquya, T.J., Lengsfeldb, C.S. 2005. Effect of jet nebulization on DNA: identifying the dominant degradation mechanism and mitigation methods. *Journal of Aerosol Science*. **36**(8): 973-990

Li, J., Leavey, A., Wang, Y., et al. 2018. Comparing the performance of 3 bioaerosol samplers for influenza virus. *J Aerosol Sci*. **115**: 133–145. doi: 10.1016/j.jaerosci.2017.08.007

Lu, Z., Zou, X., Dong, L., et al. 2008. Novel recombinant adenovirus type 41 vector and its biological properties. *The Journal of Gene Medicine*. **11**(2): 128-138. Doi: https://doi.org/10.1002/jgm.1284

Melikyan, G.B. 2014. HIV entry: a game of hide-and-fuse? *Current Opinion in Virology*. **4**: 1-7. doi: 10.1016/j.coviro.2013.09.004.

Mowbray, N.G., Ansell, J., Horwood, J., et al. 2020. Safe management of surgical smoke in the age of COVID-19. *BJS*. **107**(11). Doi: https://doi-org.abc.cardiff.ac.uk/10.1002/bjs.11679

Niazi, S., Philp, L.K., Spann, K., and Johnson, G.R. 2021. Utility of Three Nebulizers in Investigating the Infectivity of Airborne Viruses. *Appl Environ Microbiol*. **87**(16): e0049721. doi: 10.1128/AEM.00497-21.

Orgilés, M., Morales, A., Delvecchio, E., Mazzeschi, C., and Espada, J.P. 2020. *Frontiers in Psychology*. **6**. Doi: https://doi.org/10.3389/fpsyg.2020.579038

Pardon, G., Ladhani, L., Sandström, N., et al. 2015. Aerosol sampling using an electrostatic precipitator integrated with a microfluidic interface. *Sensors and Actuators B: Chemical*. **212**: 344-352. Doi: https://doi.org/10.1016/j.snb.2015.02.008

Pekker, M and Shneider, M.N. 2014. The surface charge of a cell lipid membrane. J *Phys Chem Biophys*. **5** (177). Doi: https://doi.org/10.48550/arXiv.1401.4707

Perry, K.A., Coulliette, A.D., Rose, L.J., et al. 2016. Persistence of Influenza A (H1N1) Virus on Stainless Steel Surfaces. *Applied and Environmental Microbiology*. **82**(11). Doi: https://doi-org.abc.cardiff.ac.uk/10.1128/AEM.04046-15

Piri, A. Kim, H.R., Park, D.H., and Hwang, J. 2021. Increased survivability of coronavirus and H1N1 influenza virus under electrostatic aerosol-to-hydrosol sampling. *Journal of Hazardous Materials*. **413**. 125417. Doi: https://doi.org/10.1016/j.jhazmat.2021.125417

Propper, C., Stoye, G., and Zaranko, B. 2020. The Wider Impacts of the Coronavirus Pandemic on the NHS. *The Journal of Applied Public Economics*. **41**(2): 345-356. doi: https://doi-org.abc.cardiff.ac.uk/10.1111/1475-5890.12227

Rahman, H., Taylor, J., Clack, B., et al. 2013. Effects of Storage Conditions on the Morphology and Titer of Lentiviral Vectors. *Faculty Publications*. **94**. Doi. https://scholarworks.sfasu.edu/biology/94

Ramos, C.C.R., Roque, J.L.A., Sarmiento, D.B., et al. 2020. Use of ultraviolet-C in environmental sterilization in hospitals: A systematic review on efficacy and safety. *International Journal of Health Sciences (Qassim)*. **14**(6): 52–65. Doi: https://www-ncbi-nlm-nih-gov.abc.cardiff.ac.uk/pmc/articles/PMC7644456/

Redmann, R.K., Beddingfield, B.J., Spencer, S., et al. 2022. A Micronized Electrostatic Precipitator Respirator Effectively Removes Ambient SARS-CoV-2 Bioaerosols. *BMJ*. Doi: https://doi.org/10.1101/2022.01.27.22269961

Riccaboni, M., and Verginer, L. 2022. The impact of the COVID-19 pandemic on scientific research in the life sciences. *PLOS ONE*. **17**(2). Doi: https://doi.org/10.1371/journal.pone.0263001

Richards, F., Kodjamanova, P., Chen, X., et al. 2022. Economic Burden of COVID-19: A Systematic Review. *ClinicoEconomics and Outcomes Research*. **14**: 293-307. doi: 10.2147/CEOR.S338225.

Robinson, C.M., Singh, G., Lee, J.Y., et al. 2013. Molecular evolution of human adenoviruses. *Scientific Reports*. **3**(1812). Doi: https://doi.org/10.1038/srep01812

Russel, W.C. 2009. Adenoviruses: Update on Structure and Function. *The Journal of General Virology*. **90**: 1-20 doi: 10.1099/vir.0.003087-0 https://www.microbiologyresearch.org/content/journal/jgv/10.1099/vir.0.003087-0

Saladino, V., Algeri, D., and Auriemma, V. 2020. The Psychological and Social Impact of Covid-19: New Perspectives of Well-Being. *Frontiers in Psychology*. **11**. doi: 10.3389/fpsyg.2020.577684

Santonen, T., Stockmann-Juvala, H and Zitting, A. 2010. *Review on Toxicity of Stainless Steel*. Helsinki: Finnish Institute of Occupational Health.

Sarafianos, S.G., Marchand, B., Das, K., et al. 2009. Structure and function of HIV-1 reverse transcriptase: molecular mechanisms of polymerization and inhibition. *J Mol Biol*. **385**(3): 693–713. doi: 10.1016/j.jmb.2008.10.071

Serban, D., Smarandache, C.G., Tudor, C., Duta, L.N., Dascalu, A.M., Aliuș, C. 2020. Laparoscopic Surgery in COVID-19 Era-Safety and Ethical Issues. *Diagnostics (Basel).* **10**(9):673. Doi: 10.3390/diagnostics10090673.

Scheuch, G. 2020. Breathing Is Enough: For the Spread of Influenza Virus and SARS-CoV-2 by Breathing Only. *Journal of Aerosol Medicine and Pulmonary Drug Delivery*. **33**(4): 230–234. doi: 10.1089/jamp.2020.1616

Shen, T.T., and Pereira, N.C. 1979. Electrostatic Precipitation. *Environmental Engineering*. **1**: 103–143. Doi: 10.1007/978-1-4612-6236-7_4

Schlimgen, R., Howard, J., Wooley, D., et al. 2016. Risks Associated With Lentiviral Vector Exposures and Prevention Strategies. *J Occup Environ Med*. **58**(12): 1159–1166. Doi: 10.1097/JOM.0000000000000879

Smither, S.J., Eastaugh, L.S., Findlay, J.S., and Lever, M.S. 2020. Experimental aerosol survival of SARS-CoV-2 in artificial saliva and tissue culture media at medium and high humidity. *Emerging Microbes and Infections*. **9**(1): 1415-1417. Doi: https://doi-org.abc.cardiff.ac.uk/10.1080/22221751.2020.1777906

Shretta, R. 2020. The economic impact of COVID-19. Available at: https://www.research.ox.ac.uk/article/2020-04-07-the-economic-impact-of-covid-19 [Accessed: 24/07/22]

Stanford University. 2022. *Lentivirus Fact Sheet*. Available at: https://ehs.stanford.edu/reference/lentivirus-fact-sheet#:~:text=Transmitted%20from%20person%20to%20person,.%3B%20transplacental%20transfer%20can%20occur [Available: 4/12/2022]

Stanton, R.J., McSharry, B.P., Armstrong, M., Tomasec, P., Wilkinson, G.W.G. 2008. Re-engineering adenovirus vector systems to enable high-throughput analyses of gene function. *BioTechniques*. **46**(6). doi: https://www.future-science.com/doi/full/10.2144/000112993

Stepanenko, A.A., and Chekhonin, V.P. 2018. Tropism and transduction of oncolytic adenovirus 5 vectors in cancer therapy: Focus on fiber chimerism and mosaicism, hexon and pIX. *Virus Research*. **257**: 40-51. doi: 10.1016/j.virusres.2018.08.012.

Sun, W., Reyes-Serratos, E., Barilla, D., et al. 2019. Mathematical determination of the HIV-1 matrix shell structure and its impact on the biology of HIV-1. *PLoS ONE*. **14**(11): e0224965. Doi: https://doi.org/10.1371/journal.pone.0224965

Sykes, D.L., Holdsworth, L., Jawad, N., Gunasekera, P., Morice, A.H., et al. 2021. Post-COVID-19 Symptom Burden: What is Long-COVID and How Should We Manage It? *Lung*. **199**(2): 113-119. doi: 10.1007/s00408-021-00423-z.

Tate, S.J., Sande, L.V., Ceelen, W.P., Torkington, J., and Parker, A. 2021. The Feasibility of Pressurised Intraperitoneal Aerosolised Virotherapy (PIPAV) to Administer Oncolytic Adenoviruses. *Pharmaceutics*. **13**(2043). Doi: https://doi.org/10.3390/pharmaceutics13122043

Tenny, K.M. and Keenaghan, M. 2021. Ohms Law. Treasure Island Florida: StatPearls Publishing.

Tornex Inc. 2022. Electrostatic Precipitator (ESP) – How Does it Work? Available at: https://www.tornex-world.com/?p=580 [Accessed: 24/07/22]

Tsang, T.H., Cook, S.M and Marra, M.E. 1990. Dynamic Behavior of Condensation and Evaporation of Polydisperse Volatile Aerosols. *Aerosol Science and Technology*. **12**(2): 386-398. Doi: 10.1080/02786829008959354

UK Government. 2022. Coronavirus (COVID-19) in the UK – Daily Updates. Available at: https://coronavirus.data.gov.uk/details/deaths [Accessed 24/07/22]

UK Government. 2022. COVID-19 variants identified in the UK – latest updates. Available at: https://www.gov.uk/government/news/covid-19-variants-identified-in-the-uk-latest-updates [Accessed: 11/07/22]

van Doremalen, N., Bushmaker, T., Morris, D.H., et al. 2020. Aerosol and Surface Stability of SARS-CoV-2 as Compared with SARS-CoV-1. *New England Journal of Medicine*. **382**: 1564-1567. Doi: 10.1056/NEJMc2004973

Virology Research Services. 2022. *Enveloped vs. non-enveloped viruses*. Available at: https://virologyresearchservices.com/2022/05/22/enveloped-vs-non-enveloped-viruses/ [Available: 4/12/2022]

Wang, C.C., Prather, K.A., Sznitman, J., et al. 2021. Airborne transmission of respiratory viruses. *Science*. **373**(6558). Doi: 10.1126/science.abd9149

Wang, M., Zhao, R., Gao, L., Gao, X., Wang, D., and Cao, J. 2020. SARS-CoV-2: Structure, Biology, and Structure-Based Therapeutics Development. *Frontiers in Cellular and Infection Microbiology*. **10**: 587269. doi: 10.3389/fcimb.2020.587269

Wickham, T.J., Mathias, P., Cheresh, D.A., Nemerow, G.R. 1993. Integrins αvβ3 and αvβ5 promote adenovirus internalization but not virus attachment. *Cell*. **73**(2): 309-319. Doi: https://doi.org/10.1016/0092-8674(93)90231-E.

Wigand, R., Bartha, A., Dreizin, R., et al. 1982. Adenoviridae: Second Report. *Intervirology*. **18**:169–176. Doi: https://doi.org/10.1159/000149322

Willaert, W., Van de Sande, L., Van Daele, E., et al. 2019. Safety and preliminary efficacy of electrostatic precipitation during pressurized intraperitoneal aerosol chemotherapy (PIPAC) for unresectable carcinomatosis. *Eur J Surg Oncol*. **45**(12):2302-2309. Doi: 10.1016/j.ejso.2019.06.018.

World Health Organisation. 2022. COVID-19 Vaccines. Available at: https://www-who-int.abc.cardiff.ac.uk/emergencies/diseases/novel-coronavirus-2019/covid-19-vaccines [Accessed: 11/07/22]

Yesudhas, D., Srivastava, A., Gromiha, M.M. 2021. COVID-19 outbreak: history, mechanism, transmission, structural studies and therapeutics. *Infection*. **49**(2): 199-213. doi: 10.1007/s15010-020-01516-2.

Yu, B., Zhou, Y., Wu, H., Wang, Z., Zhan, Y., Feng, X., Geng, R., Wu, Y., Kong, W., Yu, X. 2012. Seroprevalence of neutralizing antibodies to human adenovirus type 5 in healthy adults in China. *Journal of Medical Virology.* **84**(9): 1408-14. doi: 10.1002/jmv.23325.

9. Appendix

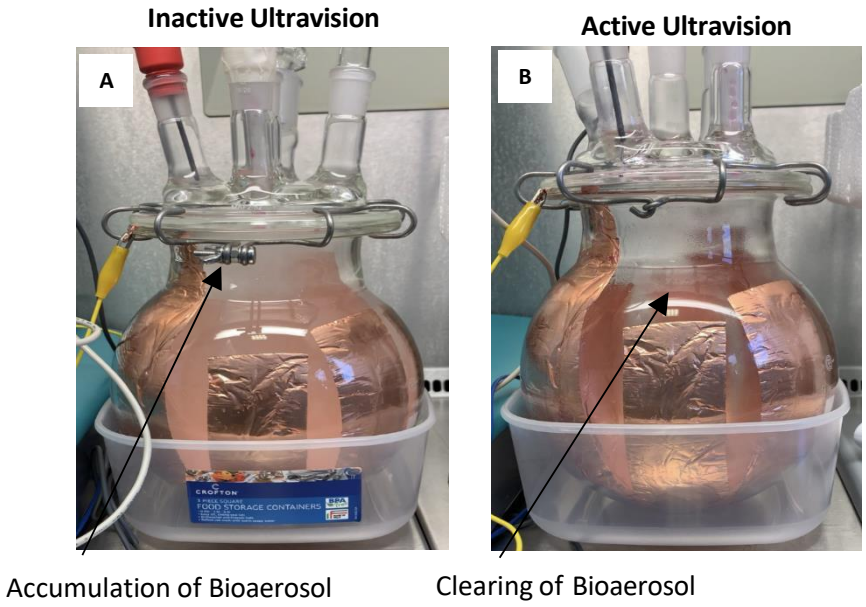

***Figure 9.1**. **Photographic images taken of the reaction kettle during sample aerosolisation**. **A**) Aerosol sample exposed to inactive Ultravision. Visual evidence of aerosol accumulation within the reaction kettle. **B**) Aerosol sample exposed to active Ultravision. Visual evidence of aerosol clearing, due to electrostatic precipitation. Aerosol particles precipitated onto the positively charged copper tape, upon direct contact with the Ultravision Ion Wand.*

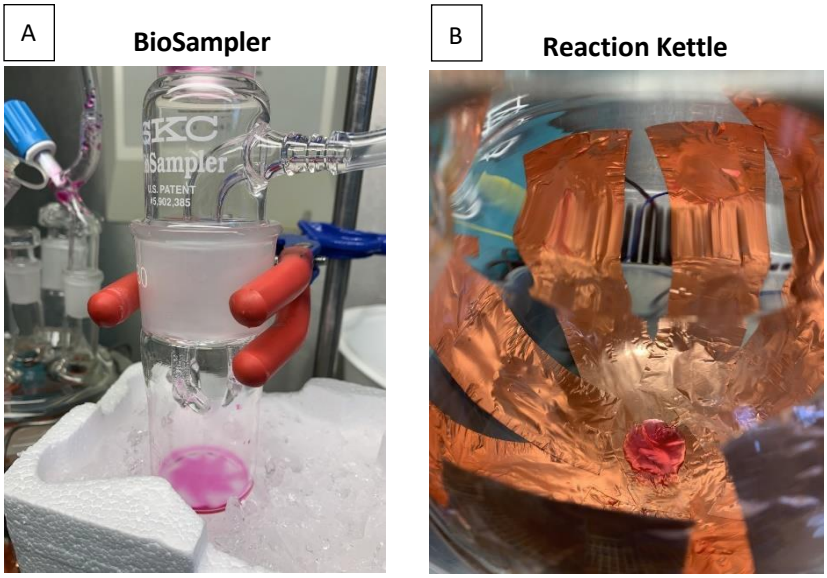

***Figure 9.2**. **Regions of Sample Collection within the Closed-System Model. A**) Following sample exposure to the Ultravision Ion Wand within the reaction kettle, the aerosol was suctioned into the BioSampler via a vacuum unit. The aerosol was collected in 2ml of SF media within the BioSampler. Following each experimental run, the media sample was obtained from the BioSampler and stored at -80°C, in preparation for analysis. **B**) Due to practical issues with the nebuliser and closed-system model, unknown volumes of the aerosolised samples were prematurely condensed during each experimental run. The condensation accumulated in the bottom of the reaction kettle and was also collected and stored for experimental analysis.*